Spring 5-15-2019

Improved Orthopaedic Repairs through Mechanically Optimized, Adhesive Biomaterials

Stephen Wheeler Linderman
Washington University in St. Louis

WASHINGTON UNIVERSITY IN ST. LOUIS

School of Engineering & Applied Science
Department of Biomedical Engineering

Dissertation Examination Committee:
Stavros Thomopoulos, Chair
Matthew J. Silva, Co-Chair
Richard H. Gelberman
Guy M. Genin
Shelly E. Sakiyama-Elbert
Larry A. Taber

Improved Orthopaedic Repairs through Mechanically Optimized, Adhesive Biomaterials

by
Stephen Wheeler Linderman

A dissertation presented to
the Graduate School
of Washington University in
partial fulfillment of the
requirements for the degree
of Doctor of Philosophy

May 2019
St. Louis, Missouri

Contents

List of Figures

List of Tables

Acknowledgments

The completion of this dissertation was only possible with the scientific and personal support of many advisors, family members, and friends. First, I would like to thank my primary mentor, Professor Stavros Thomopoulos, for his unwavering commitment to my scientific, professional, and personal growth. Steve supported (and reasonably cautioned) me as I forged a new and exciting direction in the laboratory, pursuing a project outside of his core expertise. He is an incredible role model for developing a strong network of scientific collaborations to find the necessary combination of expertise for any project. He helped me create new collaborations with biomaterials experts around the country in order to bring my dream doctoral project to fruition. Steve has pushed me to become a better scientist, helping me learn to design, execute, and write about a cohesive project from grants to publications. Even after Steve took a well-earned promotion 1,000 miles away to become Vice Chair of Orthopaedic Surgery at Columbia University Medical Center, he always remained encouraging, supportive, and a close mentor despite the physical distance. I was able to visit New York several times to meet orthopedic surgeons, professors, and lab members at Columbia to do some very exciting human cadaver studies.

I have been blessed to receive strong scientific, clinical, and professional mentorship from many outstanding faculty at Washington University and around the country. My mentors have helped me bring together many disparate disciplines to pursue my passion for becoming a physician scientist, translating medical and engineering research into new treatments that directly improve patient care. I am excited to work at the intersection engineering, biomechanics, biomaterials, medical science, preclinical experimentation and trials, and medical care, with close mentors in each area committed to helping me train and develop professionally. Alongside Steve, Professor Guy Genin has been an outstanding co-mentor and friend. Guy is an exceptionally smart mechanical engineer who has helped me hone my knowledge and application of theory to understand a problem at its core. He has an impressive intuition and an even more impressive wit, helping me always remember to keep research fun and interesting. I could not have completed this doctoral thesis without Guy's consistent encouragement, guidance, and support, even in the face of experimental

setbacks. Professor Matt Silva graciously continued supporting me in the combined biomechanics lab at the Washington University Musculoskeletal Research Center, ensuring that I always had all the resources, guidance, and support I needed as I navigated the last 18 months of my PhD work with Steve in New York. My biomaterials mentors and collaborators, including Prof. Shelly Sakiyama-Elbert at University of Texas at Austin, Prof. Younan Xia at Georgia Institute of Technology, Prof. David Kaplan at Tufts University, and Prof. Kollbe Ahn at University of California Santa Barbara, have been impressively patient as I've learned about completely new scientific areas, outside my or Steve Thomopoulos' expertise. They have let me struggle with ideas that were doomed, but always guided me back in the right direction. They have been equally patient with video conferences as we looped in mentors from several cities around the country and world into the same meetings. My clinical research mentor, Dr. Richard Gelberman, and collaborators Dr. William Levine and Dr. Leesa Galatz, have helped me keep all of my research grounded in clinical application. I will be forever grateful for their mentorship and support helping me learn to simultaneously live in the worlds of physicians and scientists.

I would like to thank my lab mates, those here at Washington University and those that moved to Columbia University, for their friendship, encouragement, and support. John Boyle has been an amazing help and inspiration for everything code or computer related. Mikhail Golman, Annie Schwartz, and Alix Black have all taken countless hours, sometimes late into the night, to help me get through important experiments. I could not hope for a more interesting, fun, intelligent, and patient group of friends and colleagues.

Outside of the lab, I kept busy as President of Sling Health, formerly known as IDEA Labs, a student run biotechnology incubator that has taught me about a whole different side of translating and commercializing medical technology. My many close friends on the leadership team, especially my co-founders and MD-PhD classmates Avik Som, Joshua Siegel, LeMoyne Habimana-Griffin, and Ravi Chacko, have kept me always excited, goal-focused, and sane through my time at Washington University. I have been fortunate to work with so many passionate students and wonderful mentors here in St. Louis and around the country as we grew from a small club into a national nonprofit and movement. In addition to developing as a multidisciplinary scientist, these years as a PhD student have helped me envision and build a career studying interfaces while working at the interfaces of medicine, engineering, and industry. The extensive network of friends, colleagues, and mentors involved with Sling Health have shaped my career.

Finally, I would like to thank my loving family for helping me get here and making my life so enjoyable over the last several years. They put up with me incessantly talking about my crazy ideas, projects, and hobbies. More importantly, they always grounded me through the sometimes rapid onslaught of highs and lows as I moved in too many directions at once. My brothers Scott, Matthew, and Randy are some of the smartest and best people I know, always inspiring

me to take on interesting, challenging problems. I especially thank my mother and father for believing in me, pushing me, and supporting me unconditionally as I've moved far away to England and then the Midwest in pursuit of my academic dreams, blending their own lives' work: medicine and engineering.

This dissertation was supported by an amazing group of administrative and support staff across the Department of Biomedical Engineering, the Department of Orthopaedic Surgery, the Department of Mechanical Engineering, and the Medical Scientist Training Program at Washington University in St. Louis. I cannot imagine completing experiments without their support. Financially, this work was supported by the Washington University in St. Louis Medical Scientist Training Program training grant (T32 GM007200), the Washington University Musculoskeletal Research Center training grant (T32 AR060719), and a National Institutes of Health individual predoctoral MD-PhD training fellowship (F30 AR06491) through the National Institute of Arthritis and Musculoskeletal and Skin Disorders. The research experiments described herein were financially supported by the National Institutes of Health, a Washington University Musculoskeletal Research Center Translational Grant, and a translational research grant through the Washington University Bear Cub competition and the Institute of Clinical and Translational Sciences.

Stephen W. Linderman

Washington University in St. Louis

May 2019

ABSTRACT OF THE DISSERTATION

Improved Orthopaedic Repairs through Mechanically Optimized, Adhesive Biomaterials

by

Stephen Wheeler Linderman

Doctor of Philosophy in Biomedical Engineering

Washington University in St. Louis, 2019

Professor Stavros Thomopoulos, Chair

Professor Matthew J. Silva, Co-Chair

Despite countless surgical advances over the last several decades refining surgical approaches, repair techniques, and tools to treat tendon and tendon-to-bone injuries, we are still left with repair solutions that rely on fairly crude underlying mechanical principles. Musculoskeletal soft tissues have evolved to transfer high loads by optimizing stress distribution profiles across the tissue at each length scale. However, instead of mimicking these natural load transfer mechanisms, conventional suture approaches are limited by high load transfer across only a small number of anchor points within tissue. This leads to stress concentrations at anchor points that often cause repair failure as the sutures cut longitudinally through the fibrous tendon tissue like a wire cutting through cheese. Most tendon reconstruction ruptures occur within the first several weeks to months after repair, indicating that the initial strength of the repair is critical for its success. Over time under favorable conditions, the healing response can strengthen the repair sufficiently to function under typical physiologic forces.

Here, we developed adhesive-based technologies to distribute load transfer more effectively across tendon and tendon-to-bone repairs, thus reducing peak stress and enabling repairs to sustain higher load before failure. First, we hypothesized that using the lateral surfaces along the length of suture to transfer load in shear would improve repair strength. We evaluated the mechanical principles of an adhesive-coated suture using a shear lag model to identify properties of suitable adhesives. Examination of the design space for an optimal adhesive demonstrated requirements for strong adhesion and low stiffness to maximize the strength of the adhesive-coated suture repair construct. When this design space was compared to real material properties in an Ashby plot, the model anticipated theoretical load transfer improvements of more than 7-fold over current tendon suture repairs using optimal elastomeric adhesives. We validated these model predictions experimentally using idealized single-strand pullout tests and clinically relevant flexor tendon repairs in cadaver canine flexor tendon. Clinically relevant repairs performed with Loctite 4903 cyanoacrylate-coated suture had significantly higher strength (17%) compared to standard repairs without adhesive. Notably, cyanoacrylate provided strong adhesion with high stiffness and brittle behavior, and was therefore not an ideal adhesive for enhancing

suture repair. Nevertheless, the improvement in repair properties in a clinically relevant setting, even using a non-ideal adhesive, demonstrated the potential for the proposed approach to improve outcomes for treatments requiring suture fixation.

We expanded this approach to assess the potential of adhesive films to increase the load tolerance of tendon-to-bone repairs. We hypothesized that adhesive films would redistribute load over the tendon footprint area where tendon inserts into bone, instead of focusing stress at just a few anchor points where suture from bone anchors punctures through tendon. Based on a shear lag model corroborated by a finite element model to establish the limits of the shear lag assumptions for thick or stiff adhesives, desirable adhesives again required compliance and high strength under shear loading. Models predicted an opportunity to increase transfer across tendon-to-bone repairs by over 10-fold. To rapidly evaluate adhesive mechanical properties for both applications using relevant tissue adherends, we developed a new method for consistent lap shear testing using tendon and bone planks. We validated shear lag predictions using this idealized test scenario and further assessed the ability of adhesives to provide additive benefit to rotator cuff repair strength using a clinically relevant human cadaver rotator cuff repair model with and without adhesive. Using this idealized adhesive testing platform, we demonstrated the potential of the proposed approach to improve outcomes in arthroscopic repair settings by applying a catechol-derived, marine mussel-mimetic adhesive with relevant mechanical properties that binds under water. Further study is needed to optimize adhesive binding properties and assess this approach in preclinical surgical tendon-to-bone repair scenarios.

Finally, we developed a new approach to deliver adhesives and biofactors in tendon repairs using sutures with a porous outer sheath. These porous sutures were mechanically non-inferior to conventional sutures in single strand tests and clinically relevant tendon repairs. The porosity dramatically increased the suture surface area, which we conjectured would facilitate adhesive interdigitation and strong binding. Furthermore, this porous suture enabled growth factor or other bioactive factor addition to the inside of the suture for increased loading capacity and sustained release over the first 14 days, determined using connective tissue growth factor. In a clinically relevant canine *in vivo* injury and repair model, we assessed the effects of porous suture delivery of CTGF on the proliferative stage of repair at 14 days. This approach is hypothesized to act as a "biological adhesive," increasing repair strength by modulating healing and encouraging tissue ingrowth into the suture pores. Taken together, these technologies represent dramatic departures from the traditional mechanical principles underlying tendon and tendon-to-bone repair, enabling large improvements in surgical repair strength without significantly changing the procedure in the operating room.

Chapter 1

Introduction

Portions of this chapter were previously published in: Linderman SW, Gelberman RH, Thomopoulos S, Shen H. Cell and Biologic-Based Treatment of Flexor Tendon Injuries. Operative Techniques in Orthopaedics. 26(3):206–215, 2016, DOI: 10.1053/j.oto.2016.06.011

Tendon, ligament, and tendon-to-bone insertion sites are frequently injured tissues that directly impact people's ability to function in their daily lives, generating a significant burden on society. Despite many decades of improvements to surgical repair techniques, surgical tools and materials, and pre- and post-operative care, musculoskeletal soft tissue repair failure rates remain high. These repairs are required to withstand high forces to accommodate normal function. Most repair ruptures occur within the first several weeks following repair, before the tissue can heal adequately to improve load tolerance. The odds of successful tendon-to-bone repair are even slimmer due to the inherent material property mismatch, which concentrates stress on the injured site.

Previous surgical repair gains have derived from the use of stronger materials and more effective tissue grasping techniques that distribute load transfer over a larger area, thereby reducing stresses. However, these gains have plateaued, while failure rates remain unacceptably high. Much of orthopedic soft tissue pre-clinical research now focuses on delivering bioactive factors and scaffold matrices to guide the healing process, aiming to strengthen repairs and create a normal tissue over several weeks following repairs. While these approaches hold great opportunity to modulate the healing response and guide tissue regeneration, they rely on the tissue remaining well apposed by the surgical repair without gap formation between the tissue ends or tissue retraction from the injury site. Furthermore, biofactor thera-

pies rely on optimized delivery approaches to provide sustained biofactor delivery without unnecessary tissue damage or tissue bulking during surgical delivery or the biological response to the reparative agent. This doctoral dissertation presents a means to reduce stress concentration and improve the overall strength of repairs using adhesive-coated sutures (Chapter 2) and adhesive films (Chapter 3) with low shear stiffness but high shear strength to distribute load transfer over larger areas. Chapter 4 presents a suture with a porous outer sheath to facilitate adhesive binding and delivery. In addition to direct application of adhesives for strength improvements at early post-surgical time points, porous sutures facilitate delivery of biofactors directly to the injury site without introducing additional damage or unnecessary bulking to the repair. Chapter 5 discusses steps to implement these technologies in clinical repairs, and describes opportunities for combining these approaches with other promising therapies to improve orthopedic soft tissue repair.

1.1 Clinical significance of tendon and ligament injury

Musculoskeletal injuries are a leading cause of disability and pain, with over 50 million injuries per year costing over $125 billion annually [1, 2]. Approximately 35-45% of these injuries involve tendons and ligaments [3]. Musculoskeletal injuries cause pain and limit strength and movement, thus impairing patients' ability to perform activities of daily living, work, and otherwise maintain quality of life [4, 5]. Decreased activity from disability can lead to other significant health concerns, including depression and weight gain. Musculoskeletal injuries fuel entire industries, including physical therapy, occupational therapy, and orthopedic surgery. Several clinically important examples of tendon and ligament injuries are discussed below. Tendinopathies can be classified by size (partial or full thickness), location (tendon midsubstance or tendon-to-bone interface), environment (intrasynovial or extrasynovial), and chronicity (acute or chronic) [6, 7]. Each classification generates important considerations for treatment.

Flexor digitorum profundus tendon: Among the most common and challenging hand injuries, intrasynovial flexor tendon transections have motivated over five decades of research designed to improve primary operative and rehabilitation techniques [8, 9, 10, 11, 12, 13, 14, 15, 16, 17]. Finger lacerations are the most common upper extremity injury encountered in the emergency room, with an incidence of 221 per 100,000 person-years or 1 in 452 people per year [18], mostly caused by glass or knives [19]. As such, flexor tendon injuries are typically acute transections without chronic degenerataion. Even small lacerations < 2 cm presenting to the emergency room often cause deep tendon injuries ($\sim$60% of cases) [19]. Major repair technique advances by Kessler [16], then Pennington [17], and

then Winters and Gelberman [11] have changed zone II intrasynovial flexor digitorum profundus (FDP) tendon treatment from an inoperable "no man's land" [15] to a common surgical procedure. Following several decades of repair [11, 16, 17, 10, 20, 21, 22, 23, 24, 25, 26, 27, 28, 29] and rehabilitation [30, 31, 32] improvements, we have reached a plateau in zone II flexor tendon repair outcomes with current methods. Clinical outcomes remain highly variable, necessitating alternative approaches [10, 33, 34].

Rotator cuff: Rotator cuff tears, a quintessential example of tendon-to-bone attachment site injuries, are one of the most common causes of shoulder pain and upper extremity disability [35], affecting over 17 million individuals in the US [6]. Shoulder pain presents over 4.5 million times annually in the U.S. [36]. Approximately half of the U.S. population over 60 years old has a rotator cuff tear [37, 38], leading to over 500,000 repairs of symptomatic shoulders annually [39]. Most tears involve the supraspinatus tendon [6]. Re-tear rates following surgery are quite high, starting at 20% for young, healthy athletes and increasing as high as 94% for elderly patients with large or massive tears [40, 41]. These high post-repair rupture rates, combined with asymptomatic tears, lead to a large disparity between the prevalence of injury and the surgical repair rates. Rotator cuff tears can be classified as acute (e.g., sports injury) or chronic following years of degeneration. Chronic rotator cuff tendon injury is typically accompanied by fatty infiltration, which negatively impacts the mechanical properties and healing capacity of the tissue [42]. Nevertheless, economic analyses have demonstrated that rotator cuff repair is cost effective for all ages and generates net cost savings for patients younger than 61 years old [4]. Repair is clinically recommended for all symptomatic, full thickness rotator cuff tears [43].

Knee ligaments: The anterior cruciate ligament (ACL), in the intrasynovial environment within the knee, plays an important role in knee stability by preventing anterior movement of the tibia relative to the femur. It is commonly injured by valgus stress while landing or planting in sports that require a twisting or pivoting motion. The medial collateral ligament (MCL) and occasionally the meniscus are commonly injured at the same time ("unhappy triad" [44, 45]). There is an incidence of approximately 200,000 ACL injuries leading to 100,000 reconstructions in the U.S. annually. This is affiliated with $2.7 – $4.3 billion in medical costs annually, due largely to rehabilitation and long term osteoarthritis [5]. Instead of attempting a primary suture repair, current treatments remove the torn ACL and implant a bone–tendon–bone graft from the middle third of the patellar tendon, the hamstring tendon, or allograft tissue [46]. Bone–patellar tendon–bone grafts are most successful in the ACL since they include natural biological fixation to subchondral bone; however, there is a high incidence of iatrogenic donor site morbidity [47, 48, 49]. As many as 78% of patients develop osteoarthritis within 14 years [50]. Tears in the extrasynovial MCL, by contrast, heal

in nearly all patients with non-operative management [46].

Achilles tendon: The Achilles tendon is the largest and strongest tendon in the body, but is still susceptible to overuse injury [51]. Achilles tendinopathy includes strain, tendon midsubstance rupture, and tendon avulsion injuries. Most ruptures occur in the midsubstance, 2 – 6 cm proximal to the insertion into the calcaneus [52]. Approximately 8 – 18 per 100,000 people rupture their Achilles tendon each year, mostly commonly due to acute or chronic sports injuries in middle aged men [51, 53]. Achilles tendinopathy has substantial morbidity, impacting patients' ability to walk, or participate in physical activities. The re-rupture rate is only approximately 3.5% for these midsubstance repairs [54, 55, 56], making Achilles repair one of the more successful tendon repairs discussed here. Still, given the essential nature of the Achilles for physical activity, improved repair techniques reducing rupture rates even further would have a substantial impact on patient morbidity.

1.2 Natural healing response

1.2.1 Tendon midsubstance

Similar to healing paradigms in other tissues, tendons follow three successive, overlapping stages of healing: acute inflammation (days 0–7 post injury), proliferation (days 3–14), and remodeling (days 10+) [57, 58, 59]. Healing outcomes vary greatly between intrasynovial and extrasynovial tendons. Intrasynovial tendons or tendon segments are enclosed within a synovial sheath, which contains synovial fluid as a lubricant and nutrition source [6]. Intrasynovial tendons are commonly located in regions where the tendon goes through a pulley to exert force on a joint which it is crossing, before inserting further distally into bone. Intrasynovial ligaments pass directly through joint spaces that require lubrication. The flexor tendon and ACL are examples of intrasynovial tendons and ligaments, respectively. Extrasynovial tendons and ligaments (e.g., patellar tendon, Achilles tendon, MCL) lack a synovial sheath or lubricant, but instead have higher vascularity for nutrition [60].

The zone II flexor tendon provides an example of intrasynovial healing [61]. The tendon lies within a synovium-lined fibro-osseous sheath that extends from the distal aspect of the palm to the distal aspect of the A4 pulley (Figure 1.1A,B). Intrasynovial flexor tendons are paucicellular [62] and hypovascular [63, 64], with limited blood supply delivered by long and short vinculae originating from the digital arteries and supplying the tendon segmentally (Figure 1.1C) [65]. In addition, the tendon receives nutrients and lubrication from the synovial fluid produced by the tendon sheath

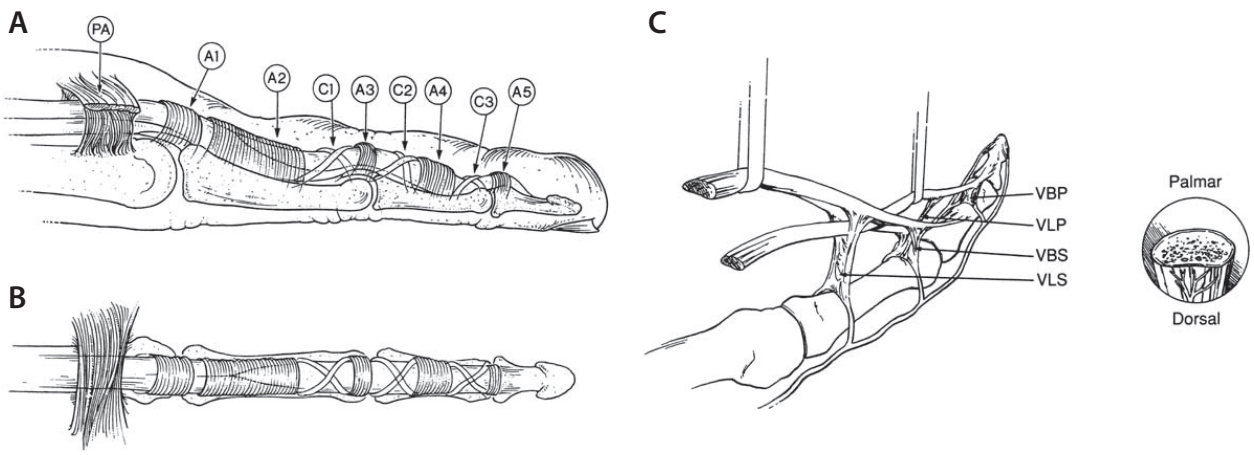

Figure 1.1: (A and B) "Lateral and palmar views of a finger depict the components of the digital flexor sheath. The sturdy annular pulleys (A1, A2, A3, A4, and A5) are important biomechanically in keeping the tendons closely applied to the phalanges. The thin, pliable cruciate pulleys (C1, C2, and C3) collapse to allow full digital flexion." (C) "The blood supply to the flexor tendons within the digital sheath. The segmental vascular supply to the flexor tendons is by means of long and short vincular connections. The vinculum brevis superficialis (VBS) and the vinculum brevis profundus (VBP) consist of small triangular mesenteries near the insertion of the FDS and FDP tendons, respectively. The vinculum longum to the superficialis tendon (VLS) arises from the floor of the digital sheath of the proximal phalanx. The vinculum longum to the profundus tendon (VLP) arises from the superficialis at the level of the proximal interphalangeal joint. The cutaway view depicts the relative avascularity of the palmar side of the flexor tendons in zones I and II compared with the richer blood supply on the dorsal side, which connects with the vincula." This figure was reprinted with permission from [25].

[10, 58]. As healing intrasynovial tendon has few intrinsic cells and has limited vascularization, there is little intrinsic healing from tendon fibroblasts until delayed time points. At early time points, cell proliferation and matrix synthesis are dominated by cells that migrate to the injury site (Figure 1.2) [58, 59, 66]. As a result, zone II flexor tendon injuries have substantially poorer healing outcomes following operative repair than do tendon injuries to extrasynovial flexor tendons [15, 10, 22].

Acute inflammation in the first several days after tendon injury attracts circulating inflammatory cells to the injured tendon [68, 69, 59]. This inflammatory infiltrate is dominated by polymorphonuclear cells during the first day, especially in the fibrin clot that forms at the repair site, followed by a transition to macrophages and monocytes by the third day [57]. Activated macrophages exhibit two phenotypes: M1 and M2. The M1 macrophages, prevalent during acute inflammation [70, 71], promote extracellular matrix deposition (scar formation) and inflammation [69, 72], bridging the transected tendon ends but also leading to adhesions. Following acute inflammation, the proliferative phase of healing ensues. In addition to M1 macrophages [69], there is an increase in the number of fibroblast-like cells synthesizing extracellular matrix at the proliferative phase [57]. Most of the fibroblast-like cells are likely derived from epitenon cells [57] and resident tendon fibroblasts [73]. Morphologic studies of repaired canine tendons at 7 days after

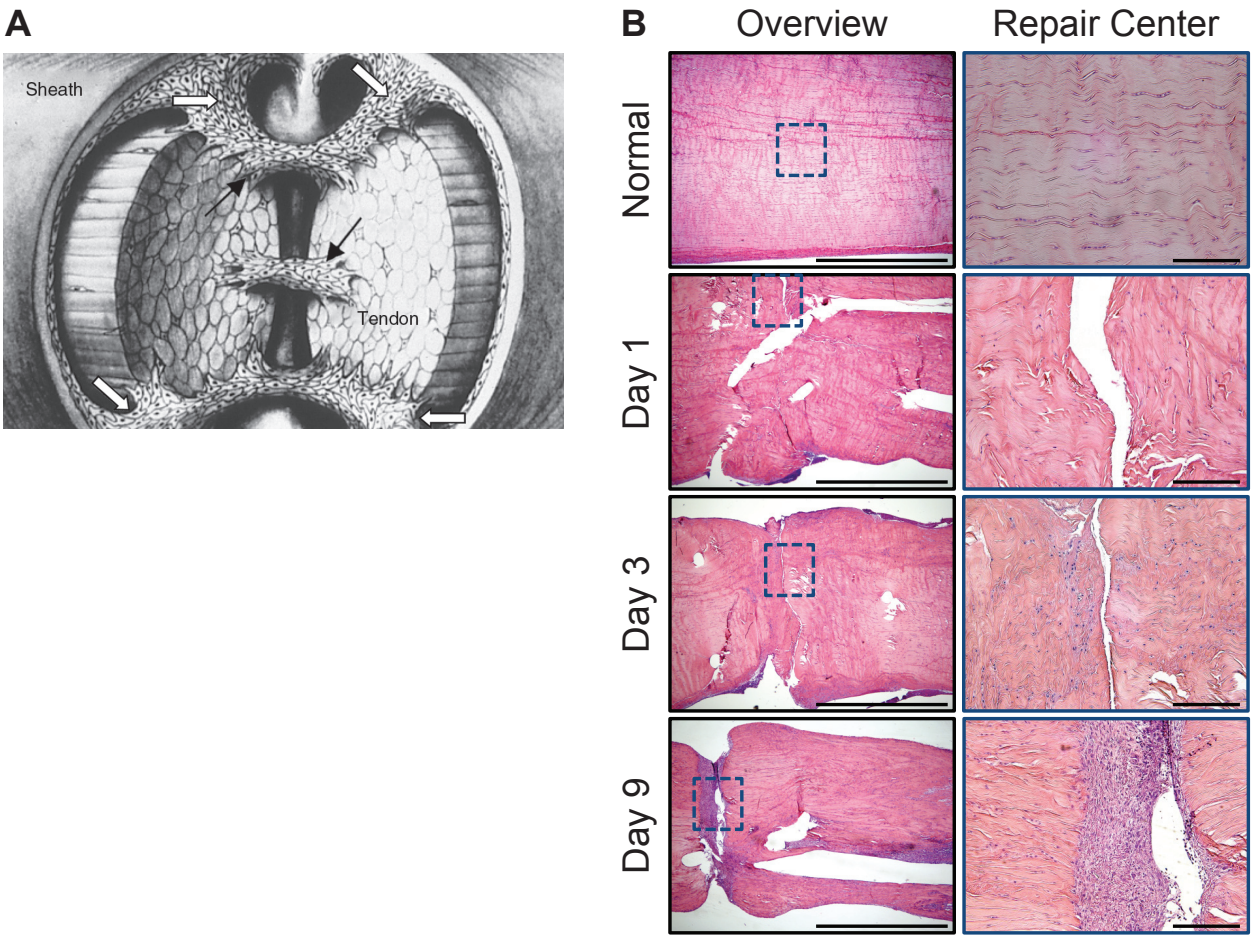

Figure 1.2: (A) Schematic of intrasynovial tendon healing, showing infiltration of fibroblasts from the outer and inner surfaces of tendon (black arrows). Adhesions between the outer surface of tendon and the sheath can reduce range of motion (white block arrows). (B) Representative histologic sections of healthy and repaired canine flexor tendons 1, 3, and 9 days post-operatively. The sections were stained with H&E and viewed under bright field for cell identification. An overview of a representative section from each time point is shown to the left (4× objective, 2 mm scale bar). High magnification images (20× objective, 200 mm scale bar) of the section outlined in blue are shown to the right. Inflammatory cells are seen infiltrating the repair site via the tendon surface on Day 1. The inflammatory response decreases over time and fibroblasts invaginate and fill the repair by Day 9. New blood vessel formation on the tendon surface is evident on Day 9. Figure (A) reprinted from [67, 6]. Figure (B) modified from [57], with permission.

tendon transection and repair show that regions with well coapted collagen fibers had a stronger endotendon response compared to those where the gap only had a few fibrinous strands serving as a scaffold for epitenon cell migration [59]. New blood vessels emerge at the surface of canine tendons 9 days following suture [57]. By 14 days, repaired canine tendon stumps show spontaneous neo-vascularization [59]. The final phase, remodeling, lasts many weeks to months, during which M1 macrophages subside and M2 macrophages appear. M2 macrophages suppress inflammation, promote matrix deposition, and facilitate tissue remodeling [74, 69, 70]. Reorganization of the granulation tissue at the repair site leads to improved tendon strength in tendon repairs that survive without gap formation. Intrasynovial tendon healing frequently leads to adhesion formation between the tendon surface and the surrounding sheath, increasing gliding resistance and decreasing range of motion (Figure 1.2A). Synovial fluid may directly inhibit the healing response as well [75].

Extrasynovial tendons heal by a similar sequence of events; however, extrinsic healing is greatly accelerated by the increased tissue vascularity. Extrasynovial tendons generally operate in a less confined space, so adhesion formation is less of a problem for joint motion. This accelerated healing response strengthens tendons and often leads to better repair outcomes [60].

1.2.2 Tendon-to-bone

Tendon-to-bone healing, e.g., for rotator cuff tears, has an added challenge compared to tendon midsubstance in that the healing tissue needs to bridge two tissues with vastly different mechanical properties. The healthy tendon enthesis facilitates load transfer from tendon to bone in several ways, including by (i) distributing force over a relatively large footprint area to reduce local stresses, (ii) using a compliant transitional fibrocartilaginous tissue to optimize stress concentrations and toughen the attachment [76, 77, 78, 79], and (iii) interdigitating fibrocartilage with bone [80]. Unfortunately, the natural healing process forms a fibrovascular scar [81, 82] that fails to recreate these stress-dissipation mechanisms. Repairs do not approach normal mechanical strength, even many months after surgery [83]. Instead, large quantities of mechanically inferior scar tissue remain at the interface between tendon and bone [82].

Rotator cuff tendon repair is one of the most common orthopaedic procedures, since the high mobility of the shoulder joint makes these tendons particularly susceptible to injury. In addition to the challenges inherent to healing the interface between tissues with different mechanical properties, rotator cuff tears frequently coincide with fatty infiltration and muscular atrophy [84]. Full-thickness tears lead to further muscle degeneration and retraction, fibrosis, and decreased collagen expression that worsen with the size and chronicity of injury [85, 86, 87]. This baseline of already

inferior tissue further impairs repair outcomes [42, 88].

ACL primary repair, which is both intrasynovial and ligament-to-bone, has such poor healing outcomes that instead reconstructions attempt to circumvent the challenges associated with ligament-to-bone healing by implanting bone–tendon–bone grafts, as discussed above [48, 49]. The bony plugs then heal with adjacent bone via a callus [89, 46]. This approach leads to im proved functional repair outcomes locally, though donor site morbidity remains a problem.

1.3 Current surgical repair techniques

1.3.1 General tendon healing and repair themes

The natural healing for different tendon repair categories emphasizes several important themes that guide operative management:

1. Extrasynovial tendon heals better than intrasynovial tendon [90, 60, 91, 92]. Controlled motion is important to prevent adhesion formation in intrasynovial tendons [65, 13], but is less important in extrasynovial tendons and ligaments such as the MCL [46] which can still function with higher gliding resistance. Extrasynovial tendon allows faster blood vessel infiltration and robust tendon matrix production [6].

2. Bone-to-bone units have improved healing capacity compared to intrasynovial tendon or ligament midsubstance, due to increased vascular supply and inherent ability to mend after fractures through callus formation [89].

3. Tendon-to-bone healing is difficult, requiring healing between tissues with vastly different tissue properties [82, 77, 93]. The normal transitional tissue at the enthesis (i.e., tendon-to-bone junction) is typically lost during injury and/or surgically removed prior to repair. Fibrovascular scar does not recreate natural tissue gradations and stress dissipation mechanisms, and repaired tissue never reaches the same strength [6].

4. Frayed tendon or ligament ends are difficult to repair, especially in an intrasynovial environment such as the ACL. Debridement reduces tendon length and applies tension across the repaired tissue. Thus, sharp transections have better post-operative outcomes than injuries that fray the tendon stumps [6].

5. Many tendon repairs exhibit a critical danger period of approximately 6 weeks during the healing process [12, 33]. Rotator cuff re-tears typically occur within the first 3–6 months following operation [94, 95]. After this point, the remodeling stage of healing often sufficiently stabilizes the repair to limit the risk of re-rupture [7].

Patient care with rehabilitation and use of a repaired tendon likely exacerbates this effect: patients that overload repairs are likely to have failures, while more cautious patients may avoid these adverse events.

Readers are referred to a review by Butler, Juncosa, and Dressler on the "functional efficacy of [the] tendon repair process" for a detailed description of considerations for tendon suture and repair assessment [96].

The technologies developed throughout this dissertation are applicable to tendon and tendon-to-bone repair generally, with additional potential applications in other soft tissue surgeries. In the following sections we focus on the flexor digitorum profundus tendon and the rotator cuff tendons to provide case studies of particular tendon and tendon-to-bone repairs, respectively, that would benefit from improved treatment alternatives.

1.3.2 Focused example: Flexor digitorum profundus tendon repair and rehabilitation

General considerations and themes: The two primary factors leading to poor results in flexor tendon repair are adhesion formation within the digital sheath and repair-site elongation and rupture. Adhesions severe enough to limit range of motion occur in up to 40% of flexor tendon repairs [97]. While adhesions can be decreased with passive motion rehabilitation [13, 98], they still occur frequently, even with closely controlled techniques [32, 99]. Experimental studies report repair-site elongation and gap formation preventing satisfactory healing in up to 48% of canine FDP tendons undergoing state-of-the-art operative repairs. In a clinically relevant, controlled canine repair model, repair site gap formation during the first six postoperative weeks did not correlate with formation of intrasynovial adhesions or loss of digital motion [100]. In clinical settings, surgeons pursue a balance between repair and rehabilitation approaches promoting tendon strength and digital excursion [58]. Flexor tendon repair complications are attributed to a slow accrual of repair-site strength and stiffness and to an increase in gliding resistance within the digital sheath during the first few weeks following tendon suture [66, 101, 59, 100, 102, 103, 58, 104, 105]. The healing of paucicellular, hypovascular intrasynovial tendon appears to be limited by the relatively low levels of collagen synthesis and remodeling during the early stages of healing [106, 65].

Surgical repair: Prior approaches have focused on improving surgical technique and rehabilitation in order to reduce the risk of repair site elongation and adhesion formation. Investigators, including Kessler, Winters and Gelberman, Tajima, Becker, and Savage have extensively varied the configuration of the core suture strands, altering the number of strands crossing the repair site and changing core suture caliber and material to produce a mechanically competent

repair (Figure 1.3) [10, 25]. If the repair is not sufficient to maintain tendon coaptation while proliferation and remodeling occurs, the repair will elongate or rupture. Canine studies consistently show that repairs that minimize gap formation and maintain closely coapted fibers have improved healing results, while those with gaps of greater than 3 mm between the tendon ends have insufficient healing and lack accrual of repair site strength over time [100, 59].

In addition, investigators have varied the pattern and depth of placement of the circumferential epitenon suture to maximize repair strength and tissue re-apposition while simultaneously debulking the tendon by smoothing the surface [10, 21, 20, 22, 23]. Suture technique innovations with larger caliber suture and larger number of strands bear the most load [11]; however, increased bulk of the repair site can reduce tendon gliding. Repairs with slightly smaller suture caliber but increased numbers of grasping points improve strength while limiting bulking [107]. Locking suture loop configurations also increase tendon holding capacity, improving repair strength [108, 109, 24, 17] (as discussed and improved in Appendix A), though some types of locking configurations may strangulate tissue.

Rehabilitation: Passive range of motion: The improved surgical techniques then allowed for the testing of controlled motion rehabilitation strategies to mitigate the risk of adhesion formation and maintain range of motion without endangering gap formation between the repaired tendon stumps. Rehabilitation variables consist of low levels of tendon excursion and *in vivo* tendon force (up to 3 mm of excursion and 5 N of force [30]. Greater magnitudes of tendon excursion does not appear to enhance healing further [31, 32] for this tendon repair type with current surgical approaches. However, this may be partially limited by gap formation under current repairs. If repair strength was improved, more aggressive rehabilitation could be evaluated to determine if rehabilitation could stimulate faster healing.

These studies have led to a plateau in zone II flexor tendon repair outcomes with current suture methods, necessitating alternative approaches. Repair failures typically occur by suture pullout through the tendon tissue, like a wire cutting through cheese, as described in detail in Appendix A.

1.3.3 Focused example: Rotator cuff tendon repair

General considerations and themes: The rotator cuff muscles and corresponding tendons are essential for glenohumeral joint stability in the shoulder. The complex loading environment combined with common degeneration of rotator cuff tendons with age leads to high tear prevalence. As with other surgical repairs, rotator cuff repairs aim to create a strong connection between the repaired tissue with minimal gap formation in order to facilitate healing [85].

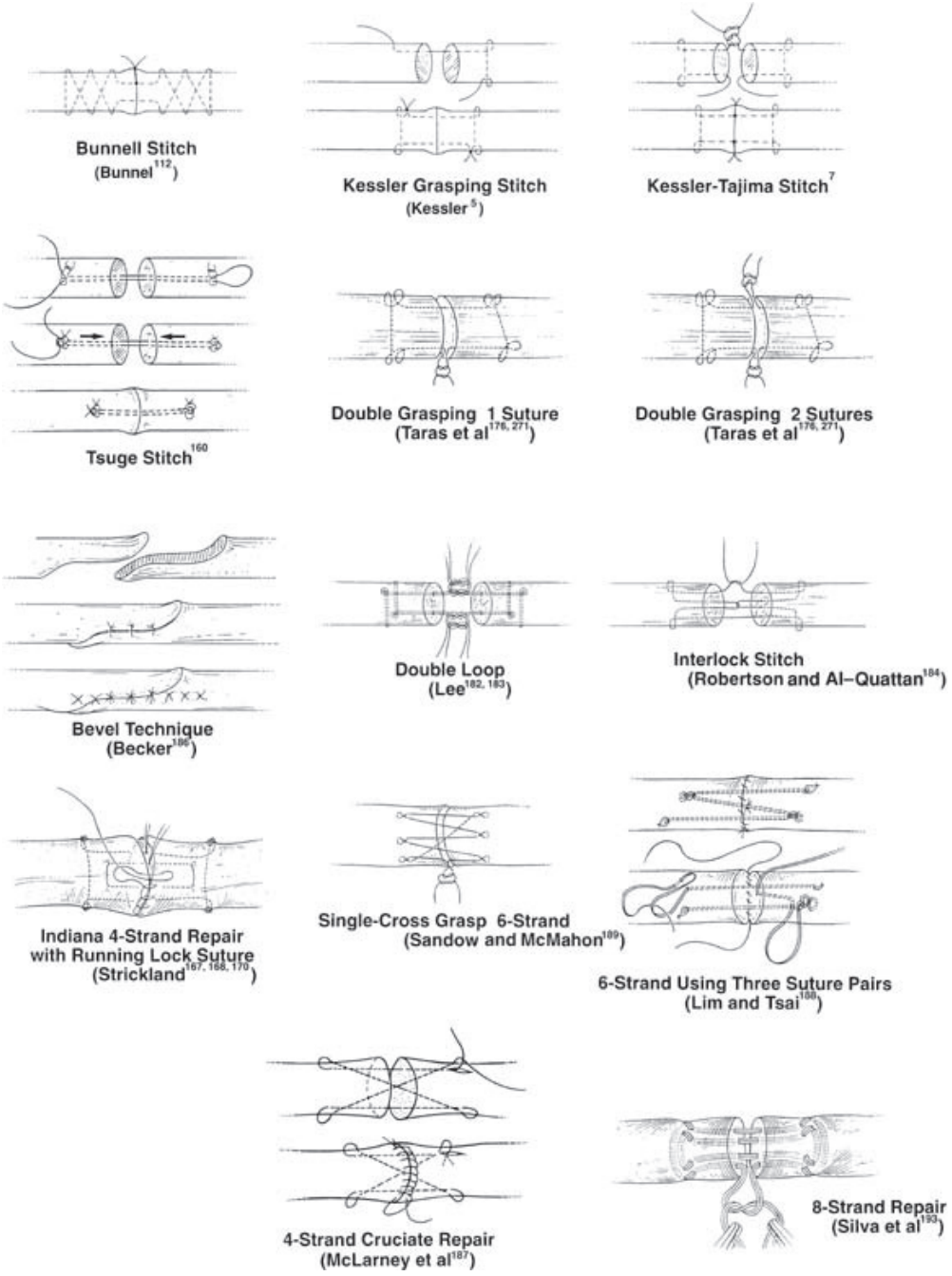

Figure 1.3: Techniques for flexor digitorum profundus tendon midsubstance end-to-end repair. This figure was reprinted with permission from [25]. Despite surgical technique improvements, clinical outcomes following FDP suture remain highly variable.

While healthy rotator cuff tendons effectively transfer load by inserting into a large footprint area on the humeral head using a specialized fibrocartilaginous transition tissue (i.e., enthesis), surgical repairs merely hope to hold the tendon in close proximity to the footprint using compression from suture. Tendon-to-bone healing requires biomechanical forces across the repair [110, 111], and immobilization leads to shoulder stiffness and discomfort [112, 113], but rehabilitation is challenging to implement without damaging the structural integrity of the repair [114]. Furthermore, patient compliance with rehabilitation protocols that require patients not to use their arm may be limited. Due to concerns over micro-motion or overt repair anatomic failure limiting healing, most orthopaedic surgeons recommend controlled passive motion for the first several weeks following repair [85]. Since current rotator cuff repairs have high anatomic failure rates [41, 40], surgical outcomes instead frequently focus on pain reduction as a means to improve shoulder use [115]. Improved surgical approaches that prevent micro-motion at the healing repair site during use of the arm, in addition to simply maintaining macroscopic tendon-to-bone apposition where the tissue passes under sutures, should greatly improve the tissue healing capacity.

Surgical repair – Arthroscopic vs. open repair: Over the last two decades, improvements in surgical treatment of rotator cuff tears have largely focused on transitioning from fully open surgical fields to "mini-open" [116] repairs with limited deltoid-splitting to fully arthroscopic repairs [85, 117, 118]. Traditional open surgical treatments allowed transosseous suture repair, which was the gold standard based on strength and tendon reapposition to the footprint. However, open surgeries lead to large scars, significant damage to the deltoid muscle, and limited visualization of articular surface of the tendon [85]. Mini-open repairs reduce deltoid damage and scar formation, and facilitate accelerated rehabilitation, while maintaining the fairly straightforward surgical approach [118]. Fully arthroscopic surgeries are quickly becoming the gold standard due to decreased infection rates, preservation of the deltoid, and improved visualization to resolve other pathology during the surgery [85, 119]. However, arthroscopic repairs are much more technically challenging, potentially more time consuming, and costly [120]. Arthroscopic devices have dramatically improved, but still come with increased risk of device failure compared to mini-open techniques [121]. In cases with complicated tears, less experienced surgeons may have higher success with mini-open or open techniques. Nevertheless, the substantial benefits of arthroscopic repairs indicate that any improvements on current treatment must be compatible with the confined, fluid-filled, arthroscopic environment.

Surgical repair – Single-row vs. double-row repair: Early arthroscopic approaches applied a simple single-row suture technique (Figure 1.4A,B), largely because of speed and simplicity in the technically challenging arthroscopic setting. However, this approach demonstrated high anatomic failure (i.e., re-tear) rates [40] and inferior mechanical

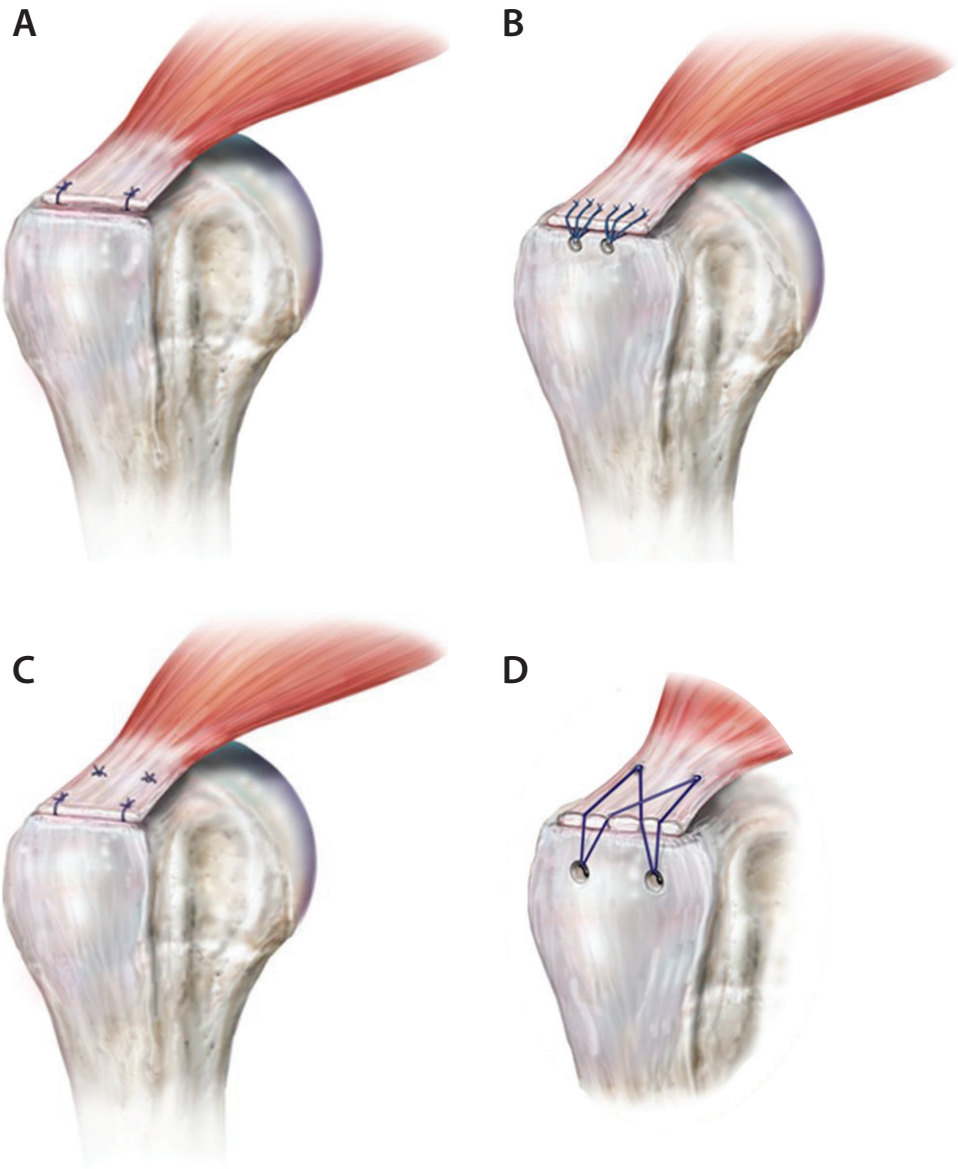

Figure 1.4: Schematics of (A) traditional single-row and (C) traditional double-row arthroscopic rotator cuff tendon repairs compared with improved variants (B,D). As a modification to the traditional single-row construct, triple-loaded suture anchors (B) have been developed to increase the number of suture passes required to secure the tendon back to its footprint. The transosseous-equivalent double-row technique (D) crosses the medial and lateral suture limbs to reinforce repairs. Double-row repairs increase mechanical fixation strength and reappose a larger percentage of the tendon-to-bone footprint than single-row repairs. Figure reprinted from [122] with minor modification.

properties compared to transosseous open repairs. Single-row repairs left half (average 52.7%) of the tendon-to-bone footprint uncovered [123]. Double-row suture configurations (Figure 1.4C,D), which include a medial and a lateral row of suture anchors, increase mechanical fixation strength and reappose a significantly larger percentage of the rotator cuff tendon footprint area [123, 124, 125, 126, 85, 127]. This strength improvement corresponds to decreased gap formation and increased resistance to cyclic displacement [128, 129, 130, 131]. This improvement in strength comes at both a financial and a physical cost: surgical repair times significantly increase [131], and the bone anchors can spatially crowd the humeral head and interfere with each other [85]. High levels of non-physiologic compressive force on the tendon from the sutures risks tissue strangulation and necrosis [132, 133]. Most importantly, there is substantial debate about whether increased macro-scale fixation strength of double row repairs improve functional outcomes. Several randomized controlled studies were unable to find a difference in functional outcomes between the repair types [134, 135, 136], though some clinicians have argued that no rigorous, adequately powered studies have been performed [122]. While single row repairs may be sufficient for small tears that only affect a small portion of the tendon insertion site, double row repairs are likely more appropriate for large tears that encompass the entire tendon or multiple rotator cuff tendons. In either repair style, repair failures commonly occur at the musculotendinous junction where the proximal suture anchors puncture through the tendon [133]. High stresses concentrated on these points, in addition to micro-motion between the tendon and the underlying bone [137], likely negatively impacts healing and causes anatomic failure of repairs.

1.4 Experimental approaches to improve outcomes

1.4.1 Experimental flexor digitorum profundus tendon repair

Animal models - FDP tendon

The most commonly used animal models for studying flexor tendon repair and tendon rehabilitation [138, 25] are the canine, mouse, horse [139, 140, 141], rabbit [142], and chicken [143, 144, 145, 146]. The canine model for zone II FDP tendon laceration and repair has been extensively used since 1962 [147, 8]. Canine flexor tendons are similar to human flexor tendons in both anatomy and function [148, 138], as well as in response to tendon injury, repair, and rehabilitation [31, 10]. The canine FDP tendon size is approximately one half the size of a human FDP tendon. Approximate size match enables surgeons both to perform surgical repairs identical to those performed clinically and

to achieve similar time-zero mechanical strength to that seen in humans [149, 150]. The canine zone II FDP tendon repair surgical model allows direct testing of surgical modifications and biological approaches before performing clinical trials in humans [32, 31, 151, 152, 153, 154, 155]. Due to these advantages, we employed the canine flexor tendon model *ex vivo* and *in vivo* in this dissertation as a prototypical intrasynovial tendon repair model with immediate clinical implications (Chapter 2 and Chapter 4).

Several groups are currently investigating murine models for flexor tendon repair [156, 68, 157, 158, 73, 159, 160]. These models offer high genetic versatility and low cost, enabling *in vivo* studies of the healing response, biology of adhesion formation [68, 73, 159], and effects of biological interventions [157]. However, the models and hypotheses tested need to be considered carefully due to anatomic and technical challenges that limit clinical relevance. Specifically, the small size of the tendon requires a simpler surgical technique using 8–0 caliber or smaller suture. Furthermore, to prevent repair rupture, all murine models to date require either partial laceration, which modifies the healing process, or proximal unloading. Wong and colleagues perform a partial laceration in zone II in the murine digit [68]. Other groups opted to fully or partially lacerate the extrasynovial zone III tendon and perform proximal transection to protect the repair [160, 73, 158], leading to large scar formation between tendon ends [159]. Finally, rehabilitation postoperatively cannot be controlled due to the small size of the animal. Despite these limitations, the availability of transgenic mouse models opens up possibilities for mechanistic basic science experiments, including cell lineage tracing, gene deletion, and cell ablation.

Biomechanical approaches

Some new approaches in the canine model seek to increase time-zero strength by increasing interaction between the suture and tendon tissue. Crosslinking agents including 1-ethyl-3-(3-dimethylaminopropyl) carbo-diimide hydrochloride (EDC) and cyanoacrylate have been used on suture in canine flexor tendon on transverse suture passes, perpendicular to the tendon longitudinal axis, to increase suture-tendon interactions and crosslink the tendon tissue immediately adjacent to the suture [161, 153]. These mechanical approaches offer an opportunity to improve repair strength, which should facilitate improved healing, but do not inherently do anything to decrease adhesions. In contrast, surface treatments using lubricin have been able to inhibit adhesion formation; however, this improvement in range of motion sacrifices repair strength, tempering our enthusiasm [162, 163, 157, 151, 164]. We build on work to increase tendon–suture interactions in this dissertation (Chapter 2).

Biological approaches

Biological approaches, such as the application of growth factors and mesenchymal stem cells (MSCs), will likely augment mechanical improvements in next generation therapies. The major goals of biological treatments are to (i) limit deleterious inflammatory effects and disordered bulk scar formation, (ii) stimulate matrix synthesis within the tendon midsubstance, and (iii) block adhesion formation at the tendon surface. Some of these approaches are discussed as potential combinatorial approaches in Chapter 5.

A number of recent reports have indicated that biological approaches, such as the application of growth factors and mesenchymal stem cells (MSCs), have the potential to improve tendon and ligament repair [103, 105, 165, 166, 151, 167]. By introducing cells into the paucicellular intrasynovial flexor tendon milieu and inducing a developmental paradigm between the repaired tendon ends, biological approaches attempt to accelerate healing and regenerate normal tissue. Multipotent MSCs from a variety of adult tissues have an excellent capacity to differentiate into the relevant tissue-specific phenotype and to provide potent immunosuppressive and anti-inflammatory effects [168, 169]. However, MSC delivery in isolation has been ineffective in improving the strength and stiffness and in reducing adhesion formation following the repair of intrasynovial tendons *in vivo* [151]. Similarly, likely due to the paucity of tendon fibroblasts in the region of repair, growth factor application in isolation has been unsuccessful in stimulating enhanced tensile properties following tendon suture, although some improvements have been achieved in digital range of motion [105, 103, 155]. This has led to more recent focus on combinations of growth factors, cells, and specialized delivery approaches to improve flexor tendon repair.

Delivery of biofactors: Several biofactor delivery approaches have been investigated to improve healing after flexor tendon suture. The simplest delivery method, systemic drug delivery, has not been widely adopted clinically due to low bioavailability at the tendon and concern of side effects. Oral nonsteroidal anti-inflammatory drugs (NSAIDs, e.g., ibuprofen) have been used, with varying results, to limit adhesions experimentally and clinically [170, 171, 172, 173]. Local bolus delivery of cells [174] or growth factors [175, 176] by simple injection has yielded limited results, since few cells graft to host tissue without a supporting scaffold and the delivered growth factor is rapidly cleared from the repair site [177]. Recent studies have shown that biological interventions require controlled spatiotemporal delivery to the repair site to improve tendon healing [178, 105, 179, 180, 181].

In order to effectively deliver cells and growth factors to the repair site, two major tissue engineering paradigms have been investigated using a variety of scaffold biomaterials. Approaches typically either interpose cell- and/or

growth factor-seeded scaffolds between the repaired tendon stumps [93, 182, 183] or deliver scaffolds on the surface of the repaired tendon [184, 151]. Interposition delivers factors directly to the injury site where they are needed for repair, but scaffolds may form a barrier between the tendon stumps that is detrimental for healing [185]. Our group has explored scaffold delivery in a longitudinal slit made within the canine flexor tendon, enabling factor delivery to the injured site while retaining tendon stump coaptation. The slit was found to have injurious mechanical effects, however, that must be overcome before improvement in healing can be achieved [186, 167, 155]. Alternatively, scaffolds placed on the surface of tendon adjacent to the repair site deliver factors to the general vicinity but rely on biofactor diffusion or migration to impact the repair itself. Furthermore, scaffolds wrapped around the tendon may induce adhesions or cause excessive bulking that limits tendon gliding within the fibro-osseous sheath. To minimize adhesion formation, lubricating biomaterials such as lubricin and hyaluronic acid [151, 162, 157, 163, 187, 188, 189] and anti-mitotic drugs such as 5-fluorouracil [66, 190] have been successfully utilized in animal models. While these materials improve tendon gliding, some studies have shown deleterious effects on repair strength [162, 151, 191]. Other materials including silicone, polyethylene, and cellophane have been used clinically as an artificial sheath to reduce adhesions, but have not gained widespread acceptance in the United States [9, 192, 193, 10].

Biomaterial selection is crucial to the function of tissue engineered scaffolds. Fibrin delivery systems with heparin-bound growth factors have enabled sustained drug delivery during healing [194, 195, 155, 105, 178, 167, 186], as have some microsphere-based approaches [196, 197, 198]. Here, we describe more recent work on these materials in Chapter 5 [199]. The scaffold backbone is also essential for promoting stem cell integration and differentiation. Scaffold mechanical properties and fiber diameter influence cell activity and differentiation [200]. Synthetic polymer approaches using electrospun polylactic co-glycolic acid (PLGA) nanofiber scaffolds have provided a strong, fibrous backbone and delivered viable cells and growth factors to the repair site (Figure 1.5). However, these scaffolds release acidic byproducts that increase the proinflammatory cytokine IL-1β and negatively impact healing [186, 167]. Naturally occurring polymers, including collagen- and fibrin/heparin-based delivery systems, have been explored for their enhanced biocompatibility. Future delivery approaches should be biocompatible, appropriate for cell seeding, able to provide sustained growth factor delivery, and have appropriate surgical handling characteristics for implantation into the relatively dense tendon tissue. One such new approach is developed here in Chapter 4 for adhesive and biofactor delivery.

Growth factor treatments: The growth factors bone morphogenic protein (BMP) 12, BMP13, and BMP14, (a.k.a., GDF7, GDF6, and GDF5, respectively) which are expressed in developing tendons and ligaments, have been shown

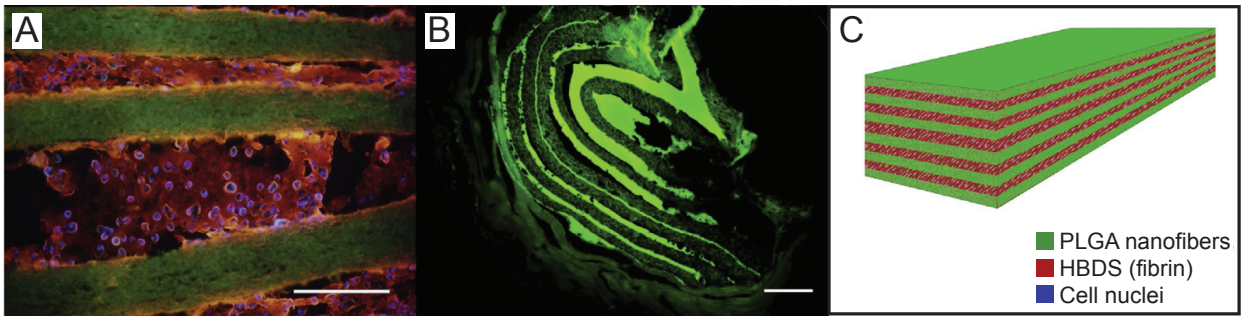

Figure 1.5: A representative PLGA-fibrin scaffold with 11 alternating layers of aligned electrospun PLGA nanofiber mats separated by fibrin containing adipose-derived MSCs. (A) Micrograph showing the scaffold in vitro; the PLGA was labeled with FITC (green), the fibrin was labeled with Alexa Fluor 546 (red) and the adipose-derived MSC nuclei were labeled with Hoescht 33258 (blue) (scale bar = 200 μm). (B) Micrograph showing the scaffold in vivo 9 days after implantation in a canine flexor tendon repair (scale bar = 100 μm). (C) A schematic of the layered scaffold is shown. Figure modified from [167], with permission.

to have the greatest potential for improving tendon healing [165, 201, 202, 203, 204, 205]. These BMPs act by inducing tenogenesis in stem cells *in vitro* via Smad 1/5/8 phosphorylation [201, 204, 165, 206]. BMP12 effectively increased the expression of the tendon markers scleraxis and tenomodulin in canine adipose-derived mesenchymal stromal cells (ASCs) *in vitro* at both mRNA and protein levels [165]. Consistent with these results, BMP12 induced scleraxis promoter driven-GFP and tenomodulin expression in mouse ASCs. BMP12 administration concurrently reduced expression of the bone marker osteocalcin, but not the osteogenic transcription factor runx-2. There was a mild increase in the expression of the cartilage matrix gene aggrecan, though still to considerably lower levels than those detected in tendon fibroblasts. BMP14 had similar but less potent effects [165]. However, these factors alone, without concurrent cell delivery, have not been sufficient to improve repair strength. Hayashi et al. interposed collagen gels with BMP14 without cells between cut ends of canine FDP tendon under *in vitro* tissue culture conditions, but this did not significantly change ultimate healing strength or stiffness compared to repaired controls [166]. Similarly, adenoviral-mediated gene transfer of human BMP13 did not improve healing in a rat rotator cuff repair model [207].

Several other growth factor approaches have attempted to promote cell proliferation and matrix synthesis in order to improve flexor tendon healing. I refer the reader to a review article that I recently published on the topic for more information [208].

A promising recent growth factor approach is based on connective tissue growth factor (CTGF), which has been shown to induce MSC differentiation into tendon fibroblasts and/or chondrocytes [209, 210, 211]. Similar to BMP12, *in vitro* CTGF effectively increased the expression of the tenocyte lineage markers scleraxis and tenomodulin, as well as the fibroblast proteins collagen I and tenascin-C [210]. During rat rotator cuff healing, CTGF is highly expressed

in the tendon midsubstance and at the tendon-to-bone insertion for several weeks following injury [212]. In chicken flexor tendons, CTGF is relatively highly expressed in normal tendons and throughout healing [213]. CTGF and cell combination studies are described below, and form the basis of the work described in Chapter 4 delivering CTGF *in vivo* in a canine flexor tendon injury and repair model using sutures with porous outer sheaths to increase loading capacity.

Cell treatments: As noted above, early enthusiasm for cell therapy, based on patellar tendon [174, 214] and Achilles tendon [215] results, has been largely unsuccessful in rotator cuff [216] and flexor tendon animal models. In two studies using a canine *in vitro* tissue culture model, interposition of a multilayered collagen patch seeded with bone marrow-derived MSCs into the repair site did not improve flexor tendon healing mechanics compared with control repairs without interposed patches [166, 217]. MSC implantation *in vivo* in rabbits decreased adhesions but did not improve biomechanical properties 3 or 8 weeks after surgery [218]. Racehorses that received direct injection of bone marrow-derived MSCs during superficial digital flexor tendon repair had reduced re-injury rates compared with historical controls [219, 220, 221]; however, the equine superficial digital flexor tendon has substantially different functional, structural, and material properties from human FDP tendon [222, 139].

Cell-growth factor combination treatments: Though cells and growth factors in isolation have not markedly improved flexor tendon healing, combination therapies offer greater potential to improve outcomes. While interposition of bone marrow-derived MSCs only or BMP14 only did not improve repair mechanics in an *in vitro* canine flexor tendon tissue culture model, the combination of MSCs with BMP14 or platelet-rich plasma on collagen patches improved strength and stiffness [166, 217]. This approach, combined with surface lubricin for *in vivo* canine flexor tendon repairs to decrease adhesions, unfortunately resulted in substantially worse repair strength 42 days after repair [151]. Similarly, application of adipose-derived MSCs in combination with BMP12 in an *in vivo* canine zone II flexor tendon repair using PLGA and fibrin scaffolds led to increased total collagen compared to repairs with acellular scaffolds, but did not improve tensile properties at 28 days after surgery compared to the acellular group. The delivery method used in these studies was a critical component driving the outcomes: the PLGA-fibrin scaffolds had a deleterious effect that may have counteracted any beneficial effects from the MSCs and/or BMP12 [186]. A previous study delivering the same PLGA-fibrin scaffolds containing MSCs and PDGF-BB demonstrated retained cell viability after 10 days, but also mild inflammatory reactions, possibly due to the PLGA scaffold (Figure 1.5) [167].

Connective tissue growth factor and cell combination approaches have not been thoroughly evaluated in flexor tendon

in vivo, but CTGF-based approaches show promise in other tendon repair scenarios. Tendon-derived CD146+ stem cells cultured with CTGF promoted tenogenic differentiation *in vitro* [223]. Tendon-derived stem cell sheets stimulated with CTGF promoted improved anterior cruciate ligament graft healing and biomechanics *in vivo* in rats, including improved osteointegration [224]. Similarly, cell sheets with CTGF and ascorbic acid enhanced biomechanical and histology-based outcomes at 8 weeks in an *in vivo* rat patellar tendon repair model. While this work is in a rat model that is far from a clinically relevant scenario, it is an intriguing for additional study. Further studies introducing CTGF and/or BMP growth factors on biocompatible matrices, possibly with cells, will be important for defining the next generation of therapies for flexor tendon repair. In Chapter 4, we employed porous sutures to delivery CTGF in a sustained, biocompatible fashion directly to the interior of repaired tendons.

1.4.2 Experimental rotator cuff repair

Animal models

Similar to flexor tendon research, several animal models have been employed to study rotator cuff injury and repair. The most commonly used animal models are rat [225, 226, 227, 228, 229, 230], goat [83], sheep [231, 132], and rabbit [232, 233, 234]. Goats and sheep are the animal models with rotator cuffs closest in size to human rotator cuffs. However, unlike humans, they lack a coracoacromial arch and the tendon is extrasynovial [235]. The rat model developed by Dr. Louis Soslowsky is structurally and physiologically the most similar to a human shoulder, and has been used for over 20 years [225]. While the rat model allows for basic science studies of biological and simple mechanical treatments, the small size prohibits repairs that truly mimic the human mechanical loading scenario [235]. Furthermore, all of these animal models are quadripeds, resulting in different loading requirements on the shoulder compared to humans. Due to these limitations in animal models, we elected to study mechanical impacts of adhesive films in human cadaver rotator cuff repairs in Chapter 3.

Biological approaches and delivery scaffolds

Due to poor healing rates in rotator cuff repair, there has been an intense research focus on delivery of biological factors (in addition to the surgical modifications discussed above) as a means to improve the healing process [236]. Clinicians and patients are desperate for ways to improve repair outcomes, especially since improved holding strength by compression with double-row repairs has not shown definitive evidence of improved repair outcomes. Platelet-rich

plasma (PRP) injections received great interest over the last decade as a potential means to induce cell migration into the repair site, differentiation, and proliferation [237, 238]. Autologous PRP contains many growth factors implicated in tendon-to-bone development and repair, including PDGF and VEGF [236]. However, despite clinical enthusiasm and several trials evaluating efficacy in patients, use of PRP has limited scientific basis or evidence of success [238, 239, 240].

More refined biological approaches to treat rotator cuff tears follow the typical tissue engineering paradigms, as outlined above for flexor tendon repair. Appropriate spatiotemporal delivery of cells and growth factors, integrated into scaffolds with relevant biophysical properties, has potential to mimic developmental paradigms to guide the healing process [235, 236, 241, 242, 243, 228]. Biological factors that have been evaluated in research settings of tendon-to-bone repair include transforming growth factor-β3 (TGF-β3) to stimulate cell proliferation [244, 228, 245] and bone morphogenic proteins BMP-2 [245] and BMP13 [207] to stimulate bone formation at the repair site [212]. While MSCs did not have a positive effect on repairs when used alone [216], MSCs did stimulate improved mechanical properties in rats following transduction with the scleraxis [246, 6], a transcription factor involved in tendon development (as discussed above for flexor tendon) [241]. Other interesting tissue engineering approaches seek to bridge the disparate mechanical properties of tendon and bone using multiphasic scaffolds, each phase with its own cell and growth factor seeding [93, 47]. While these and related approaches [247] are moving in the right direction to bridge tendon and bone mechanical properties, a review recently emphasized the need to optimize scaffold properties [248]. Iterations on these approaches have substantial potential to impact clinical rotator cuff repairs. Unfortunately, any single-factor therapy is likely insufficient in the complicated biological and mechanical milieu of the healing rotator cuff [6, 236]. The intricate requirements for biological and mechanical factor delivery timed spatially and temporally during the repair process, as well as the regulatory requirements to approve such therapies, indicates that these therapies are likely still several years from clinical application. While specific biological approaches to enhance tendon-to-bone repair are largely outside the scope of this dissertation, they still offer an interesting opportunity for future combinatorial therapy approaches with porous sutures or adhesive biomaterial films as more research establishes which biofactors are most important. This is analogous to the combinatorial approaches discussed for tendon midsubstance repair in Chapter 4 and Chapter 5.

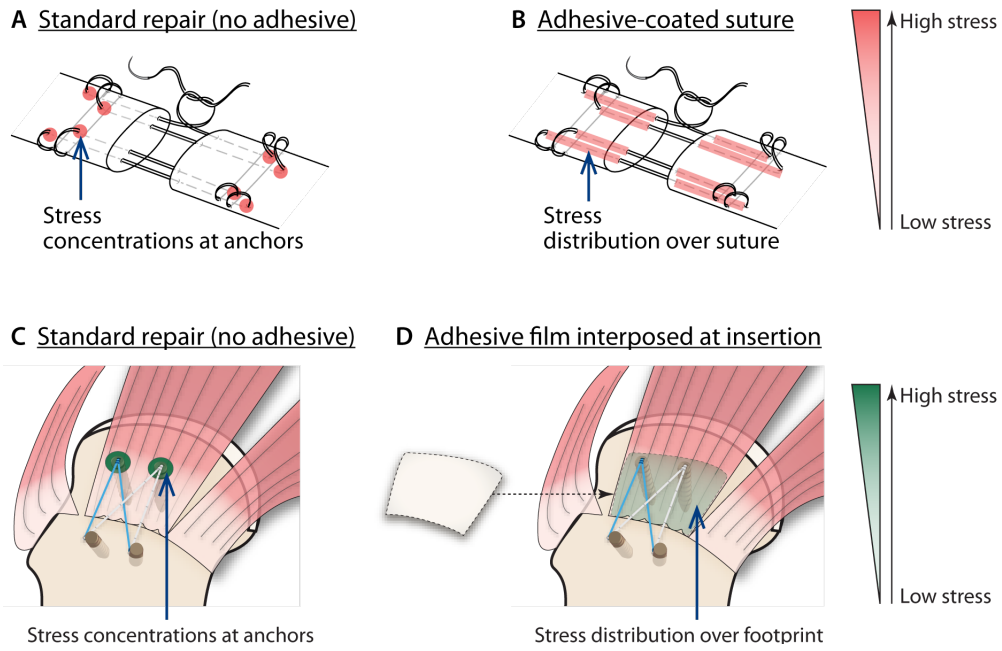

Figure 1.6: Approximate stress distributions for standard clinical tendon (A) and tendon-to-bone (C) repairs vs. repairs augmented with mechanically optimized, adhesive biomaterials (B,D). Adhesives were hypothesized to use increased surface area for load transfer, reducing peak stresses and improving overall repair mechanics. Stress is indicated by red (A,B) or green (C,D) shading.

1.5 Thesis aims and hypotheses

While modern repair techniques are sufficient to hold together many tissues, tendon and ligament repairs have elongation and rupture rates as high as 48% for flexor tendon [33, 100, 249, 250] and 94% for rotator cuff [40, 41, 251, 39, 252]. These repair failures lead to reoperations, worsening injuries, and even permanent disability [253]. Musculoskeletal tissue reconstructions such as tendon or ligament repair demand high biomechanical strength to accommodate activities of daily living without risking rupture. Improved orthopaedic surgical repair mechanics facilitate improved tissue healing and regained function. Unfortunately, surgical suturing is a crude mechanical solution. Sutures are in tension along their length, but the load is predominantly transferred to the surrounding tissue where sutures bend at anchor points (Figure 1.6A). Tendon-to-bone repairs are even worse from a mechanical perspective: almost all of the force transferred from muscle to bone concentrates across two anchor points, where the suture from a bone anchor punctures through the tendon (Figure 1.6C). This fails to recreate natural load transfer mechanisms across this interface. In both cases, high stress concentrations at these anchor points lead to repair failure [254, 152, 255]. Improved repair schemes would minimize stress concentrations and increase repair strength, reducing rupture and gap formation between the repaired tissues [33, 100].

Here, we propose to improve surgical repair outcomes through adhesive biomaterial approaches. Our global hypothesis is that mechanically optimized adhesive biomaterials that redistribute load transfer over larger physiologically-relevant surface areas will reduce stress concentrations, thereby improving load tolerance of repaired tendons (Figure 1.6B,D).

Aim 1: Assess potential of adhesive-coated sutures to transfer load along suture length. To test this hypothesis, we derived and employed a shear lag mechanical model to predict load transfer along adhesive-coated sutures for tendon midsubstance repair (Chapter 2) in order to guide research on elastomeric adhesives suitable for use in clinical settings. We validated this model using idealized and clinically relevant cadaver repairs.

Aim 2: Assess potential of adhesive films between tendon and bone to augment surgical repair strength. We then extended this model from tendon midsubstance repairs using adhesive-coated sutures to tendon-to-bone repairs using adhesive films (Chapter 3). Following idealized and clinically-relevant validation, we established a protocol for rapid, repeatable testing of adhesive mechanical properties while binding bone and tendon planks.

Aim 3: Develop implementation strategies to deliver adhesive on suture surfaces. The goal was to advance mechanically optimized adhesives that bind strongly to tissue and to sutures, and whose mechanical properties lie within the range predicted by our mechanical models to improve repair site strength, toward clinical implementation for tendon midsubstance or tendon-to-bone insertion repairs. To achieve this, we collaborated on development of sutures with porous outer sheaths to increase adhesive or biofactor loading capacity and binding strength. We then evaluated the mechanical and biological potential of loaded porous sutures to improve tendon repair *ex vivo* and in an *in vivo* canine flexor tendon injury and repair model (Chapter 4). Finally, we postulated on future directions to advance these technologies individually and in combination with biological approaches to improve tendon midsubstance and tendon-to-bone repair outcomes (Chapter 5).

Chapter 2

Enhanced tendon repair through adhesive-coated sutures

Portions of this chapter were previously published in: Linderman SW, Kormpakis I, Gelberman RH, Birman V, Wegst UG, Genin GM, Thomopoulos S. Shear lag sutures: Improved suture repair through the use of adhesives. Acta Biomater. 23:229-39, 2015. PMID: 26022966. [256]

2.1 Abstract

Suture materials and surgical knot tying techniques have improved dramatically since their first use over five millennia ago. However, the approach remains limited by the ability of the suture to transfer load to tissue at suture anchor points. Here, we predict that adhesive-coated sutures can improve mechanical load transfer beyond the range of performance of existing suture methods, thereby strengthening repairs and decreasing the risk of failure. The mechanical properties of suitable adhesives were identified using a shear lag model. Examination of the design space for an optimal adhesive demonstrated requirements for strong adhesion and low stiffness to maximize the strength of the adhesive-coated suture repair construct. To experimentally assess the model, we evaluated single strands of sutures coated with flexible cyanoacrylates (Loctite 4903 and 4902), cyanoacrylate (Loctite QuickTite Instant Adhesive Gel), rubber cement, rubber/gasket adhesive (1300 Scotch-Weld Neoprene High Performance Rubber & Gasket Ad-

PBS	Phosphate buffered saline	x	position along suture
$\tau(x)$	shear stress in the adhesive layer	τ_{ave}	average shear stress
τ_{fail}	failure shear stress of adhesive-coated suture	$\bar{\sigma}_s(x)$	normal stress in suture normalized by normal stress at $x = 0$
E_s	suture elastic modulus	E_s^*	suture elastic modulus normalized by tendon elastic modulus
E_t	tendon elastic modulus	G_a	adhesive shear modulus
G_a^*	adhesive shear modulus normalized by tendon elastic modulus		
L	suture purchase length	$L_{intersect}$	suture length where asymptotic limits for load transfer intersect
P_s	normal force in suture at the interface, $x = 0$	P_k	resultant normal force in suture at the anchor point
r_s	suture radius	r_t^*	tendon radius normalized by suture radius
r_t	tendon radius	ρ_t^*	effective radius of tendon, normalized by suture radius
t_a	adhesive thickness	t_a^*	adhesive thickness normalized by suture radius
β_s	characteristic (inverse) length scale related to geometry and material properties	χ	variable related to geometry and material properties

Table 2.1: Abbreviations and variables used throughout Chapter 2.

hesive), an albumin-glutaraldehyde adhesive (BioGlue), or poly(dopamine). As a clinically relevant proof-of-concept, cyanoacrylate-coated sutures were then used to perform flexor digitorum tendon repair in cadaver tissues. The repairs performed with adhesive-coated suture had significantly higher strength compared to the standard repairs without adhesive. Notably, cyanoacrylate provided strong adhesion with high stiffness and brittle behavior, and was therefore not an ideal adhesive for enhancing suture repair. Nevertheless, the improvement in repair properties in a clinically relevant setting, even using a non-ideal adhesive, demonstrated the potential for the proposed approach to improve outcomes for treatments requiring suture fixation. Further study is necessary to develop a strongly adherent, compliant adhesive within the optimal design space described by the model.

2.2 Introduction

Sutures are an age-old technology: they have been used for wound closure for over 5 millennia, dating back to sutures used in ancient Egypt, as described in the Edwin Smith Papyrus from 3000 – 1600 BC [257, 258, 259]. While many improvements in suture materials and intricate knot tying techniques have been introduced over the years, the core method of directly sewing tissues together remains a crude mechanical solution. Sutures typically work in pure tension along most of their length. Tension is transferred to the tissue only at anchor points (Figure 2.1). High stress concentrations at these anchor points can lead to sutures breaking or cutting through the surrounding tissue. This phenomenon limits the maximum force that can be transferred across the repair site. While current suturing techniques are sufficient to maintain the integrity of many surgical repairs, musculoskeletal tissue reconstruction (e.g., tendon and ligament repair) typically demand strong biomechanical resilience to accommodate activities of daily living without risking rupture. For example, repair-site elongation and rupture rates of up to 48% have been described after flexor tendon repair, even with modern suturing and rehabilitation protocols [250, 100, 20, 260]. Rotator cuff

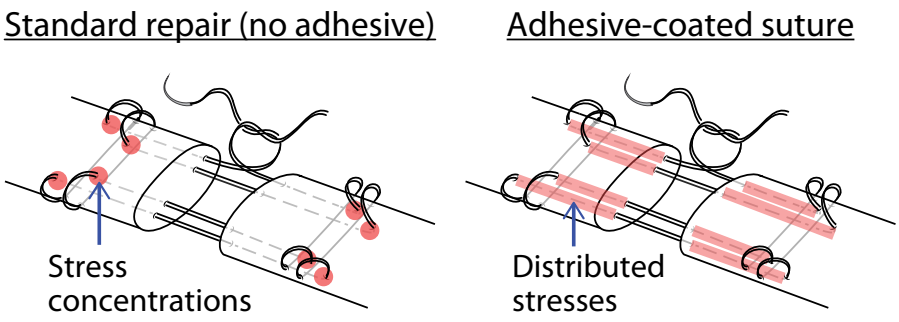

Figure 2.1: An 8-stranded Winters-Gelberman suture repair technique is shown for human flexor digitorum profundus tendon repair [11]. Red shading indicates location of load transfer. Current suturing techniques generate stress concentrations at anchor points where the suture bends within tissue. Adhesive-coated sutures could distribute that load transfer along the entire length of the suture, reducing peak stresses and improving overall repair construct mechanics.

repairs, which require reattachment of materials with disparate mechanical properties (tendon and bone), have recently reported failure rates as high as 94% [40, 41, 118]. Improved suturing schemes would allow for the transfer of greater loads across the repair site, reducing rupture and gap formation between the repaired tissues and improving healing outcomes, not only by strengthening repairs but also by enabling more aggressive rehabilitation protocols. By holding the tissues together for longer time intervals, mechanical solutions that prevent gap formation and development could provide more time for the biological healing response to generate a strong, organized tissue instead of disorganized scar [100, 11, 261].

Here, a new approach is proposed to augment standard suturing technology. Conventional sutures have a relatively large surface area passing through the tendon that is currently not utilized for load transfer. We envisioned a modified suture with an adsorbed or covalently bound adhesive that tightly binds collagen along the suture's length, thereby reducing stress concentrations and better distributing load (Figure 2.1). We hypothesized that adhesives along the length of the suture would transfer load more effectively than conventional suture without adhesive. This improvement in load transfer is expected to result in an improvement in overall repair construct mechanical properties. Note that achieving the full strength of an uninjured tendon is unnecessary, as tendons are over-designed and are typically able to accommodate many times more load than is applied physiologically [179, 262, 263]. We aim to generate functional repairs that are sufficient to accommodate *in vivo* loads and enhanced rehabilitation protocols. We focus here on single stranded sutures or pseudomonofilament sutures, including multiple fibers within an outer casing, because these are used surgically for flexor tendon repair [11].

In order to predict the ability of adhesive-coated sutures to improve load transfer, we employed a shear lag model [264, 265, 266, 267] of suture within a cylindrical tissue (e.g., a tendon). Using this model, we identified desirable

adhesive mechanical properties to improve load transfer across a repair site. We then biomechanically tested sutures coated with adhesives to validate the model and experimentally assess the capacity to improve load transfer.

2.3 Theory

2.3.1 Terminology

Throughout this chapter, "suture" refers to the core strand of suture, "adhesive" refers to the adhesive layer, "assembly" and "adhesive-coated suture" refer to the combination of suture with adhesive surrounding it, and "repair" refers to the complete tissue repair, including several strands of adhesive-coated suture and a region of tissue in which these are embedded.

2.3.2 Shear lag model

A shear lag model was studied to identify adhesives with desirable properties for suture repair (Appendix 2.A). The model predicted load sharing between the sutures and an idealized isotropic, homogeneous repaired tendon.

The load P_s on an assembly that would cause adhesive failure was estimated from the following expression for the shear stress $\tau(x)$ as a function of the position, x, along a suture (Figure 2.2):

$$\frac{\tau(x)}{\tau_{ave}} = \frac{\beta_s L}{\chi \sinh(\beta_s L)} \left[(\chi - 1)\cosh(\beta_s(x - L)) - \left(\frac{P_k}{P_s}\chi - 1 \right) \cosh(\beta_s x) \right] \tag{2.1}$$

where $\tau_{ave} = \frac{P_s}{2\pi r_s L}$ is the average shear stress; L is the suture purchase length (i.e., the length of the straight section of the suture within the connected section of the tendon); P_k is the resultant normal force in the suture at the anchor point (the knot at $x = L$); P_s is the normal force in the suture at the interface ($x = 0$); and χ and the characteristic (inverse) length scale β_s relate to the geometry and material properties:

$$\chi = 1 + \frac{\rho_t^{*2}}{E_s^*} \tag{2.2}$$

$$\beta_s^2 = \frac{1}{r_s^2} \frac{2G_a^*}{t_a^*} \left(\frac{1}{\rho_t^{*2}} + \frac{1}{E_s^*} \right) \tag{2.3}$$

where $\rho_t^{*2} = r_t^{*2} - (1 + t_a^*)^2$, in which r_t^* and t_a^* are, respectively, the tendon radius and adhesive thickness normalized

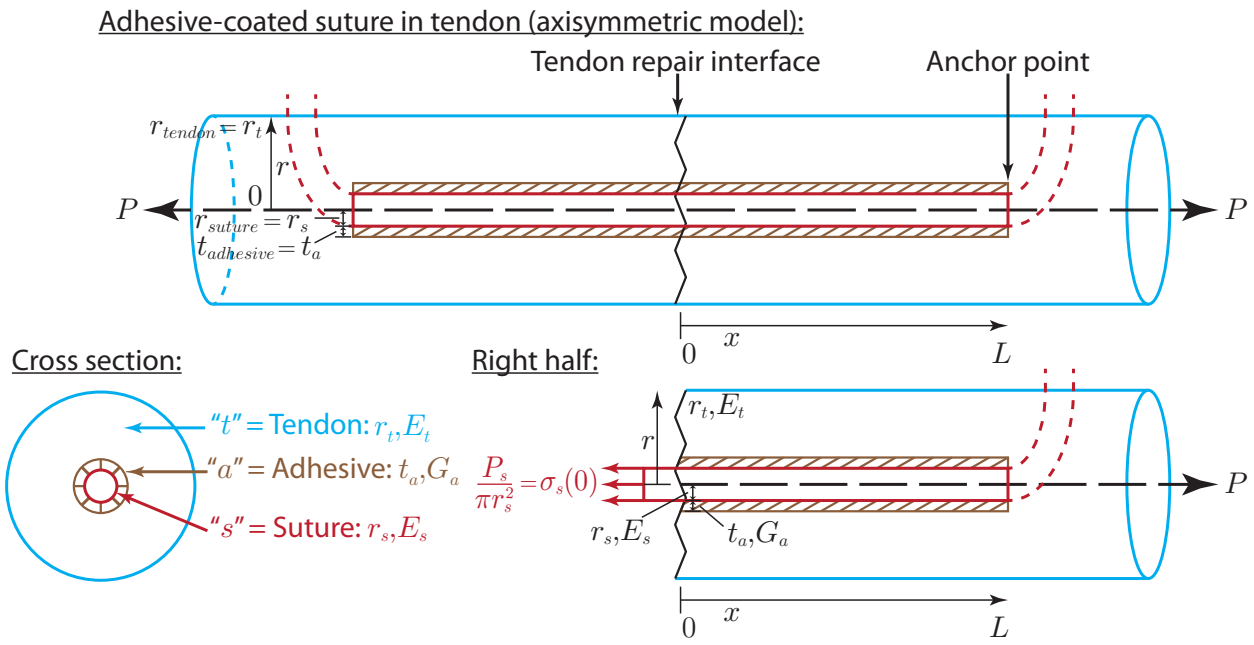

Figure 2.2: Diagram of adhesive-coated suture assembly within a cylindrical tissue, such as tendon, used to conduct shear lag analysis. P_s is the tensile load carried by the suture at the interface between repaired tissues (i.e., at $x = 0$). P_k is the load at an anchor point or knot, where the suture bends within the tissue ($x = L$). This load, when too high, leads to the assembly cutting through surrounding tissue and to rupture of the repair.

by the suture radius r_s; and E_s^* and G_a^* are, respectively, the suture elastic modulus and adhesive shear modulus normalized by the tendon elastic modulus E_t. The peak shear stress in the adhesive occurs at the interface $x = 0$ (Figure 2.3). Equating this to the adhesive failure shear stress, τ_{fail}, and solving (2.1) for the case of $P_k = 0$ yields:

$$\left(\frac{P_{max}}{2\pi r_s^2}\right) = \tau_{fail}\frac{L}{r_s}\frac{\sinh(\beta_s L)}{\beta_s L}\frac{\chi}{(\chi-1)\cosh(-\beta_s L)+1} \tag{2.4}$$

Note that τ_{fail} could be limited by failure at the interfaces with adherends (i.e., suture or surrounding tissue) or failure within the adherends themselves. This solution is nearly bilinear, with two asymptotes (Figure 2.4, Figure 2.5):

$$\lim_{L\to\infty}\left(\frac{P_{max}}{2\pi r_s^2}\right) = \tau_{fail}\left[\frac{E_s^* t_a^*}{2G_a^*}\left(1+\frac{E_s^*}{\rho_t^{*2}}\right)\right]^{\frac{1}{2}} \tag{2.5}$$

$$\lim_{G_a\to 0}\left(\frac{P_{max}}{2\pi r_s^2}\right) = \tau_{fail}\frac{L}{r_s} \tag{2.6}$$

For a given suture, the first limit ($L \to \infty$) shows that the force a suture can carry increases monotonically with decreasing adhesive shear modulus G_a^*. Below a critical adhesive shear modulus, however, the second limit ($G_a \to 0$)

shows that a cut-off exists that depends upon the suture length. Therefore, the optimum strength involves as compliant of an adhesive as possible provided that the suture length is sufficient:

$$L \geq L_{intersect} \equiv r_s \left[\frac{E_s^* t_a^*}{2G_a^*} \left(1 + \frac{E_s^*}{\rho_t^{*2}} \right) \right]^{\frac{1}{2}} \tag{2.7}$$

As a test case for a clinically relevant suture repair scenario, the model was analyzed using realistic tendon and suture material properties and a variety of realistic suture lengths and adhesive properties for a typical flexor digitorum profundus clinical repair: $L = 13$ mm, $r_t = 2$ mm, $E_t = 200$ MPa, $t_a = 100$ μm, $r_s = 100$ μm, and $E_s = 2$ GPa [107, 268, 269, 270, 271, 272, 273].

2.4 Materials and methods

2.4.1 *Ex vivo* surgical repair model

To experimentally assess the ability of adhesives to improve load transfer, a number of adhesive coatings were added to single pseudo-monofilament polycaprolactam (a.k.a. nylon 6) 4-0 suture strands (Supramid, S. Jackson, Inc., Alexandria, VA) and inserted into tendon tissue prior to preforming pullout tests. Single strands without knots were chosen to isolate the effects of the adhesive and mimic the mathematical model as closely as possible. The following adhesives were examined: highly flexible cyanoacrylates (Loctite 4903 and 4902, based on ethyl and octyl cyanoacrylate [274, 275]; Henkel Corporation, Düsseldorf, Germany), cyanoacrylate (Loctite QuickTite Instant Adhesive Gel, based on ethyl cyanoacrylate [276], Henkel Corporation, Düsseldorf, Germany), rubber cement (Elmer's Rubber Cement; Elmer's Products, Inc., Columbus, OH), rubber/gasket adhesive (1300 Scotch-Weld Neoprene High Performance Rubber & Gasket Adhesive; 3M, St. Paul, MN), BioGlue (CryoLife Inc., Kennesaw, GA), and polydopamine [277, 278] (Sigma Aldrich, St. Louis, MO). Henkel does not release the exact chemical composition of their products. Of these adhesives, only BioGlue is FDA approved for use inside the body. These commercially available adhesives were chosen solely to assess the concept proposed here, not to promote the use of any particular adhesive clinically. Loctite 4903 and 4902 have shear moduli of 538 MPa and 399 MPa, respectively [279]. BioGlue, rubber cement, and rubber/gasket adhesives [280] have shear moduli on the order of 0.5 - 5 MPa [281, 282, 283]. Suture was passed through cadaveric canine hindpaw flexor digitorum profundus tendons using a French eye needle. All tendons tested in this study were from hindpaws of healthy female adult mongrel dogs from 20-30 kg in weight (Covance Research,

Princeton, NJ), taken postmortem from an unrelated project. Canine intrasynovial flexor tendons have been used extensively by our group and others since the early 1960s as a reliable model of human tendon repair; we expect the results from this model to be comparable to those that would be obtained from human flexor tendon reconstructions [100, 284, 285, 286, 13, 138, 12, 105]. Tendons had elliptical cross sections with major and minor radii approximately 3 mm and 1 mm, respectively. The tendon was first dissected away from surrounding tissue and a complete transection was made in Zone II [61] perpendicular to the long axis of the tendon. Suture was passed from the side of the tendon 10 mm from the site of transection toward the laceration interface. The suture was pulled through the tendon so that only a single suture strand remained within the tendon. In the adhesive-coated suture tests, the adhesive was injected onto the suture and the suture was pulled into place, dragging the adhesive into the tendon. Adhesive that accumulated on the side of the tendon was cleared with gauze soaked in phosphate buffered saline (PBS). The assembly within the tendon was wrapped in PBS-soaked gauze in an airtight tube and then allowed to cure overnight at 4 °C before biomechanical testing. This curing procedure was chosen to ensure that the postmortem tissue *ex vivo* would not rot or deteriorate.

To assess the ability of adhesive to improve load transfer in a clinically relevant setting, cadaveric canine hindpaw flexor digitorum profundus tendons with Zone II lacerations [61] were repaired using an 8-strand Winters-Gelberman repair [11] ($n = 11$; Supramid 4-0 suture; S. Jackson Inc., Alexandria, VA), as diagrammed in Figure 2.1 and described previously [107]. Control repairs without adhesive were compared to repairs with Loctite 4903-coated suture. Loctite 4903 was chosen based on results of single suture pullout tests described above. All surgeries were performed by IK, an orthopaedic hand surgeon. For adhesive-augmented repairs, sutures were passed through the tendon following usual surgical technique, then for each suture pass, Loctite 4903 was injected onto the suture strands using a syringe immediately prior to pulling the adhesive-coated suture into its final position. The outside of the tendon was cleaned with PBS-soaked gauze to remove any excess adhesive. Repairs were completed with a continuous, nonlocking peripheral stitch using 5-0 nylon suture, as performed clinically [250, 11, 22, 21]. The repaired tendon and distal phalangeal bone were wrapped in PBS-soaked gauze in an airtight tube and then allowed to cure overnight at 4 °C to prevent tissue deterioration before biomechanical testing.

2.4.2 Biomechanical testing

Samples were brought to 37 °C prior to biomechanical testing. For single suture strand pullout tests, any suture and adhesive outside of the lateral tendon was first dissected away. This experimentally ensured that the effect was due to

adhesive along the length of the suture instead of adhesive accumulated at the suture entrance point. Samples were then tested in uniaxial tension on a materials testing frame (ElectroPuls E1000; Instron Corp., Norwood, MA, chosen because of a low noise load cell suitable for distinguishing milli-Newton level forces). The tendon was clamped in a stationary grip so 15 mm of tendon length was exposed. Suture was carefully placed in a jig consisting of a low friction spool and a clamp grip, which was pulled upward at 0.3 mm/s to apply tension to the suture. The gauge length between the tendon and suture grips was 8.5 cm for all samples at the start of the test. Pullout (failure) force of single adhesive-coated suture strands within tendon tissue were determined from the force-elongation curves.

Clinical repairs of cadaveric flexor digitorum profundus tendons were tested as described previously [287, 288, 103, 105]. After preconditioning, samples were pulled in uniaxial tension using a material testing machine (5866; Instron Corp., Norwood, MA, chosen because of a high capacity load cell) at 0.3 mm/s until failure. Strain was determined optically to determine when a physiologically relevant 2 mm gap formed between the repaired tendon ends. Immediately prior to testing, tendons were stained with a speckle pattern of freshly prepared VerHoeff stain to provide a surface texture for optical tracking. Elongation measurements from the material testing machine were synced with optical recordings from a high resolution camera at a frame rate of 4 Hz (illunis, Minnetonka, MN), similar to described previously [30]. Optical tracking of points proximal and distal to the laceration interface enabled accurate determination of local tissue strain. From the force-elongation curves, maximum force, force required to create a 2 mm gap in the repair (a clinically relevant measure of repair strength [100]), and stiffness (slope of the linear region) were determined. From the force-strain curves, strain at 20 N force (approximating strains at physiologically relevant load levels [289, 99]) and resilience (area under the curve until yield) were determined.

2.4.3 Statistics

Statistical analysis for all experiments was performed by non-parametric Wilcoxon rank-sum using MATLAB. Statistical significance was set at $p < 0.05$ unless otherwise noted.

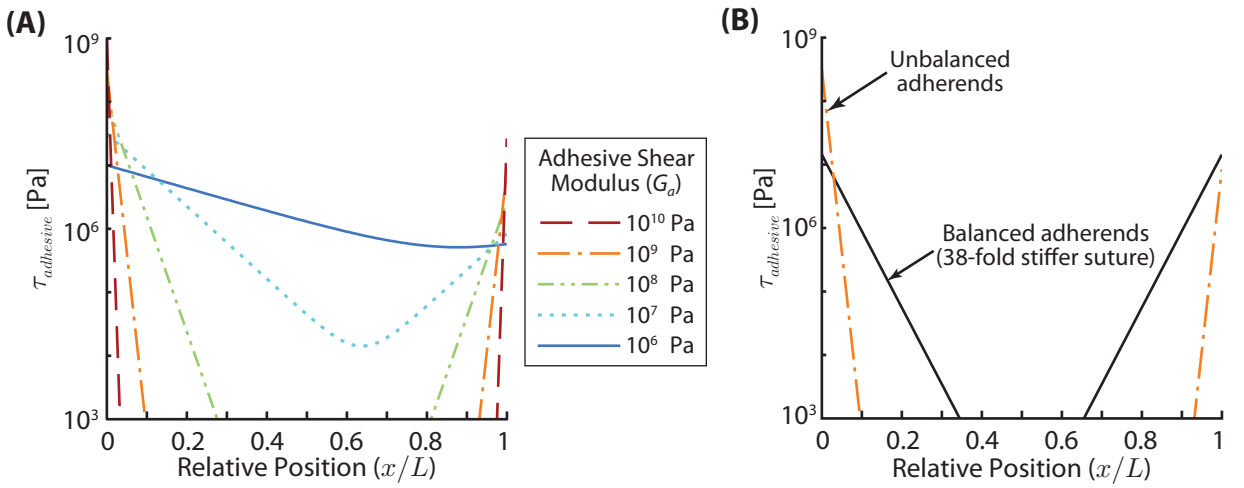

Figure 2.3: Shear stress vs. position along the length of a suture is shown. (A) The peak shear stress decreases as the adhesive shear modulus decreases because compliant adhesives distribute loads over a longer distance than stiffer adhesives. (B) A typical repair with Supramid or other sutures is unbalanced in the shear lag sense (i.e., $\rho_t^{*2} > E_s^*$, orange line, $G_a = 1$ GPa), resulting in higher peak stresses. If a 38x stiffer suture were available to balance the adherends (black line, still using $G_a = 1$ GPa), the peak stress would drop by a factor of 8.5. In these calculations $P_k = 0$ N, so that all of the load carried by the suture was transferred to the surrounding tissue via the adhesive.

2.5 Results

2.5.1 Shear lag model analysis

Shear lag modeling predicted that adhesive coatings on sutures would improve load transfer compared to conventional sutures for a certain range of properties (white band, Figure 2.4). Mechanically desirable adhesives would be compliant in shear while maintaining high binding and shear strengths. Compliant adhesives allow greater deformation, thereby distributing loads over a larger length than stiff adhesives (Figure 2.3a). This distribution reduces stress concentrations at the suture anchor points, leading to an adhesive-coated suture assembly that carries greater load before failure. In addition to adhesive properties, the maximum shear stress in the adhesive is minimized by balancing the adherends [290] (i.e., tissue and suture) so that $E_s^* = \rho_t^{*2}$ (Appendix 2.A). These adherends are not balanced with current Supramid surgical suture and tendon. When adherends (tendon and suture) are balanced by assuming 38-fold stiffer suture, the peak stress is 8.5-fold lower than in conventional suture repair (Figure 2.3b).

Shear lag modeling also predicted that maximum load transfer would increase with increasing adhesive-coated suture length. However, varying the ratio of suture length to $L_{intersect}$ demonstrates that adhesive-coated sutures approach the limit for maximum load transferred when the suture length, L, is 2-3 times $L_{intersect}$ (Figure 2.5a). The length

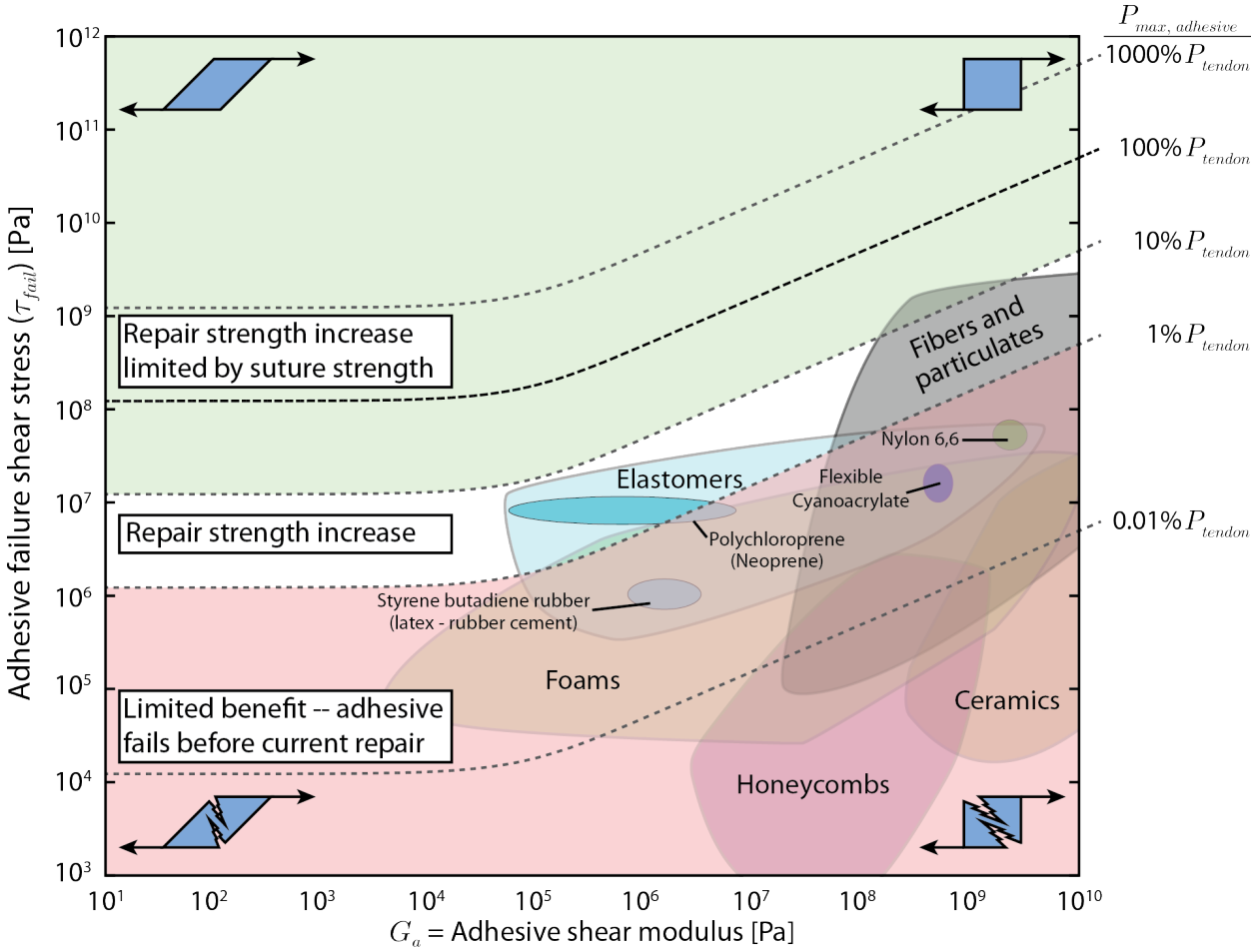

Figure 2.4: Contour map of maximum load transferred across the repair by an adhesive-coated suture strand, calculated from a wide array of theoretical adhesive shear moduli and adhesive failure shear stresses (i.e., strengths) given properties described in the methods, and overlaid with real material properties for several material types [279, 280, 281, 282, 291, 292, 293]. Maximum load transfer isoclines were normalized by the strength of healthy human flexor tendons ($P_{tendon} \approx 1000$ N) [294]. Maximum load transfer occurred with an infinitely compliant and infinitely strong adhesive, toward the upper left corner of this contour plot. Current flexor tendon repairs carry approximately 10 N per suture strand, so relevant adhesive coatings would have failure loads above this level. Adhesive mechanical properties that are not expected to improve load transfer are shaded red (lower portion). Note that the suture strand itself breaks above approximately 15.5 N for Supramid 4-0 or 23.5 N for Supramid 3-0 suture [107], so adhesive failure loads above this level would not further improve load transfer (shaded green, upper portion). Also note that shear modulus and failure shear stress are related for a given real material, so not all theoretical combinations are realistic.

of suture used is limited surgically by the particular tissue being repaired. Suture length of 13 mm was used in the model to make results relevant to flexor digitorum profundus tendon repair (Figure 2.5b) [22]. A contour map of maximum load transfer given various adhesive properties was generated using this length (Figure 2.4). Properties of several real materials were then overlaid on this contour map to identify promising candidate materials. Only a small fraction of the material classes shown are relevant materials; the remainder are included for comparison as is standard with an Ashby plot, and to highlight the importance of appropriate adhesive material selection. Assuming a compliant adhesive ($G_a = 100$ kPa) with a strong shear strength ($\tau = 10$ MPa) and the current clinical suture length of 13 mm, maximum load transfer per strand would approach 70 N of force. For the typical 4- and 8-strand methods used in flexor tendon repair, this would result in theoretical improvements of up to 280 N and 560 N, $\sim$4-fold and $\sim$8-fold improvements over current methods, respectively.

2.5.2 *Ex vivo* experimental results

Biomechanical tests of single strands of adhesive-coated suture within tendon tissue supported the model prediction that adhesive coatings can increase force required to pull out a suture. Loctite 4903, a "flexible" cyanoacrylate, improved the maximum load to pull out a single suture strand in tendon from 0.076 N ($\pm$ 0.104 N standard deviation) without adhesive to 3.24 N ($\pm$ 2.11 N; $p = 3.11 * 10^{-4}$) with an adhesive-coated suture strand (Figure 2.6). The more compliant adhesives tested did not meaningfully increase the maximum load necessary to pull out the suture, likely because of poor binding to suture and tissue.

The strongest single strands of adhesive-coated suture in tendon were further evaluated in a clinically relevant 8-stranded cadaveric canine flexor tendon repair. Since the results for Quicktite, Loctite 4902, and Loctite 4903 were comparable, the choice amongst them was arbitrary from the mechanics perspective. In the clinically relevant *ex vivo* repairs, Loctite 4903-coated sutures increased maximum load transfer by 17.0% (Control = 72.7 $\pm$ 11.3 N; Loctite 4903 = 85.0 $\pm$ 8.6 N; $p = 0.009$) and load to create a clinically relevant 2 mm gap by 17.5% (Control = 59.2 $\pm$ 8.8 N; Loctite 4903 = 69.5 $\pm$ 11.2 N; $p = 0.032$) compared to standard 8-stranded suture repairs without adhesive coatings (Figure 2.7; $n = 11$ per group). Resilience, stiffness, and strain at 20 N applied force did not change significantly (Table 2.1).

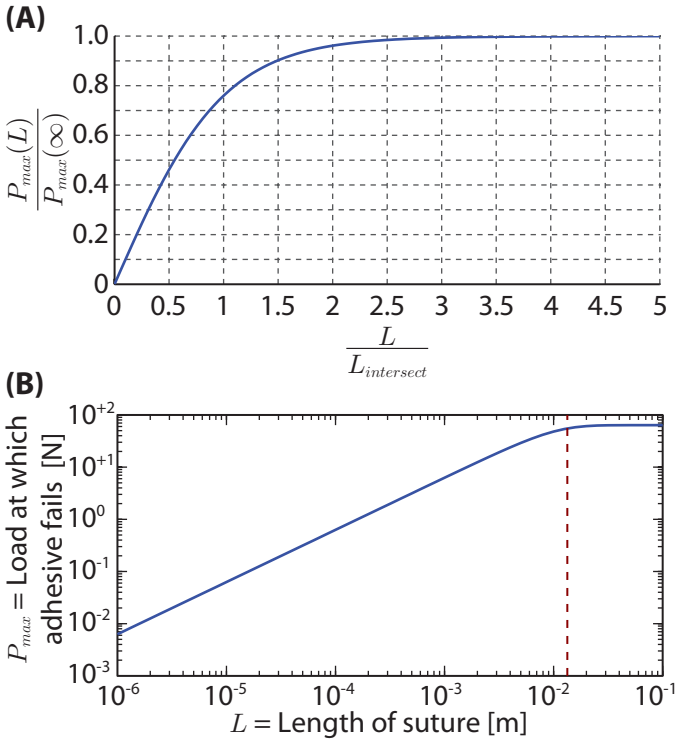

Figure 2.5: Increasing suture length increases maximum load carried by assembly, i.e., load causing adhesive to fail, only until a point. Above a transitional suture length, load capacity is governed by an asymptote independent of suture length. (A) Maximum load carried by an assembly, P_{max}, as a function of suture length, L, with respect to the length $L_{intersect}$. Maximum load is normalized by the maximum load transferred by an infinitely long suture, $P_{max}(\infty)$. At $L = L_{intersect}$, the maximum load is 76.0% of the asymptotic maximum load for an infinitely long suture. Note that this is an invariant curve that is true for any combination of t_a, G_a, E_s, r_s, E_t, and r_t that yields a particular value of $L_{intersect}$. (B) Maximum load carried by an assembly as a function of suture length for particular suture, tendon, and adhesive material and geometric properties relevant to flexor tendon repair. Here the adhesive failure shear stress $\tau_{fail} = 10$ MPa, adhesive shear modulus $G_a = 100$ kPa, adhesive thickness $t_a = 0.1$ mm, and $P_k = 0$ N. Current suture length used in flexor tendon repair is 13 mm into each tendon end, as denoted by the dashed line.

	Resilience	**Stiffness**	**Strain at 20 N**
Repair with Loctite 4903-coated suture	9.12 ± 2.46 N	27.2 ± 4.4 N/mm	$8.00 \pm 1.36\%$
Control repair (no adhesive)	7.39 ± 2.22 N	24.0 ± 7.0 N/mm	$8.81 \pm 2.91\%$
***p*-value**	0.108	0.251	0.438

Table 2.2: Repair resilience, stiffness, and strain at 20 N load are shown for a cadaveric canine flexor digitorum profundus tendon repair using standard clinical surgical technique (8 stranded repair with 4-0 Supramid suture) compared with the same repair style where suture was coated with Loctite 4903 (cyanoacrylate adhesive). Modified resilience shown here is calculated from the force-strain curve.

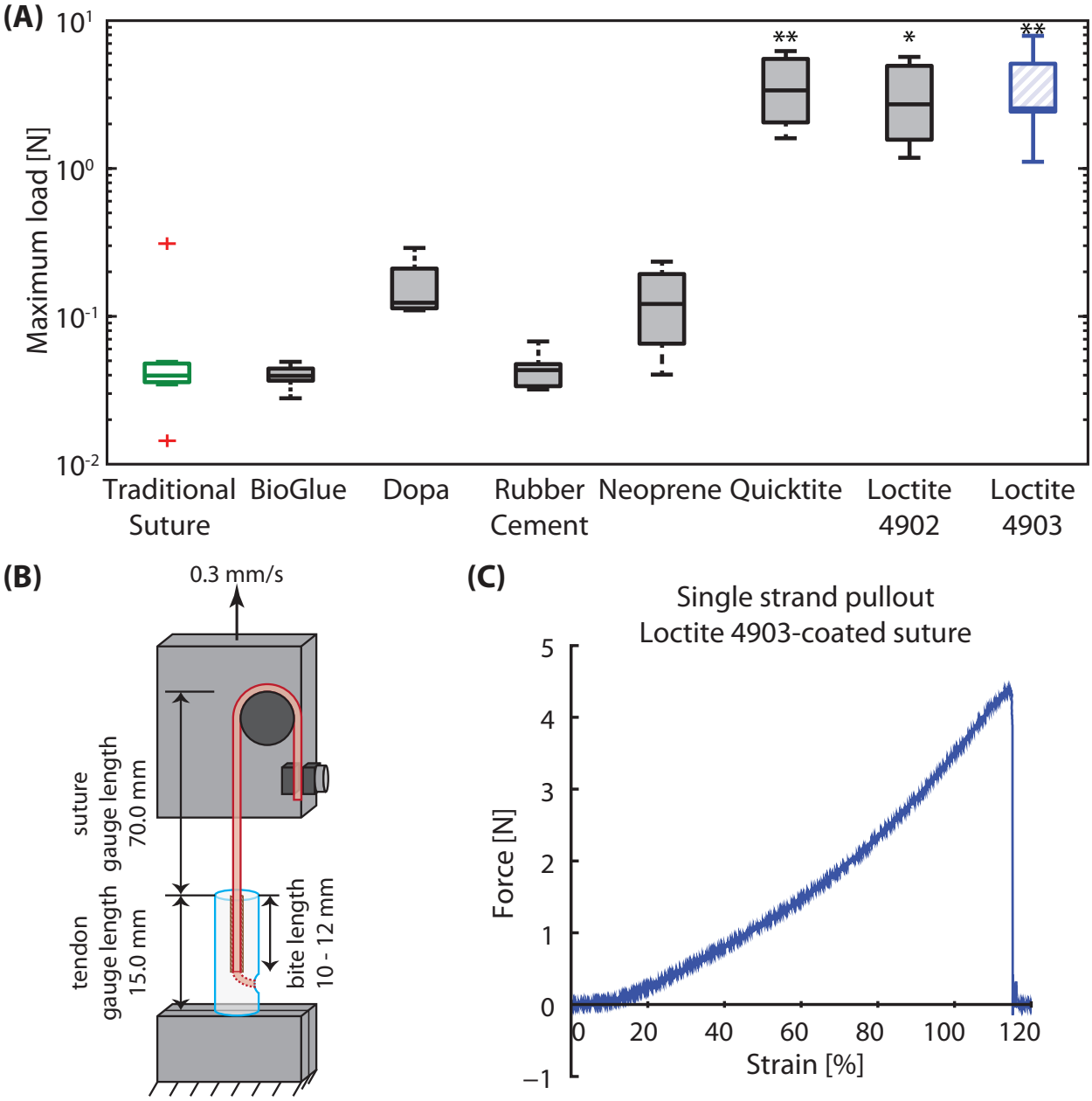

Figure 2.6: (A) Maximum loads resisted by single 4-0 Supramid suture strands coated with nothing (traditional suture), CryoLife BioGlue, Dopamine, Elmer's rubber cement, 3M rubber and gasket adhesive 1300 (neoprene), Loctite Quicktite (cyanoacrylate), Loctite 4902 or Loctite 4903 (flexible cyanoacrylates) in cadaveric canine flexor digitorum profundus tendon. The middle line within the box plots represents the median, the outer edges denote the 25 percentile and 75 percentile samples, and the whiskers extend to the extreme data points. Outliers are denoted by (+). Asterisks denote statistically significant differences compared to traditional suture (* $p < 0.05$, ** $p < 0.01$). (B) Schematic of testing setup for single strand adhesive-coated suture pullout from tendon. (C) Representative force-elongation curve for Loctite 4903-coated suture pullout.

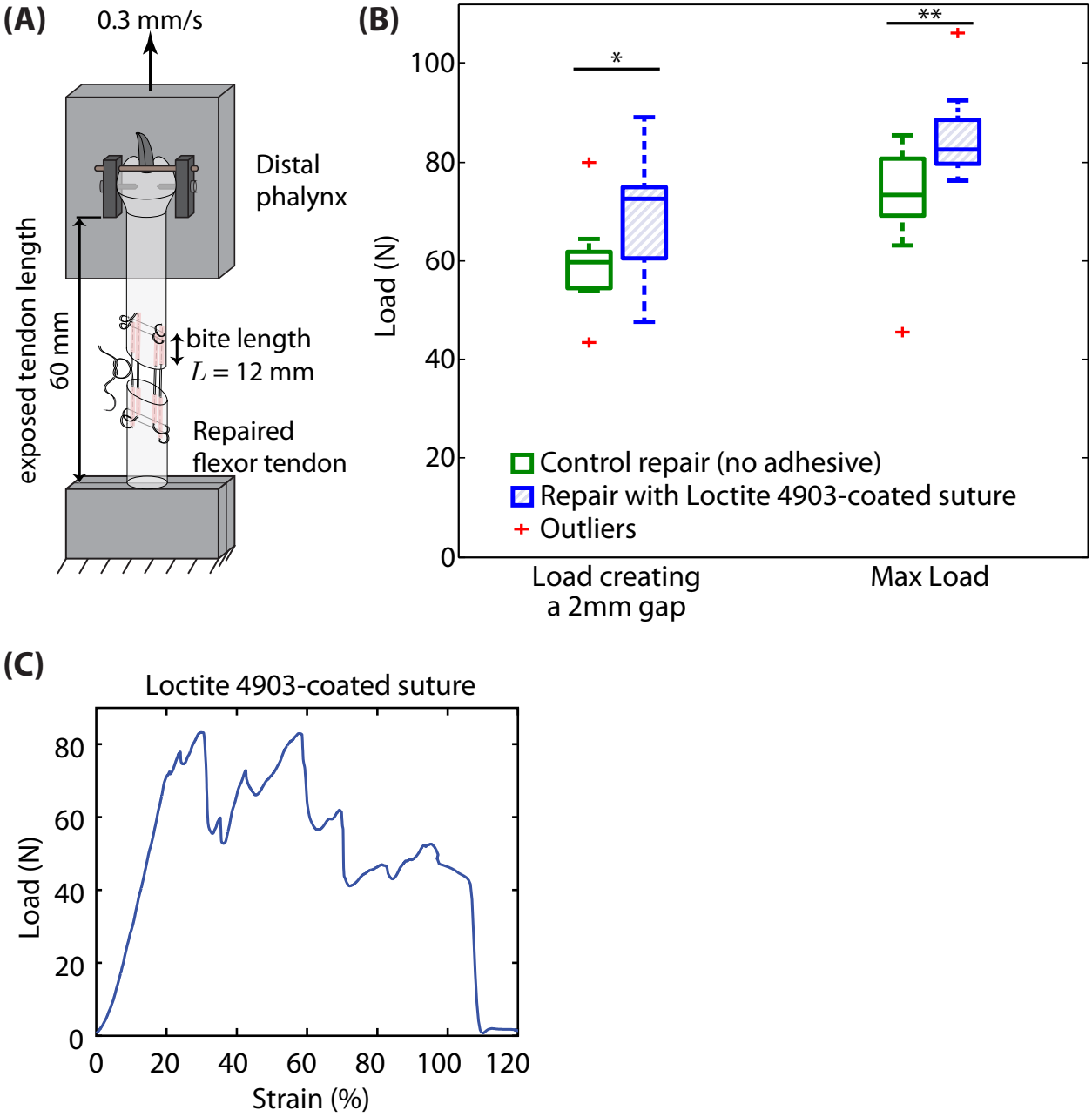

Figure 2.7: Tendon repair load tolerance with and without adhesive. (A) Schematic of testing setup for clinically relevant repairs with adhesive-coated suture. (B) The plot shows load creating a 2 mm gap and maximum load for a cadaveric canine flexor digitorum profundus tendon repair using standard clinical surgical technique (8 stranded repair with 4-0 Supramid suture, green) compared with the same repair style where suture was coated with Loctite 4903 (cyanoacrylate adhesive, blue with hash marks). The middle line within the box plots represents the median, the outer edges denote the 25 percentile and 75 percentile samples, and the whiskers extend to the extreme data points. Outliers are denoted by (+). Overbars and asterisks denote statistically significant differences (* $p < 0.05$, ** $p < 0.01$). (C) Representative force-strain curve for 8-stranded repair with Loctite 4903-coated suture.

2.6 Discussion

Although adhesives, especially cyanoacrylates [295], have been used for decades in surgical repairs to replace or augment suture for closing the skin and other tissues [296, 297], their application has been almost entirely limited to the interface between the aligned tissues. The application of adhesive to the lateral faces of sutures has never been reported for a tissue that works in tension. To our knowledge, only one previous study used adhesive-soaked sutures, reporting an increase in re-bonding strength of repaired meniscal tissue under compression compared to either suture alone or adhesive alone [298]. We hypothesized that the load distribution along sutures and the load tolerance of the repaired tissues could be optimized using a mechanical model that predicts load transfer as a function of adhesive mechanical properties. Modeling and *ex vivo* experimental results demonstrated that adhesive-coated sutures have the potential to improve the strength of tensile tissue repairs, especially with the development of adhesives with optimal mechanical properties.

The modeling indicated that adhesives that are compliant in shear facilitate load transfer from the suture to the tendon by lowering stress concentrations (Figure 2.3). This strategy is somewhat analogous to the tendon enthesis, where a compliant interfacial zone between tendon and bone [76, 77, 78] has been shown to optimize stress transfer and is hypothesized to toughen the interface [79]. Similarly, a collagen-binding adhesive that directly attaches to the suture via a small compliant layer in between the suture and the collagen would be expected to better distribute load to minimize stress concentrations, enabling more effective load transfer across the repair. Finally, we note that compliant interfaces between fibers and matrix are associated with additional modes of toughening through crack deflection [299]; this can lead to toughening of the repair as a whole through decreased sensitivity to flaws that might otherwise lead to failure [300, 301].

Adhesives with a broad range of physical properties are expected to improve load repair strength. When the derived isoclines are plotted over the properties of real materials, as in a standard Ashby plot [292, 291, 293], the model highlights a range of potential materials with appropriate mechanical properties (Figure 2.4). Many of these are not biocompatible, but elastomers such as polychloroprene, polyurethane rubber, and natural rubber do have appropriate shear moduli and shear strength to be used as base materials for adhesive development. Some biological materials, e.g., those based on elastin, could also be valuable for creating bio-adhesives. Note that the shear strength used in this model may be limited by either bulk failure within the adhesive material or interfacial failure between the adhesive and adherends (i.e., suture and tendon). Therefore, both the bulk adhesive mechanical properties and the strength of adhesion are crucial factors for successful application of this approach.

The proof-of-concept experiments performed here demonstrate substantial improvements in load transfer across single strand pullout and clinically relevant tendon repairs, even though Loctite 4903 used in these tests is a stiff cyanoacrylate that is far from ideal according to the shear lag model. The 3.24 N $\pm$ 2.11 N failure load found experimentally for a single strand of cyanoacrylate-coated suture within tendon tissue (Figure 2.6) very closely matches the predicted maximum load for cyanoacrylates from the shear lag model (Figure 2.4). The 17% improvement in load tolerance for a complete 8-stranded repair (Figure 2.7), amounting to improvement of 10–15 N, could substantially decrease rupture rate in flexor tendon repairs. The expected load transfer for clinically relevant repairs comes partially from the shear lag load transfer through adhesive and partially from the basal strength of a suture repair with knots. This 17% improvement in load transfer across a clinically relevant repair represents 47% of the additive improvement expected for an 8-strand repair based on the single strand experiments.[1] We hypothesize that this discrepancy is due to imbalanced load sharing among strands in the surgical repair. Perfectly balanced repairs are not possible even for the highly trained orthopaedic hand surgeons who performed the procedures in this study because they require that (i) all strands have the exact same tension applied to them when surgical knots are tied, (ii) the strands be perfectly aligned with the longitudinal axis of the tendon, and (iii) the tendon be loaded perfectly longitudinally. Therefore, some strands will carry more load than others in clinically relevant repairs, reducing the maximum load transfer.

The compliant adhesives tested here did not substantially improve load transfer as anticipated by overlaying their bulk material properties on the shear lag model (Figure 2.6). This discrepancy highlights the importance of compatibility between the different materials (i.e., suture, adhesive, and tendon) and the resulting interfacial shear strengths. Overall shear strength could be limited by any of three factors: (i) the interfacial shear strength between suture and adhesive, (ii) the interfacial shear strength between adhesive and surrounding tissue, and (iii) the bulk shear strength of the adhesive material. This study experimentally evaluated the model using several commercially available adhesives without prior knowledge of their binding strength to Supramid (polycaprolactam) sutures or tendon tissue. Notably, these commercially available adhesives were not optimized to adhere to suture and tissue, whereas strength parameters used in the model represented an optimal scenario where the interfacial shear strengths were at least as strong as bulk shear strength of the adhesives. Poor binding strength of these commercially available adhesives to suture or tissue might have limited the failure shear stress and efficacy for load transfer. While we tested Supramid sutures because of their surgical use in flexor tendon repair, different suture materials may have improved compatibility with particular adhesives. In addition, multifilament sutures have increased surface area for adhesive integration and binding, serving as a potential mechanism to increase interfacial failure shear stress.

[1] Each pass of an 8-stranded Winters-Gelberman repair includes 2 strands of a looped suture. Therefore, the 8 strands are bundled in 4 groups of 2 strands. If an adhesive-coated bundle of 2 strands is assumed to act as a single unit for transferring load in shear, then the load transfer improvement observed in clinically relevant repairs represents 94% of the expected additive improvement based on single strand experiments.

Since adhesives were simply injected onto the suture surface before the suture was pulled into tissue, the compliant adhesives may have sheared off of the suture when pulled into place, before adequately curing could take place. One limitation of this experimental validation is the lack of suitable visualization of adhesive within the tissue along the length of the suture. We hope to overcome this limitation in future work. The modeling performed here is applicable even for thin adhesive layers compared to the tissue and suture width. Furthermore, the methods described above ensure that the effects seen experimentally were due to adhesive along the length of the suture instead of adhesive at the entry point into tissue (Figure 2.6).

Despite these limitations, the single-strand pullout results for cyanoacrylates were accurately predicted by the mathematical model. This is possibly because Henkel publishes lap shear strength for cyanoacrylates instead of block shear strength, so the shear data includes interfacial adhesive strength. Additionally, cyanoacrylates are highly reactive compounds that may generate sufficient interfacial adhesive strength via covalent bonding with suture and with tendon that they were instead limited by failure within the adhesive bulk.

The promising mechanical improvement seen in these proof-of-concept studies with sub-optimal adhesives is still an order of magnitude below the predicted improvement that could be achieved with an optimal adhesive. While current repairs are not strong enough to sustain physiologic loading in all patients, even modest mechanical improvements are expected to make a substantial difference clinically. Therefore, we anticipate this technology will be useful clinically even if we only see half of the maximum expected improvement based on single-strand testing for a specifically engineered compliant adhesive material. Note that we do not suggest the specific adhesives tested in this proof-of-concept study be used clinically. Rather, these results provide a foundation for the further development of adhesives with the desirable mechanical properties predicted here, material compatibility with sutures and tissue, delivery methods that mitigate adhesives shearing off of suture, and appropriate biocompatibility for use in patients.

This shear lag model describes the importance of adhesive mechanical properties for creating a successful adhesive-coated suture; however, most currently used adhesives are not designed for this purpose. Specifically engineering an adhesive material to bind suture and surrounding tissue tightly, while maintaining compliance to shear stress, could lead to substantially improved adhesive-coated sutures. In addition to having appropriate mechanical properties once in place, an ideal adhesive-coated suture should be inert for storage and surgical handling before it is placed into the body. We envision several potential approaches to generate adhesive coatings that only activate when in place within tissue.

The shear lag model used in the current study employed several simplifying assumptions. First, shear lag models

treat the displacement field as one-dimensional. Only displacements along the long axis of the tendon/suture were considered. This approximation has, however, proven effective for a broad range of fibrous composites [265, 302, 303]. Second, the adhesive layer was considered to be very thin. For a thicker layer, deformation of the adhesive must be considered explicitly, accounting for both axial displacements varying through the thickness as well as radial displacements, especially for highly compliant adhesives. Third, the stress field in the suture was assumed to be independent of radial position, an approximation valid only for relatively stiff sutures. Because non-absorbable sutures used in tendon repair can be assumed rigid in tension in the range of the failure forces of the repair, this approximation should be acceptable, especially for estimates of load transfer. Despite limitations listed above, this simplified model of suture-tendon interaction allows for adequate determination of the design space for an adhesive-coated suture for tissue repair. When used in combination with an Ashby plot showing real material properties [292], this model can identify promising base materials for adhesive-coated suture development.

2.7 Conclusion

Strengthening surgical repairs should lead to improved healing outcomes for mechanically sensitive tissues, such as tendon. Our models and proof-of-concept experiments suggest that coating sutures with adhesives that are appropriately designed hold promise for achieving repairs that have higher levels of resistance to gap formation and catastrophic failure. While Loctite 4903 shows promising results that would be valuable clinically, it is far from an ideal adhesive according to the model due to its high shear modulus. We intend to develop biocompatible adhesives with optimized mechanical and chemical properties to further increase load transfer and improve clinical repairs for tendon, ligament, and other tissue injuries.

2.8 Acknowledgements

This study was supported by the National Institutes of Health (NIH): U01 EB016422 (to ST and GMG), R01 AR062947 (to ST and RHG), T32 AR060719 (to SWL) and T32 GM007200 (to Medical Scientist Training Program, Washington University in St. Louis). Loctite 4902 and 4903 were gifts from Henkel Corporation (Düsseldorf, Germany).

2.9 Author contributions

SWL derived the shear lag model with help from VB and GMG. SWL designed and performed all experiments with guidance from ST, RHG, VB, and GMG. IK performed the surgeries and provided input into how to apply adhesives to sutures during surgeries. UGKW provided input and data comparing model results to real material properties. SWL wrote the manuscript, and ST, GMG, IK, RHG, VB, and UGKW provided edits.

2.10 Supplemental material

2.10.1 Shear lag analysis of an adhesive suture

The shear lag model applied was analogous to the [264] and [265] double lap joint solutions, and to the [266] axisymmetric solution (cf. Section 2.10.2). We present a derivation here to highlight our approximations and how adhesive properties arise in the final expression.

The model was based upon the free body diagram in Figure 2.S1) and the following assumptions: (a) the suture, adhesive, and tendon are linear elastic materials; (b) viscous effects are negligible; and (c) radial displacements, strains, and stresses are small. The latter is appropriate for a thin adhesive layer. These validity of these assumptions has been established in composites with short [302, 265] and long fibers (e.g., [303]), and by comparison to solutions in which these assumptions were not made [304, 305]. We note as well that, although adhesives often exhibit nonlinearity and viscoelasticity, the linear analysis is adequate and useful for the target design range in which the adhesive is not close to failure.

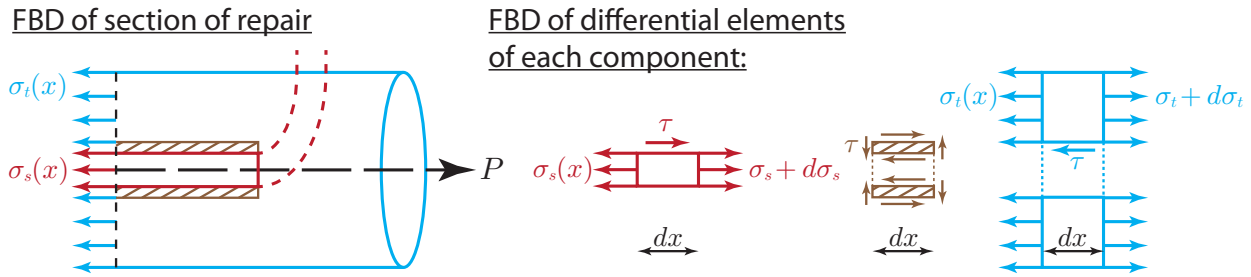

Figure 2.S1: Free body diagram showing an axisymmetric model of adhesive-coated suture within a cylindrical tendon tissue. Simultaneously analyzing a section of the repair (left) and each component independently (i.e., suture, adhesive, and tendon; right) allows derivation of a shear lag model to estimate shear stress within the adhesive. Note that this model reduces to a one-dimensional set of equations along the x-axis.

The differential equation governing the normal stress in the suture at position x is [265, 266]:

$$\frac{d^2\bar{\sigma}_s(x)}{dx^2} - \beta_s^2\bar{\sigma}_s(x) + \frac{\beta_s^2}{\chi} = 0 \tag{2.8}$$

where $\bar{\sigma}_s(x)$ is normal stress in the suture normalized by the stress $P_s/\pi r_s^2$ at $x = 0$, and β_s and χ are defined in the main text. Solving and applying the boundary condition $\bar{\sigma}_s(0) = 1$ at the interface between repaired tendon ends and $\bar{\sigma}_s(L) = P_k/P_s$ at the anchor or knot yields:

$$\begin{aligned}\bar{\sigma}_s(x) \quad = \quad & \frac{1}{\chi} + \left(1 - \frac{1}{\chi}\right)\cosh\left(\beta_s x\right) \\ & + \frac{\sinh\left(\beta_s x\right)}{\sinh\left(\beta_s L\right)}\left(\frac{P_k}{P_s} - \frac{1}{\chi} + \left(\frac{1}{\chi} - 1\right)\cosh\left(\beta_s L\right)\right)\end{aligned} \tag{2.9}$$

Inserting this into the equilibrium equation yields an expression for the shear stress $\tau(x)$ (Equation 2.1).

Note that, as with lap joints (e.g. [290]), parametric analysis of Equation 2.1 confirmed that peak stress is minimized if the inner and outer adherends (tendon and suture) are "balanced" so that $E_s^* = \rho_t^{*2}$ (Figure 2.3). This is not the case for current Supramid surgical suture and tendon. Balancing requires a 38-fold stiffer suture, and would reduce the peak stress by a factor of 8.5 (assuming geometry and material properties used in the main text).

2.10.2 Derivation from Nairn's (1997) general, optimized shear lag solution

[266] presented a general shear lag solution for n concentric, transversely isotropic cylinders that sustain an average axial stress of σ_0. We verify in this appendix that, for the case of $n = 3$ an expression analogous to that of Section 2.10.1 can be derived from this solution. Nairn's governing equation for the interfacial shear stress $\tau_{rz}(r)$ at suture/adhesive interface is:

$$2\left[-\tau_{rz}(r_s)\left(\frac{1}{E_s^*} + \frac{1}{E_a^*(t_a^{*2} + 2t_a^*)}\right) + \frac{(1+t_a^*)\tau_{rz}(r_s + t_a)}{E_a^*(t_a^{*2} + 2t_a^*)}\right]$$

$$\begin{aligned} = \quad & -\tau_{rz}''(r_s)\left[\frac{1}{4G_s^*} + \frac{(1+t_a^*)^2}{2G_a^*(t_a^{*2} + 2t_a^*)}\left(\frac{(1+t_a^*)^2}{t_a^{*2} + 2t_a^*}\ln\left(1+t_a^*\right) - 1 + \frac{t_a^{*2} + 2t_a^*}{2(1+t_a^*)^2}\right)\right] \\ & + \frac{(1+t_a^*)^3\tau_{rz}''(r_s + t_a)}{2G_a^*(t_a^{*2} + 2t_a^*)}\left(\frac{1}{t_a^{*2} + 2t_a^*}\ln\left(1+t_a^*\right) - 1 + \frac{t_a^{*2} + 2t_a^*}{2(1+t_a^*)^2}\right)\end{aligned} \tag{2.10}$$

where G_s^* is the shear modulus of the suture normalized by the elastic modulus of the tendon and all other variables are as defined in Section 2.10.1. For the adhesive/tendon interface,

$$2\left[\frac{\tau_{rz}(r_s)}{E_a^*(t_a^{*2}+2t_a)} - (1+t_a^*)\tau_{rz}(r_s+t_a)\left(\frac{1}{E_a^*(t_a^{*2}+2t_a)}+\frac{1}{\rho_t^{*2}}\right)\right]$$

$$\begin{aligned} = \quad & \frac{\tau_{rz}^{''}(r_s)}{2G_a^*(t_a^{*2}+2t_a^*)}\left(\frac{(1+t_a^*)^2}{t_a^{*2}+2t_a^*}\ln(1+t_a^*) - 1 + \frac{t_a^{*2}+2t_a^*}{2}\right) \\ & -(1+t_a^*)\tau_{rz}^{''}(r_s+t_a)\left[\frac{1}{2G_a^*(t_a^{*2}+2t_a^*)}\left(\frac{1}{t_a^{*2}+2t_a^*}\ln(1+t_a^*) - 1 + \frac{t_a^{*2}+2t_a^*}{2}\right)\right. \\ & \left. +\frac{r_t^{*2}}{2G_t^*\rho_t^{*2}}\left(\frac{r_t^{*2}}{\rho_t^{*2}}\ln\frac{r_t^{*2}}{(1+t_a^*)^2} - 1 + \frac{\rho_t^{*2}}{2r_t^{*2}}\right)\right] \end{aligned} \tag{2.11}$$

where G_t^* is the shear modulus of the tendon normalized by the elastic modulus of the tendon.

We model the case of a thin adhesive layer ($t_a^* \ll 1$) that is compliant compared to the suture and tendon ($G_a^* \ll G_s^*$ and $G_a^* \ll G_t^*$). We also assume that the shear stress to be uniform throughout the adhesive layer, as is reasonable for a thin layer. Thus, $\tau_{rz}(r_s) \approx \tau_{rz}(r_s+t_a)$ and $\tau_{rz}^{''}(r_s) \approx \tau_{rz}^{''}(r_s+t_a)$.

Making the two assumptions noted above and rewriting the above equations in the form

$$\tau_{rz}^{''} - \beta_N^2\tau_{rz} = 0$$

yields:

$$\beta_N^2 \approx \frac{1}{r_s^2}\frac{2G_a^*}{t_a^*}\left(\frac{1+t_a^*}{\rho_t^{*2}}+\frac{1}{E_s^*}\right) \tag{2.12}$$

which is equal to the expression in Equation (2.2) for $t_a^* \ll 1$.

Chapter 3

Enhanced tendon-to-bone repair through adhesive films

Portions of this chapter were previously published in: Linderman SW, Golman M, Gardner TR, Yoon D, Birman V, Ahn K, Genin GM, Thomopoulos S. Enhanced tendon-to-bone repair through adhesive films. Acta Biomater. 70:165-176, 2018. PMID: 29427745. [306]

3.1 Abstract

Tendon-to-bone surgical repairs have unacceptably high failure rates, possibly due to their inability to recreate the load transfer mechanisms of the native enthesis. Instead of using a large footprint area to distribute load, surgical repairs concentrate shear stress on a small number of points where sutures connected to bone anchors penetrate through tendon tissue. Expanding on the approach described in Chapter 2 to distribute load over the length of adhesive-coated sutures, here, we present predictions and proof-of-concept experiments showing that mechanically-optimized adhesive films can mimic the natural load transfer mechanisms of the healthy attachment and increase the load tolerance of a repair. The mechanical properties of suitable adhesives were identified using a shear lag model, corroborated by a finite element model to establish the limits of the theoretical scaling law for thick or stiff adhesives. Examination of the design space for an optimal adhesive demonstrated that strong adhesion and low stiffness are needed to maximize

the strength of the repair construct. Adhesives with optimized properties can theoretically improve load transfer across tendon-to-bone repairs by over 10-fold, decreasing the chance of rupture. To rapidly evaluate adhesive properties with relevant adherends and assess adhesive usefulness for tendon-to-bone repair, we developed a new method for lap shear testing using tendon and bone planks. Using this idealized lap shear testing method, we experimentally validated the mechanical models for a relevant range of adhesive stiffnesses and strengths. As a clinically relevant proof-of-concept, multipartite adhesives were then applied to *ex vivo* human supraspinatus repairs in cadaver tissues. The cadaver repairs performed with and without adhesives suggested that the adhesive provided an additive improvement in repair strength. Finally, a catechol-derived, marine mussel-mimetic adhesive with relevant mechanical properties that binds under water was applied to demonstrate the potential of the proposed approach to improve outcomes in arthroscopic repair settings. Further study is needed to optimize adhesive binding properties and assess this approach in pre-clinical surgical tendon-to-bone repair scenarios.

3.2 Introduction

The concept of enhanced tendon repair strength through improved load distribution is broadly applicable across various surgical repair scenarios. In the previous chapter, adhesive-coated sutures were presented for tendon or ligament repair; the approach took advantage of the previously unused lateral surfaces of sutures to transfer higher loads in small repair areas (Chapter 2). In the current chapter, adhesion was added to repair sites with larger attachment areas, such as those typical seen in tendon-to-bone repair. Although these repairs have the potential to transfer high loads across a relatively large surface, current surgical repair techniques continue to rely on load transfer concentrated across a small number of suture anchor points. We therefore investigated adhesive application to tendon-to-bone repairs in order to

PBS	phosphate buffered saline	THPC	tetrakis (hydroxymethyl) phosphonium chloride
x	position along adhesive lap	L	adhesive lap length
$\tau(x)$	shear stress in the adhesive layer	τ_{ave}	average shear stress, i.e., P/wL
τ_{fail}	failure shear stress of adhesive	$\bar{\sigma}_t(x)$	normal stress in tendon normalized by normal stress at $x = 0$
E_b	bone elastic modulus	x/L	position along adhesive lap normalized by lap length
E_t	tendon elastic modulus	E_t^*	tendon elastic modulus normalized by bone elastic modulus
G_a	adhesive shear modulus	G_a^*	adhesive shear modulus normalized by bone elastic modulus
t_t	tendon thickness	t_t^*	tendon thickness normalized by bone thickness
t_a	adhesive thickness	t_a^*	adhesive thickness normalized by bone thickness
t_b	bone thickness	P	normal force across joint far from insertion, i.e., $x = 0$ and $x = L$
P_{max}	force P causing joint failure	$L_{intersect}$	lap length where asymptotic limits for load transfer intersect
χ	variable related to geometry and material properties	β	characteristic (inverse) length scale related to geometry and material properties

Table 3.1: Abbreviations and variables used throughout Chapter 3.

improve strength across the tendon-to-bone repair site.

Tendon-to-bone repair presents a challenging mechanical problem: repairs require high strength and resilience to accommodate forces from activities of daily living and to avoid repair site elongation or rupture; the strong anchor sutures used for repairs cause stress concentrations that limit attachment strength. This is compounded by stress concentrations associated with the mismatch between compliant tendon and stiff bone [307]. The healthy tendon enthesis facilitates load transfer from tendon to bone in several ways, including by (i) distributing force over a relatively large footprint area to reduce local stresses, (ii) using a compliant transitional fibrocartilaginous tissue to minimize stress concentrations and toughen the attachment [76, 77, 78, 79], and (iii) using randomness of composition and structure where fibrocartilage interdigitates with bone to distribute stress during failure [80].

Surgical repairs have high failure rates, possibly because they not only fail to recreate these resilience mechanisms, but also introduce stress concentrations at sutures. For example, rotator cuff healing after repair is notoriously challenging, with post-repair rupture rates ranging from 20% for young, healthy athletes with small tears to as high as 94% for massive tears in elderly patients [40, 41]. These failure rates are not surprising from a mechanical perspective. While current double-row suture bridge repair techniques apply compression to the tendon over a large portion (78%) of the bony footprint [308], almost all of the force from muscle to bone is transferred in shear across only two anchor points, where the suture from a bone anchor punctures through the tendon near the musculotendinous junction (Figure 3.1A). These stress concentrations, coupled with possible vascular compromise in the same region due to strangulation from inappropriately tensioned repairs [133], lead to the vast majority (86%) of rotator cuff repair ruptures by the tendon pulling through the sutures at those anchor points [255]. Approaches that distribute shear stresses and increase strength without causing tissue strangulation would theoretically decrease failure rates. Approximately half of the US population over 60 years old has a rotator cuff tear, leading to over 500,000 repairs annually [39]. With a growing aging and elderly population, improving on these failure rates is critical to reinstate shoulder function in these patients.

Here, an adhesive-film based approach is proposed to augment standard tendon-to-bone repairs, with a particular focus on supraspinatus tendon rotator cuff repairs for proof-of-concept. This adhesive-based surgical augmentation mimics the natural stress distribution across the repair site to improve repair strength and limit ruptures. We hypothesized that, unlike conventional suture repairs with only a few anchor points (Figure 3.1A), this adhesive repair scheme would reinstate load transfer over the entire tendon-to-bone insertion footprint (Figure 3.1B). This increase in load transfer is expected to result in an improvement in overall repair construct mechanical properties, similar to the adhesive-coated suture case examined in Chapter 2. As with flexor tendon repairs discussed previously, achieving the full strength of a healthy tendon enthesis may not be necessary, since the enthesis can accommodate higher loads than are applied

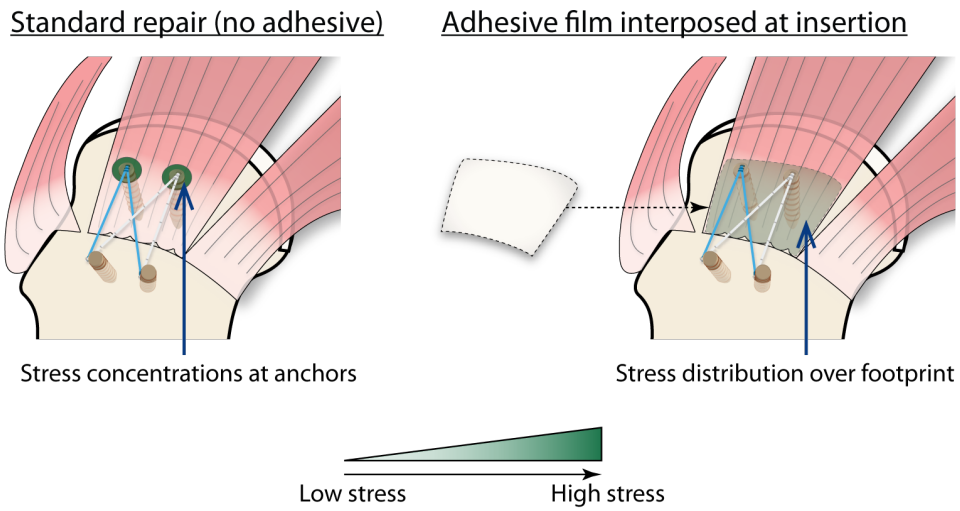

Figure 3.1: A double-row suture anchor technique is shown for repairing human supraspinatus tendon avulsions [124]. Green shading indicates location and magnitude of load transfer. (A) Current repair techniques generate stress concentrations at anchor points where the sutures from bone anchors puncture through the tendon, correlating with tissue failure at those points [255]. (B) Adhesive films interposed between the tendon and bone could distribute load transfer over the entire insertion footprint, similar to native tissue, thereby reducing peak stresses and improving overall repair construct mechanics.

physiologically during non-traumatic activities. We therefore aim to generate functional repairs that are capable of sustaining activities of daily living and enhanced rehabilitation protocols.

Following a similar approach to Chapter 2 [256], we employed a shear lag analysis to predict the ability of adhesive interlayers to improve load transfer across a repaired tendon-to-bone enthesis. We then analyzed a finite element model with the same geometric and material properties to establish the limits of the scaling law from shear lag analysis for adhesive thickness and adhesive shear modulus. Using these models, we identified desirable adhesive mechanical properties for use in adhesive films for tendon-to-bone repair. We then biomechanically tested adhesives between tendon and bone planks and in human cadaver rotator cuff repairs to validate the models and assess adhesives' potential for clinical usefulness.

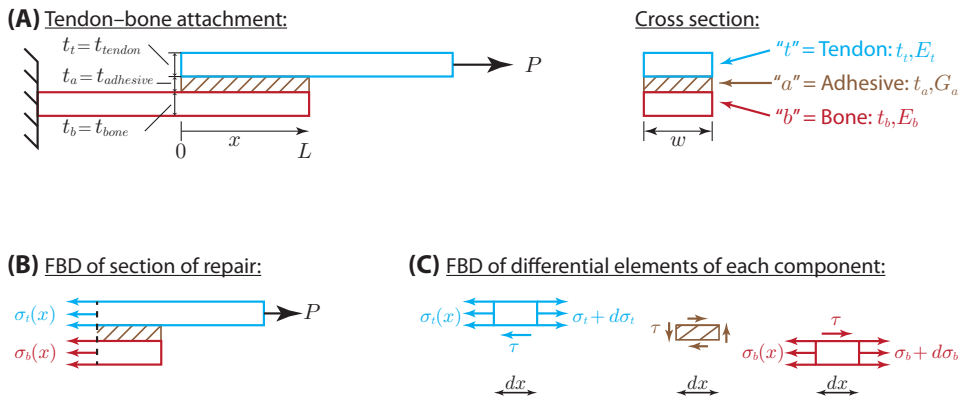

Figure 3.2: Diagram of an idealized tendon-to-bone insertion site, repaired with an interposed adhesive layer (A). Simultaneously analyzing the free body diagrams (FBD) of a section of the repair (B) and each component independently (i.e., tendon, adhesive, and bone; C) allows derivation of a shear lag model to estimate shear stress within the adhesive. Note that this model reduces to a one-dimensional set of equations along the x-axis.

3.3 Theory

3.3.1 Shear lag model

As in Chapter 2 [256], a shear lag model was studied to (i) identify adhesives with desirable properties for tendon-to-bone repair, and (ii) anticipate load transfer in idealized experiments to assess adhesive properties. The model predicted load sharing across an idealized tendon-to-bone insertion site using an interposed adhesive layer at the interface. The idealized repaired tendon and bone were both modeled as isotropic, homogenous tissue planks for this one-dimensional model.

The model, following Volkersen [264] and Cox [265], is based on the free body diagram in Figure 3.2 and the following assumptions: (i) the tendon, adhesive, and bone are linear elastic materials, (ii) viscous effects are negligible, and (iii) thickness-axis displacements, strains, and stresses are small. The latter assumption is appropriate for thin adhesive layers. These results are also corroborated by two-dimensional finite element modeling with different assumptions, as described in the following section (3.3.2 Finite element model). While adhesives and tissues often exhibit nonlinearity and viscoelasticity [76, 307, 309], the linear analysis is adequate and useful for order-of-magnitude stress estimates, and for the target design range in which the adhesive is not close to failure.

As derived by Volkersen [264] directly from equilibrium, constitutive, and strain-displacement equations for the components (i.e., tendon, adhesive, and bone, Figure 3.2C), the differential equation governing the normal stress in the

Geometric properties		SLA	FEM	Plank tests	Human
L	adhesive lap length i.e., supraspinatus tendon insertion size (medial-lateral)	13 mm	13 mm	10 mm	13 mm
$L_{b,free}$	free length of bone plank before grip	—	26 mm	5 mm	—
$L_{t,free}$	free length of tendon plank before grip	—	26 mm	25 mm	—
w	lap width i.e., supraspinatus tendon insertion size (anterior-posterior)	∞	∞	15 mm	20 mm
t_t	tendon thickness	2 mm	2 mm	3.2 mm	2 mm
t_a	adhesive thickness	[1 nm – 1 cm]	[1 µm – 1 cm]	$\approx$ 0.5 mm	$\approx$ 0.5 mm
t_b	bone cortical shell thickness	7.5 mm	7.5 mm	7.5 mm	7.5 mm
Mechanical properties					
P	force applied to tendon to model shear and normal stresses	50 N	50 N	*to failure*	—
E_t	tendon elastic modulus	$2 \cdot 10^8$ Pa	$2 \cdot 10^8$ Pa	—	—
E_b	bone elastic modulus	$2 \cdot 10^{10}$ Pa	$2 \cdot 10^{10}$ Pa	—	—
G_a	adhesive shear modulus	[10^3 – 10^{11} Pa]	[10^4 – 10^{11} Pa]	—	—
E_a	adhesive elastic modulus	—	$2G_a(1+\nu_a)$	—	—
ν_t	tendon Poisson's ratio	—	0.2	—	—
ν_a	adhesive Poisson's ratio	—	0.49	—	—
ν_b	bone Poisson's ratio	—	0.3	—	—
τ_{fail}	adhesive shear ultimate strength	[10^3 – 10^{10} Pa]	—	—	—

Table 3.2: Property values used throughout modeling and testing for shear lag analysis (SLA), finite element modeling (FEM), idealized tendon-to-bone plank tests, and human cadaver supraspinatus repair tests. Model geometry was chosen to replicate human rotator cuff supraspinatus anatomy as closely as possible [310]. Tendon and bone elastic modulus and Poisson's ratio were based on literature values [311, 312, 313].

tendon at position x is:

$$\frac{d^2\bar{\sigma}_t(x)}{dx^2} - \beta^2\bar{\sigma}_t(x) + \frac{\beta^2}{\chi} = 0 \tag{3.1}$$

where $\bar{\sigma}_t(x)$ is the dimensionless axial stress in the tendon, normalized by the stress P/wt_t at $x = L$, and χ and the characteristic (inverse) length scale β relate to the geometry and material properties:

$$\chi = \frac{E_b t_b}{E_t t_t} + 1 \qquad = \frac{1}{E_t^* t_t^*} + 1 \tag{3.2}$$

$$\beta^2 = \frac{G_a}{t_a}\left(\frac{1}{E_t t_t} + \frac{1}{E_b t_b}\right) \qquad = \frac{1}{t_b^2}\frac{G_a^*}{t_a^*}\left(\frac{1}{E_t^* t_t^*} + 1\right) \tag{3.3}$$

where E_t^* and G_a^* are, respectively, the Young's modulus of tendon and the shear modulus of adhesive normalized by the Young's modulus of bone E_b; t_t^* and t_a^* are, respectively, the thickness of the tendon and the thickness of the adhesive normalized by the thickness of the bone cortical layer t_b; and w is the width of the attachment. Solving and applying the boundary condition $\bar{\sigma}_t(0) = 0$ at the distal end of the insertion footprint and $\bar{\sigma}_t(L) = 1$ at the proximal end of the insertion footprint yields (Figure 3.4):

$$\bar{\sigma}_t(x) = \frac{1 - \cosh(\beta x)}{\chi} + \frac{\sinh(\beta x)}{\sinh(\beta L)}\left(1 + \frac{\cosh(\beta L) - 1}{\chi}\right) \tag{3.4}$$

Combining Equation 3.4 with the equilibrium equation for an infinitesimal segment of tendon, $\frac{d\bar{\sigma}_t}{dx} = \frac{\tau(x)}{P/w}$, yields a prediction for the shear stress distribution $\tau(x)$, normalized by the average shear stress $\tau_{ave} = \frac{P}{wL}$, as predicted by Volkersen:

$$\frac{\tau(x)}{\tau_{ave}} = \frac{\beta L}{\chi \sinh(\beta L)} \left[\cosh(\beta(L-x)) + (\chi - 1)\cosh(\beta x)\right] \tag{3.5}$$

This shear lag model predicts that shear stress is highest at the edges of the lap joint, i.e., at positions $x = 0$ and $x = L$, and that shear stress decreases exponentially toward more central positions (Figure 3.5). Note that as previously demonstrated for lap joints (e.g. [290]), parametric analysis of Equation 3.5 confirmed that peak stress is minimized if the adherends (tendon and bone) are "balanced" so that $E_t^* = (t_t^*)^{-1}$ (Figure 3.5). However, this is not possible for the attachment of tendon to bone. Indeed, the material mismatch at a tendon-to-bone attachment leads to stress concentrations and makes surgical repair particularly challenging.

For the geometric and material properties of a tendon-to-bone repair (Table 3.2), the peak shear stress occurs at position $x = L$ (Figure 3.5), with stress concentration factor τ_{SCF} (Figure 3.6):

$$\tau_{SCF} = \left.\frac{\tau}{\tau_{ave}}\right|_{x=L} = \frac{\beta L}{\chi \sinh(\beta L)} \left[1 + (\chi - 1)\cosh(\beta L)\right] \tag{3.6}$$

Equating the peak shear stress (at position $x = L$) to the failure shear stress value, τ_{fail}, yields the maximum load transferred across the joint via the adhesive:

$$\left(\frac{P_{max}}{w}\right) = \tau_{fail} L \frac{\sinh(\beta L)}{\beta L} \left[\frac{\chi}{(\chi - 1)\cosh(\beta L) + 1}\right] \tag{3.7}$$

This scaling law for maximum load transfer enabled prediction of desirable adhesive mechanical properties for surgical use in tendon-to-bone repairs (Figure 3.7). The shear lag model theory herein is applicable to tendon- or ligament-to-bone repairs generally, by simply updating the properties in (Table 3.2) according to the soft tissue-to-bone insertion site of interest. Note that τ_{fail} could be limited by failure (i) within the adhesive bulk, (ii) at the interfaces with adherends (i.e., the junction with the tendon or bone), or (iii) within the adherends themselves. This solution is nearly bilinear, with two asymptotes (Figure 3.7):

$$\lim_{L\to\infty}\left(\frac{P_{max}}{w}\right) = \tau_{fail}\frac{\chi}{\beta(\chi-1)} \qquad = \tau_{fail} t_b \left[\frac{E_t^* t_t^* t_a^*}{G_a^*}\left(1 + E_t^* t_t^*\right)\right]^{\frac{1}{2}} \tag{3.8}$$

$$\lim_{G_a\to 0}\left(\frac{P_{max}}{w}\right) = \lim_{\beta\to 0}\left(\frac{P_{max}}{w}\right) \qquad = \tau_{fail} L \tag{3.9}$$

For a given tendon-to-bone repair, the first limit ($L \to \infty$) shows that the force the repair can carry increases monotonically with decreasing adhesive shear modulus G_a^*. Below a critical adhesive shear modulus, however, the second limit ($G_a \to 0$) shows that a cut-off exists that depends on the length of the tendon-to-bone interface L. The intersection between the two asymptotes defines a critical interface length (Equation S1, Figure 3.S1).

3.3.2 Finite element model

To establish the limits of the scaling law described in the previous section (3.3.1 Shear lag model), we evaluated a two-dimensional finite element model in the commercial package COMSOL Multiphysics (COMSOL, Inc., Burlington, MA USA). This finite element model was developed by Mr. Mikhail Golman, M.S., using the same geometric and material properties as the shear lag model and evaluated with a range of adhesive thicknesses and shear moduli (Table 3.2, Figure 3.S2). The tendon, adhesive, and bone were modeled as linear elastic materials for direct comparison to the shear lag model. The adhesive layer was discretized into 8,000 triangular finite elements sized from 1 – 50 μm. The interfaces between adhesive and tendon or bone were modeled as perfectly fused unions, with the same mesh nodes in each section. Far from the adhesive joint, the bone was held fixed from movement or rotation in the x or y directions. The tendon boundary was constrained to stay vertical and loaded in the x direction with a 50 N force to simulate muscular contraction (Table 3.2, Figure 3.S2).

3.4 Materials and Methods

3.4.1 Idealized ex vivo repairs

Lap shear tests are a standard method to determine adhesive mechanical properties for engineering applications; however, the applications described herein (Chapter 2 and Chapter 3) require binding to biological tissues instead of metal or plastic adherends. To evaluate how the performance of the adhesive system depends upon the adhesive strength between the adherends and the stiffness of the adhesive material, a modified lap shear test was developed. A series of idealized tendon-to-bone plank repairs was performed using 1/8" thick bovine deep digital flexor tendon planks adhered to 1/4" thick bovine femur cortical bone planks (both planks were 15 mm wide, with 10 mm overlap length; Table 3.2). Fresh-frozen bovine deep digital flexor tendons (age 14-30 months; Animal Technologies, Tyler, TX) were leveled into planks while embedded in Tissue-Plus optimum cutting temperature compound (OCT, Fisher HealthCare,

Waltham, MA) using a freezing stage (BFS-30MP, Physitemp, Clifton, NJ) sledge microtome (Leica 1400, Buffalo Grove, IL) to plane both sides to a uniform, desired thickness, similar to previously described methods [314]. The desired thickness was measured using a sacrificial layer of polytetrafluoroethylene (PFTE, commonly called "Teflon", McMaster-Carr, Elmhurst, IL) on the microtome alongside the tendon samples. After being leveled into planks, samples were frozen in PBS-soaked gauze and stored at -20 °C. Samples were thawed overnight at 4 °C and trimmed to 15 mm wide with a razor blade before use. The width was chosen based on the size of bovine deep digital flexor tendons, and to maintain a high width-to-thickness aspect ratio $\sim 5:1$. Pilot experiments performed on tendon samples planed on only one side had high variability in shear strength, likely due to variable tissue curvature, necessitating planing samples on both sides. Fresh-frozen bovine femurs obtained from a local butcher were cut into bone planks using a diamond wafer blade (IsoMet, Buehler, Lake Bluff, IL). In addition, to rapidly assess adhesive mechanical properties with relevant adherends for use in either tendon-to-bone repair or on adhesive-coated sutures, a series of idealized tendon-to-tendon plank repairs were performed using two 1/8" thick bovine deep digital flexor tendon planks but no bone planks.

Effects of adhesive stiffness: To experimentally assess the impact of varying adhesive stiffness without modifying interfacial binding strength, a series of multipartite adhesive systems was evaluated. Each multipartite adhesive consisted of a 1/16" thick bovine tendon to provide a compliant bulk, attached to the adjacent tendon and bone using 50 µL of a flexible cyanoacrylate on each interface (Loctite 4903, based on ethyl and octyl cyanoacrylate [275]; Henkel Corporation, Düsseldorf, Germany) to provide the necessary bond strength. The 1/16" thick tendon bulk was first treated with PBS containing 0 mM, 20 mM, or 100 mM tetrakis (hydroxymethyl) phosphonium chloride (THPC, Sigma Aldrich, St. Louis, MO) for 15 minutes to assess the impact of a two-fold stronger adhesive bulk material ($n = 6$ each).[1] After treatment with THPC, the 1/16" tendon bulk was washed twice in excess PBS (40 mL) on a rocker for 5 minutes before use in the multipartite adhesive system. Two tendon plank samples in this experimental series were discarded because the samples were discolored and dramatically stiffer than the other samples, likely due to dehydration and oxidation at some point during the tendon plank processing (a.k.a., "freezer burn"). There were at least $n = 5$ samples in each final group. The adherends and the 1/16" thick tendon bulk pieces were blotted dry with Kimwipes (Kimberly-Clark Professional, Roswell, GA) three times before applying cyanoacrylate. This was cured for 3 hours at room temperature under 100 kPa compressive pressure, wrapped in PBS-soaked gauze, before lap shear testing.

In addition to evaluating the multipartite adhesive directly, the elastic modulus of tendon planks treated with THPC

[1] THPC covalently crosslinks amine groups in proteins.

was determined by direct tensile testing. A series of 1/8" thick tendon planks, treated with PBS containing 0 mM, 20 mM, or 100 mM THPC for 15 minutes before two washes in PBS, was mechanically evaluated ($n = 4$ each). Two samples were discarded due to discoloration and stiffness before testing, leaving at least $n = 3$ samples per group.

Catechol-derived adhesives: Given the advances in arthroscopic surgical repairs over the last two decades, any adhesive applied to a tendon-to-bone repair will need to function in an underwater environment. In collaboration with Professor Kollbe Ahn at the University of California in Santa Barbara, we tested a series of marine mussel-mimetic, catechol-derived adhesive polymers [315] in our idealized tendon-bone and tendon-tendon plank single lap shear model. These polymers are high molecular weight and elastomeric, with catechol-derived chemical binding groups. After thawing the 1/8" thick tendon samples at 4 °C overnight, then trimming them to 15 mm wide and 60 mm long, 100 μL of high molecular weight adhesive homopolymer (no crosslinking polymer) or heteropolymer (including a crosslinking polymer for bulk shear strength upon curing) was applied to a 15 mm wide by 10 mm long tendon plank segment on each plank, all while fully submerged in PBS at pH 7.4. In a different group of samples, the polymer was applied to a wet but not submerged tendon to avoid polymer dissipation in the fluid bath during application. After waiting 30 seconds for partial gelation and phase change, the samples were pressed together under a 100 kPa compressive pressure and re-submerged in PBS, as described above. Samples were cured in PBS either overnight at 4 °C, or over 72 hours at 37 °C to induce oxidation and stronger binding, before biomechanical testing.

3.4.2 Human cadaver rotator cuff repairs

To assess the potential for adhesive application in a clinically relevant rotator cuff repair setting, paired human cadaver rotator cuff samples were dissected. Human cadaver shoulders were obtained from Anatomy Gifts Registry (Anatomic Gift Foundation, Inc., Hanover, MD). Supraspinatus tendons were dissected away from the humeral head to ensure full detachment, then tendons were repaired with an open, double-row suture bridge technique, in a paired fashion either with or without the multipartite adhesive system described above (Loctite 4903 with a 1/16" thick bovine flexor tendon plank compliant interlayer; $n = 2$ per group). Repairs were performed by Dr. William Levine, an experienced, fellowship-trained orthopaedic surgeon at Columbia University specializing in the shoulder. To assess the strength of the multipartite adhesive system without suture, the infraspinatus tendons from the same cadaver samples were dissected away from the humeral head, then adhered the tendons to their insertion sites using the same adhesive system before mechanically testing to failure. Tissue was kept hydrated using PBS-soaked gauze throughout this process, once it was dissected. After repair, the humerus and rotator cuff tendons and muscles were carefully dissected

from the scapula and surrounding tissue and stored at 4 °C overnight before biomechanical testing the following day.

3.4.3 Biomechanical testing

Idealized tendon-tendon and tendon-bone plank repairs were tested similar to previously described protocols for testing flexor tendons [287, 288, 103, 105]. After 5 cycles of triangular-ramp preconditioning to 1 mm displacement, samples were pulled in uniaxial tension using a material testing machine (5866; Instron Corp., Norwood, MA, chosen because of a high capacity load cell) at 0.3 mm/s until failure. Video of the test was recorded for optical strain tracking. Immediately prior to testing, tendons were stained with a speckle pattern of freshly prepared VerHoeff stain to provide a surface texture for optical tracking. Elongation measurements from the material testing machine were synced with optical recordings from a high resolution camera at a frame rate of 30 Hz (Google Nexus 6p, Mountain View, CA), similar to described previously [30, 256]. Optical tracking of points on the tendon and bone immediately surrounding the interface enabled accurate determination of semi-local tissue strain. This allowed for more accurate adhesive material property assessment, without confounding the viscoelastic effects or strain-energy storage of the tendon plank proximal to the interface. From the force-elongation curves, maximum force and yield force were determined. From the force-strain curves, strain at 20 N force (approximating strains at physiologically relevant load levels [289, 99]), modulus (slope of the linear portion), and resilience (area under the curve until yield) were determined.

Human cadaver rotator cuff repairs were tested with an MTS 858 Bionix (MTS Eden Prairie, MN, USA) testing system at Columbia University's Carroll Laboratory, similar to previously described methods [316]. Briefly, dissected samples were returned to room temperature and secured in black pipe with two orthogonal bolts and Rockite cement. The pipe was secured very close to the humeral head to prevent flexion. The insertion site was speckle-coated with VerHoeff stain to facilitate optical tracking. The rotator cuff muscle being tested was secured in a frozen clamp using liquid CO_2. The humerus was angled so the muscle was being pulled in line with the direction of the tendon fibers at the insertion. Supraspinatus samples (repaired with double-row suture $\pm$ adhesive) were first preconditioned with 10 haversine cycles from 1 – 25 N at 0.5 Hz, followed by a ramp to 10 N at 1 N/s and then a hold at constant load for 5 seconds. Infraspinatus samples (repaired with adhesive only) were preconditioned with 10 haversine cycles from 1 – 5 N at 0.5 Hz, followed by a ramp to 2.5 N at 1 N/s and then a hold at constant load for 5 seconds. After this preconditioning regimen, samples were pulled in uniaxial tension to failure at 0.5 mm/s with time, force, and MTS grip displacement data measured at a 20 Hz sampling rate. Video was simultaneously recorded from front and side views at 30 Hz. Optical tracking of points on the tendon and bone immediately surrounding the interface, performed

using custom MATLAB code, enabled accurate determination of semi-local tissue strain, as with idealized plank tests.

3.4.4 Biomechanics analysis

Fully automated biomechanics analysis was performed using a custom MALAB code following the algorithm given in the flow chart in Figure 3.3. Modulus, stiffness, and rigidity were calculated using random sample correlation (RANSAC) based on Ke Yan's 2011 implementation[2] to quickly find the best fitting line of sufficient bin width. Data is first trimmed to remove data before 10% of max stress and after 95% of max stress to isolate the region of interest. Two points were selected at random and a line was drawn between them, for $n = 1000$ iterations. All data points within a threshold range of 0.5% of the robust fit stress at the 80th percentile were counted as within an acceptable range of the best fit line. Of the n iterations, the iteration with the most inliers was deemed the best fit. This approach represents a "robust" fit, which minimizes the effect of outlier points on the best fit line compared to a least squared errors fit. This is confirmed by visual inspection. The "yield" point was determined as the point where the smoothed data first deviated from the RANSAC fit line by 0.1% of the expected stress.

3.4.5 Statistics

Statistical analysis for all experiments was performed by non-parametric Wilcoxon rank-sum using MATLAB, as some results were not normally distributed. Statistical significance was set at $p < 0.05$, unless otherwise noted.

[2] https://www.mathworks.com/matlabcentral/fileexchange/30809-ransac-algorithm-with-example-of%2Dfinding-homography

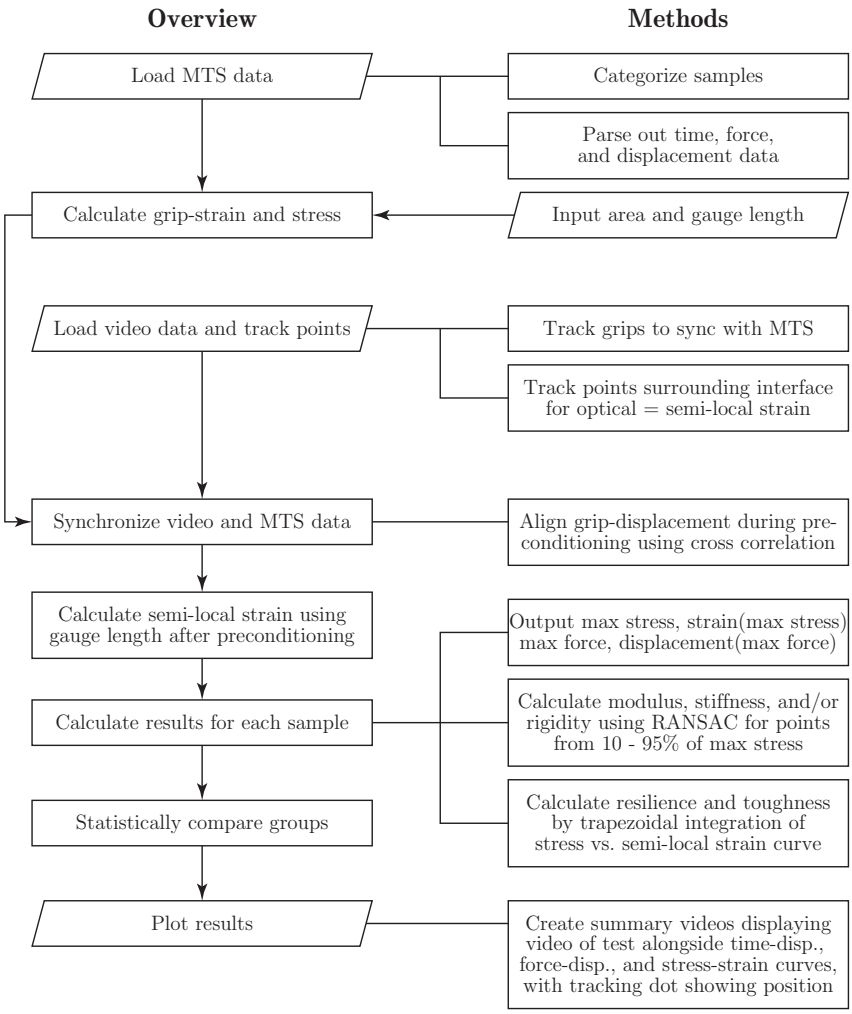

Figure 3.3: Biomechanical analysis flowchart, describing how custom MATLAB code analyzed mechanical and video data.

3.5 Results

3.5.1 Shear lag and finite element models

Shear lag and finite element modeling revealed an ideal design space for adhesive mechanical properties to improve load transfer across tendon-to-bone repairs (Figure 3.7, band inside blue dotted box, including the elastomer material class). As with adhesive-coatings on sutures (Chapter 2), mechanically desirable adhesives should be compliant in shear while maintaining high binding and shear strengths. Higher deformation of compliant adhesives facilitates load distribution over larger lengths than stiff adhesives, reducing the peak stress (Figure 3.5, 3.4). Similarly, thick

adhesives allow higher deformation than thin adhesives, reducing the shear stress concentration factor. Shear lag analysis predicted stress concentration factors of approximately $1 - 200$ for the experimentally relevant ranges of adhesive shear modulus and thickness ($G_a = 10^4 - 10^8$ Pa and $t_a = 1$ µm $- 1$ mm, respectively) (Figure 3.6). While these models assumed a 13 mm adhesive interface length based on rotator cuff anatomy, note that much shorter adhesive lengths are expected to transfer nearly the same load (Figure 3.S1).

While shear lag analyses generate simple, closed form solutions, the simplifying assumptions described in the Theory section (3.3.1 Shear lag model) lead to inaccurate stress predictions at edges ($x = 0$ and $x = L$) and in cases of stiff or thick adhesives layers. The finite element predictions of normal stress distribution in the tendon and shear stress distribution in the adhesive (Figure 3.4B and 3.5B, respectively) closely resembled the shear lag predictions for compliant adhesive layers (Figure 3.4A and 3.5A), but deviated for adhesive shear moduli greater than $\sim 10^8 - 10^9$ Pa. However, the predicted peak shear stress (i.e., at position $x = L$ for shear lag predictions, slightly in from position $x = L$ for finite element predictions) remained similar for the two models even for $G_a > 10^8$ Pa, and only substantially deviated for $G_a \geq 10^{10}$ Pa. The finite element model corroborated the shear stress concentration factor predictions from shear lag analysis for adhesives up to 1 mm thick (Figure 3.S3).

A contour map of maximum load transfer given various adhesive properties was generated from Equation 3.7 using an adhesive thickness of 0.5 mm (Figure 3.7). Properties of several real materials were then overlaid on this contour map to identify promising candidate materials. Only a small fraction of the material classes shown are relevant materials; the remainder are included for comparison as is standard with an Ashby plot, and to highlight the importance of appropriate adhesive material selection. Assuming a compliant adhesive ($G_a = 1$ MPa) with a strong shear strength ($\tau = 10$ MPa) and the average adult supraspinatus tendon insertion geometric properties (Table 3.2), maximum load transfer through would approach 3,000 N. This would result in theoretical improvements of up to ~10-fold over current methods using a double row suture anchor repair, causing repair strength to be limited by tissue strength. The maximum load transfer prediction herein uses supraspinatus tendon insertions as an example to calculate values, but it is relevant for surgical connective tissue-to-bone attachments throughout the body.

3.5.2 Ex vivo experiments

Biomechanical tests of idealized tendon-to-bone planks in lap shear using multipartite adhesives (comprised of 1/16" tendon plank interlayers with Loctite 4903 at interfaces) matched model predictions of maximum load (Figure 3.8). To evaluate a range of adhesive stiffnesses, the 1/16" tendon plank interlayers were first treated with 0 mM, 20 mM,

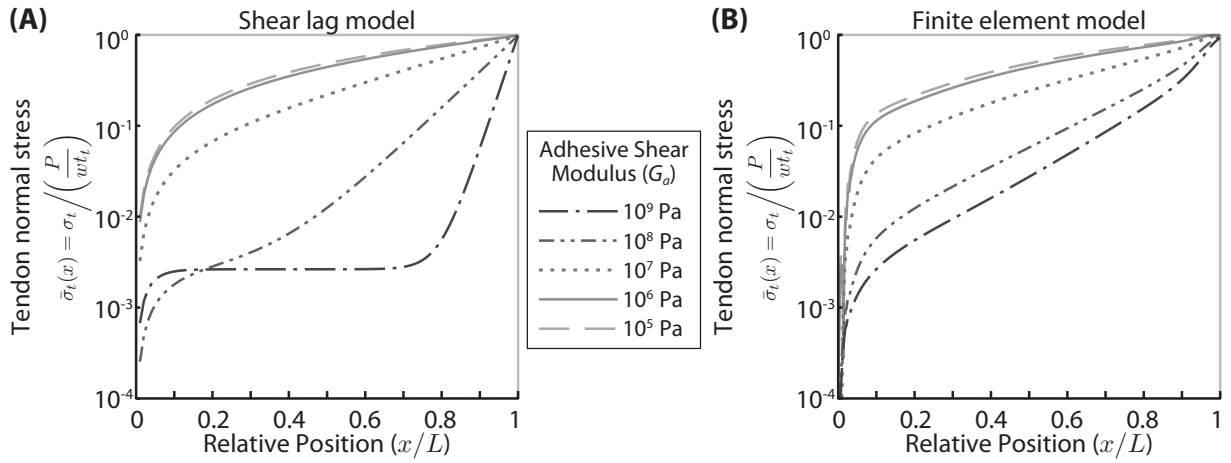

Figure 3.4: Normal stress in the tendon vs. position, normalized, as predicted by shear lag modeling (A) and finite element modeling (B) for a range of adhesive shear moduli from 100 kPa to 1 GPa. Since the finite element model is two-dimensional, the maximum normal stress through the thickness ($\bar{\sigma}_{t,xx}$) is plotted in (B)

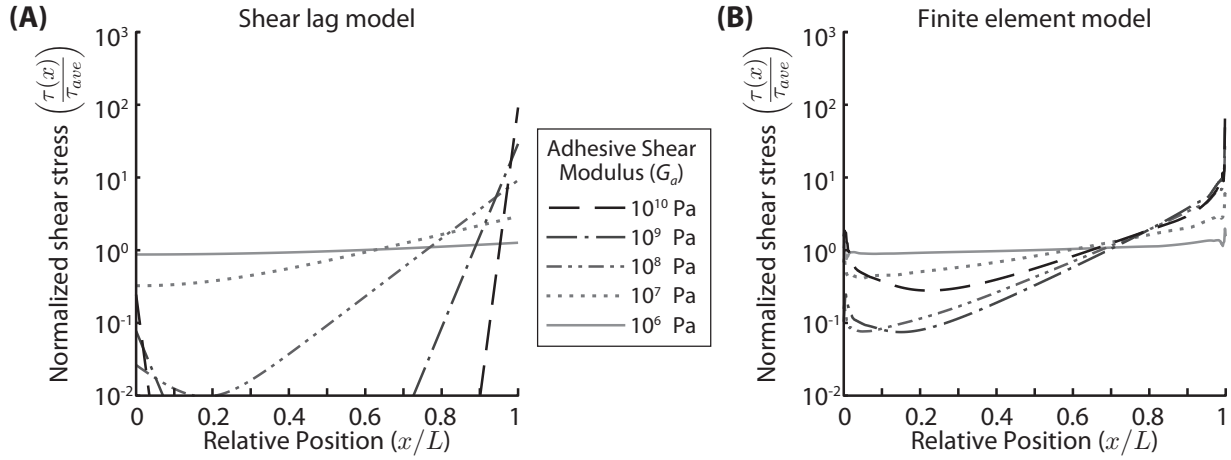

Figure 3.5: Shear stress in the adhesive vs. position, normalized, as predicted by shear lag modeling (A) and finite element modeling (B) for a range of adhesive shear moduli from 100 kPa to 1 GPa. Since the finite element model is two-dimensional, the maximum shear stress through the thickness ($\tau_{a,xy}/\tau_{ave}$) is plotted in (B).

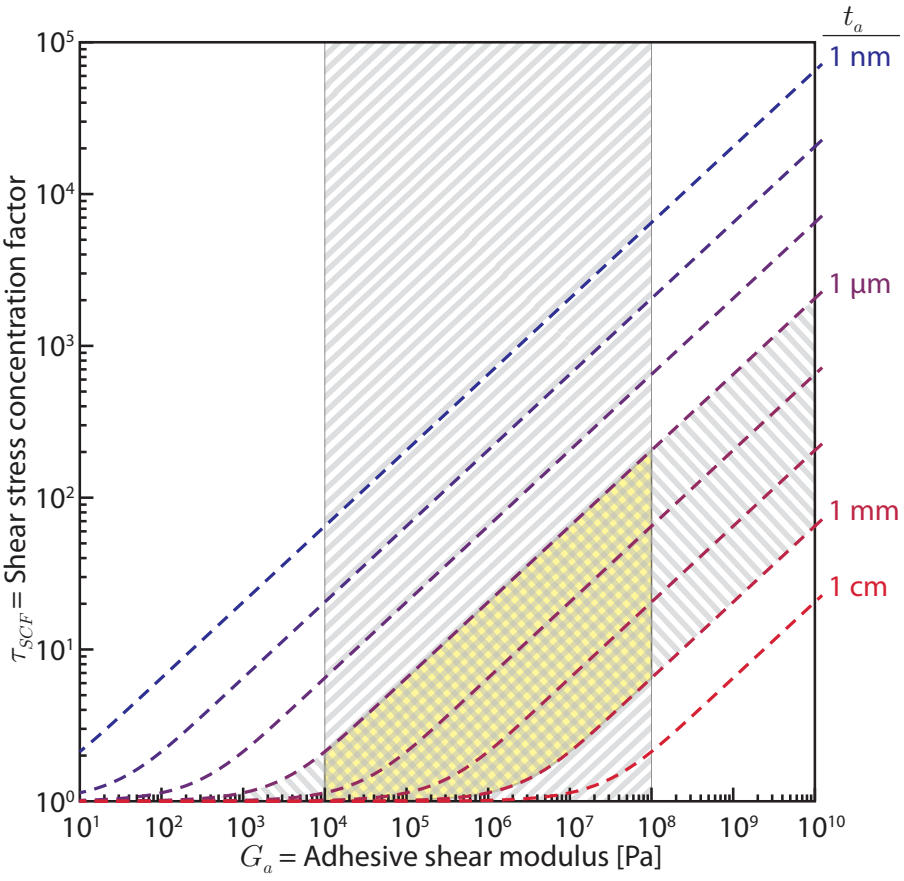

Figure 3.6: Shear lag modeling predicted the lowest stress concentration for compliant, thick adhesives. Line color represents thickness of the adhesive layer (labeled on right). Hatched, shaded regions highlight the relevant ranges of adhesive shear modulus ($G_a = 10^4 - 10^8$ Pa) and thickness ($t_a = 1$ μm $- 1$ mm), with the overlapping relevant property range highlighted in yellow. The shear lag modeling closely matched finite element modeling for adhesive thickness below 1 mm, as shown in the supplemental material (Figure 3.S3).

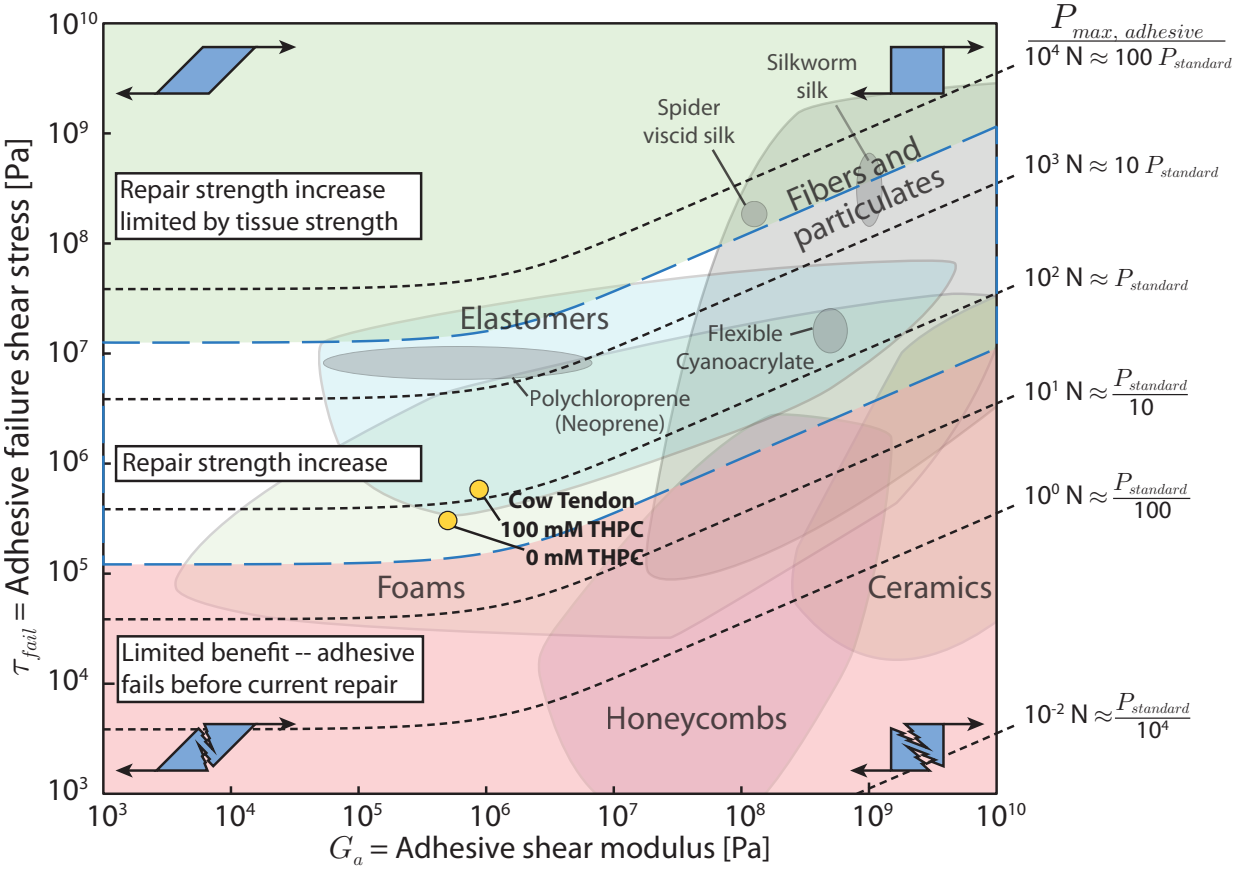

Figure 3.7: A contour map showing the design space for adhesive biomaterials for tendon-to-bone repair, using an adhesive thickness of 0.5 mm and human supraspinatus tendon attachment parameters (Table 3.2) as a representative attachment. The x-axis shows the shear modulus of the adhesive material, the y-axis shows the shear stress at which the adhesive material fails, and the contours show the total maximum force transferred across the repair site via the adhesive. $P_{standard}$ indicates the order of magnitude of strength of standard rotator cuff repairs. This domain map is overlaid with real material properties (shaded zones) to highlight promising materials for further adhesive development. The region highlighted by the blue dotted box is expected to increase rotator cuff repair strength.

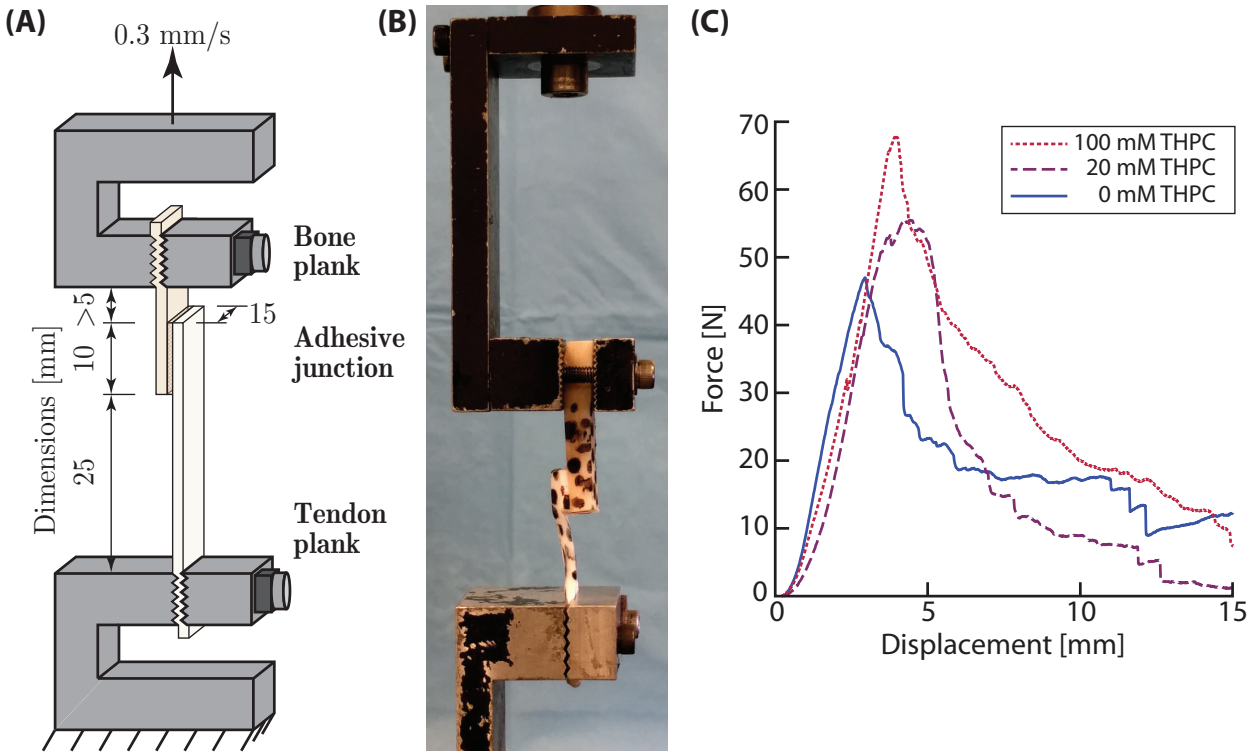

Figure 3.8: (A) Schematic and (B) picture of biomechanical testing setup for idealized single lap shear experiments using tendon and bone planks as adherends. (C) Representative force-displacement curves using multipartitite adhesives comprised of cyanoacrylate and 1/16" tendon planks treated with various concentrations of THPC.

or 100 mM THPC for 15 minutes. Elastic modulus of bovine flexor tendon planks, tested in tension, increased with THPC treatment concentration by 76% for 20 mM THPC and 112% for 100 mM THPC, as expected ($n = 4$ per group, Figure 3.9A). When applied in idealized lap shear tests, multipartite adhesive interlayers treated with 0 mM, 20 mM, and 100 mM THPC yielded maximum average shear stresses $\left(\tau_{ave} = \frac{P}{wL}\right)$ of 324 kPa ($\pm$ 61 kPa standard deviation, $n = 5$), 433 kPa ($\pm$ 132 kPa, $n = 6$), and 494 kPa ($\pm$ 90 kPa, $n = 5$, $p = 0.008$), respectively, (Figure 3.9C). This represented a 52% higher failure shear stress and 88% higher yield shear stress ($p = 0.064$, Figure 3.9D) with strengthened adhesive bulk interlayers crosslinked with 100 mM THPC, as predicted by shear lag analysis (Figure 3.7). Failure occurred within the tendon plank in all samples with THPC-crosslinked interlayers, as expected since crosslinking strengthened and stiffened the interlayer, leaving the tendon plank as the weakest point. In comparison, some samples without THPC crosslinking failed within the tendon plank while others failed in the interlayer, since the tendon plank and interlayer were approximately the same strength.

The multipartite adhesive system was further evaluated in human rotator cuff biomechanical tests to evaluate a clinically-relevant loading scenario (Figure 3.10). Cadaver infraspinatus repairs with adhesive only (no sutures) had a maximum

shear stress of 115 kPa ($\pm$ 10 kPa, $n = 4$), 35% of the strength of idealized plank tests (Figure 3.9). This equated to a maximum load of 34.5 N ($\pm$ 3.0 N), or approximately 10% of the strength of a typical rotator cuff tendon repair [132]. Finally, the multipartite adhesive system was assessed in clinical-style human cadaver supraspinatus tenotomy and repair to assess adhesive strength contributions in parallel to a suture repair. Pilot studies in cadaver human supraspinatus tendons, repaired with double-row suture bridge and multipartite adhesive between the supraspinatus tendon and humeral head, yielded approximately 40 – 50 N stronger repairs than paired contralateral control repairs (Figure 3.S4, 3.S5, 3.S6, and 3.S7). This estimated load improvement is similar to loads carried by infraspinatus tendons adhered without suture, indicating that the adhesive had an additive effect on the strength of the double-row suture bridge repair.

After validating the shear lag model in idealized and clinically-relevant *ex vivo* experimental scenarios with various stiffnesses of multipartite adhesives, we explored novel adhesives with the potential for clinical application. A series of idealized tendon-to-tendon plank lap shear tests was performed using catechol-derived adhesive polymers binding in a hydrated environment (PBS) to assess the adhesive's capacity for arthroscopic use. While homopolymer samples (no crosslinker) and heteropolymer samples (containing crosslinker) that were evaluated without oxidation did not carry meaningful load (0.0 – 1.5 N), heteropolymer samples that were allowed to oxidize by remaining at 37 °C for 72 hours had several fold higher failure load (4, 6, 18 N), approaching levels that would be clinically meaningful.

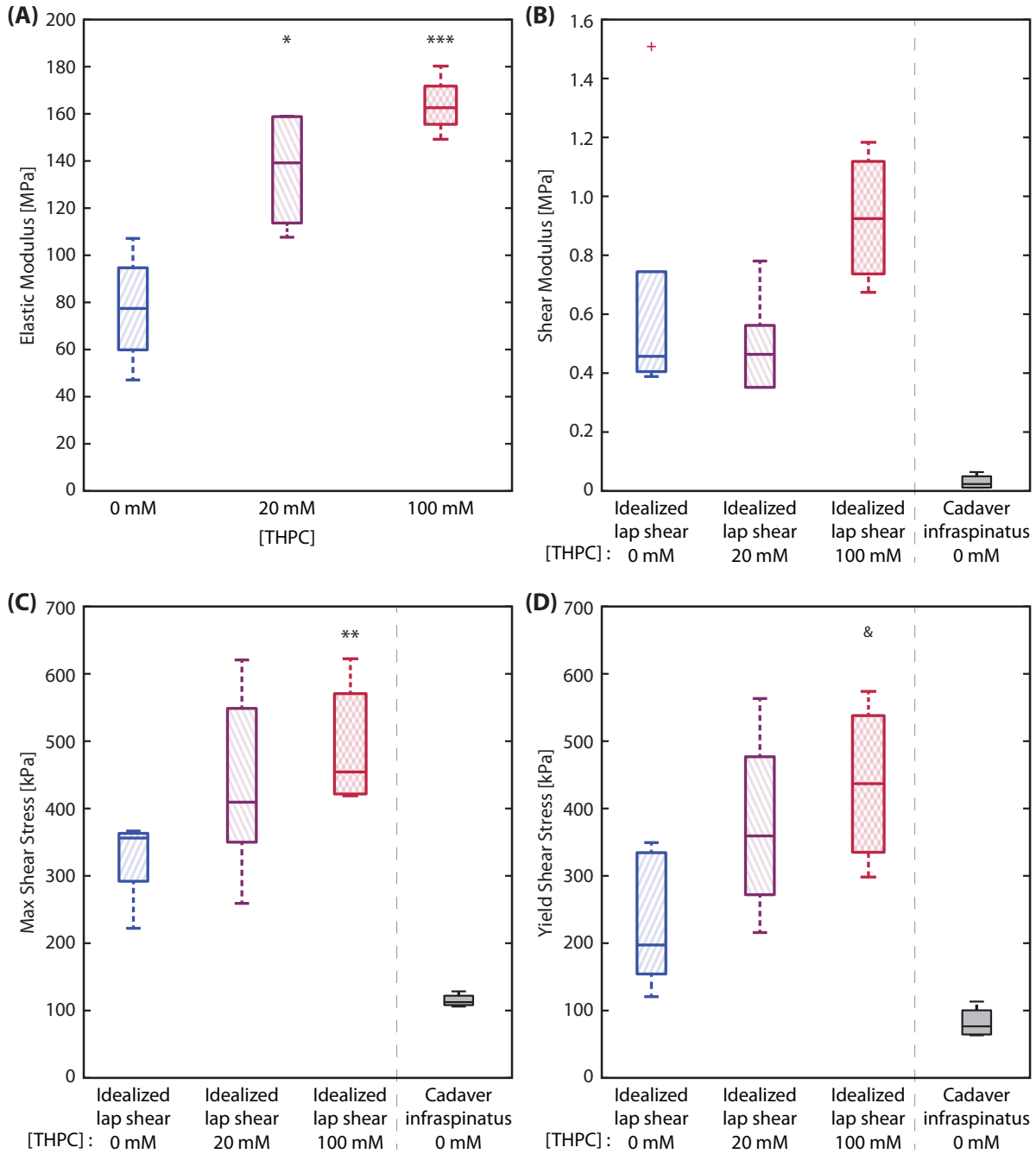

Figure 3.9: (A) Elastic modulus of 1/8" thick THPC treated tendon planks tested in tension (no adhesive or repair). (B) shear modulus, (C) Maximum shear stress, and (D) yield shear stress (τ_{ave}) of multipartite adhesive evaluated in idealized lap shear tests and cadaver infraspinatus tendon insertion repairs. Stronger adhesive materials (100 mM THPC-crosslinked) failed at 52% greater average shear stress. The middle line within the box plots represents the median, the outer edges denote the 25 percentile and 75 percentile samples, and the whiskers extend to the extreme data points. Outliers are denoted by (+). Asterisks denote statistically significant differences compared to idealized lap shear tests for 0 mM THPC group (* $p < 0.05$, ** $p < 0.01$, *** $p < 0.001$, $^{\&}$ $p = 0.064$).

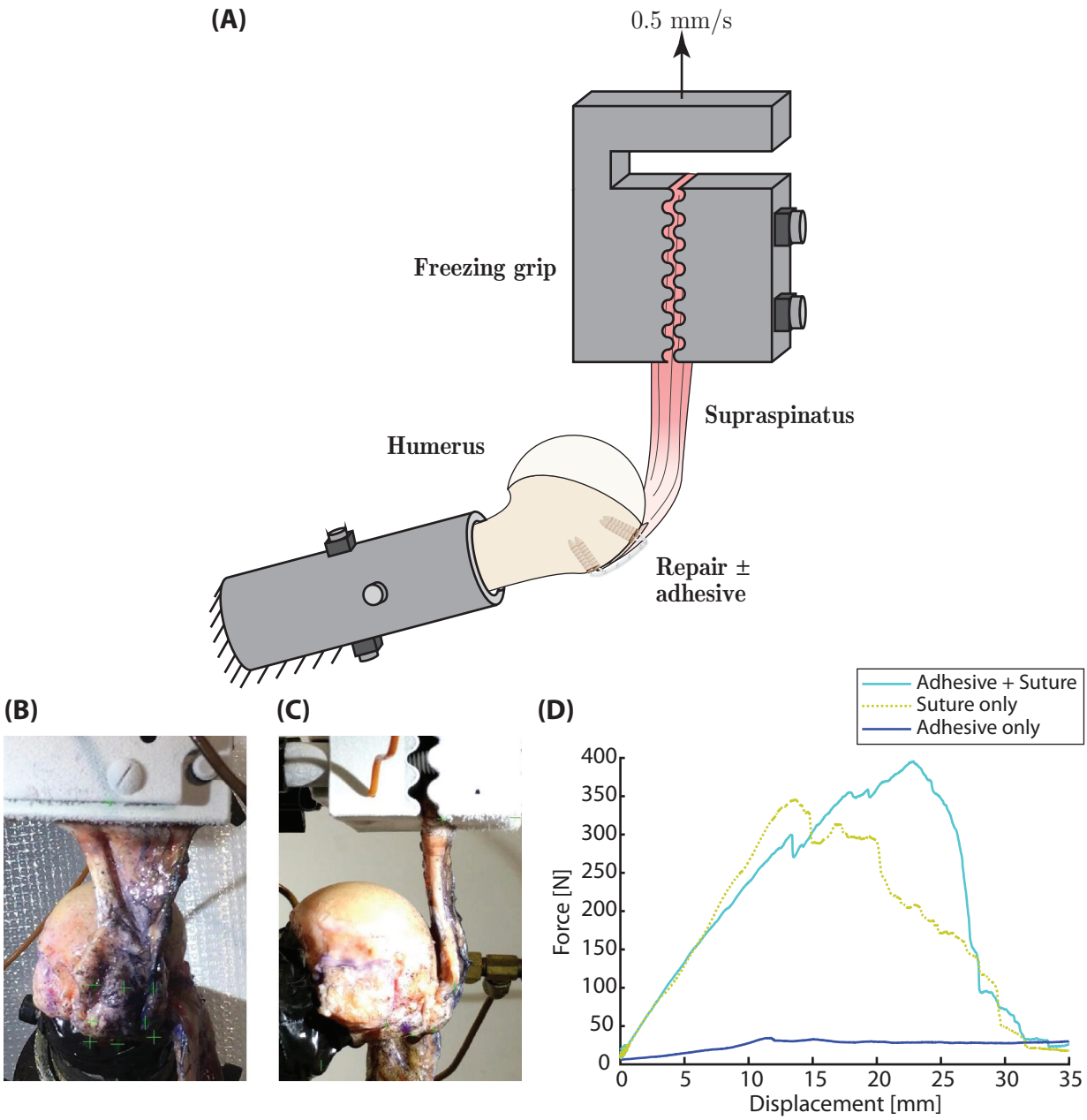

Figure 3.10: Human cadaver rotator cuff tendons were repaired to the humeral head with adhesive only (infraspinatus), double-row suture only, or adhesive and suture (supraspinatus). (A) Schematic drawing of biomechanical testing setup for clinically relevant repairs. (B) Front view and (C) side view pictures of biomechanical tests. (D) Representative force-displacement curves for biomechicanical tests of cadaver supraspinatus repairs with and without adhesive, and for infraspinatus repairs with adhesive only.

3.6 Discussion

Current operative techniques for rotator cuff tendon repair rely on load transfer across only a few points where suture anchors into bone (Figure 3.1). Variations on this approach have reached a limit for mechanical fixation, where increased numbers of strands or anchor points do not lead to improved outcomes (e.g., most studies have shown that single-row repairs and double-row repairs are equivalent clinically [317]). Recent research has instead focused on biological augmentation to facilitate improved tendon-to-bone healing instead of fibrovascular scar tissue [318], but mechanical fixation remains inadequate for holding the tissues together long enough for healing to occur. We hypothesized that, similar to adhesive-coatings on sutures for tendon repair (Chapter 2), tendon-to-bone repair mechanics could be enhanced through better load distribution across the repair site, using an adhesive biomaterial that is simultaneously strong and compliant in shear. Modeling and *ex vivo* experimental results demonstrated that an adhesive interposed between tendon and its bony footprint has the potential to dramatically improve the strength of tendon-to-bone repairs using feasible adhesive material properties. This increase in strength, combined with anticipated decreases in interfacial micro-motion from the use of an adhesive, should improve tendon-to-bone healing.

The shear lag model indicated that mechanically desirable adhesives would be of millimeter-scale thickness and compliant in shear while maintaining high binding and shear strengths. This combination of properties minimizes stress concentration and maximizes load transfer across the repair (Figure 3.6 yellow shaded region, and Figure 3.7 green shaded region). Compliant, thick adhesives allow greater deformation, thereby distributing loads over a larger length than stiff, thin adhesives (Figure 3.4, 3.5). This is analogous to a native, fibrocartilaginous tendon enthesis, where a compliant zone optimizes stress concentrations and toughens the interface [76, 77, 78, 79]. The derived load transfer isoclines, based on rotator cuff geometric and material properties (Table 3.2), indicate that adhesives with a wide range of theoretical material properties are expected to improve repair strength. When these isoclines are overlaid on real material properties, as in a standard Ashby plot [292, 291, 293], the model highlights materials with the appropriate properties to improve repair strength (Figure 3.7, region in blue dotted box). Due to the relatively large surface area compared to adhesive-coated sutures (Figure 2.4 on page 34), adhesive films would generate meaningful repair strength improvements using a much broader range of adhesive mechanical properties. For example, the entire class of elastomeric materials have appropriate mechanical properties to improve repair strength. Therefore, we are exploring biocompatible, adhesive elastomeric materials as potential bio-adhesives to improve repair strength. Optimal adhesive materials are expected to improve load transfer by over 3,000 N, or 10-fold the strength of current repair techniques (Figure 3.7). While this provides a large theoretical opportunity, an improvement of even 100 N (i.e., 22.5% of the strength of double-row suture bridge repairs) that reduces local stress concentrations would provide a clinically

meaningful improvement to surgical repairs [319, 320].

The shear lag model used here is one-dimensional, with several limiting assumptions (detailed in the Theory section, 3.3.1 Shear lag model) that lead to errors predicting stress distribution around edges and for stiff, thick adhesives on the same thickness order of magnitude as the adherends [266]. Therefore, we employed a finite element model that confirmed that the shear lag model was inaccurate for thick adhesives ($t_a > 1$ cm) and stiff adhesives ($G_a >$ approximately 1 GPa; Figure 3.S3). This finite element modeling corroborated the shear lag predictions for adhesives in the desirable range, i.e., compliant, strong adhesives with millimeter-scale or lower thickness. To further refine modeling predictions, future models could incorporate (i) non-linear elastic material assumptions and (ii) cohesion within the adhesive instead of assuming catastrophic failure [321, 322], especially to predict sensitivity to flaws in the adhesive material. Nevertheless, the current model provides sufficient predictions of load transfer to guide adhesive material development.[3]

In order to evaluate adhesive properties with relevant adherends and assess adhesive usefulness for tendon-to-bone repair, we developed a new method for lap shear testing using tendon and bone planks (Figure 3.8). Tendon plank were fabricated using a sliding microtome to create highly uniform, geometrically standardized planks. Similarly, bone planks were manufactured using a diamond blade to create precisely-sized samples. This protocol enabled rapid testing of adhesive properties via lap shear with relevant adherends for clinical application. However, note that the failure shear strength, τ_{fail}, used in the shear lag model can be limited by: (i) the bulk adhesive strength (cohesion), (ii) the interfacial binding strength to the surrounding tissue, and/or (iii) the ability of the surrounding tissue to accommodate load transfer (e.g., through distributing shear stress among tendon fibers). Since the adherends are relevant to the repair setting, the failure shear stress measured in these lap shear experiments is reflective of the failure shear stress of the adhesive.[4]

Proof-of-concept experiments demonstrated substantial improvements in load transfer for multipartite cyanoacrylate adhesives in idealized tendon-to-bone plank tests and human cadaver rotator cuff repairs. Off-the-shelf cyanoacrylate adhesives (Loctite 4903) are far more stiff than the ideal predicted by the shear lag model. Therefore, we used a

[3]The shear lag model employed herein is one-dimensional and ignores loads that are not directly in line with the tendon (considered isotropic, linear elastic herein). This is a major simplification of the rotator cuff, where the high degrees of freedom during rotation and other movements would apply multi-dimensional load to the supraspinatus attachment. However, (i) the majority of that load will be carried by other muscles and ligaments and (ii) the adhesive and repair are able to withstand some load in off-axis directions.

[4]The shear strength used in the shear lag modeling to predict load tolerance was the failure shear stress τ_{fail} at the local, material level. The shear stress measured in idealized plank tests was averaged over the interface (τ_{ave}). The optical tracking performed in the experiments used semi-local strain determination, which is more relevant than grip-to-grip strain measurements since it does not include the strain-energy stored in tissues outside the repair site. However, this analysis did not include a local strain assessment to determine the peak shear stress within the adhesive layer. Such local assessments have been effectively used for tracking strains and detecting cracks forming in biological tissues [323]; however, they are difficult to measure in thin adhesive layers due to insufficient number of pixels. Regardless, they are largely unnecessary for determining adhesive efficacy.

multipartite adhesive comprised of an interlayer (1/16" plank of bovine flexor tendon) adhered to tendon and bone using Loctite 4903 to assess a more relevant adhesive shear modulus range. The 324 kPa $\pm$ 61 kPa failure shear stress found experimentally in idealized plank tests (Figure 3.9A), equating to a 84.3 N $\pm$ 15.8 N failure load over a 2.6 cm^2 supraspinatus insertion footprint, closely matched the predicted maximum load from the shear lag model (Figure 3.7, yellow circle). Furthermore, when the tendon plank interlayer was stiffened and strengthened by crosslinking with 100 mM THPC for 15 minutes, the experimental results (494 kPa $\pm$ 90 kPa, equating to 128.5 N $\pm$ 23.4 N) again closely matched the theoretical predictions. Thus, based on idealized plank tests, even the fairly stiff, off-the-shelf cyanoacrylate-based adhesives carry enough load to improve repair strength by approximately 25 – 40% over a 2.6 cm^2 supraspinatus repair footprint, when used in conjunction with current repair techniques [132]. That 25 – 40% increase in load tolerance could substantially decrease repair rupture risk during activities of daily living, thereby facilitating improved healing.

In human cadaver rotator cuff experiments using the infraspinatus tendon, the load transferred by the adhesive was 115 kPa $\pm$ 10 kPa (Figure 3.9), equating to 34.5 N $\pm$ 3.0 N, or 35% of the anticipated load from idealized plank tests. It is likely that the human rotator cuff tenotomy and adhesion experiments demonstrated lower strength than the idealized plank tests due to the irregular, curved bony surface causing microscopic stress concentrations and the non-idealized adhesive application and testing conditions. Furthermore, the adhesive only cured for approximately 2 hours in the cadaver experiments, compared to overnight in the idealized plank tests, which may have further limited strength. The cadaver supraspinatus repairs with and without adhesive demonstrated approximate repair strength increases commensurate with the expected additive improvement based on load transferred in the adhesive-only repairs (Figure 3.10). This analysis was complicated by surgical issues with bone anchor placement in two of the four supraspinatus repairs (one adhesive and one control shoulder repair, from different pairs). Repeat suture anchor placement led to weaker attachments, with failure in one case by the anchor pulling out of the bone instead of the tendon or suture breaking. Comparing the control repairs from different samples, the sample without any surgical issues failed at 344 N (Sample 2 right, Figure 3.S6) while the sample with surgical issues failed at 308 N, or 36 N less (Sample 1 left, Figure 3.S4). The adhesive sample without any surgical issues failed at 394 N (Sample 1 right, Figure 3.S5), while the adhesive sample with surgical anchor issues failed at 348 N (Sample 2 left, Figure 3.S7). This data suggests that the adhesive treatment improved repair strength by approximately 40 – 50 N, indicating that adhesives provide additive strength improvement over the current suture repairs based on predictions from the infraspinatus adhesive-only experiments. Especially given the experimental issues with suture anchor placement, a more thorough assessment with more samples and without suture anchor failures is necessary to evaluate the adhesive's impact at the rotator cuff.

Taken as a whole, the multipartite adhesive experiments with and without THPC treatment provide evidence that (i) the shear lag model accurately predicted load transfer across tendon-to-bone for a relevant range of adhesive shear moduli (100 kPa - 1 MPa, Figure 3.9C), and (ii) clinical style repairs demonstrate approximately one-third of the additive load tolerance improvement expected based on the shear lag model and idealized tests. Even this sub-optimal multipartite adhesive material enabled load tolerance increases on the necessary order to improve rotator cuff repair outcomes. Optimal adhesive materials are expected to increase load transfer by approximately 10-fold compared to current repairs.

It is interesting to note that the proposed combination of a compliant, strong adhesive layer with a suture repair resembles bonded-bolted joints in composite structures that have been considered in engineering since 1985 [324]. Kelly conducted and experimentally validated a three-dimensional finite element analysis, which concluded that bonded-bolted joints with a thick, low-modulus adhesive layer effectively distribute load transfer between the adhesive and the bolts [325]. High-modulus adhesives provided a stiffer load path and thus transferred the majority of the load, minimizing the value of the bolts and making the joint more susceptible to crack propagation [325]. Thus, previous studies of bonded-bolted joints and the shear lag model employed here both indicate that compliant, strong adhesives are desirable. The strength of bonded-bolted joints exceeded that of bonded or bolted counterparts by 52% and 127% in experimental assessments, respectively [326]. The combination of adhesive bonds and bolts increases joint strength while minimizing peeling stresses and fracture cracks [327].

The mechanical models and experiments here provide the theoretical underpinnings of a previous study showing that a biological adhesive secreted by the Australian frog *Notaden bennetti* increased the strength of cadaver sheep infraspinatus repairs by approximately 70 – 80 N, or 2-fold, over a 16.4 $\pm$ 0.2 mm by 13.2 $\pm$ 0.1 mm infraspinatus insertion site [328]. Indeed, this robust improvement follows the same mechanical principals outlined here: the protein-based frog adhesive is elastic ($G_a = 402 \pm 7$ kPa) with approximately 65% of the adhesive strength of cyanoacrylate and a high shear strength ($\tau_{fail} = 1.7$ MPa between wood adherends) [329, 330]. The adhesive set in approximately 30 – 60 seconds and could work while hydrated [328]. While this frog-secreted adhesive, secreted and immediately applied in the operating room, is not clinically applicable in its current form, it further provides proof-of-concept validation that adhesives that are compliant in shear and strong can substantially improve repair strength.

In addition to the adhesive mechanical properties defined here, clinically useful adhesives for many tendon-to-bone repair styles need to work in an arthroscopic setting (underwater environment). Therefore, a series of elastomeric polymers with marine mussel-derived, catechol-based binding domains were evaluated. These adhesives were adhered to tissues when fully submerged in PBS to activate catechol binding chemistry and to mimic the arthroscopic environ-

ment. As expected, homopolymer adhesives (i.e., no crosslinker to stabilize cohesive strength of the polymer) did not carry clinically relevant loads in the idealized plank tests. Heteropolymer adhesives that were allowed to oxidize and crosslink carried 4-18 N of load. This is on the same order of magnitude as the cyanoacrylate-based multipartite adhesive tests, but with a much more clinically applicable adhesive. Further studies are needed to assess catechol-derived and other elastomeric bio-adhesives using the simple, standardized lap shear testing protocol described herein to hone adhesive binding and crosslinking chemistries for clinical application.

Translating this theoretical and experimental foundation into a clinically useful adhesive for tendon-to-bone repair will require co-optimization of several properties, including the adhesive mechanical properties defined here, biocompatibility, degradation *in vivo*, adhesive curing in a hydrated environment, and production cost [331]. While this study applies particularly to the time of repair and does not consider the healing process, results from many studies in orthopedic repair indicate that time zero strength properties correlate with long-term repair outcomes, e.g., [319, 320]. Ideal adhesives could either be biologically inert or guide the healing response as with a tissue engineering approach [332]: the same biomechanical design principles apply to minimizing stress concentrations for tissue engineered biomaterials at interfaces between soft and hard tissues. Current adhesive approaches to orthopedic repair primarily use bone cements (e.g., [333]), cyanoacrylate- [334, 335, 336, 337, 338] or methacrylate-based chemistries [339, 340, 341, 342], which may be appropriate for fracture repair but are significantly more stiff than desirable for tendon-to-bone repair. Furthermore, biocompatibility is limited unless all free acrylate moieties are consumed. At the other extreme, fibrin glues such as TISSELL (Baxter) form compliant clots but do not provide sufficient strength [343, 344]. Mussel-inspired, catechol-derived adhesives offer versatile, high-strength binding in hydrated environments which may be engineered into compliant, energy-dissipating, and possibly bioactive biomaterial matrices [345, 346, 347, 348, 349]. In addition to manipulating the chemical binding moiety, several recent studies of interest have incorporated carbonate, calcium phosphate, or mineral trioxide groups, as well as bone morphogenic protein 2, to enhance integration into bone [339, 350, 351, 352]. While these approaches are promising, there are no adhesives successfully used clinically for tendon-to-bone repair. We hope this work may serve to inform further bioadhesive development to maximize benefit to soft tissue-to-bone repairs.

3.7 Conclusion

Strengthening tendon-to-bone repairs is essential to enable adequate healing and functional recovery, particularly for the rotator cuff, where repair outcomes are poor. Modeling and experimental validation indicate that adhesive

films can augment current surgical approaches by transferring stress between tendon and bone over the entire enthesis footprint area, instead of relying only on a small number of anchor points. Even the sub-optimal multipartite adhesives evaluated here for model validation led to load tolerance improvements that are attractive for rotator cuff repair. Future studies investigating compliant, strong adhesive biomaterials have promise for enhancing rotator cuff repair strength and enabling the requisite tissue apposition for healing.

3.8 Acknowledgements

Mr. Donghwan (Eric) Yoon planed many of the tendon planks used here. Tendon planks were planed using a sliding microtome in Professor Spencer Lake's laboratory at Washington University in St. Louis. The work in this chapter was supported by the National Institutes of Health (NIH): U01 EB016422 (to ST and GMG), R01 AR062947 (to ST), and F30 AR069491 (to SWL). Additionally, the work in this chapter was supported by translational research grants from Washington University Institute for Translational and Clinical Sciences and Musculoskeletal Research Center (P30 AR057235).

3.9 Supplemental Material

The shear lag analysis employed here assumes tight contact between the adhesive and the adjacent bone or tendon. Tight contact may not occur between layers in a surgical setting, e.g., due to non-ideal adhesive application. However, 13 mm of continuous overlap length is not necessary to improve load transfer. Intuitively, even several discrete binding zones would distribute stress concentrations over larger areas than the few suture puncture points that are currently used clinically. This intuition is supported mathematically: the critical adhesive binding interface length is dictated by the intersection between the two load transfer asymptotes given in Equation 3.8 and 3.9:

$$L_{critical} \equiv \frac{\chi}{\beta(\chi-1)} = t_b \left[\frac{E_t^* t_t^* t_a^*}{G_a^*} \left(1 + E_t^* t_t^*\right) \right]^{\frac{1}{2}} \tag{S1}$$

At the critical interface length, the load transfer is 76% of the load transfer expected for an infinitely long adhesive interface (Figure 3.S1). At twice the critical interface length, the load transfer approaches that of an infinitely long adhesive interface (96%). For geometric and material properties given in Table 3.2 for shear lag analysis, and assuming

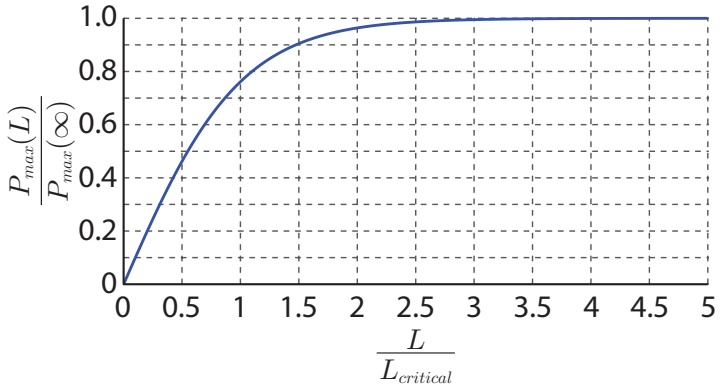

Figure 3.S1: Maximum load transfer, P_{max}, normalized by maximum load transferred by an infinitely long adhesive interface, $P_{max}(\infty)$, as a function of adhesive interface length, L, with respect to the critical interface length $L_{critical}$. Increasing adhesive interface length increases maximum load transfer, i.e., load causing the adhesive to fail, only until a point. Above a critical interface length, load capacity is governed by an asymptote independent of interface length (Equation 3.8). Note that this is an invariant curve that is true for any combination of G_a, t_a, E_b, t_b, E_t, and t_t that yields a particular value of $L_{critical}$.

an adhesive thickness of 0.5 mm and adhesive shear modulus of 100 MPa, this critical interface length is 1.4 mm. Less thick adhesive layers have a shorter critical interface length. A series of discontinuous, short adhesive binding points should therefore still improve load transfer nearly as predicted in Figure 3.7.

Figures 3.S4, 3.S5, 3.S6, and 3.S7 show biomechanical tests of supraspinatus repairs with and without multipartite adhesive. All of these figures follow the same layout: (Left) Frames from the side and front view videos at the start of mechanical testing demonstrate positioning, overlaid with (+) symbols at optical tracking points. (Right) Stress-interface strain curves (solid lines) show with strain calculated from optically tracked points on the supraspinatus tendon and the bone immediately adjacent to the repair interface, from front and side videos. Dashed lines: fitted line for modulus; •: Yield stress position. (Bottom) Table of key test results, using side view strain tracking for yield stress, modulus, and resilience calculations.

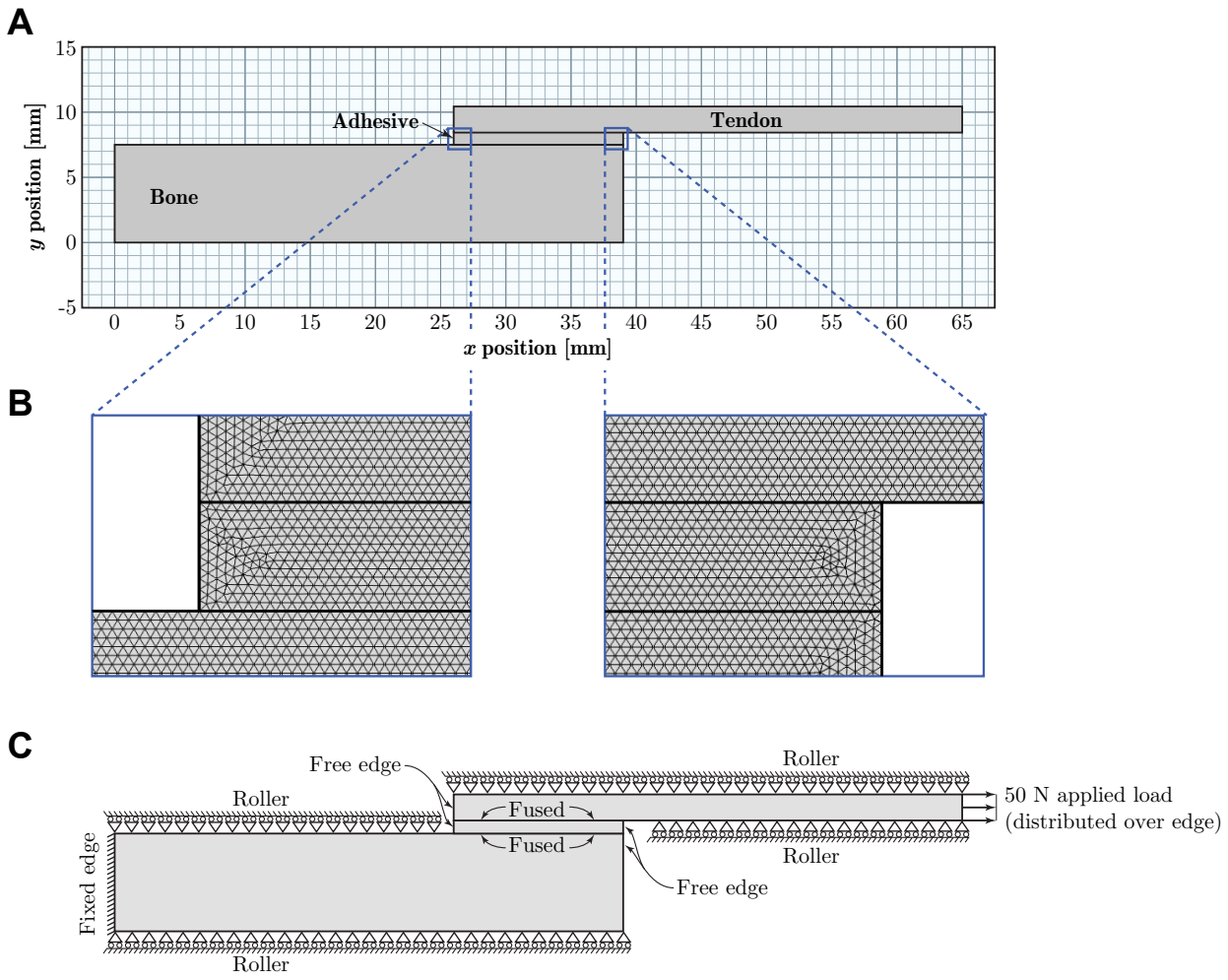

Figure 3.S2: (A) A two-dimensional finite element model was evaluated in COMSOL Multiphysics using the geometric and material properties given in Table 3.2. A range of adhesive thicknesses from 1 µm – 1 cm were evaluated. (B) The adhesive, tendon, and bone layers were discretized into finite elements sized from 1 – 50 µm. Screenshots of the finite element mesh are shown. Convergence was achieved for models with 376,000 – 505,000 triangular quadratic-interpolation elements, depending on the adhesive layer thickness. (C) Boundary conditions for the finite element model.

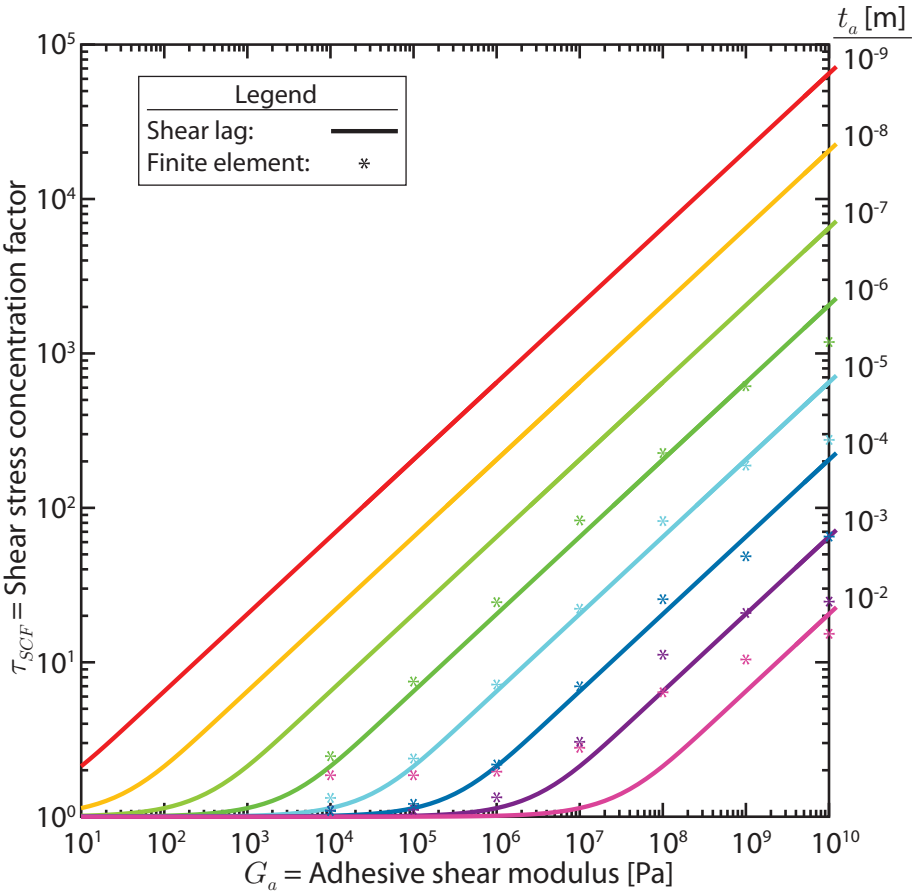

Figure 3.S3: Shear lag (lines) and finite element (*) modeling predicted the lowest stress concentration for compliant, thick adhesives. When the adhesive thickness is the same order of magnitude as the adherend thickness (~ 1 cm), the shear lag model loses accuracy. In addition, the shear lag model is inaccurate for very still adhesives ($G_a \geq 10^{10}$ Pa). Color represents thickness of the adhesive layer (labeled on right).

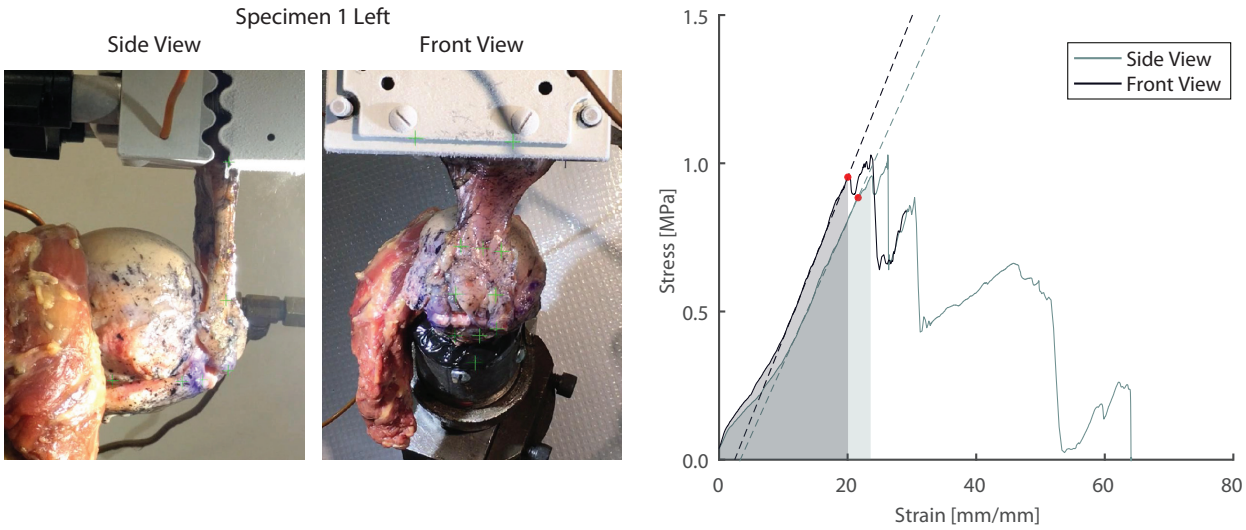

Max Force	Max Stress	Yield Stress	Modulus	Resilience
308 N	1.03 MPa	0.88 MPa	48.3 kPa	10.9 MPa $*$ strain

Figure 3.S4: Human cadaver supraspinatus double-row suture anchor repair, without adhesive, for Specimen 1 left shoulder. This repair required repeated suture anchor placement due to incorrect initial positioning. Key results (table) are calculated from strain tracking performed on the side view video.

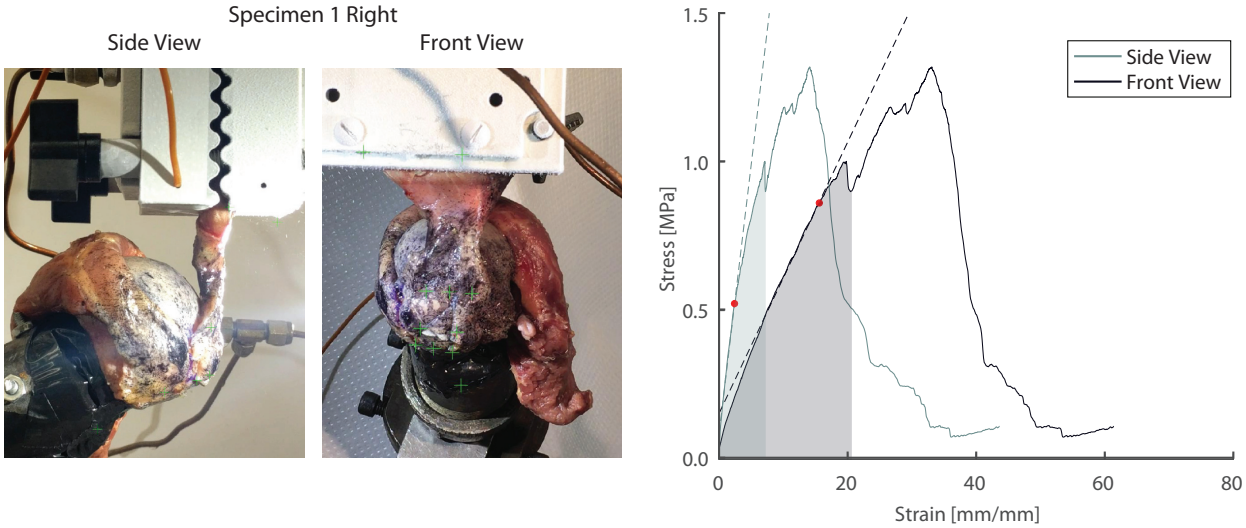

Max Force	Max Stress	Yield Stress	Modulus	Resilience
396 N	1.32 MPa	0.52 MPa	181 kPa	4.54 MPa $*$ strain

Figure 3.S5: Human cadaver supraspinatus double-row suture anchor repair, with multipartite adhesive, for Specimen 1 right shoulder. This repair did not have any surgical issues. Key results (table) are calculated from strain tracking performed on the side view video.

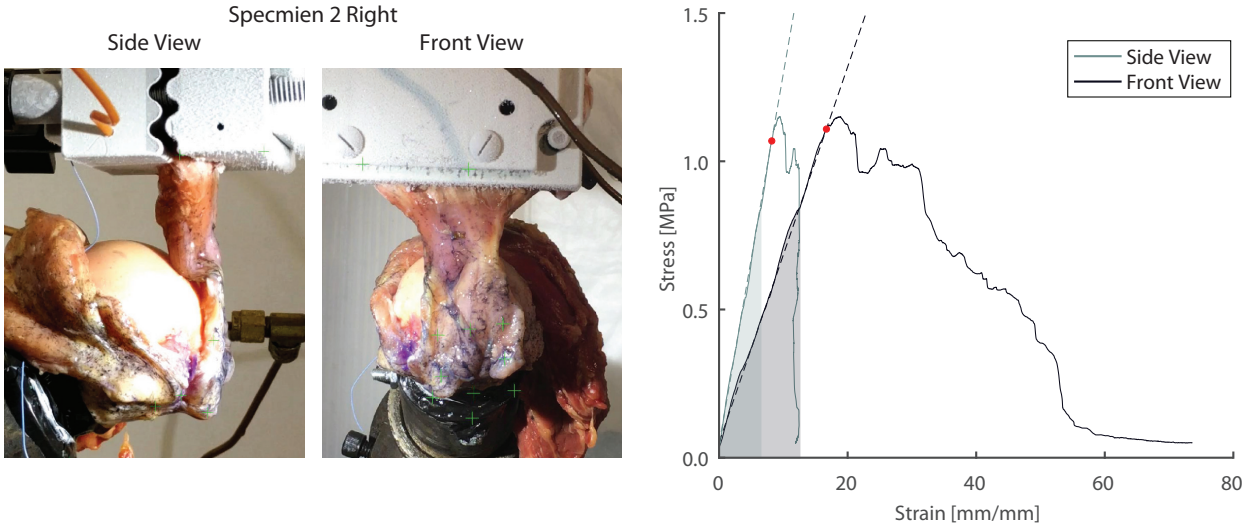

Max Force	Max Stress	Yield Stress	Modulus	Resilience
345 N	1.15 MPa	1.07 MPa	125 kPa	3.00 MPa $*$ strain

Figure 3.S6: Human cadaver supraspinatus double-row suture anchor repair, without adhesive, for sample Specimen 2 right shoulder. This repair did not have any surgical issues. Key results (table) are calculated from strain tracking performed on the side view video.

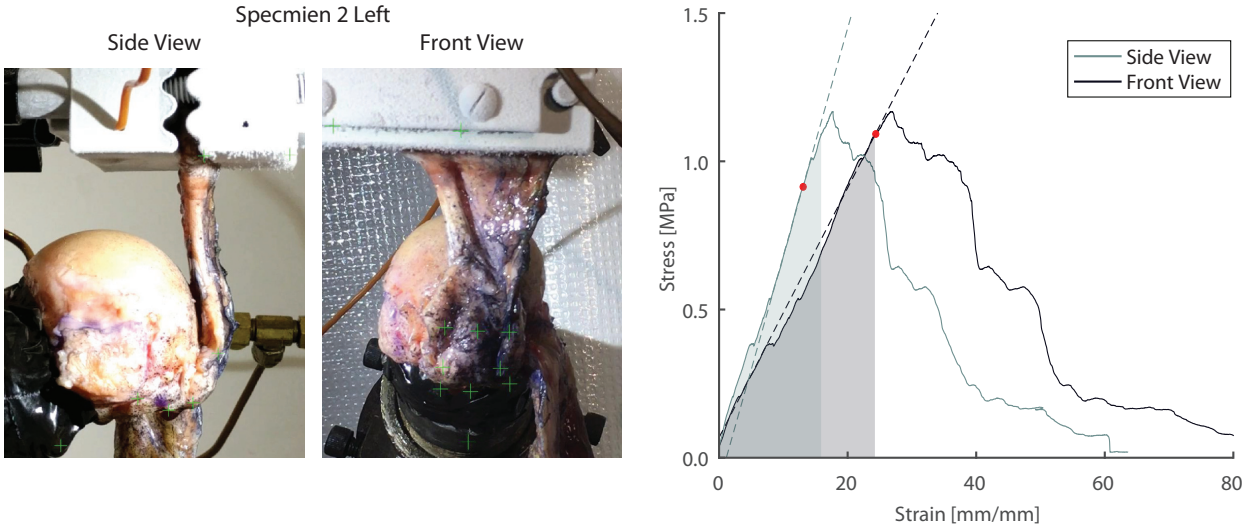

Max Force	Max Stress	Yield Stress	Modulus	Resilience
350 N	1.17 MPa	0.91 MPa	77 kPa	8.95 MPa $*$ strain

Figure 3.S7: Human cadaver supraspinatus double-row suture anchor repair, with multipartite adhesive, for Specimen 2 left shoulder. This repair required repeated suture anchor placement due to incorrect initial positioning. Key results (table) are calculated from strain tracking performed on the side view video.

Chapter 4

Adhesive and bioactive factor delivery via sutures with porous sheaths

Portions of this chapter were previously published in:

Li J, Linderman SW, Zhu C, Liu H, Thomopoulos S, Xia Y. Surgical Sutures with Porous Sheaths for the Sustained Release of Growth Factors. Adv Mater. 2016 Jun;28(23):4620-4. PMID: 27059654. [353]

Linderman SW, Shen H, Yoneda S, Jayaram R, Tanes ML, Sakiyama-Elbert SE, Xia Y, Thomopoulos S, Gelberman RH. Effect of Connective Tissue Growth Factor Delivered Via Porous Sutures on the Proliferative Stage of Intrasynovial Tendon Repair. J Orthop Res. 2018 Jul;36(7):2052-2063. PMID: 29266404. [354]

4.1 Abstract

The previous chapters analyzed mechanical models and experimental applications of adhesives for tendon and tendon-to-bone repairs. In the current chapter, we developed a novel approach to deliver adhesives and bioactive factors in tendon repairs using porous sutures. Standard Supramid (pseudomonofilament nylon) sutures were modified to create micrometer-sized pores in the outer sheath without modifying the inner, load-bearing nylon fibers. Importantly, this process did not detrimentally affect suture mechanical properties in either single suture strand tests or in cadaver canine

flexor digitorum profundus tendon repairs. The porosity dramatically increased the suture surface area, facilitating adhesive interdigitation and strong binding. In addition, this porous suture enabled growth factor or other bioactive factor addition to the inside of the suture for sustained release over time. While previous suture coating approaches had insufficient loading capacity to deliver substantial levels of factors to repair sites, the porous suture approach enabled loading several fold higher amounts of a growth factor. Using connective tissue growth factor (CTGF) as a model growth factor, release kinetics *in vitro* demonstrated an initial burst of 0.50 – 1.25 $\frac{\text{ng CTGF}}{(\text{cm suture})(\text{day})}$ followed by sustained delivery of 0.15 $\frac{\text{ng CTGF}}{(\text{cm suture})(\text{day})}$ through day 14, corresponding to concentrations of 60 – 150 ng/mL daily burst and 10 – 20 ng/mL daily sustained release from suture within 3 mm of a theoretical flexor tendon repair site. *In vitro* experiments confirmed that growth factor-loaded porous sutures retained bioactivity and did not have any negative impact on cell viability in culture. *In vivo* repairs with CTGF-laden sutures were mechanically competent and did not show any evidence of adhesions or other negative inflammatory reactions based on histology, gene expression, or proteomics analyses at 14 days following repair. CTGF-laden sutures induced local cellular infiltration and a significant biological response immediately adjacent to the suture, including histological signs of angiogenesis and collagen deposition. There were no evident widespread biological effects throughout the tendon substance. There were significant differences in gene expression of the macrophage marker CD163 and anti-apoptotic factor BCL2L1; however, these differences were not corroborated by proteomics analysis. In summary, this study provided encouraging evidence of sustained delivery of biologically active CTGF from porous sutures without signs of a negative inflammatory reaction. Future studies will evaluate porous sutures with adhesive materials, with and without embedded bioactive factors, to improve the mechanical and biological response following flexor tendon repair. This work represents a novel, highly translational approach to modify the mechanics and biology of healing with almost no changes to the surgical repair approach. Furthermore, porous sutures can be readily adapted as a delivery tool for other surgical repair settings.

4.2 Introduction

Implementation of adhesive coatings on sutures to improve tendon and other soft tissue repair strength requires specifically designed delivery approaches to maximize efficacy. Previous chapters established the mechanical engineering theoretical basis and proof-of-concept experimental validation for adhesive-coated sutures (Chapter 2) and adhesive films, and identified potential adhesive biomaterial approaches to obtain the desired mechanical properties (Chapter 3). The current chapter describes a suture with a porous outer sheath to facilitate adhesive delivery and increase load transfer between the suture and surrounding tissue. While sutures have a large lateral surface that can be used to deliver

adhesives or other biofactors, that surface was not designed for this application. To the contrary, suturing advances for tendon or tendon-to-bone repair optimize material strength and grasping techniques, but typically seek to avoid binding to the lateral surfaces, thereby creating poor suture choices for coating with adhesives [355]. Suture surfaces are typically designed with minimal friction to facilitate surgical handling for suture passage and reduce the collateral damage to tissue from the trauma of suture passage. Polytetrafluoroethylene-coated sutures (PTFE, a.k.a. teflon) are marketed to reduce inflammation and prevent bacterial adhesion, especially for stitches that contact the skin or mucosal surfaces [356, 357], analogous to intrauterine devices that have slick, monofilament threads to reduce bacterial infiltration [358]. While adhesives can still provide benefit on standard surgical suture, as shown in Figure 2.7, new suture delivery approaches are needed to optimize suture–adhesive interfacial strength.

Existing suture coating approaches are usually directly anti-adhesive, as with PTFE, or deliver antimicrobial agents or growth factors to repair sites. These approaches are not designed to maximize binding or transfer load along the lateral surface. Some previous research explores tissue ingrowth into surgical implants, such as porous tantalum for hip and knee implants [359, 360] and "mesh sutures" for abdominal hernia repair [361][1], as a method to strengthen repairs. Tissue ingrowth is a possible mechanism for strength improvement of polyfilament sutures compared to monofilament sutures, in addition to the strength improvements inherent to braided threads. Tissue ingrowth would cause interdigitation of tissue and suture material, facilitating a stronger bond analogous to the interface between tendon and bone in an enthesis [80].

In addition to delivering adhesive materials to improve stress distribution within tendon suture, sutures are aptly suited to deliver bioactive factors. Current delivery approaches used in tissue engineering research typically place scaffolds or inject fluid containing biofactors at one of the following locations: (i) at the tendon surface [199], which risks forming deleterious adhesions to surrounding tissues unless carefully performed; (ii) at the repair interface [93, 47], which could act as a barrier to tissue regrowth across the repair; or (iii) within the injured tissue, which causes excess tissue damage compared to a conventional repair [167, 186]. Sutures, on the other hand, have potential to deliver biofactors immediately within and surrounding the repair site following surgery, without introducing additional defects or materials that may cause inflammation, such as poly(lactic-co-glycolytic acid) [167, 186]. Prior work on local delivery of biofactors via sutures has primarily focused on coating the surface of a solid suture thread with a biofactor or biofactor-containing material [362, 363, 364, 365, 366, 367]. However, this approach has two major disadvantages. First, almost all of the biofactor is exposed to surrounding tissue, leading to rapid bolus release of biofactor. Even with carrier materials, most reported release profiles from sutures remain relatively short, over only several days

[1] "Mesh sutures" described by Souza *et al.* are polypropylene strips, not cylindrical sutures.

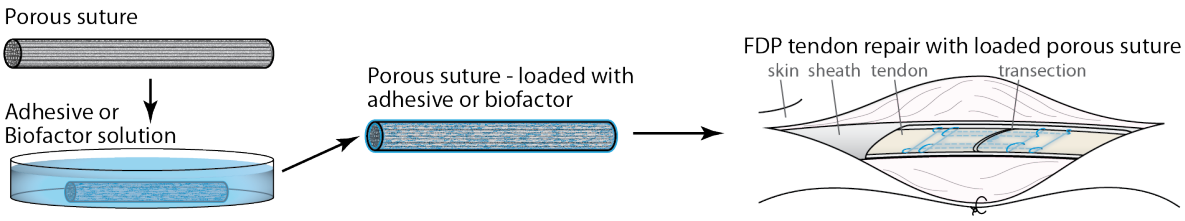

Figure 4.1: Porous sutures have high surface area and loading capacity, which can be used to deliver adhesives and/or biofactors to an injury site within a tendon.

[365, 366, 367]. Second, solid sutures have limited loading capacity on the surface, so it is challenging to obtain sufficient biofactor release to have a significant impact. Biofactors are typically restricted to thin coating layers, which can easily peel off during handling for the reasons discussed above that also limit adhesive–suture interfacial binding strength. While prior suture delivery approaches have yielded only marginal success [365, 366, 367], new approaches that increase loading capacity and enable sustained delivery have the potential to guide the healing process. Growth factors that promote the proliferative stages of repair, especially those that stimulate connective tissue extracellular matrix production and tendon regeneration such as connective tissue growth factor (CTGF) [209, 223, 368], provide an opportunity to directly promote tissue ingrowth into the suture and tissue healing at large to improve load tolerance of the healing repair.

Here, we aimed to modify the lateral surfaces of commercially available sutures to create a suture with improved properties for delivery of adhesive biomaterials or other biofactors, without compromising the mechanical integrity of the suture. First, we modified the surface of pseudo-monofilament nylon sutures to create a porous outer sheath, without impacting the inner suture fibers. We evaluated these sutures for biomechanical properties, loading capacity and release profiles, and *in vivo* impact at 14 days in a canine flexor digitorum profundus tendon transection and repair model, as shown in Figure 4.1.

4.3 Methods and Materials

4.3.1 Preparation and visualization of modified, porous sutures

N.B.: Porous suture development was performed by Jianhua Li in the laboratory of Professor Younan Xia at Georgia Institute of Technology.

To create surgical sutures with porous outer sheaths, pristine pseudo-monofilament surgical sutures (Supramid 4–0, HEA40, S. Jackson Inc., Alexandria, VA) were treated with a swelling and freeze-drying procedure. Before treatment, the commercially available sutures had a cable-type structure consisting of fine inner nylon-6,6 filaments enclosed by a nylon-6 sheath with a smooth surface. The commercially available sutures were soaked in a 500 mM $CaCl_2$ solution in methanol for 24 hours at room temperature to induce swelling of the outer sheath as Ca^{2+} ions formed coordination bonds with the carbonyl groups on nylon-6, breaking the hydrogen bonds between adjacent nylon chains [369]. By controlling the incubation time and $CaCl_2$ concentration, most of the swelling was restricted to the sheaths only before Ca^{2+} began to attack the inner filaments (supplemental data shown in [353]). Afterward, the swollen sutures were quickly frozen in liquid nitrogen (-196 °C) to crystallize and phase-separate the solvent molecules from the polymer chains. Then samples were freeze-dried in a vacuum overnight, which eventually produced a highly porous structure once the solvent molecules had been removed by sublimation [370, 371, 372]. Since all reagents used in this process were water soluble, their residues were readily removed by rinsing several times with water.

The swelling and freeze-drying approach caused the $\approx$ 10 μm outer sheath of cable-type, pseudo-monofilament nylon sutures to become porous, while the inner packed fibers remained intact with very few pores, as shown by scanning electron microscopy images before and after modification (SEM, Figure 4.2A,B). The pristine suture showed a smooth surface, which facilitated surgical handling and suture passage with low friction. In contrast, the modified suture had a highly porous surface, with pore sizes in the range of 0.5 – 5 μm (Figure 4.2C,D). The micrometer-sized pores were generated through the entire cross section of the sheath. Varying Ca^{2+} concentration controlled porosity and pore size (data shown in supplemental material of [353]).

4.3.2 Biomechanical testing

Single-strand mechanical tests: The unmodified and porous sutures were first biomechanically evaluated as individual strands in uniaxial tension using a material testing machine (5866; Instron Corp., Norwood, MA), as described

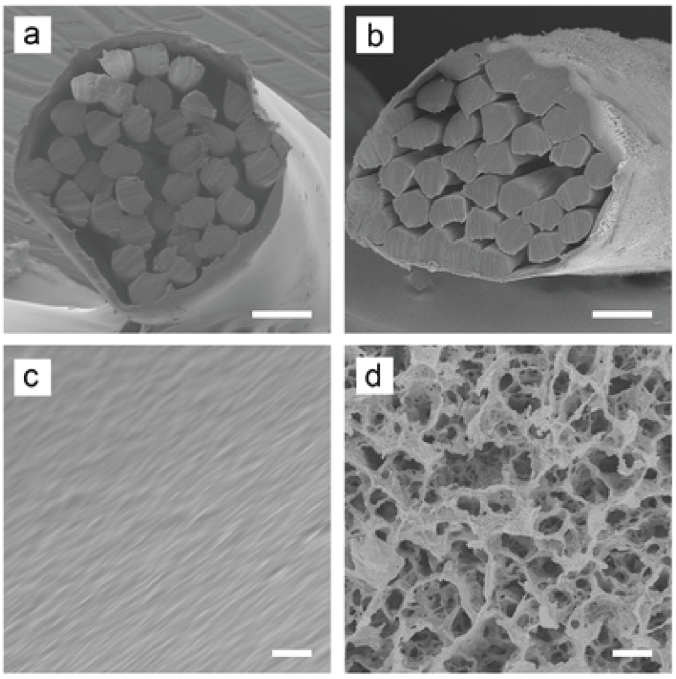

Figure 4.2: SEM images of the (A,B) cross sections and (C,D) side surfaces of the unmodified (A,C) and porous (B,D) sutures. Scale bars: 50 μm in panels (A,B) and 2 μm in panels (C,D). Figure reproduced with permission from [353].

previously [107] ($n = 7$ for unmodified sutures and $n = 6$ for modified, porous sutures). A suture was carefully placed in a jig consisting of a low-friction spool and a clamp grip, which was pulled upward at 1.0 mm/s to apply tension to the suture. The gauge length between the suture grips was 110 mm for all the samples at the beginning of the test. Maximum stress, yield strain, strain at maximum stress, and modulus were determined from the stress-strain curves using a custom MATLAB script as described in Section 3.4.4, simply using MTS grip data without any optical strain analysis.

Clinical-style repair biomechanics: Cadaver canine forepaw samples were obtained post-mortem from an unrelated study, stored at -20 °C, and thawed at 4 °C immediately before use. Flexor digitorum profundus (FDP) tendons were sharply transected in Zone II and repaired with unmodified or porous sutures 4–0 Supramid core sutures using an 8-stranded Winters-Gelberman technique followed by a 5–0 proline running epitenon suture, following the same methods as in Section 2.4.1 performed by highly experienced orthopaedic hand surgeons ($n = 10$ for modified, porous sutures and $n = 11$ for unmodified sutures). Dr. Richard Gelberman performed the *ex vivo* repairs with porous sutures and Dr. Susumu Yoneda performed the *ex vivo* control repairs with unmodified sutures using the same technique. Following clinical-style repairs, cadaver FDP tendons were biomechanically evaluated following the methods as in Section 2.4.2.

Adhesive-coatings on porous sutures: To experimentally assess the ability of porous sutures to delivery adhesives to improve load transfer, the flexible cyanoacrylate Loctite 4903 ($n = 4$ per group, based on ethyl and octyl cyanoacrylate [274, 275]; Henkel Corporation, Düsseldorf, Germany) or a catechol-derived heteropolymer adhesive ($n = 3$ per group, courtesy of Dr. Kollbe Ahn at University of California in Santa Barbara, previously evaluated in idealized tendon-to-bone plank tests in Chapter 3) was applied to single psuedomonofilament nylon sutures (unmodified, U) or nylon sutures that were first modified to have a porous outer sheath (porous, P). This idealized adhesive testing method, described in Section 2.4.1, was shown to be predictive of strength improvements in clinically relevant cadaver tendon repairs in Chapter 2. Single unmodified or porous nylon 4–0 suture strands were passed through cadaver canine hindpaw flexor tendon tissue by Dr. Susumu Yoneda by using a looped 4–0 suture with a needle to pull the tested suture segment into place. Cadaver canine hindpaw samples were obtained from healthy female adult mongrel dogs from 20–30 kg in weight (Covance Research, Princeton, NJ), taken postmortem from an unrelated study and frozen at -20 °C before use. The tendon was first dissected away from surrounding tissue and a complete transection was made in Zone II [61] perpendicular to the long axis of the tendon. Suture was passed from the side of the tendon 10.0 – 12.0 mm from the site of transection toward the laceration interface. The suture was pulled through the tendon so that only a single suture strand remained within the tendon. The adhesive was injected onto the suture on the side of the tendon and the suture was pulled into place, dragging the adhesive into the tendon. For the catechol-derived heteropolymer groups, after adhesive was injected onto the suture, the suture was placed in an oxidizing solution of 100 mM sodium (meta)periodate ($NaIO_4$, Sigma Aldrich, St. Louis, MO) in PBS for 60 seconds before pulling into the tendon to stimulate catechol oxidation and prime for binding. Adhesive that accumulated on the side of the tendon was cleared with gauze soaked in phosphate buffered saline (PBS). The assembly within the tendon was wrapped in PBS-soaked gauze with excess PBS in an airtight tube and then allowed to cure for 12 hours at room temperature followed by 12 hours at 4 °C before biomechanical testing. This curing procedure was chosen to facilitate catechol oxidation and binding, while also limiting the risk that postmortem tissue *ex vivo* would rot or deteriorate.

Samples were brought to 37 °C prior to biomechanical testing. Any suture and adhesive outside of the lateral tendon was first dissected away. This experimentally ensured that the effect was due to adhesive along the length of the suture instead of adhesive accumulated at the suture entrance point. Samples were then tested in uniaxial tension on a materials testing frame (ElectroPuls E1000; Instron Corp., Norwood, MA, chosen because of a low noise load cell suitable for distinguishing milli-Newton level forces). The tendon was clamped in a stationary grip so 15 mm of tendon length was exposed. Suture was carefully placed in a jig consisting of a low friction spool and a clamp grip, which was pulled upward at 0.3 mm/s to apply tension to the suture. The gauge length between the tendon and suture grips was 8.5 cm for all samples at the start of the test. Pullout (failure) force of single adhesive-coated suture strands

within tendon tissue were determined from the force-elongation curves.

4.3.3 Biofactor loading and *in vitro* evaluation

Dye loading and visualization: *N.B.: Porous suture dye loading and visualization experiments were performed by Jianhua Li in the laboratory of Professor Younan Xia at Georgia Institute of Technology.*
After modifying sutures to create a porous outer sheath, sutures were infiltrated with dyes and biofactor molecules to evaluate loading capacity. A small, water-soluble dye (Rhodamine B, Sigma Aldrich, St. Louis, MO) and a larger dye-labeled protein (FITC-BSA, Sigma Aldrich) were separately loaded onto unmodified and porous sutures within a fibrin matrix. Suture samples were first sterilized using 75% ethanol, then immersed in Tris-buffered saline (TBS, pH 7.2) containing 20 mg/mL fibrinogen and either Rhodamine B or FITC-BSA overnight at 4 °C. The fibrinogen- and dye-loaded sutures were then soaked in TBS containing 2 U/mL thrombin, 40 mM $CaCl_2$, and the same concentration of dye used in the previous step at room temperature for 2 hours. Laser confocal fluorescence microscopy (Zeiss LSM 700) was used to resolve distribution of the dyes and dye-labeled proteins in each suture.

Following porous modification, biofactor molecules readily infiltrated into the voids among the inner suture filaments via the interconnected pores created in the outer sheath. This was validated for small and large molecules using the small, water-soluble dye Rhodamine B (Figure 4.3B) and a large dye-labeled protein, FITC-BSA (Figure 4.3D), visualized by fluorescence micrographs of the cross-sections of loaded sutures. Both the dye and dye-labeled protein could be clearly observed filling the voids among inner filaments of porous modified sutures. In contrast, the smooth outer sheath of unmodified sutures prevented biofactor penetration. Dyes were only observed on the outer surface of unmodified sutures (Figure 4.3A,C). This result indicates that the dense sheath surrounding the filaments of unmodified sutures could not be penetrated by small or large molecular species, whereas the highly porous sheath of modified sutures could be used to access the voids among the inner filaments. The capillary action caused by the interconnected porous structure, in combination with the concentration gradient of molecules in solution, effectively drove molecules through the pores and into the voids inside the sutures (Figure 4.3E,F).

CTGF/HBDS loading: Modified, porous sutures created at Georgia Institute of Technology, lyophilized after being washed with distilled water several times ($i > 5$), were shipped to Washington University in St. Louis and loaded with recombinant human CTGF, produced in *E. coli* (BioVendor, Asheville, NC). CTGF was loaded in a heparin/fibrin delivery system (HBDS) for sustained release, as described previously [167, 194, 178]. The lyophilized sutures were

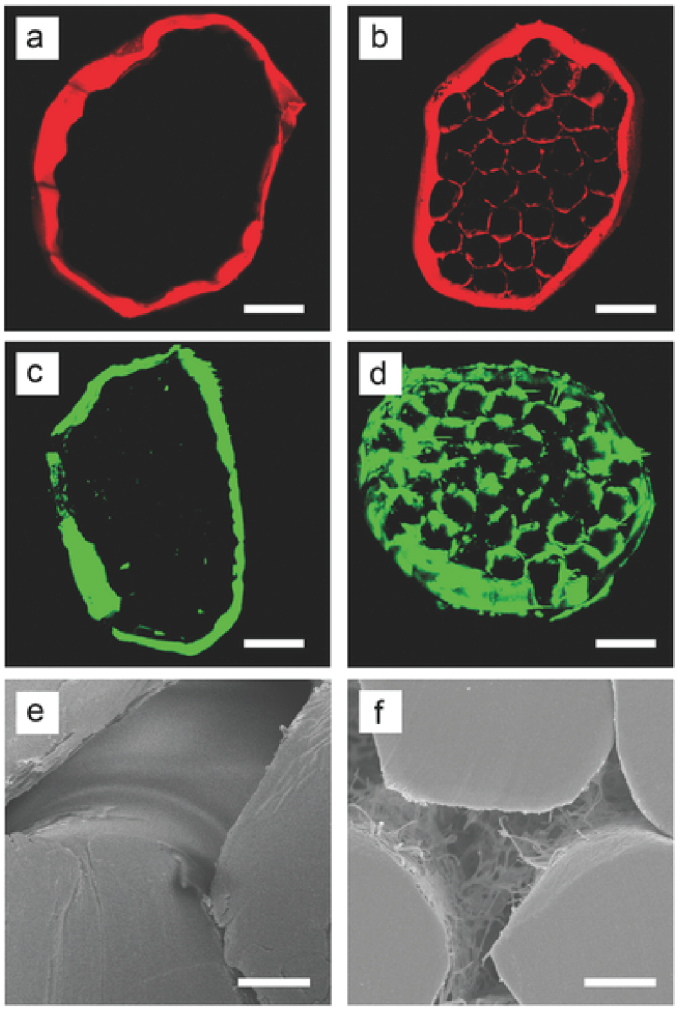

Figure 4.3: Sutures with porous sheaths showed a much higher loading capacity for both (A,B) small molecules (Rhodamine B) and (C,D) proteins (FITC-labeled BSA), as indicated by (A–D) confocal fluorescence and (E,F) scanning electron micrographs taken from the cross sections of (A,C,E) unmodified and (B,D,F) modified sutures. The fibrin matrix and dye are evident in the voids among the inner filaments of the modified suture. In contrast, dye is nearly absent from the interior of the pristine suture. Scale bars: 50 μm in panels (A–D) and 10 μm in panels (E,F). Figure reproduced with permission from [353].

first sterilzed with poly(ethylene oxide) gas, then care was taken to maintain sterility before use. Sutures only came into contact with sterile solutions (0.2 μm filtered) in a sterile biosafety cabinet, using autoclaved surgical instruments and sterile surgical gloves. All pipette tips, tubes, and tools were either silanized or rinsed with TBS containing 0.1% bovine serum albumin (BSA) prior to use to block inadvertent protein binding.

To coat with CTGF/HBDS, sterile sutures were first either cut into 15 mm pieces for *in vitro* release profile evaluation or left as 30 cm looped suture with a needle for *in vivo* surgical implantation. Sutures or suture segments were then submerged in TBS (pH 7.4) containing 0.1% w/v BSA (Sigma Aldrich), 20 mg/mL human fibrinogen (plasminogen depleted, $>$ 95% clottable proteins; EMD Millipore), and CTGF/HBDS components at 4 °C overnight to enable the components to permeate the porous suture and reach equilibrium at the desired CTGF/HDBS levels. The fibrinogen- and CTGF/HBDS-loaded sutures were then immersed in TBS containing 0.1% w/v BSA, 20 U/mL thrombin (Sigma Aldrich), and 13.7 mM $CaCl_2$ for 2 hours at 37 °C to crosslink. Suture samples were washed by rinsing in TBS with 0.1% w/v BSA to remove unbound CTGF before collecting release profiles *in vitro* or implanting suture *in vivo*.

The CTGF/HBDS components used for the two loading steps included: (i) a bi-domain HBDS peptide, (ii) heparin (Sigma Aldrich H3393), and (*iii*) CTGF at a $\left[4 : 1 : \frac{1}{135}\right]$ stoichiometric molar ratio, calculated based on final CTGF concentrations (10, 20, 30, 40, 50, or 100 μg/mL for *in vitro* release studies, $n = 2$ per group; 0 or 30 μg/mL for *in vivo* surgical studies). The HBDS peptide consisted of a factor XIIIa substrate derived from α_2-plasmin inhibitor at the N-terminus and a C-terminal heparin-binding domain from anti-thrombin II [167, 105, 106, 178, 103, 195] (sequence dLNQEQVSPK(βA)FAKLAARLYRKA-NH_2, where dL denotes dansyl leucine, purity $>$ 95%; GenScript, Piscataway, NJ). The bi-domain peptide was covalently cross-linked to fibrin during polymerization by the transglutaminase activity of factor XIIIa. The peptide electrostatically immobilized heparin to the matrix, which in turn immobilized the heparin-binding growth factor, CTGF, preventing diffusion away from the matrix. While there were small sample numbers at each loading concentration, several CTGF concentrations within a small range were evaluated to enhance reliability and enable identification of the optimal CGTF loading concentration for *in vivo* use.

CTGF release profile: After loading porous suture for *in vitro* release, 15 mm suture segments were incubated in 70 μL of TBS containing 0.1% w/v BSA in a 0.6 mL tube at 37 °C. All 70 μL of solution was collected at each time point and replaced with fresh TBS with 0.1% w/v BSA. The collected aliquots were placed in a silanized tube, centrifuged for 3 minutes at 16,100 g, and stored at -80 °C before the amount of CTGF was quantified using an enzyme-linked immunosorbent assay (BioOcean, Shoreview, MN), performed following the manufacturer's instructions, except using TBS with 0.1% w/v BSA for all dilution buffers to maintain a consistent buffer. The absorbance was read with a

microplate reader (Cytation 5 Plate Reader, BioTek, Winooski, VT) and the concentration of CTGF from each sample was determined from a calibration curve derived from CTGF solutions with known concentrations.

4.3.4 Canine flexor tendon injury and repair model

Ten 1- to 2- year-old female mongrel dogs (20 – 30 kg) were used in this study (Covance, Denver, Pennsylvania), and all procedures were approved by the institutional Animal Studies Committee. Animal housing and welfare was provided by the institutional Division of Comparative Medicine. The effects of porous sutures loaded with or without CTGF were assessed in paired intrasynovial flexor tendon repairs in canines (Figure 4.1), performed on two digits of one paw per animal ($n = 10$ tendons per group). The FDP tendons of the medial and lateral right forepaw digits (2^{nd} or 5^{th} digits) were sharply transected at the level of the proximal interphalangeal joint (within Zone II) and repaired using a porous core suture, loaded as described above with all HBDS components with or without CTGF at a 30 µg/mL soaking concentration ($CTGF^+$ group and $CTGF^-$ control group, respectively). All repairs were performed as described previously [186, 199, 103, 155, 167], using an 8-stranded Winters-Gelberman core suture technique followed by a 5–0 nylon epitenon suture [11]. Controlled passive motion exercise was applied to the digits postoperatively to replicate the clinical scenario. The paws were flexed fully and then extended to the limits of the extension block for 5 minutes daily, 6 days per week [65].

The corresponding left digital flexor tendons served as normal controls (Normal group). All animals were euthanized 14 days after repair. Of the 10 repaired tendons within each repair group and normal controls, $6/10$ were longitudinally transected into two parts consisting of approximately $2/3$ and $1/3$ of the tendon volume, within 5 mm on either side of the repair site. The smaller part was used for proteomics analysis and the larger part was used for RNA isolation and subsequent gene expression analysis. The remaining tendons ($4/10$) were used for histological study and transmission electron microscopy. One tendon ($CTGF^-$ group, histological sample) formed a gap greater than 3 mm and was therefore excluded along with the paired tendon from the same animal ($CTGF^+$ group). Some comparisons also used historical controls from different animals in other studies using the same model, including: (i) a repair with unmodified nylon 4–0 core suture (Repair-only group) and (ii) a repair with unmodified suture that was also treated with an autologous adipose-derived stem cell (ASC) sheet at the surface of the flexor tendon, then sealed with hyaluronic acid to prevent cell sheet movement or adhesion formation to the intrasynovial sheath (ASC group).

4.3.5 Histology and transmission electron microscopy

Histological section preparation: For morphological assessment, a 20 mm tendon fragment was obtained from each repaired tendon, with the transection site in the middle. The tendon fragments were trimmed at both ends to generate a center piece (10 mm in length) and two end pieces (5 mm in length). The center pieces and end pieces were used for histology and transmission electron microscopy (TEM), respectively. The histological samples were fixed in 4% paraformaldehyde overnight. After washing and dehydrating, the histology samples were embedded in paraffin and serial coronal paraffin sections (5 μm thick) were prepared [199, 373]. Hematoxylin and eosin (H&E), Russell-Movat pentachrome (American MasterTech, Lodi, CA), or reticular staining were performed. Reticular staining was chosen to assess vascular ingrowth since it is a well characterized stain, and there are no validated CD34 antibodies available for the canine. Immunohistochemical staining for CD146 and Ki67 was also performed to label for tendon-resident $CD146^+$ stem/progenitor cells and proliferating cells, respectively.

Cell counting protocol: Histological slides from the middle of the flexor tendon thickness, prepared with H&E staining, were used to assess cell counts near the suture surface ($n = 3$ tendons per group, paired by animal). Digital slides were analyzed blindly using a custom MATLAB script that manually identified the tendon laceration interface, then divided each side into thirds (approximately 3 mm long each) for cell counting. The script automatically identified the suture sections by thresholding the grayscale image, with user oversight. This enabled accurate calculation of the area of the tissue section within 70 μm of the suture surface, which was used to create output images for cell counting and also used for normalization. Cells in each section were counted manually in ImageJ and normalized by tissue area. Normalized cell counts from corresponding segments on each side of a slide were averaged as a single experimental sample.

Transmission electron microscopy (TEM): Ultrathin cross sections ($90 \sim 100$ nm) of flexor tendon were prepared from the TEM samples. Cross sections were taken from the TEM tendon sample end closest to the transection site to ensure that the samples included suture material. TEM images were taken at 2,500× and displayed at approximately 1,250× magnification. Collagen fibrils were automatically identified by thresholding the image with a custom MATLAB script, and fibril diameter and distance from the 10 closest neighboring fibrils (a measure of fibril density) were calculated.

4.3.6 Gene expression

Total RNA isolation, cDNA synthesis, and gene expression assays were performed as described previously [199, 373, 165]. The gene expression profile in repaired tendons 14 days after repair was determined using TaqMan® real-time PCR (Applied Biosystems, Woolston, UK) by the Washington University Genome Technology Access Center using the Biomark^{TM} HD system (Fluidigm, San Francisco, CA). The relative abundance of target genes in repaired digits was analyzed with the comparative Ct ($2^{-\Delta\Delta Ct}$) method using GAPDH and PPIB as endogenous reference genes. All gene expression results are shown as fold changes compared to the average gene expression levels in contralateral non-operated, normal digits (2^{nd} and 5^{th}) from the same animal. All TaqMan primers and probes used in this study were obtained from Applied Biosystems (Foster City, CA).

4.3.7 Proteomics

Protein sample preparation and quantitative proteomics analysis were performed by the Proteomics Core Laboratory at Washington University using a tandem-mass-tag-based assay, as described previously [373]. The PROC MIXED models (SAS Institute, Cary, NC, USA) were applied to proteomics data to identify proteins differentially expressed between three different conditions (Normal, CTGF^{-}, CTGF^{+}). Protein functional classification was performed on selected proteins using the UniProt Knowledgebase (UniProtKB, http://www.uniprot.org).

4.3.8 Statistics

All data are shown as box plots, with the median and range (minimum, 25^{th} percentile, 75^{th} percentile, and maximum), unless otherwise noted. For *in vitro* single strand and *ex vivo* cadaver flexor tendon biomechanics data, non-inferiority of porous sutures was evaluated using a one-sided t-test to determine whether the difference between the means was less than an acceptable equivalence margin, δ, with $\alpha = 0.05$ [374]. This is equivalent to assessing whether the $90\% = (1 - 2\alpha)100\%$ confidence interval for the difference between the means contains the equivalence margin. For cell counts, a 2-way analysis of variance (ANOVA) was performed to compare normalized cell counts grouped by CTGF delivery and position, followed by Fisher's least significant difference post hoc tests. For collagen fibril size comparisons, three representative TEM images per group were combined and fibril diameters were compared with an unpaired Wilcoxon rank-sum test. For gene expression, paired Wilcoxon signed-rank tests were used to compare the fold change compared to normal for CTGF^{-} and CTGF^{+} groups. Changes that yielded $0.05 < p < 0.1$ are marked

as nonsignificant (N.S.). For proteomics data, an ANOVA was used to compare relative protein abundance between groups. The obtained p-values were further corrected using Benjamini-Hochberg's method.

4.4 Results

4.4.1 Biomechanical results

Single-strand mechanical properties: The mechanical properties of single suture strands, with and without modification, were evaluated as shown in the schematic in Figure 4.4A. The two groups of stress–strain curves show similar patterns (Figure 4.4B), indicating that the modification did not have a substantial impact on the mechanical properties of the sutures. The maximum stress increased slightly, from 506.6 $\pm$ 17.2 MPa for the unmodified sutures to 530.4 $\pm$ 14.5 MPa for the porous sutures ($p < 0.05$, Figure 4.4C), likely due to the formation of Ca^{2+}-nylon 6 complexes [369]. The moduli of unmodified and porous sutures were 1.49 $\pm$ 0.03 GPa and 1.59 $\pm$ 0.13 GPa, respectively (Figure 4.4D). The strain at maximum stress and yield strain of the porous sutures increased by $\approx 16\%$ when compared to the unmodified sutures ($p < 0.05$) (Figure 4.4E,F). Almost all of the difference in the stress–strain curves occurred at low stresses ($\sigma < 150$ MPa, which are applied when surgeons tension the suture. As expected, the lack of modification to the inner filaments of the suture resulted in retention of mechanical properties, despite the creation of pores in the outer sheath.

Clinical-style repair biomechanics: After confirming non-inferiority of the porous sutures compared to unmodified sutures in single-strand tests [353], the uncoated porous sutures were evaluated in full clinical-style, cadaver flexor tendon repairs (Figure 4.5A). For each measured mechanical property, the 95% confidence intervals for difference between the means and the percentage change between groups are listed in Table 4.1. The loads creating a 2 mm gap, failure loads, repair rigidities, repair resiliencies, and strains created by a physiologically relevant 20 N load are displayed for each group in Figure 4.5 B, C, D, E, and G, respectively. Load versus strain curves for all samples are shown in Figure 4.5F. The maximum load and resilience of repairs were comparable between groups, indicating porous sutures were appropriate for *in vivo* use. There was a statistically significant 22% decrease in load to create a 2 mm gap using porous sutures; however, the decrease was not clinically meaningful since repairs remained substantially stronger than functional requirements for controlled rehabilitation and normal grasp strength (approximately 35 N) [375]. Similarly, the 25% decrease in rigidity and 17% increase in strain created by a 20 N load were statistically

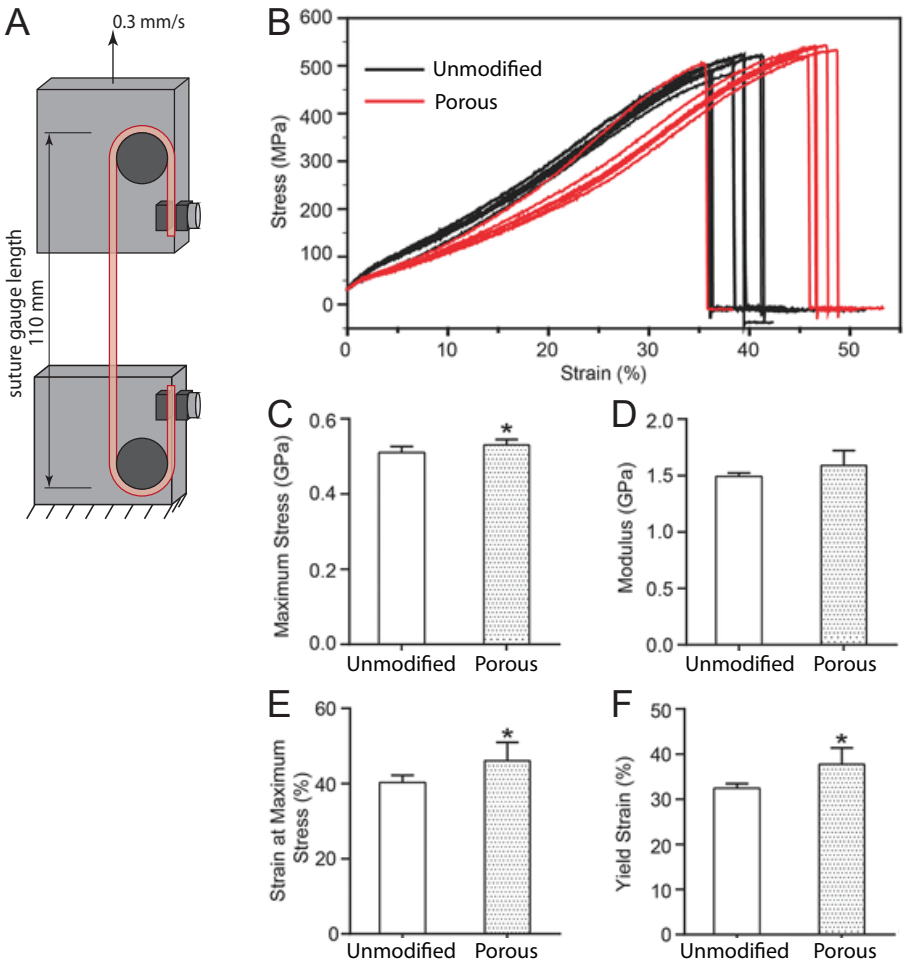

Figure 4.4: Tensile mechanical testing of the pristine and modified sutures: (A) mechanical testing schematic, (B) stress–strain behavior, (C) maximum stress, (D) modulus, (E) strain at maximum stress, and (F) yield strain. $N = 7$ for the pristine samples and $n = 6$ for the modified samples; $*p < 0.05$ (by t-test) indicates significant difference between the two types of samples. Data in (C–F) is displayed as mean $\pm$ standard deviation. Figure reproduced with permission from [353].

but not clinically significant. Of note, porous sutures were mechanically non-inferior to historical control repairs with unmodified sutures.

Surgical handling was notably different between the unmodified suture and the uncoated porous sutures in cadaver tendon. While the unmodified sutures have a smooth surface that enabled low-friction suture passage, porous sutures had substantially higher surface area that increased friction during suture passage. That difference was likely exacerbated by using cadaver instead of living tissue. The high porous suture friction was ameliorated by dripping PBS onto the suture before passage. It was expected that coating the porous sutures with CTGF/HBDS would fill the pores with fibrin hydrogel, reduce the effective surface area, and further decrease friction. Indeed, the friction experienced by the

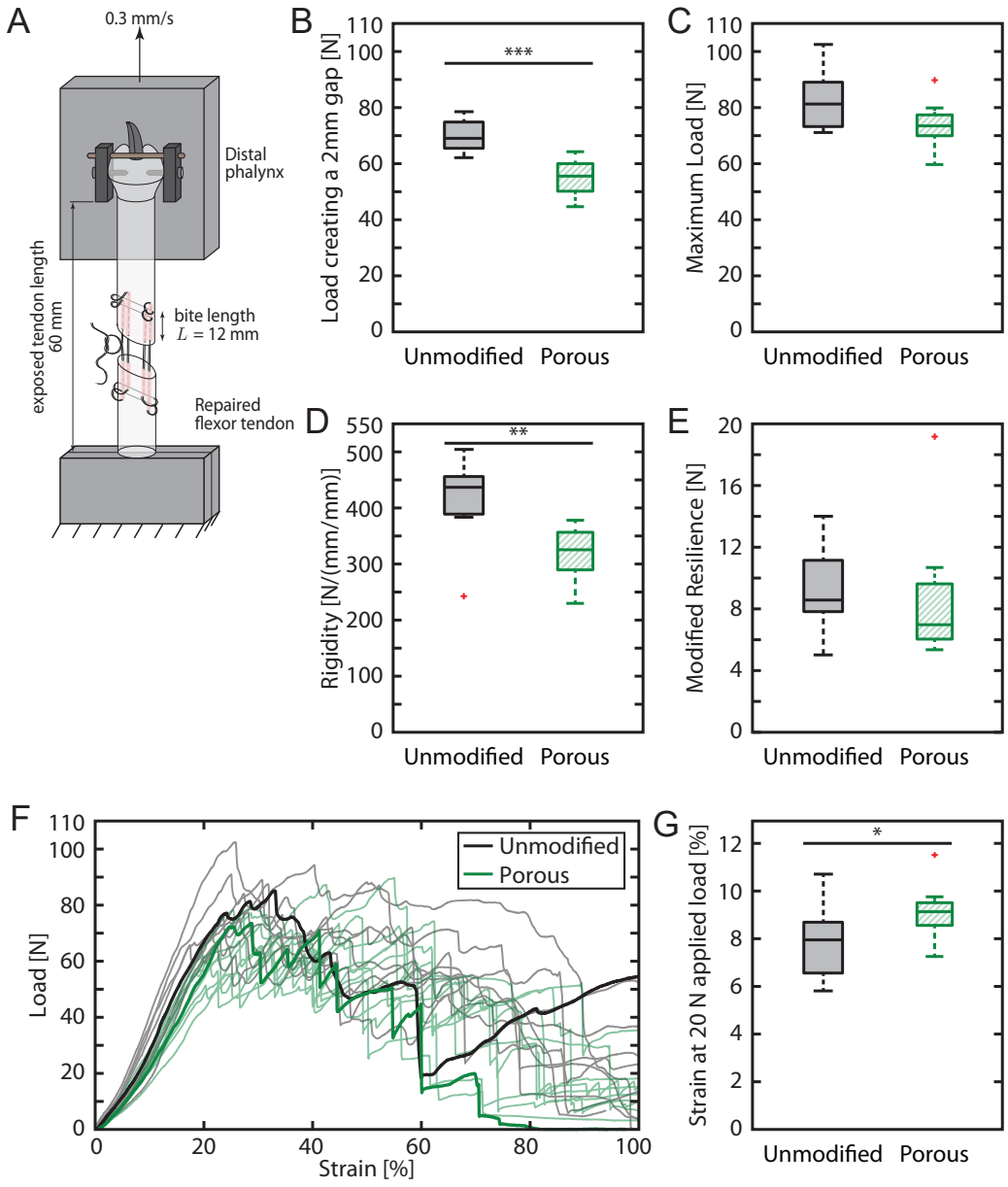

Figure 4.5: Tensile mechanical testing of the unmodified sutures (black) and porous sutures (green) in an 8-stranded Winters-Gelberman flexor digitorum profundus tendon repair: (A) mechanical testing schematic, (B) load to create a 2 mm gap, (C) maximum load, and (D) rigidity, (E) modified resilience, (F) load versus strain curves for all samples, with representative curves bolded, and (G) strain at 20 N applied load. $N = 10$ per group for the unmodified sutures and for the porous sutures. Overbars and asterisks denote statistically significant differences ($^{*}p < 0.05$, $^{**}p < 0.01$, $^{***}p < 0.001$, $n = 10 - 11$). Mechanical properties of repairs with porous sutures were modestly decreased and similar to historical control data [108, 256].

surgeon when passing sutures through tendon was qualitatively lower during *in vivo* experiments using porous sutures coated with CTGF/HBDS than it was during *ex vivo* experiments with uncoated porous sutures.

Measurement	Unit	Mean ± Standard Deviation		95% Confidence Interval	Percent Change
		Unmodified	Porous		
Load creating a 2 mm gap	N	70.0 ± 15.5	54.9 ± 6.1	[-20.6, -9.7]	- 22%
Maximum load	N	82.8 ± 10.6	74.1 ± 8.0	[-17.6, +0.1]	N.S.
Rigidity	N/(mm/mm)	419 ± 73	316 ± 51	[-163, -44]	- 25%
Resilience	N·(mm/mm)	9.1 ± 2.4	8.5 ± 4.1	[-3.6, +2.5]	N.S.
Strain created by a 20 N load	%	7.81 ± 1.47	9.11 ± 1.15	[+0.07, +2.55]	+ 17%

Table 4.1: Mechanical properties of 8 stranded Winters-Gelberman flexor digitorum profundus tendon repairs with unmodified sutures or porous sutures. N.S.: Not significant.

Adhesive-coatings on porous sutures: After demonstrating mechanical properties comparable to conventional sutures, porous sutures were evaluated for adhesive delivery capacity in idealized single strand biomechancial tests. While this pilot study did not include sufficient numbers of samples to see statistical significance ($n = 4$ for Loctite 4903 and $n = 3$ for catechol derived adhesives, per group), porous sutures had higher average suture pullout loads trending toward significance for both adhesive types (Figure 4.6).

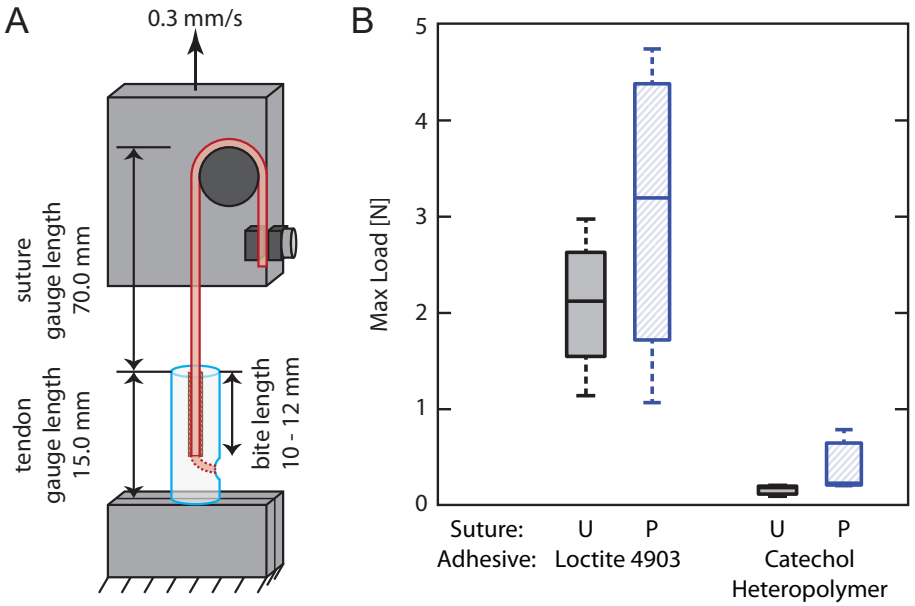

Figure 4.6: Tensile mechanical testing of the unmodified (U) and porous (P) sutures in single strand adhesive pullout tests from canine flexor digitorum profundus tendon repair. (A) mechanical testing schematic, (B) maximum load for Loctite 4903 and catechol heteropolymer tests. $N = 4$ per group for the Loctite 4903 samples and $n = 3$ per group for catechol heteropolymer samples.

CTGF Soaking Concentration	Precipitate Formation
10 µg/mL 20 µg/mL	No visible precipitate
30 µg/mL	Very slight precipitate, disappeared within 1–2 seconds
40 µg/mL	Definite precipitate, disappeared after 5–10 seconds
50 µg/mL	Most, but not all, precipitate re-dissolved over time
100 µg/mL	Substantial precipitate did not re-dissolve

Table 4.2: Precipitate formation in loading buffer containing fibrinogen + CTGF/HDBS components.

4.4.2 *Ex vivo* CTGF loading and release

A major objective of this study was to increase suture's adhesive binding capacity and biofactor loading capacity to drive a biological effect. To evaluate potential for sustained release of biofactors from porous modified sutures, sutures were loaded with various concentrations of CTGF in a heparin/fibrin based sustained delivery system (HBDS; 10, 20, 30, 40, 50, 100 µg/mL CTGF soaking concentration). Sutures demonstrated sustained release of CTGF over at least 14 days *in vitro* (Figure 4.7). Loading capacity was partially limited by CTGF and HBDS component precipitation when higher concentrations were used during loading (Table 4.2). Therefore, while the CTGF loaded into the soaking buffer progressively increased with each subsequent concentration, the effective concentration decreased when precipitate formed above $\approx$ 30 µg/mL CTGF. The maximum CTGF release was observed from porous suture segments loaded with 30 – 50 µg/mL CTGF/HBDS solution, where precipitate formation was limited but the loading concentration was still high. All samples in the 30 — 50 µg/mL CTGF loading concentration range yielded consistent release profiles. Therefore, 30 µg/mL was selected for *in vivo* experiments to minimize any unintended effects from precipitate formation. Porous sutures loaded in 30 µg/mL CTGF/HBDS demonstrated burst release of 0.50 – 1.50 $\frac{\text{ng CTGF}}{(\text{cm suture})(\text{day})}$ for the first few days, followed by sustained release of approximately 0.15 $\frac{\text{ng CTGF}}{(\text{cm suture})(\text{day})}$ through day 14. Since approximately 70 mm of suture is delivered within 3 mm of the repair site in the traversing strands and the terminal knot, this release level corresponded to concentrations of 60 – 150 ng/mL daily burst delivery and 10 – 20 ng/mL daily sustained release from suture within 3 mm of the tendon laceration site.

4.4.3 *In vivo* biological effects of CTGF-laden porous sutures

Flexor digitorum profundus tendon transections and repairs were performed with porous modified sutures loaded with 0 or 30 µg/mL CTGF in HBDS. CTGF delivery within the repaired flexor tendon was achieved without adhesion or

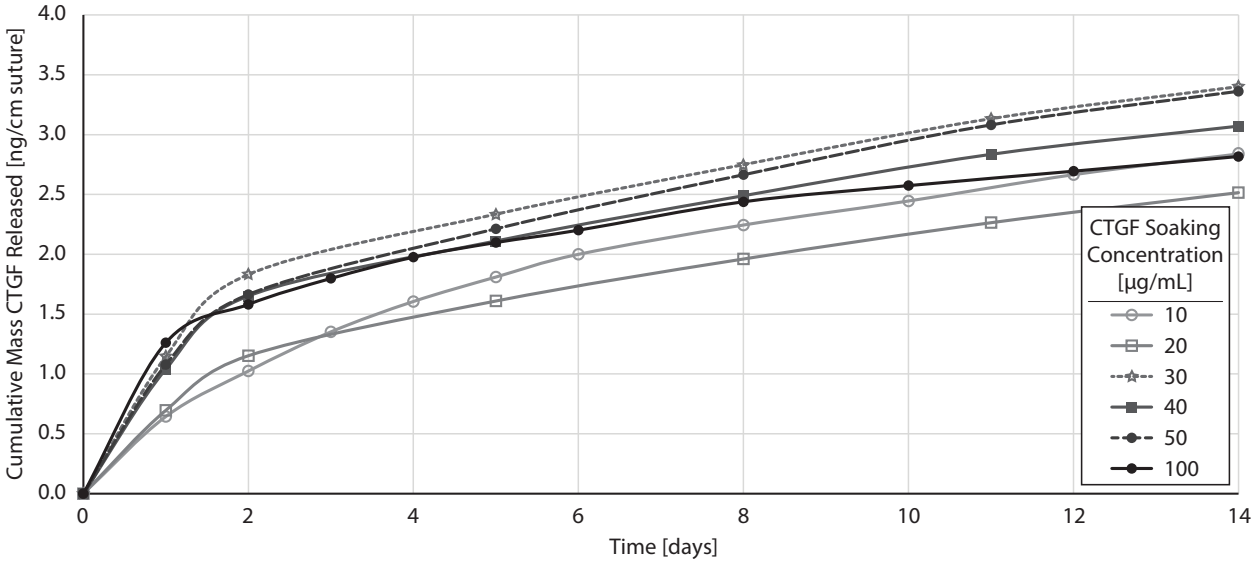

Figure 4.7: Cumulative CTGF release profiles for porous sutures loaded with a range of CTGF soaking concentrations (10–100 µg/mL) within a heparin/fibrin-based delivery system (HBDS), *in vitro* ($n = 2$ per group, averaged). Porous sutures loaded with HBDS + CTGF showed an initial burst followed by sustained release over the first 14 days. The 30 µg/mL CTGF group was the highest loading concentration that did not form precipitate in solution.

repair-site gap formation upon dissection at 14 days in the CTGF$^+$ group. In one of the 20 repaired tendons, a > 3.0 mm gap was noted (CTGF$^-$ group, histological sample), and was therefore excluded along with the paired tendon. There were no macroscopic indicators of inflammation or other deleterious effects at 14 days, such as wound dehiscence, pus formation, swelling in the digit and tendon sheath, blood within the sheath, or redness on the volar tendon surface. There were no or only very mild adhesions. This result positively contrasts with our historical experience, where canine flexor tendon repairs are highly sensitive to inflammatory stimuli [57, 186].

Histological assessment with H&E demonstrated high quality repairs with little difference between groups at low magnification (Figure 4.8, top). However, normalized cell counts under higher magnification demonstrated increased cellularity immediately surrounding the suture tracks (within 70 µm, Figure 4.8C–F, quantified in Figure 4.8G, p = 0.022 for CTGF effects and p = 0.003 for position effects, $n = 3$ per group), especially at the repair interface. There were also higher cell counts far from the repair interface in each of the three CTGF$^+$ samples than their paired CTGF$^-$ controls, though the variability precluded post hoc significance (Figure 4.8G). Pentachrome stains [376, 377] demonstrated increased staining for new collagen (yellow) instead of mature collagen (red) in CTGF$^+$ samples than CTGF$^-$ controls, both at a macroscopic level and near the suture surface (Figure 4.9A–D). Reticular staining indicated likely angiogenesis surrounding CTGF$^+$ sutures far from the repair interface (Figure 4.9H). While CD146 staining did not show apparent differences between groups (Figure 4.S1), we note that it is challenging to see differences with this

staining method since TSPCs are rare *in vivo*, and $< 1\%$ of isolated tendon cells stain for CD146 [223]. Many, but not all, cells near CTGF$^+$ suture surfaces stained for Ki67, while few cells stained for Ki67 near CTGF$^-$ suture surfaces (Figure 4.S2). This Ki67 staining pattern indicates that the increased cellularity near the CTGF$^+$ suture surface was likely due to a combination of increased cell migration and cell proliferation.

TEM images showed cell activity immediately adjacent to the CTGF$^+$ suture, with a clear layer of glycoproteins surrounding the CTGF$^-$ suture (Figure 4.10A,C) but not the CTGF$^+$ suture (Figure 4.10B,D). Collagen fibrils adjacent to the CTGF$^+$ suture were 33% smaller and 23% closer to their nearest 10 neighboring fibrils than fibrils near CTGF$^-$ suture, on average ($p < 0.001$ for both measures). The smaller, more densely packed collagen fibrils near CTGF$^+$ suture are indicative of newly synthesized collagen or a different collagen subtype compared to CTGF$^-$ control repairs (Figure 4.10E). CTGF-laden sutures also had some sites where collagen appeared to be penetrating the porous suture surface (Figure 4.10D, arrows).

Gene expression did not demonstrate large differences between CTGF$^+$ sutures and CTGF$^-$ control porous sutures, each normalized to contralateral non-operated tendons (Figure 4.11). There were 64% (N.S.), 52%, and 52% (N.S.) increases in the expression fold change of the monocyte/macrophage M2 marker *CD163*, the anti-inflammatory cytokine *IL10*, and the anti-apoptotic factor *BCL2L1*, respectively, due to CTGF. There were 24% and 19% (N.S.) decreases in the expression fold change of collagen 2 and *IL6*, respectively. However, despite this anti-inflammatory and anti-apoptotic gene expression increase, expression levels of collagen 1 and 3 and tenogenic markers scleraxis and tenomodulin were similar between groups. There were no significant differences in the expression of the matrix metalloproteinase *MMP9* or the cytokine related genes *IL1-RN* or *IL4*.

Proteomics analysis identified 512 proteins from normal and suture repaired flexor tendons. Compared to normal tendons, the relative abundances of 129 proteins were modified after tendon injury and suture repair in the presence or absence of CTGF, while no apparent differences in protein abundances were detected between the two suture treatments. Consistently, principal component analysis separated normal tendons from sutured tendons, but did not separate treatment groups with and without CTGF according to the first three principal components (Figure 4.12). Further characterization of the 129 modified proteins using the Panther Classification System revealed the function of 108 proteins (Table 4.S1 and Table 4.S2). Only a small percentage of proteins were engaged in immune system processes (4.9%) and biological adhesion (2.5%) that potentially impact tendon healing. There were no differences in inflammatory protein levels (e.g., NCF2, PTGR1, SOD3) between the tendons repaired with CTGF$^+$ or CTGF$^-$ porous sutures and historical repair-only controls with unmodified suture [373].

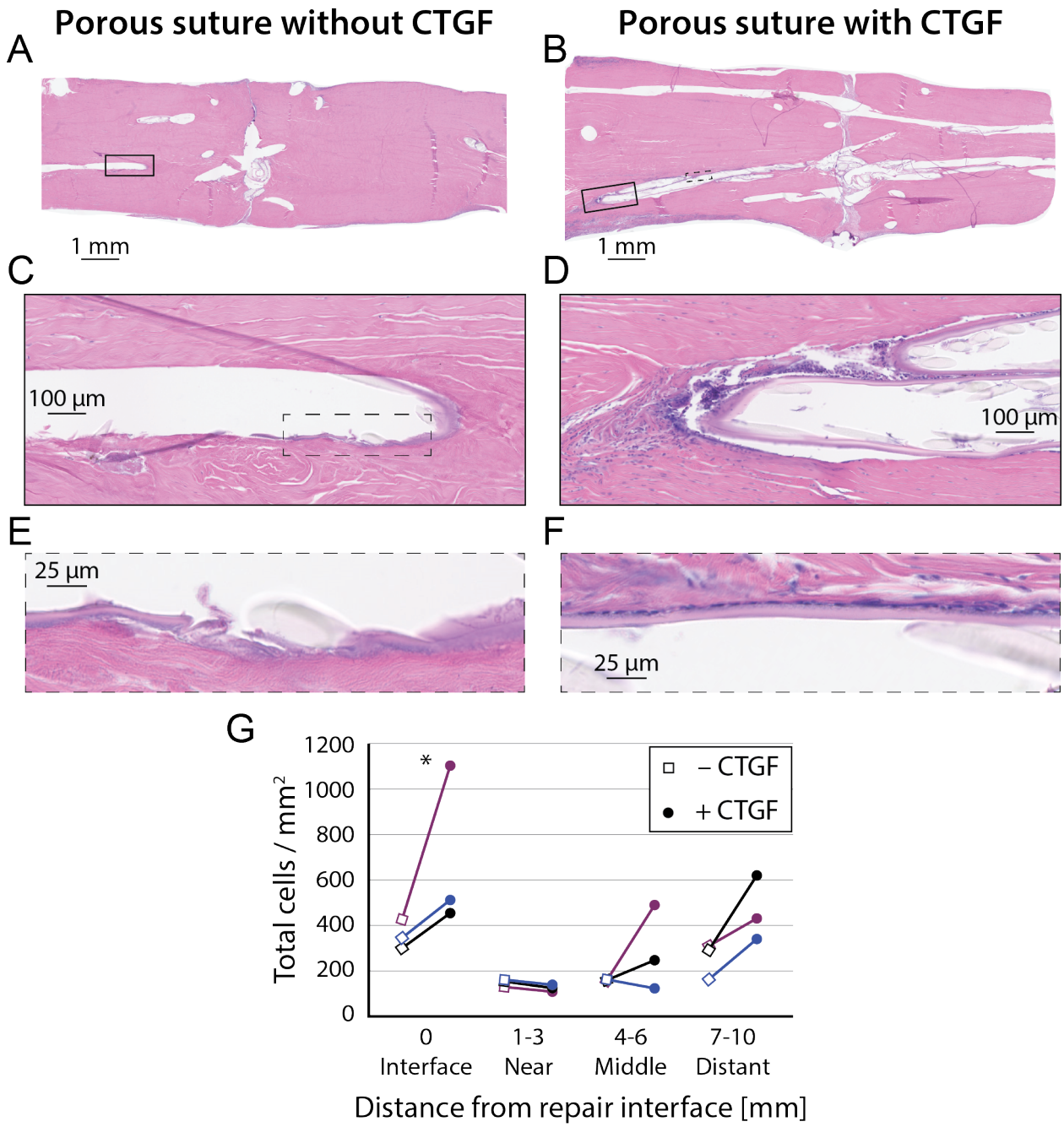

Figure 4.8: Histologic sections from canine FDP tendon 14 days after surgery with porous suture controls (A,C,E, no CTGF) or sutures containing CTGF (B,D,F), stained with H&E. (G) Normalized cell counts within 70 µm of the suture surface or within the repair interface region for paired samples. CTGF and position had significant effects on cell activity in the local region near the suture, as determined by 3-way ANOVA. $^*p < 0.05$ by Fisher's least significant difference post hoc analysis ($n = 3$ per group).

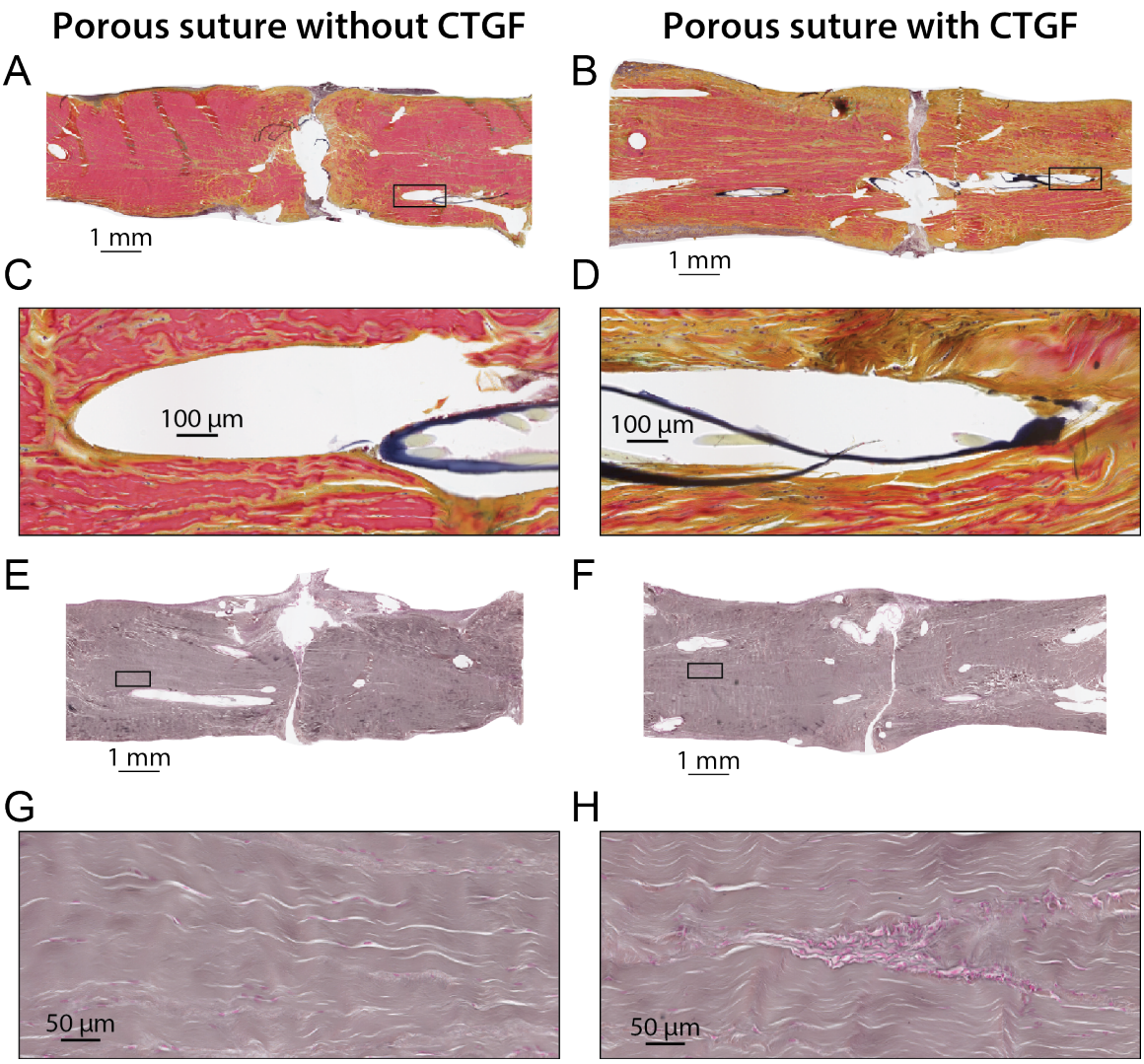

Figure 4.9: Histologic sections from canine FDP tendon 14 days after surgery with porous suture controls (A,C,E, no CTGF) or sutures containing CTGF (B,D,F), stained with pentachrome stain (A–D) or reticular stain (E–H). Tendons repaird with CTGF-laden sutures had increased staining for new collagen (yellow pentachrome stain) and evidence of likely capillary formation (reticular stain) throughout the tissue, especially adjacent to the suture. (H) The accumulation of cells in a cylindrical pattern in the tendon midsubstance is atypical for the avascular zone of flexor tendons, suggesting angiogenesis. (C,D,G,H) are 10× higher power views of the whole-tendon slides above them (A,B,E,F, respectively). Sections (A,E and B,F) were paired repairs from the same animal.

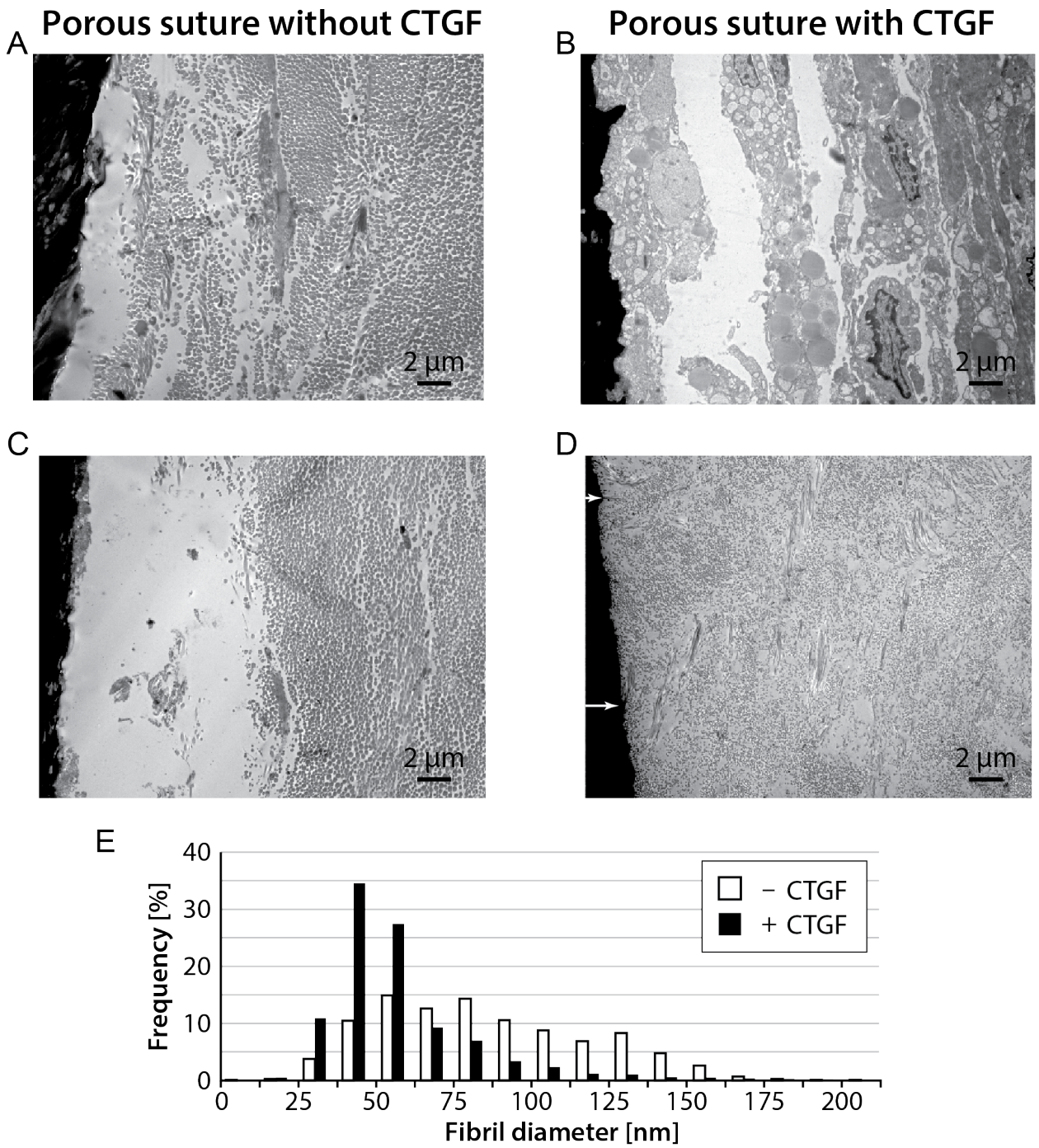

Figure 4.10: Transmission electron microscopy images of canine FDP tendon 14 days after surgery. Sutures appear black on the left side of each micrograph. (A,C) Porous suture controls lacking CTGF had large collagen fibrils anda clear glycoproteinaceous layer next to the suture. (B,D) CTGF-laden porous sutures induced increased cellular responses (B) and decreased collagen fibril size (D) compared to controls. (E) Histogram of collagen fibril diameters, combining $n = 3$ representative TEM images per group. CTGF-laden porous sutures induced a 33% decrease in average fibril diameter surrounding the suture ($p < 0.001$, $n = 2$ tendons per group).

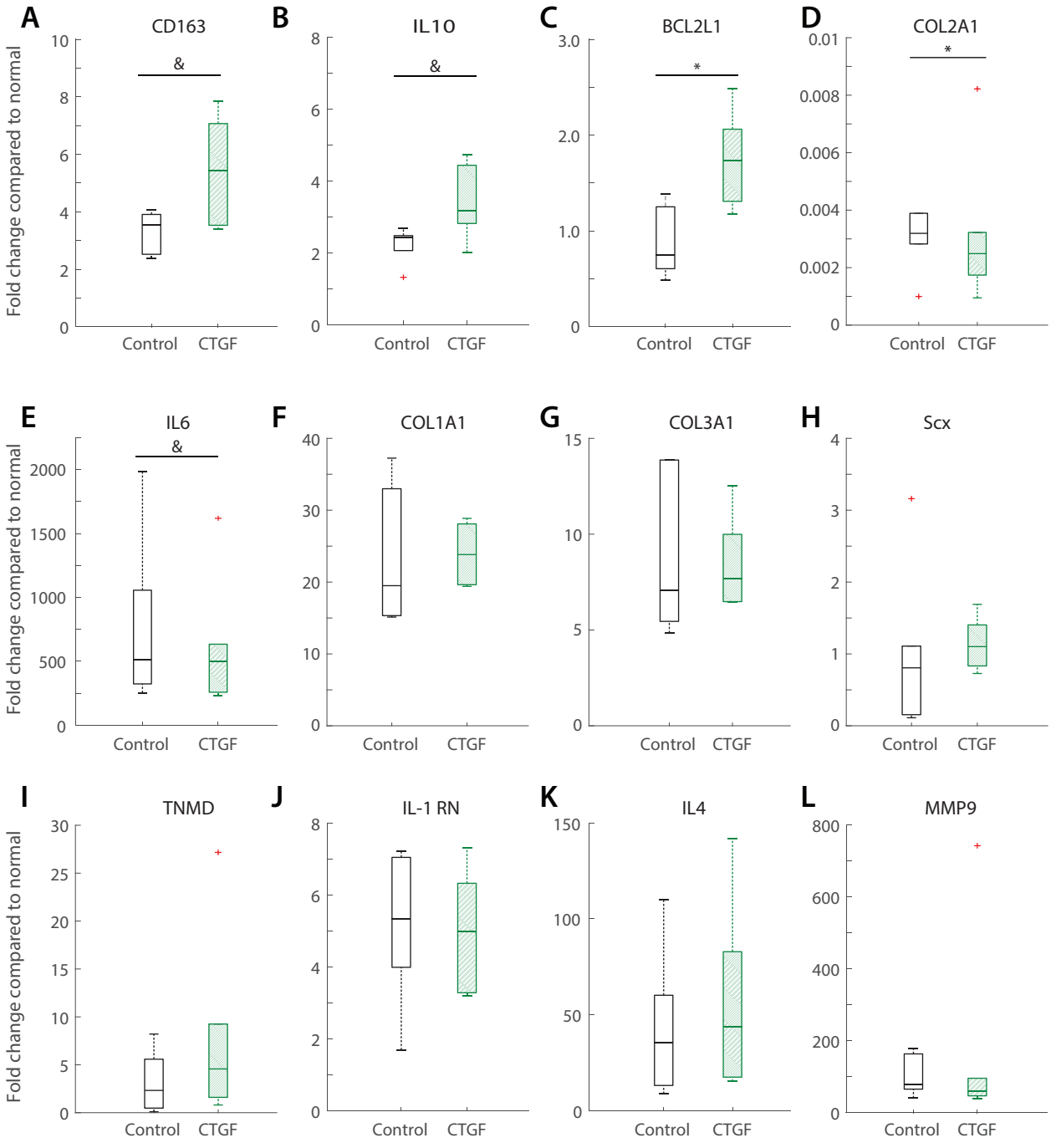

Figure 4.11: Gene expression fold changes in repaired tendons using porous suture loaded with or without CTGF compared to normal, non-operated contralateral digits for (A) macrophage/monocyte marker *CD163*, (B) anti-inflammatory cytokine *IL10*, (C) anti-apoptitic factor *BCL2L1*, (D) extracellular matrix protein *COL2A1*, (E) cytokine *IL6*, extracellular matrix proteins (F) *COL1A1* and (G) *COL3A1*, tenogenic markers (H) *Scx* and (I) *TNMD*, cytokines (J) *IL1RN* and (K) *IL4*, and (L) matrix metalloproteinase *MMP9*. $^{*}p < 0.05$, $^{\&}p < 0.1$ between groups by Wilcoxon signed-rank test ($n = 6$ per group).

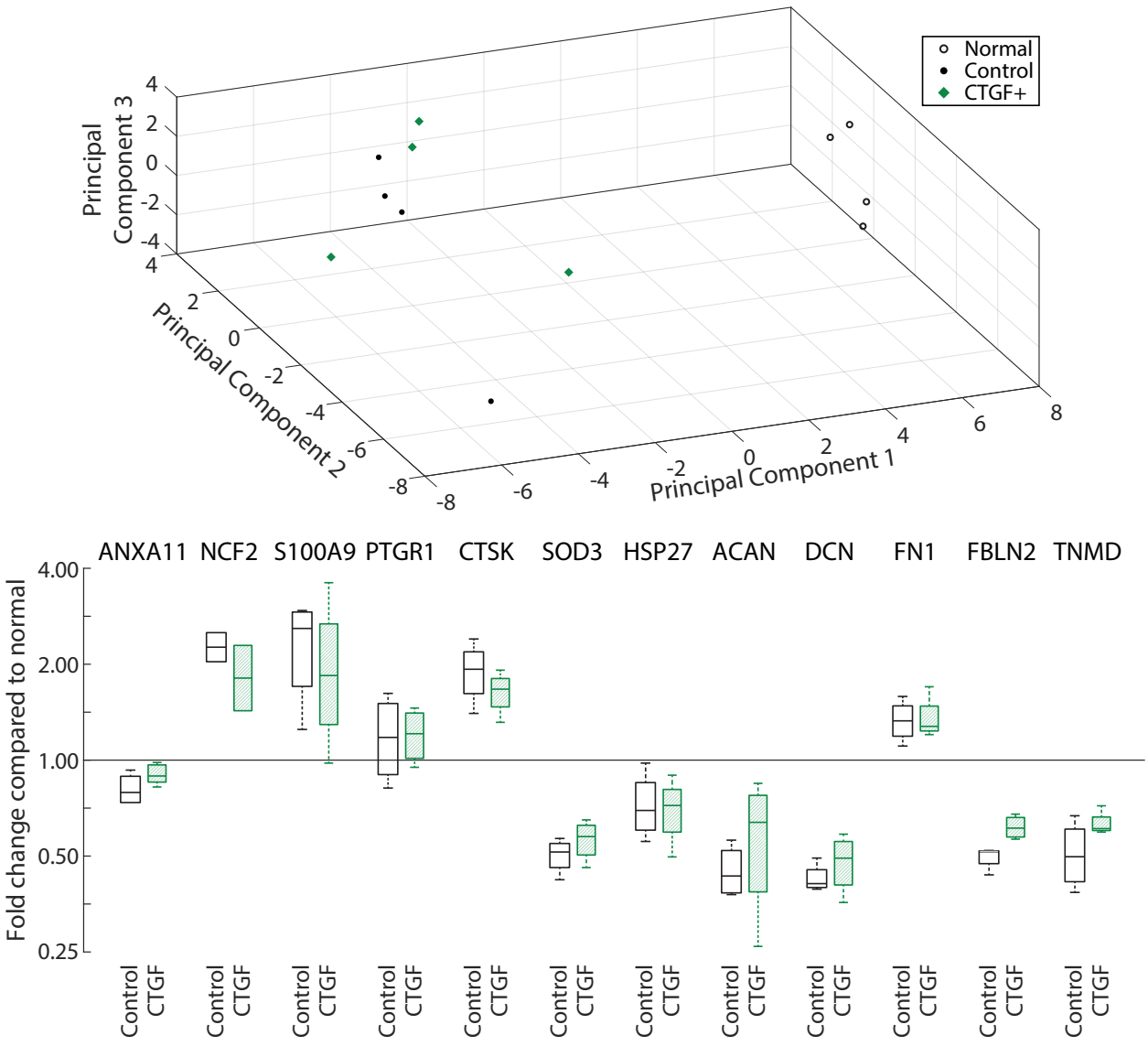

Figure 4.12: Protein expression principal component analysis (top) and fold changes compared to normal, non-operated contralateral digits (bottom, note log scale). Inflammatory proteins: ANXA11 = annexin A11; NCF2 = neutrophil cytosol factor 2; PTGR1 = prostaglandin reductase 1; CTSK = cathepsin K, SOD3 = superoxide dismutase 3; HSP27 = heat shock protein 27. Extracellular matrix proteins: ACAN = aggrecan; DCN = decorin; FN1 = fibronectin 1; FBLN2 = fibulin 2. TNMD = tenomodulin. *There were no significant differences in protein expression ($n = 4$ per group).

4.5 Discussion

While adhesive coatings on sutures have potential to reduce stress concentrations and improve load tolerance of soft tissue repairs, e.g., tendon repairs (Chapter 2), current sutures are not designed to facilitate adhesive binding. Existing approaches to coat sutures with antimicrobial agents or growth factors yield thin layers that are usually weakly bound to the suture and may be stripped off the suture with passage through tissue. Here, we developed and implemented sutures with micrometer-sized porous outer sheaths to aid adhesive binding and biofactor delivery (Figure 4.2). Porous sheaths simultaneously allow adhesive interdigitation with suture, likely toughening the interface [80], and increase the surface area available for binding. This approach enables adhesive to directly contact the load-bearing elements of the suture by penetrating through pores into the voids between inner filaments.

Furthermore, the porous structure provides an opportunity for delivery of growth factors, which can stimulate tissue ingrowth into the suture during healing in a process similar to strategies using porous structures for abdominal hernia repair [378, 379] and bone implants [380, 381, 359, 382]. Tissue ingrowth into suture should have a strengthening effect on the repair by facilitating load transfer between suture and the surrounding tissue along the suture length, following a similar mechanical principle to adhesive coatings. Sutures have several additional attractive properties for growth factor delivery in tendon repair. First, they are commonly used in conventional repairs and therefore do not require additional material that could damage tissue or cause inflammation. Second, the suture strands and knot reside within the tendon midsubstance and the repair interface, where growth factors may directly stimulate cell migration, differentiation, and matrix synthesis. Third, neovascularization and cell infiltration within tendon has been shown to occur along suture tracks [383], so growth factor delivery along these tracks may accelerate and guide these processes. Over the last two decades, several experiments have evaluated growth factor delivery on sutures for intrasynovial flexor tendon [384], Achilles tendon [385, 386], and rotator cuff tendon [367] repair, with mixed preliminary success. None of these approaches have progressed to clinical use. Prior approaches have focused on coating the surface of a solid suture with growth factors. Solid suture, however, has limited surface area and exposes the growth factor directly to the surrounding tissue. As a result, bolus release of growth factor typically occurs within a few hours to days following application [367, 365, 366, 387]. Furthermore, the growth factor dose is markedly limited since the thin coatings contain very low volumes. In addition, thin surface films are often weakly bound, so growth factor are easily stripped off of the suture during implantation [353]. Despite these challenges, suture remains a promising delivery approach, provided that methods can be developed for the administration of increased dosages over sustained time-courses following repair.

This work demonstrates a simple, versatile approach to modify currently existing suture materials to improve lateral surface area for adhesive binding. One key requirement for this approach is that the modification does not reduce the strength of the suture material or the surgical repair. Nylon sutures, modified with porous outer sheaths, retained sufficient mechanical properties for surgical use, as demonstrated by non-inferiority compared to commercially available sutures in biomechanical assessments of single suture strands (Figure 4.4). The mechanical properties of clinical-style repairs using porous sutures were reduced by some measures but still within 25% of controls (Figure 4.5). This difference is partially attributable to surgeon-to-surgeon variability, given that the mechanical properties of porous suture repairs were non-inferior to controls using the same techniques for other studies (Chapter 2, Appendix A). The modestly altered mechanical properties were sufficiently close to controls and non-inferior to historical data elsewhere in this thesis to assuage concerns over surgical implementation. The time zero biomechanics results described here are sufficient to withstand passive range of motion and normal hand function (approximately 35 N) [375] throughout the healing process. Importantly, only one tendon out of twenty had gapping (5%, in the CTGF^{-} group), despite our previous experience of $\sim$15% rupture rates in this model (and clinically) when using regular sutures [186, 373].

In order to demonstrate the ability of porous sutures to carry and deliver relevant factors (e.g., adhesives, growth factors), sutures were first loaded with small molecule (rhodamine B) or large protein (BSA-FITC) dyes encapsulated in fibrin-network gels (Figure 4.3). Dyes penetrated through the interconnected pores in the outer sheath of suture, into the voids between the inner suture fibers. This increased loading capacity by several-fold compared to unmodified sutures, where dyes only surrounded the outer sheath. Porous sutures were then compared to unmodified sutures for adhesive delivery. The pilot experiment performed here did not include sufficient numbers of samples to make strong statistical comparisons ($n = 3$ and $n = 4$), but the porous sutures did display a higher average suture pullout load for both adhesive types tested (Figure 4.6). It is important to note that while porous sutures can increase adhesive delivery and interfacial strength, these idealized pilot mechanical tests are somewhat challenging to interpret since the increased surface area inherently increases friction and pullout force compared to unmodified suture. This surface area effect on friction would be particularly notable for tests of adhesives bearing low loads. Furthermore, if the adhesive-coated suture fails instead within the adhesive bulk or at the interface with tendon, then the single strand tests would not be sensitive to increases in adhesive–suture interfacial strength.

In addition to being used to evaluate chemical adhesive delivery, porous sutures were impregnated and coated with a sustained delivery system [195, 155] to deliver CTGF. CTGF has been shown to stimulate extracellular matrix production [223, 209], acting as a biological "adhesive coating" analog to improve the interaction between suture and tendon and to promote healing generally. CTGF has been shown to improve tendon repair outcomes in a rat patellar

tendon model [223, 209]. CTGF acts by stimulating $CD146^{+}$ tendon progenitor cell proliferation and inhibiting inflammation. This stem/progenitor cell proliferation leads to additional aligned collagen matrix production during the proliferative stages of repair. In this study, porous sutures soaked in 30 µg/mL CTGF/HBDS demonstrated maximal growth factor release, sustained over at least 14 days (Figure 4.7). Approximately 70 mm of suture is estimated to be within 3 mm of the transection and repair site, based on repairs containing 8 suture strands plus the suture length contained in the terminal surgical knot, which is buried in the repair at the interface between tissues. This suture length is sufficient to deliver a burst of 60 – 150 ng CTGF/mL tendon volume within 3 mm of the repair site, followed by sustained release over the first 14 days of approximately 10 – 20 ng CTGF/mL tendon volume, which is at the lower end of the effective range used *in vitro* [209].

The promising *ex vivo* mechanical and biological characteristics of the porous sutures encouraged us to assess their efficacy in a clinically relevant *in vivo* canine flexor tendon repair model. The porous sutures, with and without growth factor, did not elicit an inflammatory response at 14 days following surgical repair based on histological, gene expression, and proteomics evaluations. Based on historical experience with this animal model, proteomics has been particularly sensitive for identifying inflammatory effects [186, 199, 373]. The lack of significant differences in inflammatory protein markers between porous suture groups with and without CTGF and historical controls using unmodified suture indicates that this porous suture delivery approach is non-inflammatory and not deleterious to the repair. This safe, targeted, sustained delivery approach represents a significant improvement compared to previous growth factor delivery strategies for tendon repair [186, 208, 345].

Histological assessment provided encouraging indications of local biological effects around the suture surface in the $CTGF^{+}$ group. Cell numbers increased at the repair interface and along the suture track of CTGF-laden sutures, indicating increased local cell migration and/or proliferation (Figure 4.8, Figure 4.S2). The most pronounced cellular effect along the suture strand-tendon interface was in regions distant from the repair site. This pattern was expected based on typical neovascularization patterns following intrasynovial flexor tendon repair: since the canine lacks a vinculum longum and the repair was performed in the middle of a 3 cm avascular zone, neovascular ingrowth occurs progressively from the proximal and distal stumps toward the repair interface [383]. Furthermore, CTGF was delivered along the entire length of the suture, so we expect effects both at the repair site where the suture knot is buried and along suture distant from the repair interface. Pentachrome and reticular stains also indicated increased collagen production and angiogenesis in areas adjacent to the CTGF-laden porous sutures compared to porous sutures without CTGF (Figure 4.9). Light and transmission electron microscopic sections provided evidence of cellular alignment along the suture surface and possible tissue ingrowth into the porous suture structure (Figure 4.8, Figure 4.9, and Figure 4.10).

Tissue ingrowth into porous structures for abdominal hernia repair [378, 379] and bone implants [380, 381, 359, 382] has been shown to strengthen the repair. Similarly, tissue ingrowth into suture would have a strengthening effect on tendon repair by facilitating load transfer between suture and the surrounding tissue along the suture length.

There are several limitations to this study of *in vivo* CTGF delivery on porous sutures. It is possible that the CTGF dosage we employed was insufficient to induce a substantial effect throughout the healing tendon. We performed a dose-response study and selected the loading concentration that led to the greatest *in vitro* CTGF release. Despite dose maximization, *in vitro* CTGF release was at the lower end of a biologically effective range in culture. Potential opportunities for increasing CTGF effects include increasing the suture pore size in order to create greater capacity within the suture sheath, developing an alternative sustained release system to achieve higher loading yield, or utilizing a modified version of CTGF. Effective CTGF levels are determined not only by flux into the tendon, but also by clearance out of the tissue (half-life) and by potency of the released growth factor. Similarly, protein engineering approaches to modify the binding site may generate a CTGF protein drug with higher binding affinity to the cell surface receptor and more potent effect. The delivery approach could be revisited using an alternative growth factor, though side effects from pleiotropic growth factors require careful monitoring. Finally, this study evaluated effects at a time point within the proliferative stage of repair. The biological effects seen locally around the suture may induce a larger effect over time as those cells continue to proliferate and produce matrix. While 14 days may be too short for functional outcome measurement in this clinically relevant model, it does provide data that encourages functional biomechanical assessment at later time-points.

While porous sutures offer benefits for adhesive or biofactor binding and delivery, as well as opportunities for tissue ingrowth, there are several potential limitations that need to be further assessed before clinical use. First, surgical handling challenges while passing the higher friction suture may lead to additional, unnecessary tissue damage during repair. While uncoated porous sutures have high surface area for adhesive binding and generate high friction when passed through tissue, the coating decreases the effective surface area and smooths the surface to nearer the level of a conventional suture. Future work should assess the level of friction of unmodified, uncoated-porous, and coated-porous suture strands passing through tendon tissue, similar to the single-strand biomechanical tests in (Chapter 2). Second, the increased surface area of polyfilament sutures compared to monofilament sutures may increase inflammatory effects and bacterial adhesion. Porous sutures may therefore increase infection risk, especially if used in stitches that contact the skin, epithelial, or mucosal surfaces, analogous to the infection dangers of the original intrauterine devices due to polyfilament strings enabling bacterial migration into the uterus. This infection risk is less of a concern in internal, sterile environments such as those for tendon repairs. Furthermore, the lack of detectable inflammation argues

against clinical impact of these concerns. Third, adhesive infiltration into the voids between inner suture strands could deleteriously stiffen sutures, limiting surgical handling ability. This potential effect will need to be evaluated with particular adhesive and suture combinations prior to clinical use. Despite these concerns, this approach for generating sutures with porous outer sheaths remains promising for delivery of adhesives, biofactors, or combinatorial therapies directly into repair sites without introducing additional foreign materials or surgical defects.

4.6 Conclusion

In this chapter we developed sutures with porous outer sheaths in order to deliver adhesives for mechanical benefit, biofactors to modulate the healing response, or combinatorial therapies including both adhesives and biofactors. The mechanical properties of these sutures are comparable to unmodified sutures. Future studies are needed to directly apply bioadhesive materials, such as those developed in Chapter 3, to sutures with porous sheaths. This chapter demonstrated the first *in vivo* use of a new approach to deliver biologically active factors into the repair site, successfully mitigating the inflammatory concerns that were noted with prior biofactor delivery approaches [388, 167, 186]. While whole-tendon biological effects were not seen in this experiment, the findings noted here showed encouraging local biological effects that warrant future investigation to increase biofactor delivery from suture with porous outer sheaths. This simple, versatile suture modification method is a general technique that can enhance suture functionality without compromising mechanical properties. This delivery approach can be applied to different suture types, tissue repairs, or biofactors. Indeed, porous sutures may facilitate improved binding and loading capacity of coated materials for local delivery of antimicrobial factors, anti-inflammatory factors, anti-coagulant factors for vascular repair, or other biologically active factors in a wide array of surgical applications.

4.7 Acknowledgements

Dr. Jianhua Li and Ms. Zifei Sun modified nylon sutures to create porous outer sheaths. The Washington University Musculoskeletal Histology and Morphometry Core, Molecular Microbiology Imaging Facility, Genome Technology Access Center, and Proteomics Core Laboratory assisted with assessing outcomes following surgical repair. This work was supported by National Institutes of Health grants R01-AR062947 (to RHG, ST, and SSE), F30-AR069491 (to SWL), and a Washington University Musculoskeletal Research Center Translational Research Award (NIH P30-AR057235).

4.8 Supplemental Material

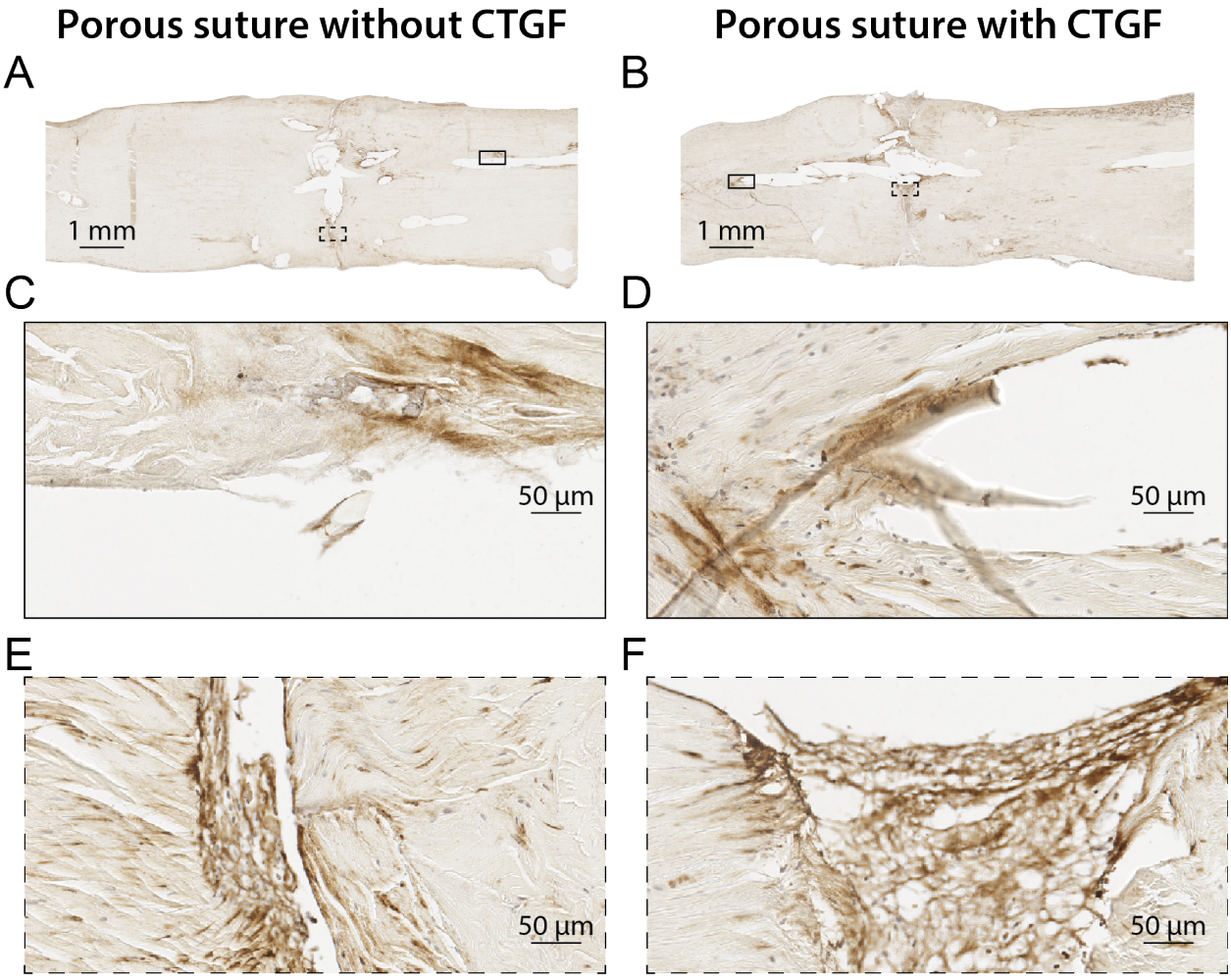

Figure 4.S1: Histologic sections from paired canine FDP tendons 14 days after surgery with porous suture controls (A,C,E no CTGF) or sutures containing CTGF (B,D,F), immunohistochemically stained for CD146. Higher magnification sections near suture (C,D) and at the repair interface (E,F) exhibit mostly nonspecific staining of tissue stroma instead of specific staining of individual cells. There were no apparent differences between groups. However, it is challenging to see clear differences with this staining method since TSPCs are rare *in vivo*, and $<1\%$ of isolated tendon cells stain for CD146.

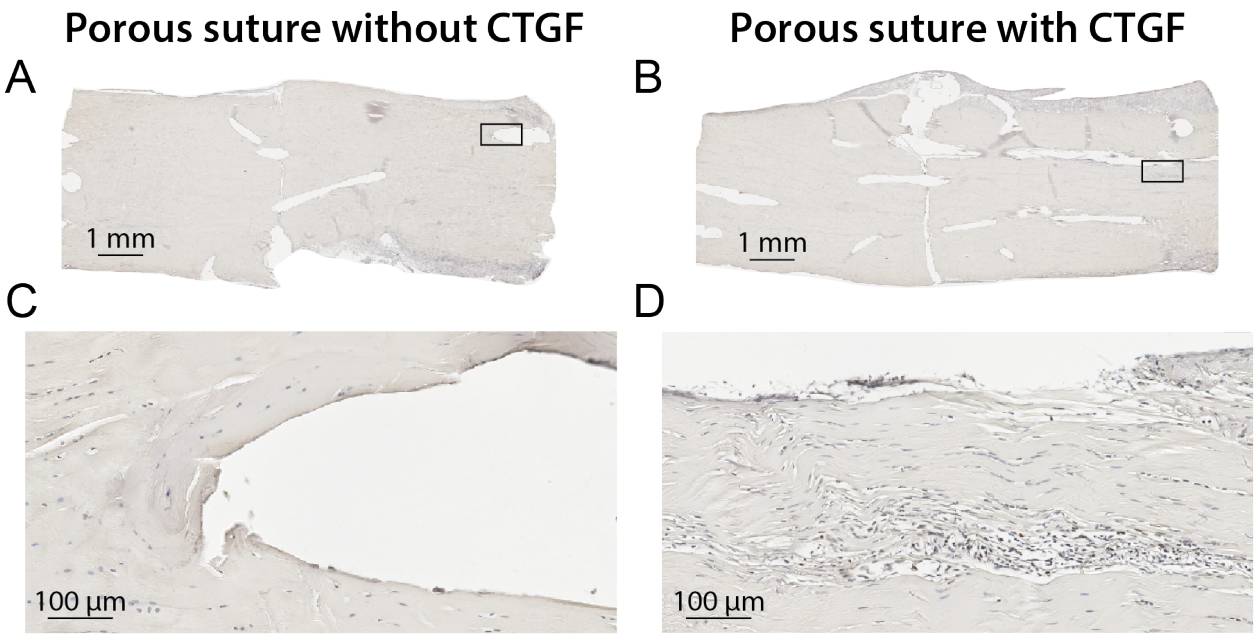

Figure 4.S2: Histologic sections from paired canine FDP tendons 14 days after surgery with porous suture controls (A,C, no CTGF) or sutures containing CTGF (B,D), immunohistochemically stained for Ki67. There was increased cellularity near CGTF^{+} sutures compared to controls, consistent with quantified cell counts from H&E stains (Figure 4.8G). In addition, many cells near CTGF^{+} suture surfaces stained positive for Ki67 (D), while few cells near CTGF^{-} sutures stained for Ki67 (C). Since many, but not all, cells near CTGF^{+} sutures stained positive for Ki67, the increased cellularity near the suture surface was likely due to a combination of increased cell migration and cell proliferation.

[CTGF$^-$ control]: unique	[CTGF$^+$]: unique	[CTGF$^-$ control] and [CTGF$^+$]:	
E2QSZ5_CANLF	J9NYX1_CANLF	G1K267_CANLF	F1PR66_CANLF
E2RQ14_CANLF	RS3_CANLF	E2QWN7_CANLF	J9PBN6_CANLF
B4YY02_CANLF	F1PIC7_CANLF	F1PRU3_CANLF	F1PQN5_CANLF
F1PKX2_CANLF	PEBP1_CANLF	Q5W425_CANLF	F1Q1H3_CANLF
E2RD95_CANLF	E2R4J1_CANLF	E2RNR0_CANLF	F6XIK8_CANLF
E2QUY2_CANLF	E2RGQ5_CANLF	F6V234_CANLF	J9NVC6_CANLF
E2R7T5_CANLF	F1P6P2_CANLF	PGS2_CANLF	J9P1J5_CANLF
J9NYC0_CANLF	F6V790_CANLF	F6Y3P9_CANLF	E2RAL0_CANLF
F6XWS5_CANLF	F1Q129_CANLF	F1P9U4_CANLF	J9NTG7_CANLF
E2RL80_CANLF	F1P790_CANLF	F1PHK9_CANLF	F1PIJ6_CANLF
F1P6B7_CANLF	E2RD86_CANLF	F1Q432_CANLF	F1PQM7_CANLF
E2R416_CANLF	F1Q3Y0_CANLF	F1PEK5_CANLF	E2RLY5_CANLF
F1PMH6_CANLF	FRIL_CANLF	LMAN2_CANLF	F1PFM6_CANLF
F1PSS2_CANLF	F6XRY2_CANLF	E2R0T6_CANLF	E2R612_CANLF
F1PFZ5_CANLF	MYH9_CANLF	F1PLN5_CANLF	F1PTL1_CANLF
A0A097HUC9_CANLF	F1P7Y6_CANLF	E2QRS3_CANLF	F1PB08_CANLF
F1PXT8_CANLF	J9P923_CANLF	E2RSI6_CANLF	E2QU08_CANLF
F1PKX3_CANLF	E2RIV1_CANLF	E2RJE0_CANLF	E2R9R2_CANLF
J9NZK5_CANLF	F6V659_CANLF	F1PBI6_CANLF	F1Q133_CANLF
J9P8M2_CANLF	E2RLA2_CANLF	MYOC_CANLF	F1PLV6_CANLF
F1P679_CANLF	ENPL_CANLF	E2R5B9_CANLF	F1P975_CANLF
TPSN_CANLF	G1K2D8_CANLF	F2Z4Q7_CANLF	E2RB37_CANLF
E2R0I9_CANLF	E2RHM4_CANLF	E2RGD3_CANLF	F1PJP5_CANLF
E2RHY7_CANLF	E2QSF4_CANLF	F1PAS8_CANLF	E2R6K5_CANLF
Q4KKT6_CANLF	FRIH_CANLF	F1PR39_CANLF	E2QZA8_CANLF
J9P315_CANLF	J9NV93_CANLF	E2RC23_CANLF	F1PL97_CANLF
E2R2G1_CANLF	APOA1_CANLF	CATK_CANLF	H9GWB4_CANLF
E2RAN6_CANLF	E2R4L7_CANLF	E2RAP5_CANLF	F1Q147_CANLF
		A7E3K7_CANLF	E2QZ50_CANLF
		F1PGH3_CANLF	E2RNB0_CANLF
		F1PXG4_CANLF	F1PM26_CANLF
		F2Z4Q1_CANLF	E2R413_CANLF
		F1PW10_CANLF	F6UYJ9_CANLF
		E2RPQ6_CANLF	F1PPZ2_CANLF
		E2RSC5_CANLF	F1PEI2_CANLF
		F1PIA3_CANLF	F1PUX4_CANLF
		CATC_CANLF	
28	28	73	

Table 4.S1: Proteins expressed by only tendons in the CTGF$^-$ group, by only tendons in the CTGF$^+$ group, or by tendons in both groups.

Gene ID	Gene Name/ Gene Symbol	Panther Family/Subfamily	Panther Protein Class
F1PQN5_CANLF	Uncharacterized protein; CFL1; ortholog	Cofilin-1 (PTHR11913:SF17)	non-motor actin binding protein (PC00165)
A7E3K7_CANLF	Predicted NADPH oxidase-2; Nox2; ortholog	Cytochrome b-245 heavy chain (PTHR11972:SF60)	oxidase (PC00175)
F2Z4Q1_CANLF	40S ribosomal protein S4; RPS4X; ortholog	SUBFAMILY NOT NAMED (PTHR11581:SF3)	ribosomal protein (PC00202)
RS3_CANLF	40S ribosomal protein S3; RPS3; ortholog	40S ribosomal protein S3 (PTHR11760:SF9)	ribosomal protein (PC00202)
F1PIJ6_CANLF	Uncharacterized protein; PPA1; ortholog	Inorganic pyrophosphatase (PTHR10286:SF3)	pyrophosphatase (PC00196)
E2RLY_CANLF	Uncharacterized protein; LAP3; ortholog	Cytosol aminopeptidase (PTHR11963:SF30)	
F1PM26_CANLF	Uncharacterized protein; CD109; ortholog	CD109 antigen (PTHR11412:SF136)	expressed by CD34+ acute myeloid leukemia cell lines, T-cell lines, activated T lymphoblasts, endothelial cells, and activated platelets
E2RQ14_CANLF	Annexin;ANXA5; ortholog	Annexin A5 (PTHR10502:SF26)	
F1PJP5_CANLF	Uncharacterized protein; STT3A; ortholog	Dolichyl-diphosphooligosaccharide–protein glycosyltransferase subunit STT3A (PTHR13872:SF1)	glycosyltransferase (PC00111)
E2RAN6_CANLF	Uncharacterized protein; FBP1; ortholog	Fructose-1,6-bisphosphatase 1 (PTHR11556:SF11)	carbohydrate phosphatase (PC00066)
J9NVC6_CANLF	Uncharacterized protein; unassigned; ortholog	Ig heavy chain V-III region 23 (PTHR23266:SF204)	
FRIL_CANLF	Ferritin light chain;FTL; ortholog	Ferritin light chain (PTHR11431:SF47)	storage protein (PC00210)

continued on next page

continued from previous page

Gene ID	Gene Name/ Gene Symbol	Panther Family/Subfamily	Panther Protein Class
F1PIA3_CANLF	Uncharacterized protein; FBN1; ortholog	Fibrillin-1 (PTHR24039:SF22)	annexin (PC00050); calmodulin (PC00061); cell adhesion molecule (PC00069); extracellular matrix glycoprotein (PC00100); extracellular matrix structural protein (PC00103); signaling molecule (PC00207)
E2RNB0_CANLF	Histone H2A; H2AFX; ortholog	Histone H2AX (PTHR23430:SF199)	histone (PC00118)
F1PUX4_CANLF	60S acidic ribosomal protein P0; RPLP0; ortholog	60S acidic ribosomal protein P0-related (PTHR21141:SF3)	ribosomal protein (PC00202)
E2RLA2_CANLF	Uncharacterized protein; P4HA1; ortholog	Prolyl 4-hydroxylase subunit alpha-1 (PTHR10869:SF101)	
J9P315_CANLF	Uncharacterized protein; LRP1; ortholog	Prolow-density lipoprotein receptor-related protein 1 (PTHR44025:SF2)	
F1P9U4_CANLF	Uncharacterized protein; DPYSL2; ortholog	Dihydropyrimidinase-related protein 2 (PTHR11647:SF56)	hydrolase (PC00121)
E2R6K5_CANLF	Histone H3;H3F3B; ortholog	Histone H3.3 (PTHR11426:SF179)	histone (PC00118)
E2RJE0_CANLF	Uncharacterized protein; COMP; ortholog	Cartilage oligomeric matrix protein (PTHR10199:SF88)	
E2QUY2_CANLF	Uncharacterized protein; ABRACL; ortholog	Costars family protein ABRACL (PTHR22739:SF0)	
E2QRS3_CANLF	Uncharacterized protein; CHAD; ortholog	Chondroadherin (PTHR44607:SF1)	Chondroadherin is a cartilage matrix protein thought to mediate adhesion of isolated chondrocytes
F1PR66_CANLF	Uncharacterized protein; LAMA4; ortholog	Laminin subunit alpha-4 (PTHR44537:SF1)	
E2R4L7_CANLF	Serine hydroxymethyl-transferase; SHMT2; ortholog	Serine hydroxymethyltransferase, mitochondrial (PTHR11680:SF17)	methyltransferase (PC00155)

continued on next page

continued from previous page

Gene ID	Gene Name/ Gene Symbol	Panther Family/Subfamily	Panther Protein Class
CATC_CANLF	Dipeptidyl peptidase 1 (Fragment);CTSC; ortholog	Dipeptidyl peptidase 1 (PTHR12411:SF354)	cysteine protease (PC00081)
F6Y3P9_CANLF	Uncharacterized protein; GSN; ortholog	Gelsolin (PTHR11977:SF29)	non-motor actin binding protein (PC00165)
F6V790_CANLF	Uncharacterized protein; CILP; ortholog	Cartilage intermediate layer protein 1 (PTHR15031:SF3)	
F1P790_CANLF	Histone H2A; HIST3H2A; ortholog	Histone H2A type 3 (PTHR23430:SF59)	histone (PC00118)
J9NYC0_CANLF	Uncharacterized protein; MFAP4; ortholog	Microfibril-associated glycoprotein 4 (PTHR19143:SF225)	signaling molecule (PC00207)
J9P923_CANLF	Uncharacterized protein; PTRF; ortholog	Polymerase I and transcript release factor (PTHR15240:SF3)	transcription factor (PC00218)
F1P6B7_CANLF	Annexin;ANXA1; ortholog	Annexin A1 (PTHR10502:SF17)	Annexin A1 both suppresses phospholipase A2, thereby blocking eicosanoid production, and inhibits various leukocyte inflammatory events (epithelial adhesion, emigration, chemotaxis, phagocytosis, respiratory burst, etc.).
F1PKX2_CANLF	Uncharacterized protein; ABI3BP; ortholog	Target of Nesh-SH3 (PTHR23197:SF10)	
F6V659_CANLF	Uncharacterized protein; DDX1; ortholog	ATP-dependent RNA helicase DDX1 (PTHR24031:SF307)	RNA helicase (PC00032)
E2RNR0_CANLF	Uncharacterized protein; OGN; ortholog	Mimecan (PTHR24373:SF122)	extracellular matrix protein (PC00102); receptor (PC00197)
F1PHK9_CANLF	Uncharacterized protein; LAMC1; ortholog	Laminin subunit gamma-1 (PTHR10574:SF270)	extracellular matrix linker protein (PC00101); receptor (PC00197)
F1P679_CANLF	Uncharacterized protein; ACTR3; ortholog	Actin-related protein 3-related (PTHR11937:SF175)	actin and actin related protein (PC00039)

continued on next page

continued from previous page

Gene ID	Gene Name/ Gene Symbol	Panther Family/Subfamily	Panther Protein Class
F1Q3Y0_CANLF	Profilin;PFN1; ortholog	Profilin-1 (PTHR13936:SF14)	
E2R0T6_CANLF	Uncharacterized protein; HSPA8; ortholog	Heat shock cognate 71 kDa protein (PTHR19375:SF239)	
PGS2_CANLF	Decorin; DCN; ortholog	Decorin (PTHR44053:SF2)	
F1PEK5_CANLF	Uncharacterized protein; SEPT2; ortholog	Septin-2 (PTHR18884:SF67)	cytoskeletal protein (PC00085); small GTPase (PC00208)
F1P975_CANLF	Uncharacterized protein; CAPN2; ortholog	Calpain-2 catalytic subunit (PTHR10183:SF268)	annexin (PC00050); calmodulin (PC00061); cysteine protease (PC00081)
PEBP1_CANLF	Phosphatidyl-ethanolamine-binding protein 1; PEBP1; ortholog	Phosphatidylethanolamine-binding protein 1 (PTHR11362:SF28)	
E2R2G1_CANLF	Uncharacterized protein; ANGPTL7; ortholog	Angiopoietin-related protein 7 (PTHR19143:SF40)	signaling molecule (PC00207)
LMAN2_CANLF	Vesicular integral-membrane protein VIP36; LMAN2; ortholog	Vesicular integral-membrane protein VIP36 (PTHR12223:SF28)	membrane traffic protein (PC00150)
F1PFM6_CANLF	Uncharacterized protein; COL6A1; ortholog	Collagen alpha-1(VI) chain (PTHR44172:SF3)	
B4YY02_CANLF	Adenylate kinase isoenzyme 1; AK1; ortholog	Adenylate kinase isoenzyme 1 (PTHR23359:SF59)	nucleotide kinase (PC00172)
E2RSI6_CANLF	Uncharacterized protein; EZR; ortholog	Ezrin (PTHR23281:SF13)	actin family cytoskeletal protein (PC00041)
F1P6P2_CANLF	Transgelin; TAGLN2; ortholog	Transgelin-2 (PTHR18959:SF41)	non-motor actin binding protein (PC00165)
E2QZ50_CANLF	Adenylyl cyclase-associated protein; CAP1; ortholog	Adenylyl cyclase-associated protein 1 (PTHR10652:SF1)	actin family cytoskeletal protein (PC00041)

continued on next page

continued from previous page

Gene ID	Gene Name/ Gene Symbol	Panther Family/Subfamily	Panther Protein Class
E2QSZ5_CANLF	Coronin; CORO1A; ortholog	Coronin-1A (PTHR10856:SF18)	non-motor actin binding protein (PC00165)
F1Q147_CANLF	Uncharacterized protein; MYO1C; ortholog	Unconventional myosin-Ic (PTHR13140:SF255)	G-protein modulator (PC00022); actin binding motor protein (PC00040); cell junction protein (PC00070)
J9NZK5_CANLF	Uncharacterized protein; LOX; ortholog	Lysyl oxidase homolog 1-related (PTHR19331:SF4)	oxidase (PC00175); receptor (PC00197); serine protease (PC00203)
APOA1_CANLF	Apolipoprotein A-I; APOA1; ortholog	Apolipoprotein A-I (PTHR18976:SF11)	
E2RL80_CANLF	Uncharacterized protein; PRELP; ortholog	Prolargin (PTHR24373:SF152)	extracellular matrix protein (PC00102); receptor (PC00197)
F1PL97_CANLF	Protein disulfide-isomerase; P4HB; ortholog	Protein disulfide-isomerase (PTHR18929:SF101)	
F1PSS2_CANLF	Uncharacterized protein; THBS4; ortholog	Thrombospondin-4 (PTHR10199:SF92)	Thrombospondin family members are adhesive glycoproteins that mediate cell-to-cell and cell-to-matrix interactions. This protein forms a pentamer and can bind to heparin and calcium.
F1PIC7_CANLF	Uncharacterized protein; HSPA5; ortholog	78 kDa glucose-regulated protein (PTHR19375:SF144)	
E2RAP5_CANLF	Uncharacterized protein; TNMD; ortholog	Tenomodulin (PTHR14064:SF3)	membrane-bound signaling molecule (PC00152)
E2RC23_CANLF	Uncharacterized protein; PCOLCE; ortholog	Procollagen C-endopeptidase enhancer 1 (PTHR44264:SF2)	
J9P1J5_CANLF	Uncharacterized protein; DSTN; ortholog	Destrin (PTHR11913:SF18)	non-motor actin binding protein (PC00165)
E2RHY7_CANLF	Uncharacterized protein; SERPINH1; ortholog	Serpin H1 (PTHR11461:SF27)	serine protease inhibitor (PC00204)

continued on next page

continued from previous page

Gene ID	Gene Name/ Gene Symbol	Panther Family/Subfamily	Panther Protein Class
E2QU08_CANLF	Uncharacterized protein; ASS1; ortholog	Argininosuccinate synthase (PTHR11587:SF2)	ligase (PC00142)
E2RSC5_CANLF	Uncharacterized protein; TLN2; ortholog	Talin-2 (PTHR19981:SF1)	actin family cytoskeletal protein (PC00041); cell adhesion molecule (PC00069)
E2RD86_CANLF	Protein disulfide-isomerase; PDIA3; ortholog	Protein disulfide-isomerase A3 (PTHR18929:SF132)	
E2QZA8_CANLF	Uncharacterized protein; FKBP10; ortholog	Peptidyl-prolyl cis-trans isomerase FKBP10 (PTHR10516:SF247)	calcium-binding protein (PC00060); chaperone (PC00072); isomerase (PC00135)
F1PBI6_CANLF	Uncharacterized protein; THBS1; ortholog	Thrombospondin-1 (PTHR10199:SF78)	
MYH9_CANLF	Myosin-9;MYH9; ortholog	Myosin-9 (PTHR13140:SF317)	G-protein modulator (PC00022); actin binding motor protein (PC00040); cell junction protein (PC00070)
TPSN_CANLF	Tapasin; TAPBP; ortholog	Tapasin (PTHR23411:SF5)	immunoglobulin receptor superfamily (PC00124)
F1PLV6_CANLF	Fibulin-1; FBLN1; ortholog	Fibulin-1 (PTHR44476:SF1)	
E2R413_CANLF	Uncharacterized protein; CAPG; ortholog	Macrophage-capping protein (PTHR11977:SF13)	non-motor actin binding protein (PC00165)
F1PTL1_CANLF	Uncharacterized protein; RAD23A; ortholog	UV excision repair protein RAD23 homolog A (PTHR10621:SF0)	damaged DNA-binding protein (PC00086)
E2QSF4_CANLF	Uncharacterized protein; TUBB; ortholog	Tubulin beta chain (PTHR11588:SF61)	tubulin (PC00228)
F2Z4Q7_CANLF	Uncharacterized protein; SERPINF1; ortholog	Pigment epithelium-derived factor (PTHR11461:SF84)	serine protease inhibitor (PC00204)
F6XIK8_CANLF	Uncharacterized protein; SYNCRIP; ortholog	Heterogeneous nuclear ribonucleoprotein Q (PTHR44088:SF3)	ribosomal protein (PC00202)
J9NTG7_CANLF	Uncharacterized protein; CD55; ortholog	Complement decay-accelerating factor (PTHR19325:SF317)	

continued on next page

continued from previous page

Gene ID	Gene Name/ Gene Symbol	Panther Family/Subfamily	Panther Protein Class
F1PFZ5_CANLF	Uncharacterized protein; MFGE8; ortholog	Lactadherin (PTHR44122:SF1)	
F1Q133_CANLF	Uncharacterized protein; COL4A1; ortholog	Collagen alpha-1(IV) chain (PTHR24023:SF854)	
E2RGD3_CANLF	Uncharacterized protein; TWF2; ortholog	Twinfilin-2 (PTHR13759:SF2)	non-motor actin binding protein (PC00165)
F1PLN5_CANLF	Uncharacterized protein; FMOD; ortholog	Fibromodulin (PTHR24373:SF127)	extracellular matrix protein (PC00102); receptor (PC00197)
F1P7Y6_CANLF	Uncharacterized protein; NID2; ortholog	SUBFAMILY NOT NAMED (PTHR44583:SF1)	
E2R416_CANLF	Uncharacterized protein; LUM; ortholog	Lumican (PTHR24373:SF119)	extracellular matrix protein (PC00102); receptor (PC00197)
F1PAS8_CANLF	Superoxide dismutase [Cu-Zn]; SOD3; ortholog	Extracellular superoxide dismutase [Cu-Zn] (PTHR10003:SF59)	oxidoreductase (PC00176)
E2R9R2_CANLF	Uncharacterized protein; LOC612644; ortholog	Cytochrome c oxidase subunit 6B1 (PTHR11387:SF16)	oxidase (PC00175)
E2R5B9_CANLF	Uncharacterized protein; GSTM3; ortholog	Glutathione S-transferase Mu 3 (PTHR11571:SF133)	
E2QWN7_CANLF	Uncharacterized protein; LCP1; ortholog	Plastin-2 (PTHR19961:SF35)	non-motor actin binding protein (PC00165)
E2R4J1_CANLF	Uncharacterized protein; LAMB2; ortholog	Laminin subunit beta-2 (PTHR10574:SF36)	extracellular matrix linker protein (PC00101); receptor (PC00197)
MYOC_CANLF	Myocilin;MYOC; ortholog	Myocilin (PTHR23192:SF33)	receptor (PC00197); structural protein (PC00211)
E2RPQ6_CANLF	Uncharacterized protein; DPT; ortholog	Dermatopontin (PTHR15040:SF2)	extracellular matrix protein (PC00102)
F6XRY2_CANLF	Uncharacterized protein; EEF2; ortholog	Elongation factor 2 (PTHR42908:SF10)	G-protein (PC00020); hydrolase (PC00121); translation elongation factor (PC00222);translation initiation factor (PC00224)

continued on next page

continued from previous page

Gene ID	Gene Name/ Gene Symbol	Panther Family/Subfamily	Panther Protein Class
ENPL_CANLF	Endoplasmin; HSP90B1; ortholog	Endoplasmin-related (PTHR11528:SF73)	
CATK_CANLF	Cathepsin K; CTSK; ortholog	Cathepsin K (PTHR12411:SF55)	cysteine protease (PC00081)
J9NV93_CANLF	Peptidyl-prolyl cis-trans isomerase;unassigned; ortholog	SUBFAMILY NOT NAMED (PTHR11071:SF400)	isomerase (PC00135)
F1PQM7_CANLF	Tetraspanin; CD9; ortholog	CD9 antigen (PTHR19282:SF163)	cell adhesion molecule (PC00069); membrane-bound signaling molecule (PC00152); receptor (PC00197)
FRIH_CANLF	Ferritin heavy chain; FTH1; ortholog	Ferritin heavy chain (PTHR11431:SF37)	storage protein (PC00210)
F1PPZ2_CANLF	Ribonuclease A B1; RNASE4; ortholog	Ribonuclease 4 (PTHR11437:SF10)	endoribonuclease (PC00094); enzyme modulator (PC00095); hydrolase (PC00121)
E2R612_CANLF	Uncharacterized protein; EFEMP1; ortholog	EGF-containing fibulin-like extracellular matrix protein 1 (PTHR44074:SF2)	
G1K267_CANLF	Uncharacterized protein; unassigned; ortholog	Heat shock 70 kDa protein 1A-related (PTHR19375:SF223)	
E2RAL0_CANLF	Uncharacterized protein; ARHGDIB; ortholog	Rho GDP-dissociation inhibitor 2 (PTHR10980:SF15)	G-protein modulator (PC00022); signaling molecule (PC00207)
E2RIV1_CANLF	AP complex subunit beta; AP2B1; ortholog	AP-2 complex subunit beta (PTHR11134:SF9)	membrane traffic protein (PC00150)
E2R7T5_CANLF	Uncharacterized protein; ALOX15; ortholog	Arachidonate 15-lipoxygenase (PTHR11771:SF33)	oxygenase (PC00177)
F1PEI2_CANLF	Uncharacterized protein; CKAP4; ortholog	Cytoskeleton-associated protein 4 (PTHR45161:SF1)	
E2RB37_CANLF	Uncharacterized protein; PDIA6; ortholog	Protein disulfide-isomerase A6 (PTHR18929:SF38)	

continued on next page

continued from previous page

Gene ID	Gene Name/ Gene Symbol	Panther Family/Subfamily	Panther Protein Class
E2RGQ5_CANLF	Uncharacterized protein; RPS10; ortholog	40S ribosomal protein S10-related (PTHR12146:SF0)	ribosomal protein (PC00202)
F1PKX3_CANLF	Uncharacterized protein; F13A1; ortholog	Coagulation factor XIII A chain (PTHR11590:SF42)	acyltransferase (PC00042)
H9GWB4_CANLF	Uncharacterized protein; LOC100855471; ortholog	Collagen alpha-2(VI) chain (PTHR44172:SF1)	
F1Q129_CANLF	Uncharacterized protein; COL4A2; ortholog	Collagen alpha-2(IV) chain (PTHR24023:SF588)	
F1PB08_CANLF	Uncharacterized protein; SEPT9; ortholog	Septin-9 (PTHR18884:SF47)	cytoskeletal protein (PC00085); small GTPase (PC00208)
F6V234_CANLF	Uncharacterized protein; PLS3; ortholog	Plastin-3 (PTHR19961:SF32)	non-motor actin binding protein (PC00165)

Table 4.S2: Panther protein class description for proteins in Table 4.S1.

Chapter 5

Implementation and future directions

5.1 Improved tendon repair through increased suture-tendon interactions

Over the last several hundred years, surgical suture improvements have focused on enhancing suture material strength, surgical handling, degradation profiles, and stitching techniques to best grasp and re-appose the tissue. However, conventional suture approaches are limited by high load transfer across only a small number of anchor points within tissue, leading to stress concentrations that often cause repair failure (Figures 2.1 and 3.1). Increasing the physical interaction between tendon and suture has the potential to improve repair load transfer, enabling better coaptation of tendon stumps and reduced tendon repair rupture rates, as theoretically and experimentally evaluated in Chapter 2. This work established a range of desirable adhesive material properties to facilitate load transfer between the tendon and the suture. In doing so, this thesis provided a theoretical basis and design direction to the literature on improved suture-tendon interactions.

Improved suture-tissue interactions have substantial potential to improve orthopedic repair strength. In addition to the direct application of adhesive to suture to improve load transfer in repairs under tensile loads, as described here, a previous study reported improved compressive properties in meniscus repairs when non-optimized adhesive coatings were added to the repair sutures compared to repairs with suture alone or adhesive alone [298]. Pursuing a similar goal, the experimental crosslinking agent 1-ethyl-3-(3-dimethylaminopropyl) carbo diimide hydrochloride (EDC) has been coated onto sutures to crosslink flexor tendon tissue immediately adjacent to the suture, with some success

[153, 161]. While EDC treatment likely did not significantly impact load transfer between tissue and suture along the length of the suture in the monofilament, the crosslinking agent was able to stiffen and strengthen the surrounding tendon tissue at the suture anchor points to improve tissue tolerance of stress concentrations. This benefit may have been due to either reduction of the mismatch between tendon and suture stiffness, thereby balancing the adherends of the repair (Figure 2.3), or increased resistance to suture cutting through the tissue. Zhao and colleagues also applied cyanoacrylate specifically to transverse suture passes within tendon tissue and saw improved load tolerance on single strand pullout tests. They hypothesized that cyanoacrylate reduced micro-motion between the suture and tendon at suture anchor points, and thus reduced the propensity for suture to saw through the surrounding fibrous tendon tissue and cause repair failure by suture pullout [153]. These approaches have both been limited by concerns of inflammation and limited efficacy due to potential cytotoxic effects and sub-optimal material properties.

Another suture material modification that can lead to increased suture-tissue interaction uses barbs on the sutures to grip tissue along the suture length. Barbs act to grip tissue at discrete locations, approximately every millimeter, analogous to the continuous bonds formed by adhesive coatings along the entire surface. The first barbed sutures were applied to canine flexor tendons, initially acting as stiff spears with hooks that were pushed into the tendon instead of being pulled through tissue trailing a needle [389, 390]. More recent approaches [391, 392, 393], including the Quill^{TM} Knotless Tissue-Closure Device (Angiotech Pharmaceuticals, Vancouver, BC, Canada) and V-Loc^{TM} Absorbable Wound Closure Device (Covidien Healthcare, Mansfield, MA), include uni- or bi-directional barbs cut into surgical suture threads, enabling the suture to be pulled into tissue for rapid closure without tying knots. Barbed sutures have been successfully used for many obstetrics and gynecological applications [394, 395, 396] and some plastic surgery applications [397], but have only generated mixed results in flexor tendon repair [398, 399]. Barbed sutures offer several advantages, including the ability to reduce tissue stress concentrations by transferring load at periodic points along the suture length, reduce tissue foreign-body irritation at bulky knots, and avoid the potential suture slippage or tissue necrosis from poorly tied knots. However, they also have several disadvantages that limit application. A meta-analysis of barbed suture used in 8 types of surgical operations indicated increased tissue irritation and complication risk [397]. Furthermore, cutting barbs into monofilament suture inherently decreases the suture fiber strength by introducing mechanical defects and stress risers. The decreased suture strength is a major drawback for high-load orthopedic applications. Nevertheless, the successful surgical implementation of barbed sutures to increase suture-tissue interaction to transfer load in some operative settings is a promising sign for the surgical potential of adhesive-coated sutures.

In addition to modifying suture materials to increase suture-tendon interaction, we and others have increased inter-

action at grasping points through the use of various types of locking stitches. A half-hitch loop technique described in Appendix A increased tendon grasping more than previous lock types [17, 24, 109], leading to repair strength improvements [108]. While locking stitches strengthen the suture-tendon interaction at locking points, reducing rupture risk, the repairs continue to rely on load transfer at only a few points. In addition, some locking stitch patterns risk tissue strangulation, causing necrosis, or excessive repair bulk, stimulating adhesion formation and reducing range of motion. Thus, increasing suture-tendon interaction has generated some improvements for repair mechanics, but both barbed sutures and locking stitches have substantial disadvantages for orthopedic repair.

The two major approaches developed and evaluated by this thesis work, adhesive coating and porosity allowing tissue ingrowth, both offer means to increase suture-tendon interaction without the negative consequences of barbed suture or locking stitches. Tissue ingrowth into porous structures, similar to ingrowth into porous bone implants [359, 360] or meshes for hernia repair [361], locks the structure in place and facilitates load transfer along the length. This is functionally equivalent to a biological 'adhesive' that forms over time during healing, forming a strong interface similar to roots grasping soil. Even fibrotic, scar tissue deposition throughout the porous suture material would be sufficient to mechanically distribute load transfer over the suture length. Thus, porous sutures may act as scaffolds for tissue regrowth. While extracellular matrix deposition occurs locally around cells, by binding the suture at several points, the healing tendon should be able to use the suture as a mechanical bridge to transfer loads over longer distances than the individual fibers of new matrix can traverse. Therefore, porous sutures have the potential to accelerate the rate at which matrix deposition and reorganization can strengthen the repair site. When porous sutures carry biofactors such as connective tissue growth factor embedded within the suture to stimulate matrix production, there is even greater potential to accelerate the healing matrix ingrowth into the suture.

While matrix deposition takes days to weeks to increase repair-site load tolerance, providing increasing benefit over time, adhesive coatings act immediately upon curing and then lose strength over time as the interfacial bonds and the bulk adhesive material are degraded. The adhesive layer only needs to hold the repair together in the short term, not indefinitely, since the repairing tissue will increase load tolerance over time. These inversely related trends create an opportunity for continued strong repair biomechanics: at early time points, a compliant adhesive interdigitated with porous suture can form a strong bond that distributes load over the suture length, then that bond can be replaced by tissue ingrowth into the suture over time. Biofactors embedded within adhesive-coated porous sutures may be able to guide this transition from tendon-adhesive-suture load transfer to tendon-suture direct load transfer along the suture length, in addition to facilitating generation of bridging fibers between the re-apposed tendon and/or bone surfaces.

5.2 Development of novel adhesive biomaterials

Novel adhesive biomaterials need to satisfy several design criteria to be useful clinically. First, the shear lag models studied here demonstrate the need for adhesives that are compliant and strong in shear, similar to elastomeric materials. Second, while most industrial adhesives work best in dry environments, biological adhesives need to work in hydrated environments. Arthroscopic surgeries require adhesives to work while fully submerged in saline. Third, adhesives need to pass through tissue easily and then bind strongly once in place. Fourth, adhesives need to be biocompatible and avoid stimulating inflammation or creating toxic degradation products. Eventual clinical use requires simple implementation by surgeons and hospitals, including inexpensive production, reasonable handling properties, and a sufficient shelf life ideally without requiring special storage conditions. While either direct mechanical benefit or biological stimulation for longer-term repair improvement would be useful independently, as discussed above, ideal products would simultaneously provide mechanical and biological benefit to facilitate tendon and tendon-to-bone healing as the adhesive begins to degrade. Meeting these specific criteria would help a new adhesive meet the five general, overarching criteria outlined by Spotnitz and Burke for new medical technologies: safety, efficacy, useability, cost, and approval by regulatory agencies [400, 295].

There are several potential adhesive material and coating approaches that achieve these desired properties for surgical use. As described in Chapter 3, we will continue to study marine mussel-mimetic, catechol-derived adhesive chemistries on elastomeric molecular backbones in order to obtain strong interfacial binding in hydrated environments with a compliant adhesive material. By modifying the elastomeric component molecular weight and crosslink density, effectively changing the length and stiffness of the molecular spring between the adhesive catechol moieties, we can tune the adhesive mechanical properties for adhesive film or adhesive-coated suture applications. If needed, we can introduce crosslinking agents such as tetrakis hydroxymethyl phosphonium chloride (THPC) and functionalize the elastomeric linker with amine groups to create additional crosslinks, stiffening the adhesive material. Since catechol moieties rely on oxidation to strengthen chemical bonds following the initial saline-driven gelation and loose binding [315], future work should explore a variety of chemical oxidizing agents such as sodium periodate and more biocompatible, biologically derived oxidizing agents with catechol-derived adhesives.

Bio-inspired adhesives are interesting because of their ability to work in hydrated environments to bind tissues. In addition to catechol-based adhesives assessed here, a compliant, strong adhesive exudate from the dorsum of the Australian frog *Notaden bennetti* has been shown to improve load transfer in sheep infraspinatus repairs [328] as predicted by shear lag models (Chapter 3). This prior work further demonstrates the value of this concept for clinical application

of mechanically-optimized adhesives in tendon-to-bone repairs. While that particular adhesive has biocompatibility concerns when used in its secreted form [401], and would not be clinically applicable since it requires immediate secretion from a frog before application within 60 seconds [330, 328], it provides another highly promising avenue for synthetic, bio-inspired adhesive development. The porous structure of the frog adhesive network described by [329] could provide additional mechanical benefit by allowing tissue ingrowth, as discussed above for sutures with porous outer sheaths.

Additional adhesive approaches include using elastomeric hydrogels bound to tissue with binding peptides or acrylate chemistry. Albumin-derived adhesives are compliant and may be a useful base with optimized interfacial binding (e.g., bovine albumin-glutaraldehyde adhesives including BioGlue, CryoLife Inc., Kennesaw, GA; egg-albumin adhesives including Mayer's Albumin) [295, 402]. Poly(ethylene glycol) diacrylate hydrogels have potential to tune elastic properties by changing the PEG linker length, while maintaining the binding strength of acrylate moieties [403, 404, 405]. A recent review by Bouten and colleagues provides an overview of adhesive materials used in clinical applications [295]. Furthermore, silk fibroin from the *Bombyx mori* silkworm has been developed into elastomeric biomaterials that could be functionalized for adhesive application [406, 407]. While existing silk hydrogels are not strong enough to transfer sufficient load [406] (Figure 5.1A), we have successfully stiffened the hydrogels to an appropriate bulk mechanical property range by partially re-crystallizing in 50–100% methanol (Figure 5.1B-D) for 60 minutes before testing the hydrogels in double lap shear. Future studies could develop adhesive materials using a partially re-crystallized silk hydrogel as a biocompatible bulk scaffold material, building from work by David Kaplan's group at Tufts University in order to enable concurrent biofactor delivery within the silk fibroin matrix.

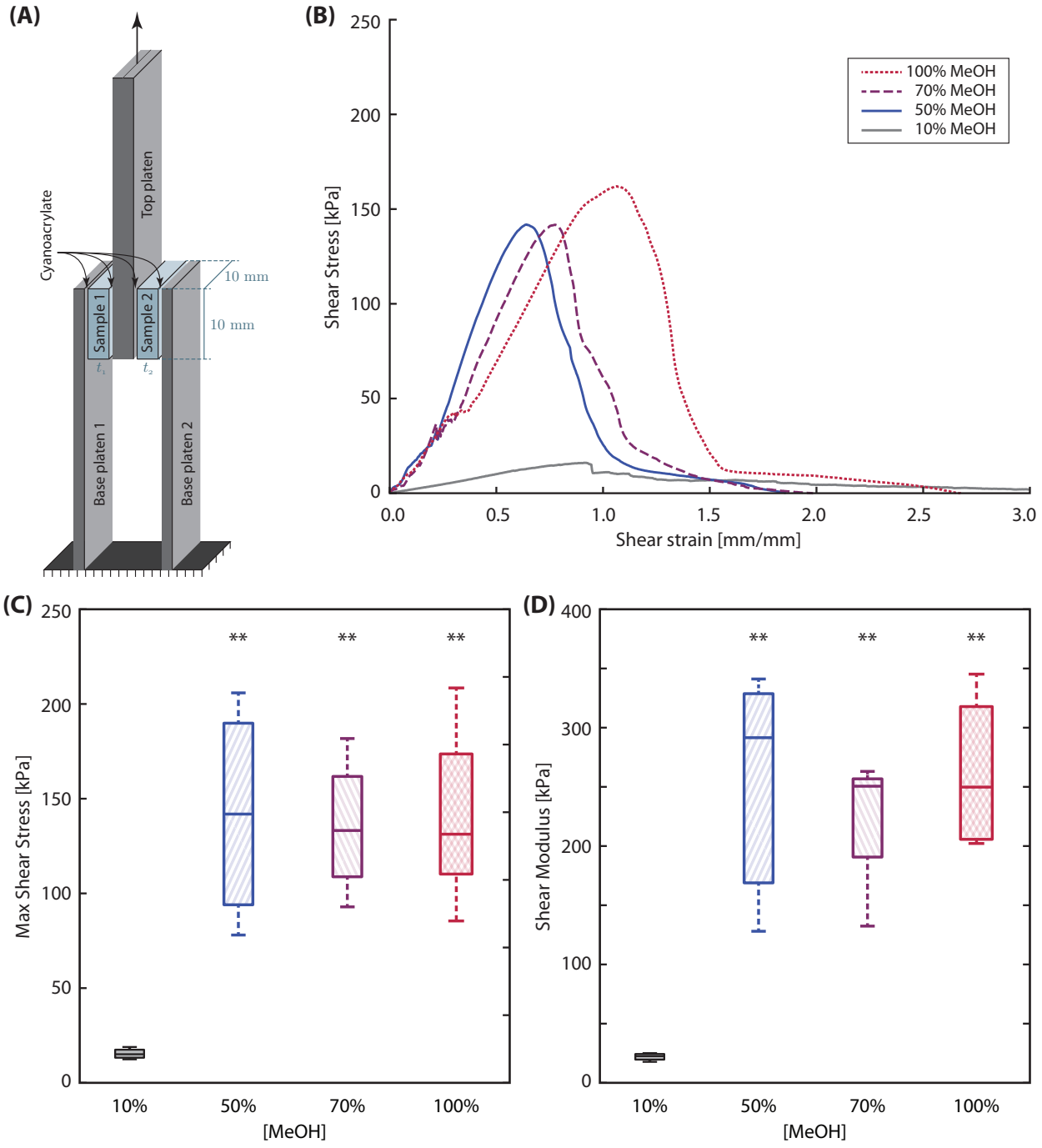

Figure 5.1: (A) Silk fibroin hydrogels, created following previously described protocols [407], were evaluated in double lap shear while adhered to poly(vinyl chloride) plastic platens using cyanoacrylate. (B) Representative shear stress – strain curves are shown for silk hydrogels partially recrystallized with various concentrations of methanol for one hour. (C) Maximum stress and (D) shear modulus increased with recrystallization, but there was no difference seen with increased methanol concentration above 50%. ** $p < 0.01$ by t-tests.

5.3 Implementation of adhesive approaches for tendon repair

Surgical implementation of adhesives for tendon repair as coatings on sutures or for tendon-to-bone repair as adhesive films requires first honing adhesive mechanical properties as discussed above, then evaluating biocompatibility. The idealized biomechanical tests performed here, which evaluate adhesives on single suture strands in tendon or in simple lap shear between tendon and bone planks, provide relevant, rapid testing protocols for assessing the usefulness of new adhesive materials. Future work should use these or similar testing models to evaluate adhesive protection and activation schemes, so sutures or films can be stable and non-binding until they are in place within tissue, and only then form a strong bond. We envision opportunities to activate adhesives by (i) temperature, using phase change materials to coat the adhesive-suture and only release the adhesive at body temperature, (ii) optical activation, possibly using near-infrared light to penetrate tissue and stimulate chemical agents within the adhesive once it is in place, and (iii) chemical priming by bringing the adhesive-suture or film into contact with priming agents immediately before surgical implantation. In addition, future studies should further evaluate theoretical improvements in adhesive–suture interfacial strength through adhesive interdigitation into suture pores. One simple experiment to evaluate this hypothesis could compare the pullout force required for porous and regular single suture strands, with or without adhesive coating, and passed longitudinally through tendon tissue *ex vivo*. Similarly, an *in vitro* tendon tissue culture experiment could compare the strength of biological bonds formed between suture and the surrounding tissue over time as tissue grows into sutures. By changing the calcium chloride concentration used to generate porous sutures, the pore size can be modulated [353] to assess the impact of pore diameter on tissue ingrowth and adhesive interdigitation strength. In addition to modifying suture surface morphology before loading, porous sutures could be further chemically modified before coating with an adhesive to prime the suture for adhesive binding. However, although adhesive interdigitation and strengthened chemical attachment may increase interfacial binding strength with the suture, this local improvement will have minimal impact on repair strength if the strength of a given adhesive is instead limited by the bulk strength, adhesive-tissue interfacial binding strength, or the ability of the tendon to successfully distribute load between adjacent fibers near the adhesive without failure.

5.3.1 Biocompatibility testing *in vitro*

Adhesive biomaterials that improve load transfer of cadaver canine flexor digitorum profundus tendon reconstructions or rotator cuff repairs should to be further evaluated for biocompatibility *in vitro* and *in vivo*. Demonstrating biocompatibility in culture and in small animal models is necessary prior to testing in clinically relevant large animal

models and translating clinically. In order to assess cellular responses to adhesive biomaterials, primary mouse, rat, or canine fibroblasts isolated from tendons should be co-cultured with the biomaterials *in vitro* as described previously [165]. Biomaterial components should be evaluated in whole and in part (with and without sutures) to elucidate the cellular response in the adhesive-influenced environment. After co-culture, biocompatibility experiments should evaluate cells under light microscopy for cell density and morphological changes, then assess changes in proliferation, cell death, matrix synthesis, inflammation, and general tendon marker gene expression using quantitative real-time RT-PCR (qRT-PCR), as described previously [165, 167, 57]. Protein expression for proliferation and matrix synthesis should be assessed using Western blots. Based on a power analysis assuming historical coefficients of variations of approximately 35% for gene and protein expression assays and 25% for cell proliferation and apoptosis assays, and a paired t-test statistical comparison, sample sizes of $n = 10$ per adhesive compound evaluated would provide the ability to statistically detect differences of 35% or greater in gene and protein expression and 25% or greater in cell proliferation and apoptosis assays ($\alpha = 0.05$, $1 - \beta = 0.8$).

5.3.2 Biocompatibility testing *in vivo*

The most promising adhesive biomaterials from *in vitro* testing should be evaluated for toxicology and inflammatory reactions *in vivo* through subcutaneous injection or implantation in rats [408, 409]. After approximately 10 days to allow the animal to react to the adhesive through the inflammatory and early proliferative stages of healing, experiments should assess overall body weight, local tissue reactions including collagen deposition, inflammatory cell recruitment, and overall cellular response in the *in vivo* setting histologically. qRT-PCR can be used to examine gene expression of inflammation-associated genes including IL-1β and TNFα, inflammation response genes including iNOS and PGE2, angiogenesis-associated genes including bFGF and PDGF, fibrosis-associated gene TGF β1, and ECM-related genes type I collagen, type III collagen, hyaluronic acid synthase, lubricin, and decorin. Assuming coefficients of variation of approximately 7% for body weight, 35% for gene expression assays, 25% for cell/proliferation and apoptosis related assays, and 25% for parameters derived from histology, and using a paired t-test statistical comparison, power analyses predict that use of 8 animals each for histology, cell proliferation, gene expression, and body weight provides the ability to detect differences of at least 29%, 29%, 41%, and 9%, respectively ($\alpha = 0.05$, $1 - \beta = 0.8$). Since individual animals can be assigned to either histology or both cell proliferation and gene expression analysis, 16 animals should be sufficient to evaluate an adhesive compound for *in vivo* biocompatibility.

If adhesive biomaterials tested for biocompatibility cause a severe inflammatory response, as determined by high cell

death and inflammatory marker expression, as well as histological assessment, the components of the biomaterial should be individually assessed for biocompatibility. After determining which component is driving the immunogenic response, that component could be replaced with an alternative component. If that still causes severe inflammatory responses, we will modify the offending material component to mitigate inflammation.

5.3.3 Large animal preclinical surgical models

Adhesive-coated sutures that exhibit appropriate mechanical and biocompatibility profiles should be evaluated in a large animal preclinical surgical model to determine clinical viability, as we have done for porous sutures (Chapter 4). Since adhesive approaches are predominantly aimed at improving the mechanical properties of repairs, rodent surgical models are too far removed from the clinical scenario to provide substantial benefit. The canine flexor digitorum profundus tendon model has been a gold standard for preclinical evaluation of intrasynovial tendon repairs since the 1960s [285, 284]. Canine flexor tendon structures, sizes, and surgical techniques are very similar to those in humans. This intrasynovial model is sensitive to inflammatory concerns [186], and demands a clinically relevant difference to demonstrate a substantial impact [167, 20, 100, 11]. Unlike previous biological factor approaches evaluated in the canine flexor tendon [106, 155, 388, 287], adhesives are expected to work quickly to improve repair biomechanics. Therefore, instead of waiting until 28 days to assess biomechanical properties, as we have done previously [186], canine repairs evaluated as early as 3 days after repair would be a useful indicators of both early inflammatory activity effects and biomechanical benefits. Since a major factor limiting clinical flexor tendon repair is adhesion formation with the intrasynovial sheath (which limits range of motion), it is especially important to evaluate potential adhesion formation resulting from adhesives.

Following preclinical evaluation, clinical application would likely require commercialization through coordination with orthopedic device and suture companies. Given the large potential benefit and the clinical need for improved flexor tendon and rotator cuff repairs, as just two example cases for adhesive-coated sutures and adhesive films, respectively, this technology investment is commercially justified. We performed a rudimentary cost-benefit analysis of publicly available data published by the U.S. Centers for Medicare and Medicaid Services (Part B National Summary Data File, previously known as BESS), which indicated that the immediate cost savings available for reducing flexor tendon repair failures is over $1 million annually, solely for surgical costs during repeat operations. This does not account for any less direct medical costs or indirect costs from lost time at work, inability to perform activities of daily living, etc. The rotator cuff market is far greater, totaling approximately $500 million annually for repairs that

mechanically fail, even though most people with a rotator cuff tear do not receive surgical treatment partially due to high failure rates. In addition to pursuing applications of adhesive-coated sutures and adhesive films within tendon and tendon-to-bone repairs, the same technologies could potentially be applied to other tissues throughout the body that are susceptible to mechanical failure, such as abdominal hernia repair.

5.4 Alternative approaches

The primary work of this thesis focused on adhesive sutures, adhesive films, and sutures with porous sheaths as mechanically-focused technologies to improve orthopedic repair strength. These simple approaches are clinically attractive because repairs can be improved without substantially changing the surgical procedure. Importantly, these technologies can be used in combination with other biologic approaches being developed to modulate healing. In parallel to the work described throughout this dissertation, we and others have developed biological approaches to modulate the healing response in the intrasynovial flexor tendon [199, 186, 164, 151, 410]. The following section describes cellular and biofactor approaches that could readily be combined with the adhesive suture approach described earlier in the thesis.

5.4.1 Adipose-derived progenitor cell sheets

N.B.: Adipose-derived stem cell sheet development was led by Dr. Hua Shen. I was a collaborating scientist on the project, involved with study design, surgical experiments, data analysis, and writing.

Portions of this section have been previously published in [199]: Shen H, Kormpakis I, Havlioglu N, Linderman SW, Sakiyama-Elbert SE, Erickson IE, Zarembinski T, Silva MJ, Gelberman RH, Thomopoulos S. The effect of mesenchymal stromal cell sheets on the inflammatory stage of flexor tendon healing. Stem Cell Res Ther. 2016 Sep 27;7(1):144.

Autologous ASC sheet preparation and surgical delivery: One exciting avenue to modify the biologic response during intrasynovial flexor tendon healing is to deliver cells directly to the surface of the repair during surgery. Previous attempts have been limited by two factors: (i) the intrasynovial tendon environment is extremely sensitive to forming adhesions with surrounding tissue that limit range of motion [388, 32, 99, 97], and (ii) cells in liquid media do not stay in place at the repair site. However, recent studies have demonstrated that autologous ASCs, co-cultured with M1 (pro-

inflammatory) macrophages, induced a macrophage phenotypic switch to the M2 (anti-inflammatory) subtype [411], suggesting therapeutic potential if the delivery challenges could be overcome. As described in detail in [199], we overcame these limitations by delivering autologous adipose-derived mesenchymal stromal cells (ASCs) on a collagen sheet, then sealing the cells in position and protecting from surface interactions with the exterior synovial sheath using a hyaluronic acid hydrogel (HA; Biotime, Inc., Almeda, CA). Briefly, subcutaneous adipose tissue was obtained 2 weeks prior to tendon repair for ASC isolation, performed as described previously [165]. Collagen sheets were prepared using 1 mL of collagen solution (pH 7.2) containing 2 mg/mL type I collagen from rat tail tendon (Corning Life Sciences, Bedford, MA), added to a ring-shaped silicone insert (ϕ19 mm). This was incubated at 37 °C for 1 hour to gel. After equilibrating collagen sheets overnight in cell media (α-MEM containing 10% fetal bovine serum and 100 U/mL penicillin-streptomycin), passage 3 ASCs were plated on top of the collagen at a cell density of 10,000 cells/cm^2. The resulting ASC sheet was cultured for 3–4 days with media changes every other day before surgical implantation.

Cell sheets were then assessed in a clinically relevant canine intrasynovial flexor digitorum profundus tendon injury and repair model. Following core and peripheral suture repair of the tendon, the collagen–ASC sheet was placed on the surface of the flexor tendon with the ASC-loaded side facing the tendon and the collagen facing the tendon sheath (Figure 5.2A). This was immobilized in position using an HA hydrogel consisting of thiol-modified hyaluronan crosslinked *in situ* with poly(ethylene glycol) diacrylate in PBS (Figure 5.2B). The HA hydrogel was mixed and allowed to gel for 5 minutes in the operating room immediately before application to the tendon surface over the cell sheet. This waiting period caused the HA hydrogel to obtain the appropriate viscosity to conform to the repair but not drip off the tendon surface. After application, the repair was left open for an additional 5 minutes to ensure complete gelation and proper adhesion of the hydrogel, before the incision was surgically closed. All repaired digits received controlled passive mobilization starting 24 hours after surgery as described previously [57, 388]. Animals were euthanized 7 days after repair.

These *in vivo* canine FDP tendon surgical experiments demonstrated that GFP-labeled ASCs were still present at the repair site 7 days following repair (whole-mount tendons, Figure 5.2C-E) and some cells infiltrated into the tendon tissue, especially at the gap between the re-apposed tendon stumps (Figure 5.2F). There were no gaps greater than 3 mm were no apparent adhesions in any of the repairs at dissection.

Real-time quantitative RT-PCR: TaqMan RT-PCR was used to determine the gene expression profile in repaired tendons after sacrifice ($n = 5$ tendons per group). Tendon fragments flanking the repair site ($\pm$ 5 mm) were dissected

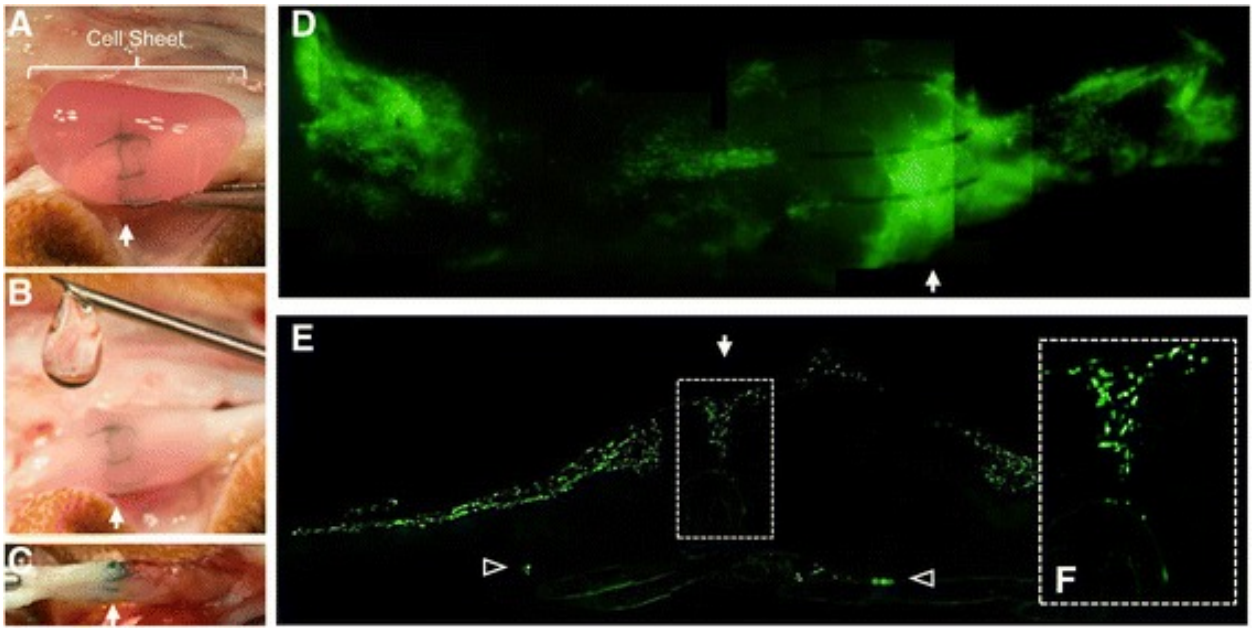

Figure 5.2: Application of an ASC sheet in tendon repair. (A,B) Representative photographs showing the process of applying (A) an ASC sheet and (B) HA to a sutured FDP tendon. (C) Representative photograph showing a FDP tendon 7 days after ASC sheet repair. (D) Representative fluorescent image of a whole-mount FDP tendon repaired with a GFP-expressing ASC sheet. (E,F) Representative fluorescent image of a longitudinal section of a FDP tendon repaired with a GFP-expressing ASC sheet. (F) Enlarged image of the boxed region in (E). *Arrows*, site of tendon repair; *open arrowheads*, GFP-expressing cells in the tendon substance. This figure is reprinted under the terms of the Creative Commons Attribution 4.0 International License (http://creativecommons.org/licenses/by/4.0/) from [199].

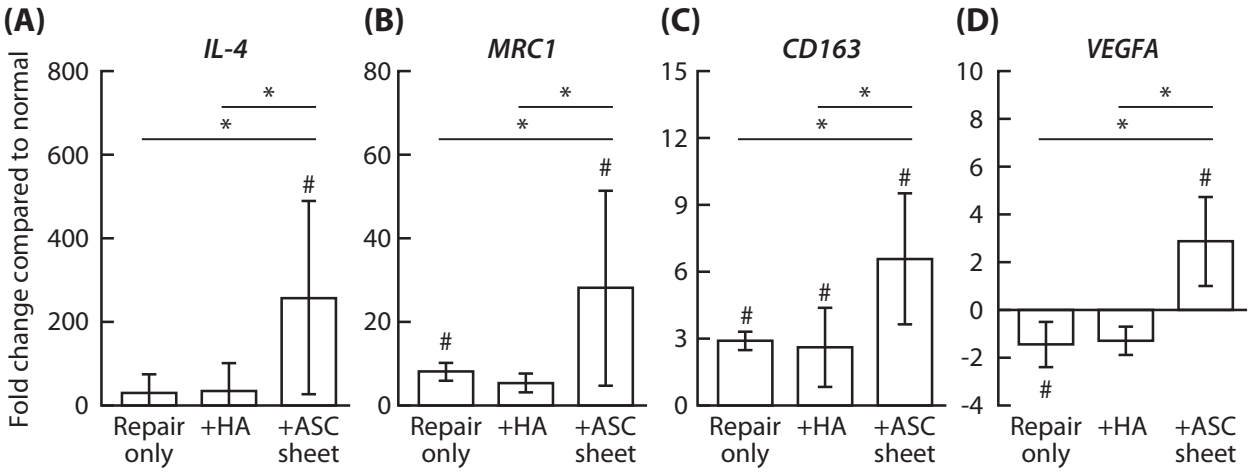

Figure 5.3: Change in expression of genes associated with macrophage polarization in FDP tendons 7 days post-operatively. (A) M2 stimulator gene *IL-4*, (B and C) M2 marker genes *MRC1* and *CD163*, and (D) downstream effector gene *VEGFA*. $^{*}p < 0.05$ between indicated groups. # $p < 0.05$ compared with normal tendons. *HA*: hyaluronan, *ASC*: adipose-derived mesenchymal stromal cell. This figure is modified from [199] under the terms of the Creative Commons Attribution 4.0 International License (http://creativecommons.org/licenses/by/4.0/).

and longitudinally split as described above, then they were diced into small pieces and flash-frozen in liquid nitrogen. Tendon fragments were pulverized with a Mikro-Dismembrator (Sartorius). Total RNA isolation, cDNA synthesis, and gene expression assays were performed as described previously [199]. All TaqMan primers and probes used in this study were purchased from Applied Biosystems. *GAPDH* and *PPIB* were used as endogenous reference genes. A one-way analysis of variance (ANOVA) followed by Student-Newman-Keuls's post-hoc testing (when appropriate) was performed to compare gene expression among the three repair groups. Two-tailed Student's t-tests and Mann-Whitney rank sum tests were used to compare the repair and normal groups for normally and non-normally distributed data, respectively. All statistical analyses were performed using SigmaStat 3.5 (Systat Software Inc., Chicago, IL, USA). The significance level was set at $p < 0.05$.

RT-PCR analysis of markers of macrophage polarization demonstrated a shift toward M2 macrophages (Figure 5.3). ASC sheets substantially increased expression of the M2 stimulator gene *IL-4* by 258-fold compared to repair alone, while there was no significant difference in the expression of M1 stimulator genes *IFNG*, *IL-1B*, *TNFA*, and *IL-6*. The expression of M2 marker genes *MRC1* and *CD163* was higher in ASC-treated tendons than in tendons from other repair groups. ASC sheet treatment also increased expression of the angiogenic factor *VEGFA*, in FDP tendons, which was significantly reduced after suture repair compared with normal. This combination of M2 stimulator, marker, and effector genes consistently indicates an anti-inflammatory, M2 macrophage phenotype following ASC sheet treatment. We hypothesize that this anti-inflammatory effect will lead to more ordered cell proliferation and extracellular matrix production, thus improving repair healing quality and rate.

5.4.2 Microsphere-based biological factor delivery

In order to evaluate the impact of these ASC sheets on the proliferative stages of repair at 14 days, ASC sheets with and without gelatin microspheres containing the tenogenic growth factor bone morphogenic protein-12 (BMP12, a.k.a. GDF7) were surgically implanted following flexor tendon injury and repair (Figure 5.4).

Sustained delivery of BMP12 via gelatin microspheres: Gelatin microspheres were synthesized as previously described [197, 412], by Phuong N. Dang in Professor Eben Alsberg's research group at Case Western Reserve University. Low ($19.5 \pm 5.65\%$) and high crosslinked (65%) microspheres were generated by crosslinking dry microspheres in 1% w/v aqueous genipin solution (Wako Chemicals USA, Inc., Richmond, VA) in distilled water at room temperature for 2 and 24.5 hours, respectively. To load BMP12, lyophilized microspheres were UV-sterilized for 10 minutes

and rehydrated in BMP12/PBS solution (pH 6) at varied concentrations for 2 hours at 37 °C. Unloaded control microspheres were soaked in PBS without BMP12. At pH 6, positively charged BMP12 and negatively charged acidic gelatin form complexes, facilitating microsphere loading [413, 414]. To determine BMP12 release kinetics, BMP12 was biotinylated with EZ-Link Sulfo-NHS-Biotin kit (Thermo Fisher Scientific) according to the manufacturer's protocol except for substituting the manufacturer's buffer with 50% (v/v) propylene glycol containing 1 M NaCl, 50 mM HEPES (pH 7.0) to stabilize BMP12. The resulting biotin-BMP12 was loaded to either high or low crosslinked microspheres at a concentration of 2 µg BMP12/mg micropsheres as described above. BMP12 release from microspheres was performed in PBS (pH 7.0) at 37 °C for 2 weeks and determined by measuring BMP12 contents in PBS at varied time points via dot blot for biotin and using biotin-BMP12 as a protein standard. As most of BMP12 was released from the low crosslinked microspheres within the first three days after loading and the high crosslinked microspheres enabled a steady 20 – 40 ng daily release of BMP12 over a 14-day period during pilot studies (Figure 5.5), the high crosslinked microspheres were used in the subsequent *in vivo* studies.

ASC + BMP12 cell sheet creation: Collagen–ASC sheets were prepared from autologous subcutaneous fat collected 2 weeks before surgery, as described above. To deliver BMP12-loaded microspheres and ASCs *in vivo*, high crosslinked microspheres were loaded with BMP12 at a concentration of 4 µg BMP12/mg microsphere. One mg of BMP12-loaded or unloaded microspheres were added to type I collagen (Corning Inc., Bedford, MA) solution (1 mL of 2 mg/mL, pH 7.2). The resulting suspension was allowed to gel at 37 °C for 1 hour in a round cast to generate a thin microsphere-containing collagen sheet (ϕ 19 mm $\times$ 500µm thick). Passage 3 ASCs were subsequently cultured on the collagen sheet at a density of 16,000 cells/cm^2 for 3 – 4 days *in vitro* and then applied *in vivo* as shown in Figure 5.2A,B. All repaired digits received controlled passive mobilization starting 24 hours after surgery as described previously [57, 388]. Animals were euthanized 14 days after repair.

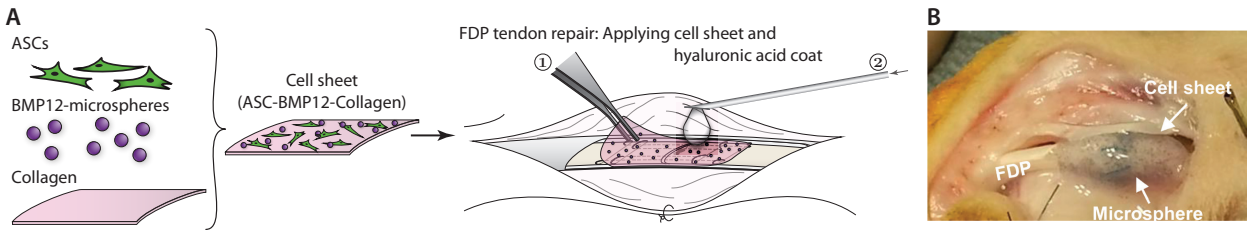

Figure 5.4: Cell sheets were generated for *in vivo* delivery of ASCs and BMP12. (A) The procedures for generation and *in vivo* delivery of cell sheets are illustrated. Hyaluronic acid (HA) was used to secure cell sheet at the repair site. (B) A representative photograph shows a cell sheet applied to a repaired flexor digitorum profundus tendon (FDP).

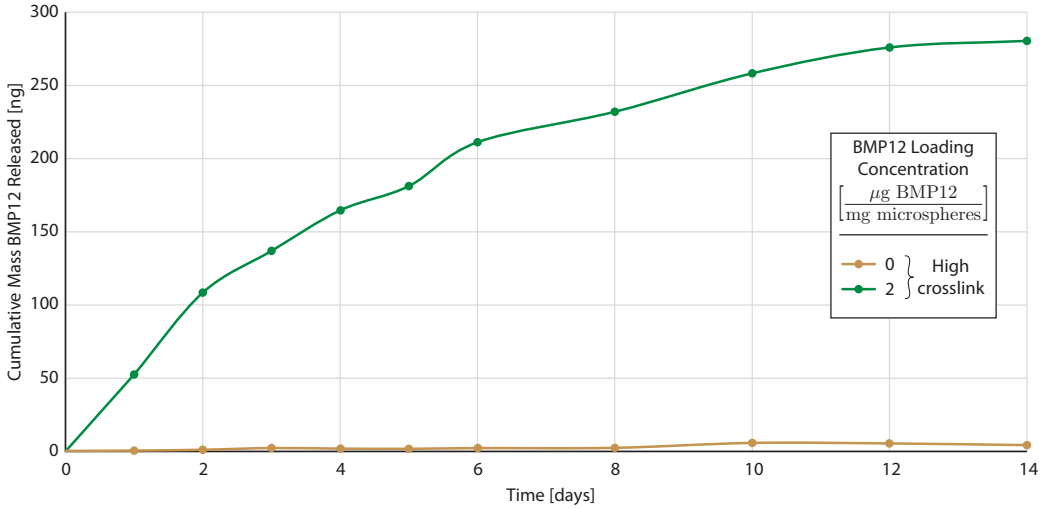

Figure 5.5: Pilot study demonstrating BMP12 growth factor release kinetics from highly crosslinked gelatin microspheres. High crosslink microspheres exhibited sustained release over the first two weeks *in vitro*.

Effects of sustained BMP12 delivery with ASC sheets: RNA was isolated and TaqMan RT-PCR was used to determine the gene expression profile in repaired tendons after sacrifice as described above ($n = 6$ tendons per group for gene expression). Compared to analysis at 7 days (Figure 5.3), RT-PCR analysis of markers of macrophage polarization at 14 days demonstrated only a moderate overall inflammatory response, as predicted for the proliferative stage of repair. At 14 days, the ASC-only group did not continue to demonstrate a statistically significant shift toward M2 macrophages, possibly due to lower total inflammatory cell counts following the anti-inflammatory effect seen at 7 days (Figure 5.6). However, there was a substantial shift toward M2 macrophages in the ASC + BMP12 treatment group. ASC sheets containing BMP12 microspheres substantially increased expression of the M2 stimulator gene *IL-4* and the M2 marker gene *CD163* compared to repair alone or the repair with ASC sheets but no BMP12 (Figure 5.6A,B). This late-stage anti-inflammatory impact of BMP12 did not change collagen production levels compared to other groups (Figure 5.6C). Future work on gene expression and proteomics analyses for these samples, as well as later stage studies assessing biomechanical properties, would help elucidate if and how the anti-inflammatory effect seen at 7 and 14 days with ASC and ASC + BMP12 treatment, respectively, impacts tendon healing and functional outcomes.

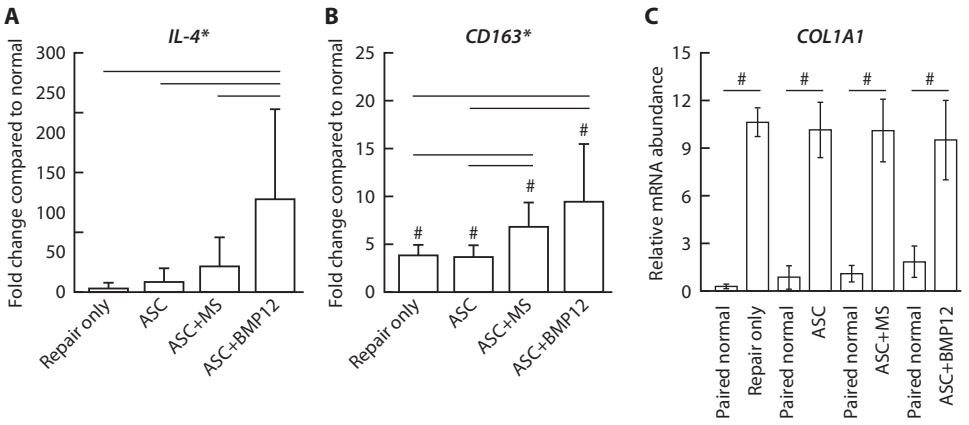

Figure 5.6: Pilot study demonstrating BMP12 growth factor release kinetics from highly crosslinked gelatin microspheres. High crosslink microspheres exhibited sustained release over the first two weeks *in vitro*.

5.4.3 Combinatorial therapy approaches

The adhesive delivery approaches developed in this thesis do not substantially change how repairs are technically performed in the operating room. Since sutures are introduced into repairs regardless, porous sutures coated with adhesives or growth factors could theoretically be combined with the cell sheet therapies described here (Figure 5.7). Such combination therapies offer an opportunity to provide synergistic benefit through early mechanical strength from the adhesive and later biologic stimulation. Future work could also explore these combinatorial approaches as a means of improving tendon or tendon-to-bone repair. By simultaneously delivering CTGF as in Chapter 4 and cell sheets as described here, CTGF could induce ASCs or ASC-influenced cells to extend matrix into the suture material and across the transected surface. This type of approach could simultaneously provide the biological instructions and the cells needed to carry out those instructions within the otherwise paucicellular intrasynovial tendon environment. However, these combinatorial approaches would add substantial complexity to the repair from the scientific, regulatory, and clinical application perspectives. Cell therapies requiring modification of autologous cells are particularly challenging, since they require multiple operations and intense care to avoid deleterious stimulation of the autologous tissue before re-implantation. Therefore, combinatorial approaches would need thorough *in vitro* and *in vivo* validation to ensure that neither factor independently or in combination negatively impacts repair outcomes.

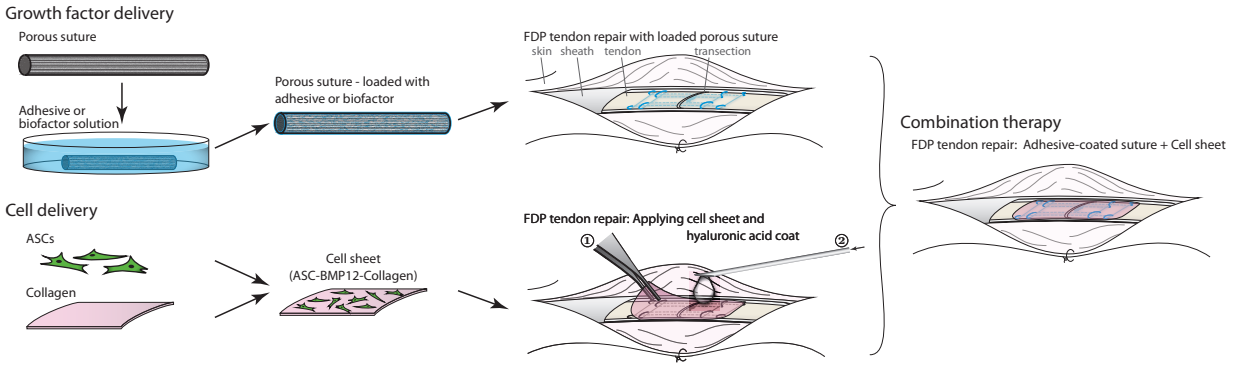

Figure 5.7: Schematic of an envisioned combinatorial therapy approach to deliver mechanically augmented sutures in addition to anti-inflammatory cell sheets. Combined biological and mechanical approaches could greatly improve repair healing. However, it is important to remember that combined approaches are inherently more complicated from scientific, clinical, regulatory perspectives, and could actually lead to negative effects due to added foreign material or unanticipated negative interactions.

5.5 Conclusions

Taken as a whole, this thesis presents a theoretical basis and experimental proof-of-concept for versatile adhesive approaches to improve the mechanical strength and toughness of tendon, tendon-to-bone, and potentially other soft tissue repairs by several fold. We have highlighted desirable adhesive material properties as well as potential adhesive biomaterials with appropriate properties. In order to evaluate adhesive candidates, we developed rapid testing platforms that are predictive of clinical-style repair strength improvements. Furthermore, we developed a simple delivery mechanism using sutures with porous outer sheaths to enhance delivery capacity and mechanical binding of chemical adhesives or biological factors. These simple technologies can theoretically be applied in combination with biological approaches being developed here and elsewhere, though such combined approaches would complicate technology development, preclinical and clinical testing, and regulatory approval. Future work assessing adhesive materials for application in either adhesive-coated (porous) sutures or adhesive films could theoretically provide greater than 500% repair strength improvements, eliminating a major source of orthopaedic repair failures.

Appendix A

Enhanced zone II flexor tendon repair through a new half hitch loop suture configuration

Ioannis Kormpakis*, Stephen W. Linderman*, Stavros Thomopoulos, Richard H. Gelberman

*These authors contributed equally to this work.

This chapter was published in PLoS One, 2016 Apr 21;11(4):e0153822. doi: 10.1371/journal.pone.0153822 [108].

A.1 Abstract

This study evaluated the impact of a new half hitch loop suture configuration on flexor tendon repair mechanics. Cadaver canine flexor digitorum profundus tendons were repaired with 4- or 8-strands, 4–0 or 3–0 suture, with and without half hitch loops. An additional group underwent repair with half hitch loops but without the terminal knot. Half hitch loops improved the strength of 8-strand repairs by 21% when 4–0, and 33% when 3–0 suture was used, and

caused a shift in failure mode from suture pullout to suture breakage. 8-strand repairs with half hitch loops but without a terminal knot produced equivalent mechanical properties to those without half hitch loops but with a terminal knot. 4-strand repairs were limited by the strength of the suture in all groups and, as a result, the presence of half hitch loops did not alter the mechanical properties. Overall, half hitch loops improved repair mechanics, allowing failure strength to reach the full capability of suture strength. Improving the mechanical properties of flexor tendon repair with half hitch loops has the potential to reduce the postoperative risk of gap formation and catastrophic rupture in the early postoperative period.

A.2 Introduction

Despite improved operative technique and postoperative rehabilitation, the outcomes of intrasynovial flexor tendon repair are highly variable [415, 11, 12, 100, 416]. The most commonly manifested complications of tendon repair are gap formation, repair-site failure, and adhesion formation between the repaired tendon and synovial sheath [31]. Typically, complications are noted within the initial few weeks following suture repair and depend, to a considerable extent, on the initial biomechanical properties of the repair [20]. Improving the biomechanical properties of repaired tendon is central to reducing the incidence of tendon rupture and gap formation, and for facilitating early controlled mobilization.

The initial mechanical properties of repaired tendon depend on the suture material and caliber and the interaction between the suture and tendon brought about by the repair technique [417, 418, 107, 250]. Numerous suture materials and repair techniques have been described, including variations in core and peripheral suture caliber and purchase, numbers of strands and knot placement [107, 419, 420]. The most commonly used surgical techniques employ a 3–0 or 4–0 caliber core suture and a 5–0 or 6–0 caliber peripheral suture. Typically, either four, six, or eight strands are used and the final knot is placed either inside or outside the interface between the tendons stumps [420, 421].

Although prior studies have demonstrated the importance of suture caliber and suture strand number on the initial mechanical properties of tendon repair [22], less consideration has been given to the mechanical effects created by the core suture loops. In the current study, our objective was to assess the mechanical interaction between tendon suture and Zone II flexor tendon (i.e., tendon grasping) as a function of the presence of a new style of half hitch loops (A.K.A. pretzel links), in an alternating configuration with the classic grasping loops, compared to repairs using grasping loops only. These half hitch loops form a small knot, gripping the tendon more than previously described

locking loops [17, 109]. Previous studies demonstrate that locking loops at every position lead to uneven tensioning and premature failure of the repair, motivating our alternating loop configuration [422]. To investigate this premise, we studied the effects of half hitch loops on 4- and 8-strand repairs performed with 3–0 and 4–0 suture. In addition, we considered a knotless configuration of the 8-strand repair using half hitch loops. Our hypothesis was that increased holding capacity between the tendon and the suture through the use of half hitch loops, in alternation with grasping loops, would improve the initial mechanical properties of 4- and 8-strand repair configurations.

A.3 Materials and Methods

A.3.1 Study design

In this *ex vivo* study, ninety-four cadaveric canine flexor digitorum profundus tendons were transected in Zone II, between the A2 and A4 pulleys. The tendons were divided into eight groups (Table A.1) with either 4-strand modified Kessler or standard 8-strand repairs, with or without half hitch loops, using 3–0 or 4–0 suture. In addition, a group of tendons was repaired with an 8-strand knotless modification with half hitch loops. All repairs were performed by an orthopaedic hand surgeon. All tendons tested in this study were from hindpaws of healthy female adult mongrel dogs 20–30 kg in weight (Covance Research, Princeton, NJ), taken postmortem from an unrelated project. The unrelated project, which investigated experimental approaches for forepaw flexor digitorum profundus tendon repair *in vivo*, was approved by the Animal Studies Committee, Office of the Vice Chancellor for Research, Washington University in St. Louis for RHG's Animal Approval Protocol #20140115. All work performed herein followed the policies and procedures for scientific research at Washington University in St. Louis, including the Research Integrity Policy by the Research Ethics and Compliance Office, Office of the Vice Chancellor for Research, Washington University in St. Louis.

A.3.2 Half hitch loop technique

The technical modification introduced here shares some characteristics with the 4-strand modified Kessler and the 8-strand Winters-Gelberman repairs. A core suture purchase of 1.2 cm and a peripheral suture purchase of 2 mm was used (Figure A.1). Supramid 4–0 or 3–0 looped double-strand suture (S. Jackson Inc., Alexandria, VA) was used for the core suture and 5–0 polypropylene was used for the peripheral suture. The repair consisted of half hitch

Technique	Strands	Caliber	*N*
Grasping	4	4–0	14
Hitched	4	4–0	12
Grasping	4	3–0	9
Hitched	4	3–0	9
Grasping	8	4–0	12
Hitched	8	4–0	12
Hitched knotless	8	4–0	12
Grasping	8	3–0	7
Hitched	8	3–0	7

Table A.1: Flexor tendon suture configurations.

and grasping loops of the core suture in an alternating fashion, which avoided the creation of consecutive hitches (Figure A.1). This configuration is symmetric, with the same number of half hitch and grasping loops on the distal and proximal stumps, medially and laterally. This setup facilitated even tensioning of the repair, where each half hitch loop secured one stump while the adjacent grasping loop allowed gliding of the suture to occur. The sliding of one loop in each pair allowed flexibility for balancing the tension of the suture strands by the surgeon, avoiding uneven load bearing among the individual strands.

To perform the half hitch loop suture in a 4-strand repair, the first and third loops were tied (Figure A.1e). To accomplish the half hitch loop configuration in an 8-strand repair, two additional alternating half hitch loops were created providing 4 hitches (second, fifth, seventh and eighth loops; Figure A.1f). In addition, a knotless version of the 8-strand repair was performed in which the terminal knot was not tied and the free end of the suture was passed through the tendon substance using a free needle. The surgeon must carefully pass the sutures in the final step of each half hitch through the space created by the previous two passes in order to achieve a successful half hitch (Figure A.1c-d).

A.3.3 Biomechanical testing

Repairs were tested biomechanically using methods described previously [103, 105]. The proximal tendon was gripped with a triangle-toothed grip and the distal phalanx was gripped in a custom grip. After preconditioning, repaired tendons were pulled in uniaxial tension until failure on a material testing machine (5866; Instron Corp., Norwood, MA). Failure mode (e.g., suture pullout or suture breakage) was recorded. The load to create a 2 mm gap (N), maximum load (N), extension at 20 N and at maximum load (mm), strain at 20 N and at maximum load (%), stiffness (N/mm) (the slope of the linear portion of the load–deformation curve), rigidity (N/%), and resilience (N strain) (the area under the load–strain curve up to the yield point) were determined using a custom-written code in MATLAB

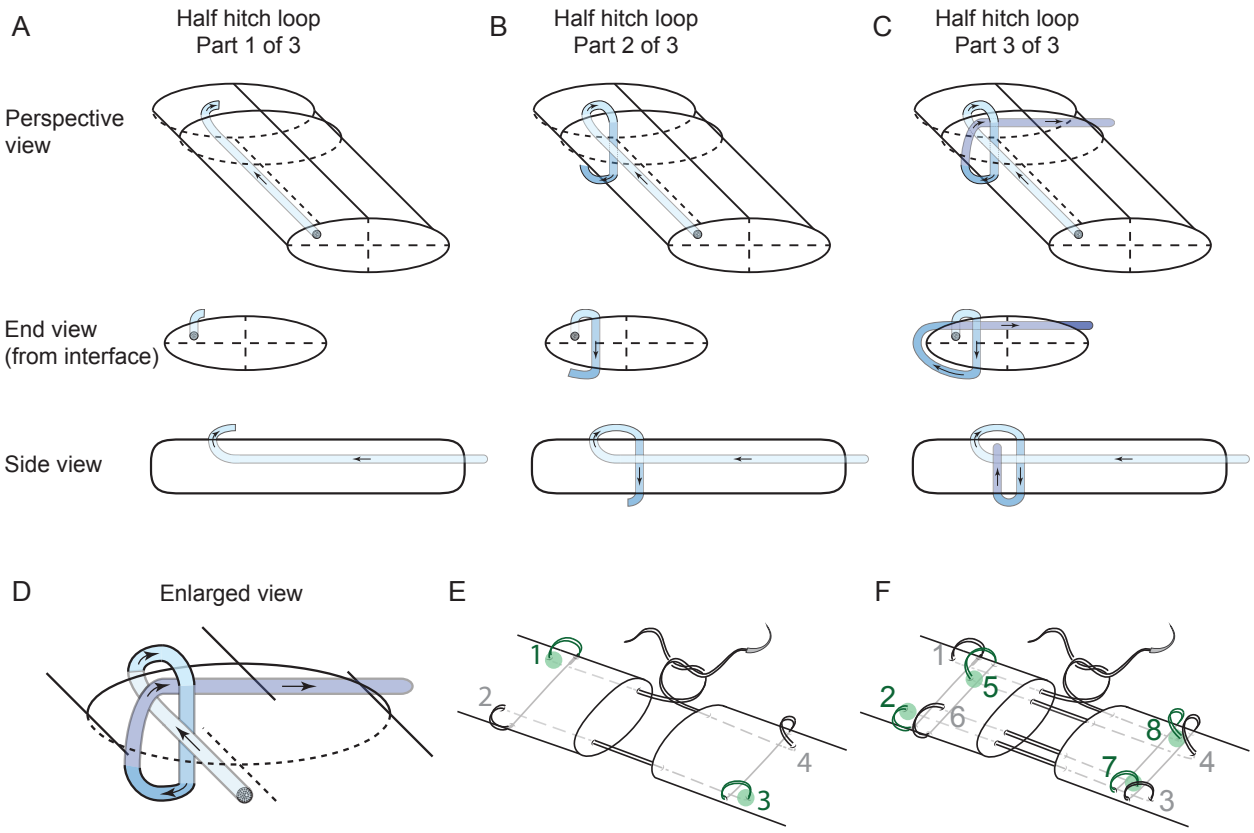

Figure A.1: **Suture configuration. (A-C)** The three suture passes required to make a single half hitch loop are shown sequentially as an end view from the transection interface, a side view, and a perspective view. This is a continuous piece of suture, where suture coloration is artificially added to aid in following the suture path, going from blue to purple. The suture diameter is enlarged two-fold for clarity. Looped suture is used surgically, but only one of each pair of suture threads is diagrammed here for simplicity. **(D)** The complete half hitch loop configuration is enlarged for clarity. **(E-F)** The locations of half hitch loops are shown in green for 4-strand modified Kessler (E) and 8-strand Winters-Gelberman (F) repairs. In 8-strand repairs, the first four passes were performed on the dorsal side and the last four passes were performed on the ventral side of the tendon.

(Natick, MA), as described previously [256]. Load to create a gap of 2 mm between tendon stump ends (a threshold level that leads to decreased repair strength and increased adhesions) was calculated by optically tracking regions nearest to the repair site [100].

A.3.4 Statistics

Groups were compared using an analysis of variance (ANOVA) followed by a Tukey's honest significant difference test for pairwise comparisons when appropriate. An alpha level of $p < 0.05$ was set for statistical significance. Results were plotted as mean $\pm$ standard deviations.

A.4 Results

A.4.1 Mechanical properties were improved when half hitch loops were incorporated into 8-strand repairs

The addition of half hitch loops significantly improved the overall mechanical properties of 8-strand repairs. Load to create a 2 mm gap, maximum load, and resilience significantly increased in half hitch repairs compared to standard 8-strand repairs for 3–0 caliber suture, and maximum load and resilience significantly increased in half hitch repairs compared to standard 8-strand repairs for 4–0 caliber suture ($p < 0.05$ for each comparison; Figure A.2). In contrast, the mechanical properties of the 4-strand repairs, with and without half hitch loops, were not significantly different ($p > 0.05$ for each comparison). Load to create a 2 mm gap, maximum load and resilience were not significantly different when comparing the modified 4-strand Kessler repair with and without half hitch loops, regardless of suture caliber (Figure A.2). Stiffness was similar for all half hitch repair groups compared to their respective controls (Figure A.2). 4-strand repairs with half hitch loops had statistically greater strain and extension to maximum load compared to modified Kessler repairs without half hitch loops (Table A.2).

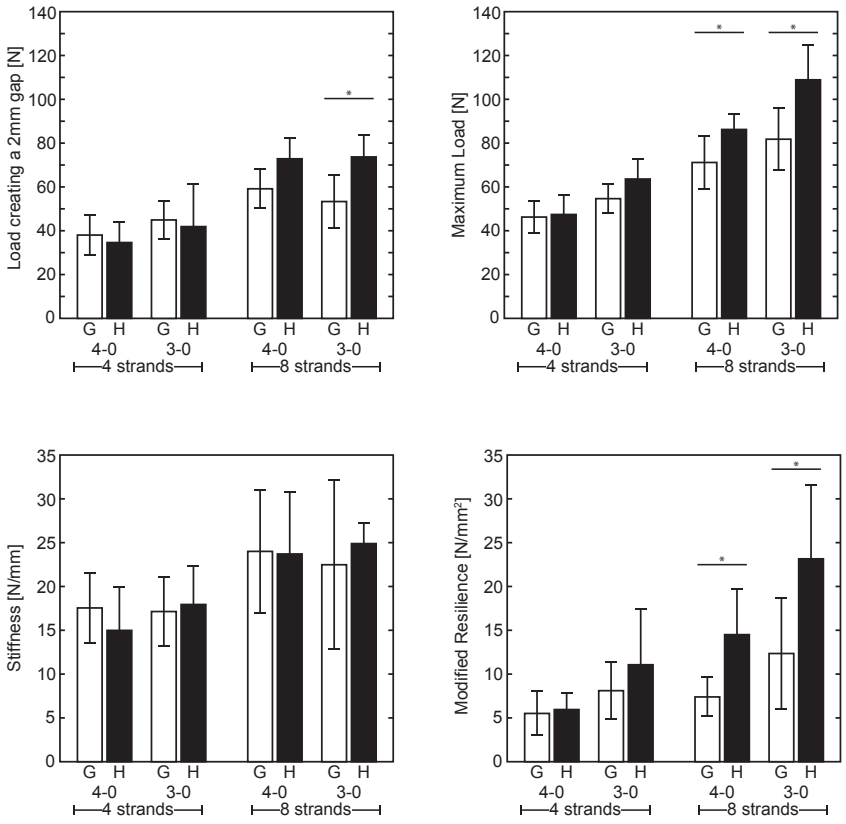

Figure A.2: **Mechanical properties.** Load creating a 2 mm gap, maximum load, and resilience were significantly improved with the addition of half hitch loops in 8 strand repairs. (G: grasping, H: hitched, * $p < 0.05$, mean $\pm$ standard deviations are shown).

Technique	**Strands**	**Caliber**	**Extension**$\vert_{20\text{ N}}$ (mm)	**Strain**$\vert_{20\text{ N}}$ (%)	**Extension**$\vert_{\text{Max Load}}$ (mm)	**Strain**$\vert_{\text{Max Load}}$ (%)	**Rigidity** (N/%)
Grasping	4	4–0	1.56 ± 0.32	10.4 ± 2.2	5.08 ± 2.31	33.7 ± 15.3	2.64 ± 0.60
Hitched	4	4–0	1.59 ± 0.33	10.6 ± 2.2	7.32 ± 2.70	48.7 ± 17.9	2.25 ± 0.75
Grasping	4	3–0	1.74 ± 0.24	11.5 ± 1.5	7.50 ± 2.43	49.5 ± 15.8	2.59 ± 0.60
Hitched	4	3–0	1.54 ± 0.36	10.2 ± 2.4	7.43 ± 3.09	49.3 ± 20.5	2.71 ± 0.66
Grasping	8	4–0	1.33 ± 0.43	8.8 ± 2.9	5.51 ± 1.97	36.6 ± 13.2	3.62 ± 1.07
Hitched	8	4–0	1.60 ± 0.64	10.6 ± 4.3	6.88 ± 2.42	45.7 ± 16.1	3.57 ± 1.06
Hitched knotless	8	4–0	1.13 ± 0.14	7.5 ± 0.9	7.42 ± 2.11	49.0 ± 13.8	3.14 ± 0.65
Grasping	8	3–0	1.10 ± 0.96	7.3 ± 6.4	7.23 ± 3.50	48.2 ± 23.3	3.37 ± 1.46
Hitched	8	3–0	1.23 ± 0.11	8.2 ± 0.7	6.39 ± 1.19	42.4 ± 7.9	3.75 ± 0.35

Table A.2: Mechanical properties of repairs (mean $\pm$ standard deviation).

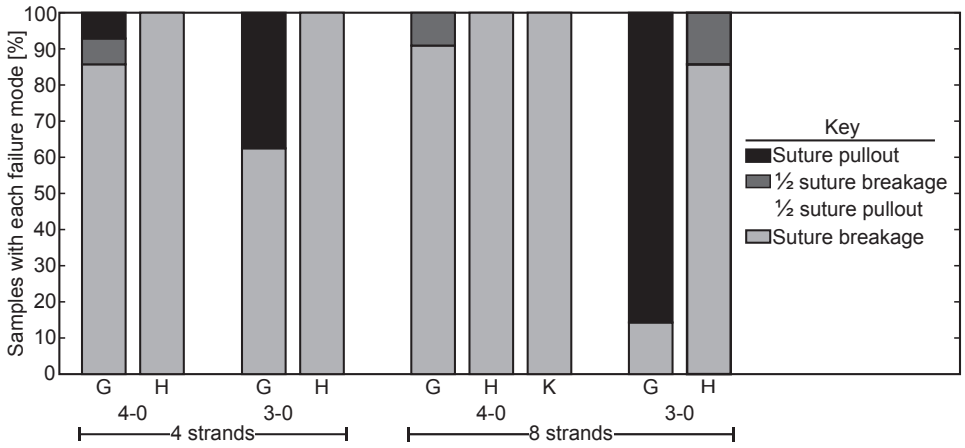

Figure A.3: **Failure modes.** Repairs completed with 4–0 caliber suture failed almost exclusively by suture breakage. Increasing suture caliber from 4–0 to 3–0 led to a shift in failure mode from suture breakage to suture pullout. The addition of half hitch loops shifted the failure mode in 3–0 suture caliber repairs back to suture breakage, indicating a significant increase in suture-tendon interaction due to the hitches. (G: grasping, H: hitched, K: hitched knotless).

A.4.2 Failure mode shifted from suture pullout to suture breakage with the addition of half hitch loops

When suture caliber was increased from 4–0 to 3–0, the failure mode of the standard 8-strand repairs without half hitch loops shifted from suture breakage to suture pullout. When half hitch loops were added to the 8-strand repairs performed with 3–0 caliber sutures, the failure mode shifted from suture pullout to suture breakage, indicating improved tendon grasping by the suture due to the half hitch loops (Figure A.3). The predominant failure mode of 4-strand repairs was suture breakage, regardless of suture caliber and the presence or absence of half hitch loops (Figure A.3).

A.4.3 The knotless configuration of the 8-strand repair with half hitch loops had equivalent mechanical properties to a standard 8-strand repair with a knot

The mechanical properties of half hitch loop repairs were similar regardless of whether or not the final knot between the tendon stumps was tied, indicating that the transfer of load occurred primarily at the half hitch loops, not at the final knot (Figure A.4). Both knotted and knotless half hitch loop repair groups had significantly higher maximum load and resilience compared to the standard 8-strand repair ($p < 0.05$ for each comparison).

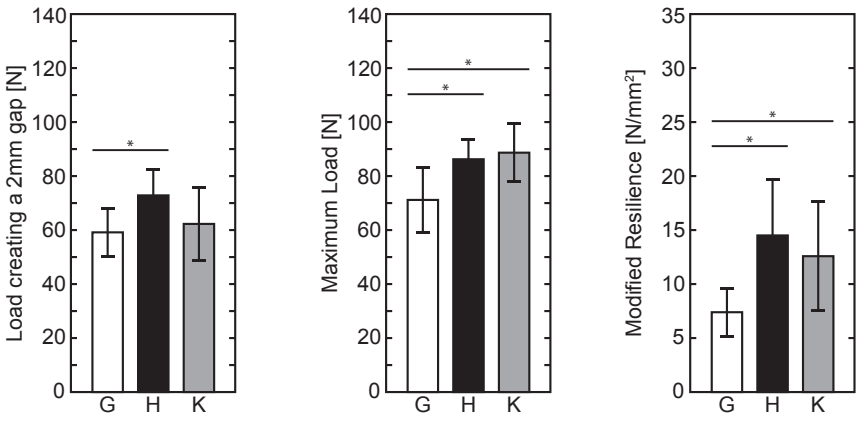

Figure A.4: **Mechanical properties of knotless repairs.** Load creating a 2 mm gap, maximum load, and resilience significantly improved with the addition of half hitch loops. Knotless repairs were either equivalent (load creating a 2 mm gap) or improved (maximum load and resilience) compared to a standard Winters-Gelberman 8-strand repair (G: grasping, H: hitched, * $p < 0.05$, mean $\pm$ standard deviations are shown).

A.5 Discussion

Prior studies have examined the effects of suture technique, suture material, and suture strand number on the time zero mechanical properties of flexor tendon repairs [418, 22]. Previous studies investigating mechanical strength of various terminal knot tying methods show improved strength using reversing half hitches [423, 424]. This common surgical knot tying technique was a motivation for testing a similar half hitch suture configuration applied to the suture loop instead of the terminal knot to improve tissue grasping at suture anchor points within the tendon. Few studies have explored the effects of increased suture-tendon interaction (i.e., improved tendon grasping) through the use of locking loops with the goal of improving mechanical properties of both 4- and 8-strand repairs. We are unaware of any previous studies investigating a similar half hitch loop for flexor tendon repair to the version described herein. In an *in vivo* study, Hatanaka et al. demonstrated that a locking suture configuration markedly enhanced ultimate strength compared to a grasping suture configuration three weeks post repair [24]. Similarly, another study showed that 3–0 caliber 4-strand cross-stitch locked repairs had significantly greater fatigue strength than did non-locked repairs and that the failure mechanism shifted from suture pullout to suture breakage [425]. On the other hand, Wong et al. showed that the consecutive locks in 6-strand repairs caused uneven load bearing among the strands, motivating the alternating half hitch and grasping loop approach described herein [422]. Employing a similar underlying principle, a recent study demonstrated that the addition of an adhesive coating to sutures in 8-strand repairs increased maximum load by 17% and load to create a 2 mm gap by 17.5% [256]. These results suggest that increasing the interaction between suture and the tendon, whether through suture half hitch loops or adhesives or a combination thereof, can lead to an improvement

in the mechanical properties of the repair.

Findings in the current experimental study indicate that the failure of tendon repair depends on both the strength of the suture and its ability to grasp the tendon stumps. Increasing the number of strands and/or increasing suture caliber only increases tendon repair strength if the suture is effective in grasping tendon substance. If suture pulls out of tendon prior to breaking, the increased strength provided by additional suture material is not realized. An *ex vivo* study showed that cadaver flexor tendon repairs tend to fail by suture pullout, particularly when they are performed with 8-strands and higher caliber suture [22]. In our study, the utilization of half hitch loops in alternation with the grasping loops increased grasping strength in 8-strand repairs through more effective load transfer between the tendon and suture and through averting the uneven load distribution that results from consecutive locks or hitches. The effect was most profound when the repairs were performed with 3–0 suture, as the failure mode shifted from suture pullout to suture breakage. Furthermore, contrasting 8-strand repair groups indicated that the presence of an alternating half hitch loop configuration appeared to be of greater importance than an increase in suture caliber. Maximum load and load to 2 mm gap failed to increase significantly when increasing caliber from 4–0 to 3–0 suture. In contrast, 8-strand half hitch repairs performed with 4–0 suture yielded similar maximum load values and statistically greater load to 2mm gap compared to classic 8-strand repairs performed with 3–0 suture. These findings indicate that the use of this half hitch pattern has a greater influence on repair mechanics than does suture caliber.

Based on the improvements in repairs with half hitch loops, we explored a knotless technique and noted equivalent or improved mechanical properties compared to the standard Winters-Gelberman 8-strand repair. This result highlights the strength of the half hitch loops for transferring load across the repair site and could have significant implications for the *in vivo* setting. Instead of relying on the terminal knot, the half hitch loops held the suture in the appropriate configuration and prevented unraveling. Previous studies have examined the effects of knot placement on the mechanical properties of the repair and on adhesions formation during healing. Momose et al. demonstrated that placing the knot outside of the repair site improves tensile strength compared to placing the knot at the interface of tendons stumps (i.e., "inside" of the repair) [421]. However, this improvement in strength comes with a penalty: knot placement outside of the repair also increases tendon gliding resistance and tissue irritation, leading to adhesion formation. In order to minimize the effect of the knots, a number of knotless approaches have been introduced using barbed sutures, with mixed outcomes [398, 399]. The knotless modification of the 8-strand repair shown here has the potential to combine the benefits to gliding and surgical operation time of a knotless repair with the benefits to tensile strength of the Winters-Gelberman repair technique.

While an improvement in mechanical properties was noted in the 8-strand repair group (increased load to create a 2 mm

gap, failure load, and resilience), the mechanical properties of the 4-strand repairs was not significantly improved. We note that 4-strand repairs failed predominantly by suture breakage, even when 3–0 caliber suture was used. Therefore, the weakest component of the 4-strand repair appears to be the strength of the suture, not the tendon grasping strength.

There were several limitations to this study that may require further investigation. First, it is possible that the 8-strand half hitch repair may cause injury to the dorsal vascular supply of tendon due to the dorsal placement of some of the loops. However, dorsal placement has been shown to be well tolerated in prior *in vivo* studies at intervals through 3 and 6 weeks post repair [31, 24]. Second, this study used canine cadaver tissue. Canine tendons may have different mechanical properties compared to human tendons. However, this animal model has been shown to have anatomic similarities to human tendons, in both *ex vivo* and *in vivo* experiments [147]. Third, we did not measure the gliding properties of the repairs in this *ex vivo* proof-of-concept study. The addition of half hitch loops to the repairs could affect gliding resistance, since more of the suture is laying on the tendon surface than in the traditional configurations. The similarity of the half hitch repairs to existing methods decreases the likelihood that gliding will be affected significantly. Future work should evaluate the work of flexion and gliding resistance prior to incorporating half hitch loops into clinical practice.

The results of this study confirm the hypothesis that increased tendon grasping strength through the use of half hitch loops, alternating with the grasping loops of the core suture, enhances the mechanical properties of 8-strand repairs, particularly when the repairs are carried out with 3–0 suture. The approach, however, did not enhance the properties of 4-strand repairs. Repair site failure mode appears to be of prime importance in predicting the mechanical properties of sutured intrasynovial tendon. In addition, the new half hitch loop configuration provided sufficient gripping capacity to allow for a knotless modification to the classical 8-strand repair. This knotless technique should be further evaluated *in vivo* for clinical utility.

A.6 Acknowledgements

Mr. Ryan Potter performed biomechanical testing for some of the repairs.

References

[1] American Academy of Orthopaedic Surgeons. Half of all musculoskeletal injuries occur in home: USBJD project draws attention to burden of musculoskeletal conditions. *AAOS Now* 2009;3(4).

[2] United States Bone and Joint Initiative. The Burden of Musculoskeletal Diseases in the United States. Third ed.; Rosemont, IL; 2014.

[3] A. Praemer, S. Furner, D. Rice. Musculoskeletal Conditions in the US. In: American Academy of Orthopaedic Surgeons. Park Ridge, IL; 1992,.

[4] R.C. Mather, A. Romeo, J. Tongue, G.W. Jr. The Societal and Economic Value of Rotator Cuff Repair. *J Bone Joint Surg Am* 2013;95(22):1993–2000.

[5] R.C. Mather, L. Koenig, M.S. Kocher, T.M. Dall, P. Gallo, D.J. Scott, B.R. Bach, K.P. Spindler, M.K. Group. Societal and economic impact of anterior cruciate ligament tears. *J Bone Joint Surg Am* 2013;95(19):1751–1759.

[6] S. Thomopoulos, P.C. Amadio, C. Zhao, R.H. Gelberman. Tendinopathy and Tendon Repair. In: R. O'Keefe, J.J. Jacobs, C.R. Chu, T.A. Einhorn, editors. Orthopaedic Basic Science: Foundations of Clinical Practice; chap. 20; Fourth ed. American Academy of Orthopaedic Surgeons; 2012, p. 329–340.

[7] S. Thomopoulos, W.C. Parks, D.B. Rifkin, K.A. Derwin. Mechanisms of tendon injury and repair. *J Orthop Res* 2015;33(6):832–839.

[8] A.D. Potenza. Tendon healing within the flexor digital sheath in the dog. *J Bone Joint Surg Am* 1962;44-A(1):49–64.

[9] I. Kessler, F. Nissim. Primary repair without immobilization of flexor tendon division within the digital sheath. An experimental and clinical study. *Acta Orthop* 1969;40:587–601.

[10] M.I. Boyer, J.W. Strickland, D.R. Engles, K. Sachar, F.J. Leversedge. Flexor Tendon Repair and Rehabilitation: State of the Art in 2002. *Instr Course Lect* 2003;52:137–61.

[11] S.C. Winters, R.H. Gelberman, S.L.Y. Woo, S.S. Chan, R. Grewal, J.G. Seiler III. The Effects of Multiple-Strand Suture Methods on the Strength and Excursion of Repaired Intrasynovial Flexor Tendons: A Biomechanical Study in Dogs. *J Hand Surg Am* 1998;23(1):97–104.

[12] S.L.Y. Woo, R.H. Gelberman, N.G. Cobb, D. Amiel, K. Lothringer, W.H. Akeson. The importance of controlled passive mobilization on flexor tendon healing. *Acta Orthop Scand* 1981;52(6):615–622.

[13] R.H. Gelberman, S.L. Woo, K. Lothringer, W.H. Akeson, D. Amiel. Effects of early intermittent passive mobilization on healing canine flexor tendons. *J Hand Surg Am* 1982;7(2):170–175.

[14] C.E. Verdan. Primary repair of flexor tendons. *J Bone Joint Surg Am* 1960;42(4):647–657.

[15] S. Bunnell. Surgery of the hand. 3rd ed.; Philadelphia: JB Lippincott; 1956.

[16] I. Kessler. The "grasping" technique for tendon repair. *Hand* 1973;5(3):253–255.

[17] D.G. Pennington. The locking loop tendon suture. *Plast Reconstr Surg* 1979;63(5):648–52.

[18] D. Ootes, K.T. Lambers, D.C. Ring. The epidemiology of upper extremity injuries presenting to the emergency department in the United States. *Hand* 2012;7(1):18–22.

[19] D. Tuncali, N. Yavuz, A. Terzioglu, G. Aslan. The rate of upper-extremity deep-structure injuries through small penetrating lacerations. *Ann Plast Surg* 2005;55(2):146–148.

[20] D.T. Fufa, D.A. Osei, R.P. Calfee, M.J. Silva, S. Thomopoulos, R.H. Gelberman. The effect of core and epitendinous suture modifications on repair of intrasynovial flexor tendons in an *in vivo* canine model. *J Hand Surg Am* 2012;37(12):2526–31.

[21] E. Diao, S. Hariharan, O. Soejima, J.C. Lotz, S. Francisco. Effect of Peripheral Suture Depth on Strength of Tendon Repairs. *J Hand Surg Am* 1996;21(2):234–239.

[22] G.N. Nelson, R. Potter, E. Ntouvali, M.J. Silva, M.I. Boyer, R.H. Gelberman, S. Thomopoulos. Intrasynovial flexor tendon repair: a biomechanical study of variations in suture application in human cadavera. *J Orthop Res* 2012;30(10):1652–9.

[23] P.J.F. Wade, R.G. Wetherell, A.A. Amis. Flexor tendon repair: Significant gain in strength from the halsted peripheral suture technique. *J Hand Surg Br* 1989;14(2):232–235.

[24] H. Hatanaka, P.R. Manske. Effect of suture size on locking and grasping flexor tendon repair techniques. *Clin Orthop Relat Res* 2000;(375):267–274.

[25] J.W. Strickland. Development of flexor tendon surgery: Twenty-five years of progress. *J Hand Surg Am* 2000;25(2):214–235.

[26] R. Savage, G. Risitano. Flexor tendon repair using a "six strand" method of repair and early active mobilisation. *J Hand Surg Br* 1989;14(4):396–9.

[27] H. Becker, M. Davidoff. Eliminating the Gap in Flexor Tendon Surgery: A New Method of Suture. *Hand* 1977;9(3):306–311.

[28] W.F. Wagner, C. Carroll, J.W. Strickland, D.a. Heck, J.P. Toombs. A biomechanical comparison of techniques of flexor tendon repair. *J Hand Surg Am* 1994;19(6):979–83.

[29] E. McLarney, H. Hoffman, S.W. Wolfe. Biomechanical analysis of the cruciate four-strand flexor tendon repair. *J Hand Surg Am* 1999;24(2):295–301.

[30] M.J. Silva, M.I. Boyer, K. Ditsios, M.E. Burns, F.L. Harwood, D. Amiel, R.H. Gelberman. The insertion site of the canine flexor digitorum profundus tendon heals slowly following injury and structure repair. *J Orthop Res* 2002;20:447–453.

[31] M.I. Boyer, R.H. Gelberman, M.E. Burns, H. Dinopoulos, R. Hofem, M.J. Silva. Intrasynovial flexor tendon repair. An experimental study comparing low and high levels of *in vivo* force during rehabilitation in canines. *J Bone Joint Surg Am* 2001;86(6):891–899.

[32] M.J. Silva, M.D. Brodt, M.I. Boyer, T.S. Morris, H. Dinopoulos, D. Amiel, R.H. Gelberman. Effects of increased In vivo excursion on digital range of motion and tendon strength following flexor tendon repair. *J Orthop Res* 1999;17:777–783.

[33] M.I. Boyer, C.a. Goldfarb, R.H. Gelberman. Recent progress in flexor tendon healing: The modulation of tendon healing with rehabilitation variables. *J Hand Ther* 2005;18:80–86.

[34] A. Khanna, M. Friel, N. Gougoulias, U.G. Longo, N. Maffulli. Prevention of adhesions in surgery of the flexor tendons of the hand: What is the evidence? *Br Med Bull* 2009;90(1):85–109.

[35] K. Chakravarty, M. Webley. Shoulder joint movement and its relationship to disability in the elderly. *J Rheumatol* 1993;20(8):1359–1361.

[36] L.S. Oh, B.R. Wolf, M.P. Hall, B.A. Levy, R.G. Marx. Indications for rotator cuff repair: a systematic review. *Clin Orthop Relat Res* 2007;455:52–63.

[37] J.S. Sher, J.W. Uribe, A. Posada, B.J. Murphy, M.B. Zlatkin. Abnormal findings on magnetic resonance images of asymptomatic shoulders. *J Bone Joint Surg Am* 1995;77:10–15.

[38] S. Tempelhof, S. Rupp, R. Seil. Age-related prevalence of rotator cuff tears in asymptomatic shoulders. *J Shoulder Elbow Surg* 1999;8(4):296–299.

[39] K. Yamaguchi. New guideline on rotator cuff problems. *AAOS Now* 2011;5(1).

[40] L.M. Galatz, C.M. Ball, S.A. Teefey, W.D. Middleton, K. Yamaguchi. The outcome and repair integrity of completely arthroscopically repaired large and massive rotator cuff tears. *J Bone Joint Surg Am* 2004;86-A(2):219–24.

[41] D.T. Harryman II, L.A. Mack, K.Y. Wang, S.E. Jackins, M.L. Richardson, F.A. Matsen III. Repairs of the rotator cuff. Correlation of functional results with integrity of the cuff. *J Bone Joint Surg Am* 1991;73(7):982–989.

[42] R. Naranja, J. Iannotti, G. Gartsman. Complications in rotator cuff surgery. In: Orthopaedic knowledge update: Shoulder and elbow. Rosemont IL, American Academy of Orthopaedic Surgeons; 1994, p. 157–166.

[43] H.E. Lähteenmäki, A. Hiltunen, P. Virolainen, O. Nelimarkka. Repair of full-thickness rotator cuff tears is recommended regardless of tear size and age: a retrospective study of 218 patients. *J Shoulder Elbow Surg* 2007;16(5):586–590.

[44] D.H. O'Donoghue. Surgical treatment of fresh injuries to the major ligaments of the knee. *J Bone Joint Surg Am* 1950;32(4):721–738.

[45] K.D. Shelbourne, P.A. Nitz. The o'donoghue triad revisited combined knee injuries involving anterior cruciate and medial collateral ligament tears. *Am J Sports Med* 1991;19(5):474–477.

[46] M.M. Murray. Current status and potential of primary acl repair. *Clinics in sports medicine* 2009;28(1):51–61.

[47] J.P. Spalazzi, E. Dagher, S.B. Doty, X.E. Guo, S.A. Rodeo, H.H. Lu. *In vivo* evaluation of a multiphased scaffold designed for orthopaedic interface tissue engineering and soft tissue-to-bone integration. *J Biomed Mater Res A* 2008;86(1):1–12.

[48] G.R. Barrett, F.K. Noojin, C.W. Hartzog, C.R. Nash. Reconstruction of the anterior cruciate ligament in females. *Arthroscopy* 2002;18(1):46–54.

[49] B.D. Beynnon, R.J. Johnson, B.C. Fleming, P. Kannus, M. Kaplan, J. Samani, P. Renström. Anterior cruciate ligament replacement: comparison of bone-patellar tendon-bone grafts with two-strand hamstring grafts. *J Bone Joint Surg Am* 2002;84(9):1503–1513.

[50] A. Von Porat, E. Roos, H. Roos. High prevalence of osteoarthritis 14 years after an anterior cruciate ligament tear in male soccer players: a study of radiographic and patient relevant outcomes. *Ann Rheum Dis* 2004;63(3):269–273.

[51] J.A. Metzl, C.S. Ahmad, W.N. Levine. The ruptured achilles tendon: operative and non-operative treatment options. *Curr Rev Musculoskelet Med* 2008;1(2):161–164.

[52] T. Lui. Fixation of tendo achilles avulsion fracture. *Foot Ankle Surg* 2009;15(2):58–61.

[53] A.A. Suchak, G. Bostick, D. Reid, S. Blitz, N. Jomha. The incidence of achilles tendon ruptures in edmonton, canada. *Foot Ankle Int* 2005;26(11):932–936.

[54] R.J. Khan, D. Fick, A. Keogh, J. Crawford, T. Brammar, M. Parker. Treatment of acute achilles tendon ruptures. *J Bone Joint Surg Am* 2005;87(10):2202–2210.

[55] H.M.J. van der Linden-van der Zwaag, R.G.H.H. Nelissen, J.B. Sintenie. Results of surgical versus non-surgical treatment of achilles tendon rupture. *Int Orthop* 2004;28(6):370–373.

[56] M. Möller, T. Movin, H. Granhed, K. Lind, E. Faxen, J. Karlsson. Acute rupture of tendo achillis. *Bone & Joint Journal* 2001;83(6):843–848.

[57] C.N. Manning, N. Havlioglu, E. Knutsen, S.E. Sakiyama-Elbert, M.J. Silva, S. Thomopoulos, R.H. Gelberman. The early inflammatory response after flexor tendon healing: a gene expression and histological analysis. *J Orthop Res* 2014;32(5):645–52.

[58] P.K. Beredjiklian. Biologic aspects of flexor tendon laceration and repair. *J Bone Joint Surg Am* 2003;85-A(3):539–550.

[59] R.H. Gelberman, J.S. Vande Berg, P.R. Manske, W.H. Akeson. The early stages of flexor tendon healing: a morphologic study of the first fourteen days. *J Hand Surg Am* 1985;10(6 Pt 1):776–784.

[60] S.O. Abrahamsson, R.H. Gelberman, S.L. Lohmander. Variations in cellular proliferation and matrix synthesis in intrasynovial and extrasynovial tendons: An in vitro study in dogs. *J Hand Surg Am* 1994;19(2):259–265.

[61] H.E. Kleinert, C. Verdan. Report of the Committee on Tendon Injuries. *J Hand Surg Am* 1983;8(5):794–798.

[62] R.H. Gelberman, J.S. Vandeberg, G.N. Lundborg, W.H. Akeson. Flexor tendon healing and restoration of the gliding surface. An ultrastructural study in dogs. *J Bone Joint Surg Am* 1983;65(1):70–80.

[63] G. Lundborg, F. Rank. Experimental intrinsic healing of flexor tendons based upon synovial fluid nutrition. *J Hand Surg Am* 1978;3(1):21–31.

[64] S.A. Fenwick, B.L. Hazleman, G.P. Riley. The vasculature and its role in the damaged and healing tendon. *Arthritis Res* 2002;4(4):252–60.

[65] R.H. Gelberman, D. Amiel, M. Gonsalves, S.L. Woo, W.H. Akeson. The Influence of Protected Passive Mobilization on the Healing of Flexor Tendons: A Biochemical and Microangiographic Study. *Hand* 1981;13(2):120–128.

[66] U. Khan, S. Kakar, A. Akali, G. Bentley, D.A. McGrouther. Modulation of the formation of adhesions during the healing of injured tendons. *J Bone Joint Surg Br* 2000;82-B(7):1054–1058.

[67] S. Woo, K. An, C. Frank, G. Livesay, C. Ma, J. Zeminski, J. Wayne, B. Myers. Anatomy, biology, and biomechanics of tendon and ligament. In: J.A. Buckwalter, T.A. Einhorn, S.R. Simon, editors. Orthopaedic Basic Science: Biology and Biomechanics of the Musculoskeletal System; Second ed. American Academy of Orthopaedic Surgeons; 2000, p. 581–616.

[68] J.K. Wong, Y.H. Lui, Z. Kapacee, K.E. Kadler, M.W. Ferguson, D.A. McGrouther. The Cellular Biology of Flexor Tendon Adhesion Formation. *Am J Pathol* 2009;175(5):1938–1951.

[69] S.G. Dakin, D. Werling, A. Hibbert, D.R.E. Abayasekara, N.J. Young, R.K.W. Smith, J. Dudhia. Macrophage sub-populations and the lipoxin A4 receptor implicate active inflammation during equine tendon repair. *PloS one* 2012;7(2):e32333.

[70] K.B. Sugg, J. Lubardic, J.P. Gumucio, C.L. Mendias. Changes in macrophage phenotype and induction of epithelial-to-mesenchymal transition genes following acute Achilles tenotomy and repair. *J Orthop Res* 2014;32(7):944–951.

[71] D. Marsolais, C.H. Côté, J. Frenette. Neutrophils and macrophages accumulate sequentially following Achilles tendon injury. *J Orthop Res* 2001;19(6):1203–1209.

[72] A. Mantovani, S.K. Biswas, M.R. Galdiero, A. Sica, M. Locati. Macrophage plasticity and polarization in tissue repair and remodelling. *J Pathology* 2013;229(2):176–185.

[73] S. Hasslund, J.A. Jacobson, T. Dadali, P. Basile, M. Ulrich-Vinther, K. Søballe, E.M. Schwarz, R.J. O'Keefe, D.J. Mitten, H.A. Awad. Adhesions in a murine flexor tendon graft model: autograft versus allograft reconstruction. *J Orthop Res* 2008;26(6):824–833.

[74] A.E. Loiselle, M. Kelly, W.C. Hammert. Biological Augmentation of Flexor Tendon Repair. *J Hand Surg Am* 2016;41(1):144–149.

[75] M.M. Murray, S. Martin, T. Martin, M. Spector. Histological changes in the human anterior cruciate ligament after rupture. *J Bone Joint Surg Am* 2000;82(10):1387–1387.

[76] S. Thomopoulos, G.R. Williams, J.A. Gimbel, M. Favata, L.J. Soslowsky. Variation of biomechanical, structural, and compositional properties along the tendon to bone insertion site. *J Orthop Res* 2003;21(3):413–9.

[77] G.M. Genin, A. Kent, V. Birman, B. Wopenka, J.D. Pasteris, P.J. Marquez, S. Thomopoulos. Functional grading of mineral and collagen in the attachment of tendon to bone. *Biophys J* 2009;97(4):976–85.

[78] Y. Liu, S. Thomopoulos, C. Chen, V. Birman, M.J. Buehler, G.M. Genin. Modelling the mechanics of partially mineralized collagen fibrils, fibres and tissue. *J R Soc Interface* 2014;11(92):20130835.

[79] Y. Liu, S. Thomopoulos, V. Birman. Bi-material attachment through a compliant interfacial system at the tendon-to-bone insertion site. *Mech Mater* 2012;44:83–92.

[80] Y. Hu, V. Birman, A. Demyier-Black, A.G. Schwartz, S. Thomopoulos, G.M. Genin. Stochastic interdigitation as a toughening mechanism at the interface between tendon and bone. *Biophys J* 2015;108(2):431–437.

[81] H. Fujioka, R. Thakur, G.J. Wang, K. Mizuno, G. Balian, S.R. Hurwitz. Comparison of surgically attached and non-attached repair of the rat achilles tendon-bone interface. cellular organization and type x collagen expression. *Connect Tissue Res* 1998;37(3-4):205–218.

[82] S. Thomopoulos, G.R. Williams, L.J. Soslowsky. Tendon to Bone Healing: Differences in Biomechanical, Structural, and Compositional Properties Due to a Range of Activity Levels. *J Biomech Eng* 2003;125(1):106.

[83] P. St Pierre, E.J. Olson, J.J. Elliott, K.C. O'Hair, L.A. McKinney, J. Ryan. Tendon-healing to cortical bone compared with healing to a cancellous trough. a biomechanical and histological evaluation in goats. *J Bone Joint Surg Am* 1995;77(12):1858–1866.

[84] P. Kannus, L. Józsa. Histopathological changes preceding spontaneous rupture of a tendon. a controlled study of 891 patients. *J Bone Joint Surg Am* 1991;73(10):1507–1525.

[85] M. Provencher, J. Kercher, L.M. Galatz, N. Elattrache, R.M. Frank, B. Cole. Evolution of rotator cuff repair techniques: are our patients really benefiting. *Instr Course Lect* 2011;60:123–136.

[86] B. Melis, M.J. DeFranco, C. Chuinard, G. Walch. Natural history of fatty infiltration and atrophy of the supraspinatus muscle in rotator cuff tears. *Clin Orthop Relat Res* 2010;468(6):1498–1505.

[87] B. Melis, C. Nemoz, G. Walch. Muscle fatty infiltration in rotator cuff tears: descriptive analysis of 1688 cases. *Orthop Traumatol Surg Res* 2009;95(5):319–324.

[88] D. Goutallier, J.M. Postel, P. Gleyze, P. Leguilloux, S. Van Driessche. Influence of cuff muscle fatty degeneration on anatomic and functional outcomes after simple suture of full-thickness tears. *J Shoulder Elbow Surg* 2003;12(6):550–554.

[89] S.H. Liu, R.S. Yang, R. Al-Shaikh, J.M. Lane. Collagen in tendon, ligament, and bone healing: A current review. *Clin Orthop Relat Res* 1995;318:265–278.

[90] S. Uchiyama, P.C. Amadio, J.H. Coert, L.J. Berglund, K.N. An. Gliding resistance of extrasynovial and intrasynovial tendons through the A2 pulley. *J Bone Joint Surg Am* 1997;79(2):219–24.

[91] T. Momose, P.C. Amadio, M.E. Zobitz, C. Zhao, K.N. An. Effect of paratenon and repetitive motion on the gliding resistance of tendon of extrasynovial origin. *Clinical Anatomy* 2002;15(3):199–205.

[92] R.H. Gelberman, D. Amiel, F. Harwood. Genetic expression for type I procollagen in the early stages of flexor tendon healing. *J Hand Surg Am* 1992;17(1):551–558.

[93] J.P. Spalazzi, S.B. Doty, K.L. Moffat, W.N. Levine, H.H. Lu. Development of controlled matrix heterogeneity on a triphasic scaffold for orthopedic interface tissue engineering. *Tissue Eng* 2006;12(12):3497–508.

[94] B.S. Miller, B.K. Downie, R.B. Kohen, T. Kijek, B. Lesniak, J.A. Jacobson, R.E. Hughes, J.E. Carpenter. When do rotator cuff repairs fail? serial ultrasound examination after arthroscopic repair of large and massive rotator cuff tears. *Am J Sports Med* 2011;39(10):2064–2070.

[95] J.P. Iannotti, A. Deutsch, A. Green, S. Rudicel, J. Christensen, S. Marraffino, S. Rodeo. Time to failure after rotator cuff repair. *J Bone Joint Surg Am* 2013;95(11):965–971.

[96] D.L. Butler, N. Juncosa, M.R. Dressler. Functional efficacy of tendon repair processes. *Annu Rev Biomed Eng* 2004;6:303–29.

[97] A. Aydin, M. Topalan, A. Mezdeği, I. Sezer, T. Ozkan, M. Erer, S. Ozkan. Single-stage flexor tendoplasty in the treatment of flexor tendon injuries. *Acta Orthop Traumatol Turc* 2004;38(1):54–9.

[98] G.D. Lister, H.E. Kleinert, J.E. Kutz, E. Atasoy. Primary flexor tendon repair followed by immediate controlled mobilization. *J Hand Surg Am* 1977;2(6):441–451.

[99] R.L. Lieber, M.J. Silva, D. Amiel, R.H. Gelberman. Wrist and digital joint motion produce unique flexor tendon force and excursion in the canine forelimb. *J Biomech* 1999;32(2):175–181.

[100] R.H. Gelberman, M.I. Boyer, M.D. Brodt, S.C. Winters, M.J. Silva. The Effect of Gap Formation at the Repair Site on the Strength and Excursion of Intrasynovial Flexor Tendons. *J Bone Joint Surg Am* 1999;81-A(7):975–982.

[101] P. Matthews, H. Richards. Factors in the adherence of flexor tendon after repair: an experimental study in the rabbit. *Bone Joint J* 1976;58(2):230–236.

[102] C. Zhao, P.C. Amadio, P. Paillard, T. Tanaka, M.E. Zobitz, D.R. Larson, K.N. An. Digital resistance and tendon strength during the first week after flexor digitorum profundus tendon repair in a canine model in vivo. *J Bone Joint Surg Am* 2004;86(2):320–327.

[103] S. Thomopoulos, E. Zampiakis, R. Das, H.M. Kim, M.J. Silva, N. Havlioglu, R.H. Gelberman. Use of a magnesium-based bone adhesive for flexor tendon-to-bone healing. *J Hand Surg Am* 2009;34(6):1066–73.

[104] P.K. Beredjiklian, M. Favata, J.S. Cartmell, C.L. Flanagan, T.M. Crombleholme, L.J. Soslowsky. Regenerative versus reparative healing in tendon: a study of biomechanical and histological properties in fetal sheep. *Ann Biomed Eng* 2003;31(10):1143–1152.

[105] R.H. Gelberman, S. Thomopoulos, S.E. Sakiyama-elbert, R. Das, M.J. Silva. The Early Effects of Sustained Platelet-Derived Functional and Structural Properties of Repaired Intrasynovial Flexor Tendons : An In Vivo Biomechanic Study at 3 Weeks in Canines. *J Hand Surg Am* 2007;32A(3):373–379.

[106] S. Thomopoulos, M.A. Zaegel, R. Das, F.L. Harwood, M.J. Silva, D. Amiel, S.E. Sakiyama-Elbert, R.H. Gelberman. PDGF-BB released in tendon repair using a novel delivery system promotes cell proliferation and collagen remodeling. *J Orthop Res* 2007;25(10):1358–68.

[107] D.A. Osei, J.G. Stepan, R.P. Calfee, S. Thomopoulos, M.I. Boyer, R. Potter, R.H. Gelberman. The Effect of Suture Caliber and Number of Core Suture Strands on Zone II Flexor Tendon Repair: A Study in Human Cadavers. *J Hand Surg Am* 2014;39(2):262–268.

[108] I. Kormpakis, S.W. Linderman, S. Thomopoulos, R.H. Gelberman. Enhanced Zone II Flexor Tendon Repair through a New Half Hitch Loop Suture Configuration. *Plos One* 2016;11(4):e0153822.

[109] X. Dong, M. He, C. Fang, T. Karjalainen, S.J. Sebastin. Direct Radiological Visualization of Loading on Four Flexor Tendon Repair Suture Configurations. *J Hand Surg Am* 2016;41(1):40–46.

[110] L.M. Galatz, N. Charlton, R. Das, H.M. Kim, N. Havlioglu, S. Thomopoulos. Complete removal of load is detrimental to rotator cuff healing. *J Shoulder Elbow Surg* 2009;18(5):669–675.

[111] S. Thomopoulos, G.M. Genin, L.M. Galatz. The development and morphogenesis of the tendon-to-bone insertion what development can teach us about healing. *J Musculoskelet Neuronal Interact* 2010;10(1):35.

[112] J.D. Keener, L.M. Galatz, G. Stobbs-Cucchi, R. Patton, K. Yamaguchi. Rehabilitation following arthroscopic rotator cuff repair. *J Bone Joint Surg Am* 2014;96(1):11–19.

[113] S.S. Koo, B. Parsley, S.S. Burkhart, J.D. Schoolfield. Reduction of postoperative stiffness after arthroscopic rotator cuff repair: results of a customized physical therapy regimen based on risk factors for stiffness. *Arthroscopy* 2011;27(2):155–160.

[114] P.J. Millett, R.B. Wilcox III, J.D. O'Holleran, J.J. Warner. Rehabilitation of the rotator cuff: An evaluation-based approach. *J Am Acad Orthop Surg* 2006;14(11):599–609.

[115] S. Namdari, R.P. Donegan, A.M. Chamberlain, L.M. Galatz, K. Yamaguchi, J.D. Keener. Factors affecting outcome after structural failure of repaired rotator cuff tears. *J Bone Joint Surg Am* 2014;96(2):99–105.

[116] H.J. Levy, J.W. Uribe, L.G. Delaney. Arthroscopic assisted rotator cuff repair: preliminary results. *Arthroscopy* 1990;6(1):55–60.

[117] K. Yamaguchi, C.M. Ball, L.M. Galatz. Arthroscopic rotator cuff repair: transition from mini-open to all-arthroscopic. *Clin Orthop Relat Res* 2001;390:83–94.

[118] K. Yamaguchi, W.N. Levine, G. Marra, L.M. Galatz, S. Klepps, E.L. Flatow. Transitioning to arthroscopic rotator cuff repair: the pros and cons. *Instr Course Lect* 2003;52(1):81–92.

[119] P. Saridakis, G. Jones. Outcomes of single-row and double-row arthroscopic rotator cuff repair: a systematic review. *J Bone Joint Surg Am* 2010;92(3):732–742.

[120] R.S. Churchill, J.K. Ghorai. Total cost and operating room time comparison of rotator cuff repair techniques at low, intermediate, and high volume centers: mini-open versus all-arthroscopic. *J Shoulder Elbow Surg* 2010;19(5):716–721.

[121] K.Ç. Köse, E. Tezen, O. Cebesoy, E. Karadeniz, D. Guner, S. Adiyaman, M. Demirtas. Mini-open versus all-arthroscopic rotator cuff repair: comparison of the operative costs and the clinical outcomes. *Adv Ther* 2008;25(3):249–259.

[122] K.M. Roth, R.J. Warth, J.T. Lee, P.J. Millett, N.S. ElAttrache. Arthroscopic single-row versus double-row repair for full-thickness posterosuperior rotator cuff tears. *JBJS Reviews* 2014;2(7):e6.

[123] P.C. Brady, P. Arrigoni, S.S. Burkhart. Evaluation of residual rotator cuff defects after in vivo single-versus double-row rotator cuff repairs. *Arthroscopy* 2006;22(10):1070–1075.

[124] I.K. Lo, S.S. Burkhart. Double-Row Athroscopic Rotator Cuff Repair: Re-Establishing the Footprint of the Rotator Cuff. *Arthroscopy* 2003;19(9):1035–1042.

[125] A.D. Mazzocca, P.J. Millett, C.A. Guanche, S.A. Santangelo, R.A. Arciero. Arthroscopic single-row versus double-row suture anchor rotator cuff repair. *Am J Sports Med* 2005;33(12):1861–1868.

[126] C.O. Nelson, M.J. Sileo, M.G. Grossman, F. Serra-Hsu. Single-row modified mason-allen versus double-row arthroscopic rotator cuff repair: a biomechanical and surface area comparison. *Arthroscopy* 2008;24(8):941–948.

[127] P. Arrigoni, P.C. Brady, S.S. Burkhart. The double-pulley technique for double-row rotator cuff repair. *Arthroscopy* 2007;23(6):675–e1.

[128] D.H. Kim, N.S. ElAttrache, J.E. Tibone, B.J. Jun, S.N. DeLaMora, R.S. Kvitne, T.Q. Lee. Biomechanical comparison of a single-row versus double-row suture anchor technique for rotator cuff repair. *Am J Sports Med* 2006;34(3):407–414.

[129] B.G. Domb, R.E. Glousman, A. Brooks, M. Hansen, T.Q. Lee, N.S. ElAttrache. High-tension double-row footprint repair compared with reduced-tension single-row repair for massive rotator cuff tears. *J Bone Joint Surg Am* 2008;90(Supplement 4):35–39.

[130] C.B. Ma, L. Comerford, J. Wilson, C.M. Puttlitz. Biomechanical evaluation of arthroscopic rotator cuff repairs: double-row compared with single-row fixation. *J Bone Joint Surg Am* 2006;88(2):403–410.

[131] J.S. Dines, A. Bedi, N.S. ElAttrache, D.M. Dines. Single-row versus double-row rotator cuff repair: Techniques and outcomes. *J Am Acad Orthop Surg* 2010;18(2):83–93.

[132] C. Gerber, A.G. Schneeberger, M. Beck, U. Schlegel. Mechanical strength of repairs of the rotator cuff. *J Bone Joint Surg Br* 1994;76(3):371–380.

[133] N.S. Cho, B.G. Lee, Y.G. Rhee. Arthroscopic rotator cuff repair using a suture bridge technique is the repair integrity actually maintained? *Am J Sports Med* 2011;39(10):2108–2116.

[134] F. Franceschi, L. Ruzzini, U.G. Longo, F.M. Martina, B.B. Zobel, N. Maffulli, V. Denaro. Equivalent clinical results of arthroscopic single-row and double-row suture anchor repair for rotator cuff tears a randomized controlled trial. *Am J Sports Med* 2007;35(8):1254–1260.

[135] J.Y. Park, S.H. Lhee, J.H. Choi, H.K. Park, J.W. Yu, J.B. Seo. Comparison of the clinical outcomes of single-and double-row repairs in rotator cuff tears. *Am J Sports Med* 2008;36(7):1310–1316.

[136] W.T. Pennington, D.J. Gibbons, B.A. Bartz, M. Dodd, J. Daun, J. Klinger, M. Popovich, B. Butler. Comparative analysis of single-row versus double-row repair of rotator cuff tears. *Arthroscopy* 2010;26(11):1419–1426.

[137] C.D. Peltz, L.M. Dourte, A.F. Kuntz, J.J. Sarver, S.Y. Kim, G.R. Williams, L.J. Soslowsky. The effect of postoperative passive motion on rotator cuff healing in a rat model. *J Bone Joint Surg Am* 2009;91(10):2421–2429.

[138] R.H. Gelberman, P.R. Manske, J.S. Vande Berg, P.a. Lesker, W.H. Akeson. Flexor tendon repair *in vitro*: a comparative histologic study of the rabbit, chicken, dog, and monkey. *J Orthop Res* 1984;2(9):39–48.

[139] C.T. Thorpe, H.L. Birch, P.D. Clegg, H.R.C. Screen. The role of the non-collagenous matrix in tendon function. *Int J Exp Pathol* 2013;94(4):248–59.

[140] C.T. Thorpe, C. Klemt, G.P. Riley, H.L. Birch, P.D. Clegg, H.R.C. Screen. Helical sub-structures in energy-storing tendons provide a possible mechanism for efficient energy storage and return. *Acta Biomater* 2013;9(8):7948–56.

[141] J.A. Cadby, E. Buehler, C. Godbout, P.R. van Weeren, J.G. Snedeker. Differences between the Cell Populations from the Peritenon and the Tendon Core with Regard to Their Potential Implication in Tendon Repair. *PloS ONE* 2014;9(3):e92474.

[142] J. Chang, D. Most, R. Thunder, B. Mehrara, M.T. Longaker, W.C. Lineaweaver. Molecular studies in flexor tendon wound healing: the role of basic fibroblast growth factor gene expression. *J Hand Surg Am* 1998;23(6):1052–1058.

[143] M.N. Halikis, P.R. Manske, H. Kubota, M. Aoki. Effect of immobilization, immediate mobilization, and delayed mobilization on the resistance to digital flexion using a tendon injury model. *J Hand Surg* 1997;22(3):464–472.

[144] R.C. Wray Jr., B. Holtman, P.M. Weeks. Clinical treatment of partial tendon lacerations without suturing and with early motion. *Plast Reconstr Surg* 1977;59(2):231–234.

[145] S. Chow, O. Yu. An experimental study on incompletely cut chicken tendons—a comparison of two methods of management. *J Hand Surg Br* 1984;9(2):121–125.

[146] J.B. Tang, Y. Cao, B. Zhu, K.Q. Xin, X.T. Wang, P.Y. Liu. Adeno-Associated Virus-2-Mediated bFGF Gene Transfer to Digital Flexor Tendons Significantly Increases Healing Strength. *J Bone Joint Surg Am* 2008;90(5):1078.

[147] A.D. Potenza. Detailed evaluation of healing processes in canine flexor digital tendons. *Mil med* 1962;127:34–47.

[148] S. Horibe, S. Woo, J. Spiegelman, J. Marcin, R. Gelberman, et al. Excursion of the flexor digitorum profundus tendon: a kinematic study of the human and canine digits. *J Orthop Res* 1990;8(2):167–174.

[149] C. Zhao, P.C. Amadio, T. Momose, P. Couvreur, M.E. Zobitz, K.N. An. The effect of suture technique on adhesion formation after flexor tendon repair for partial lacerations in a canine model. *J Trauma* 2001;51(5):917–921.

[150] C. Zhao, P.C. Amadio, M.E. Zobitz, K.N. An. Gliding characteristics of tendon repair in canine flexor digitorum profundus tendons. *J Orthop Res* 2001;19(4):580–586.

[151] C. Zhao, Y. Ozasa, R.L. Reisdorf, A.R. Thoreson, G.D. Jay, K.N. An, P.C. Amadio. Engineering Flexor Tendon Repair With Lubricant, Cells, and Cytokines in a Canine Model. *Clin Orthop Relat Res* 2014;.

[152] C. Zhao, S.L. Moran, S.S. Cha, Kai-Nan-An, P.C. Amadio. An analysis of factors associated with failure of tendon repair in the canine model. *J Hand Surg Am* 2007;32(4):518–25.

[153] C. Zhao, Y.l. Sun, M.E. Zobitz, K.n. An, P.C. Amadio. Enhancing the Strength of the Tendon–Suture Interface Using 1-Ethyl-3-(3-Dimethylaminopropyl) Carbodiimide Hydrochloride and Cyanoacrylate. *J Hand Surg Am* 2007;32A(5):606–611.

[154] M. Noguchi, J.G. Seiler, R.H. Gelberman, R.A. Sofranko, S.L.Y. Woo. In vitro biomechanical analysis of suture methods for flexor tendon repair. *J Orthop Res* 1993;11(4):603–611.

[155] S. Thomopoulos, R. Das, S. Sakiyama-Elbert, M.J. Silva, N. Charlton, R.H. Gelberman. bFGF and PDGF-BB for tendon repair: Controlled release and biologic activity by tendon fibroblasts in vitro. *Ann Biomed Eng* 2010;38(2):225–234.

[156] J. Wong, W. Bennett, M.W. Ferguson, D.A. McGrouther. Microscopic and histological examination of the mouse hindpaw digit and flexor tendon arrangement with 3d reconstruction. *J Anat* 2006;209(4):533–545.

[157] M. Hayashi, C. Zhao, A.R. Thoreson, T. Chikenji, G.D. Jay, K.N. An, P.C. Amadio. The effect of lubricin on the gliding resistance of mouse intrasynovial tendon. *PloS one* 2013;8(12):e83836.

[158] D.P. Beason, A.F. Kuntz, J.E. Hsu, K.S. Miller, L.J. Soslowsky. Development and evaluation of multiple tendon injury models in the mouse. *J Biomech* 2012;45(8):1550–1553.

[159] A.E. Loiselle, G.a. Bragdon, J.a. Jacobson, S. Hasslund, Z.E. Cortes, E.M. Schwarz, D.J. Mitten, H.a. Awad, R.J. O'Keefe. Remodeling of murine intrasynovial tendon adhesions following injury: MMP and neotendon gene expression. *J Orthop Res* 2009;27(6):833–840.

[160] S. Hasslund, R.J. O'Keefe, H.A. Awad. A mouse model of flexor tendon repair. *Methods Mol Biol* 2014;1130:73–88.

[161] A.R. Thoreson, R. Hiwatari, K.N. An, P.C. Amadio, C. Zhao. The Effect of 1-Ethyl-3-(3-Dimethylaminopropyl) Carbodiimide Suture Coating on Tendon Repair Strength and Cell Viability in a Canine Model. *J Hand Surg Am* 2015;40(10):1986–1991.

[162] C. Zhao, Y.L. Sun, R.L. Kirk, A.R. Thoreson, G.D. Jay, S.L. Moran, K.N. An, P.C. Amadio. Effects of a lubricin-containing compound on the results of flexor tendon repair in a canine model in vivo. *J Bone Joint Surg Am* 2010;92(6):1453–1461.

[163] C. Zhao, Y.L. Sun, G.D. Jay, S.L. Moran, K.N. An, P.C. Amadio. Surface modification counteracts adverse effects associated with immobilization after flexor tendon repair. *J Orthop Res* 2012;30(12):1940–1944.

[164] C. Zhao, Y. Ozasa, H. Shimura, R.L. Reisdorf, A.R. Thoreson, G. Jay, S.L. Moran, K.N. An, P.C. Amadio. Effects of lubricant and autologous bone marrow stromal cell augmentation on immobilized flexor tendon repairs. *J Orthop Res* 2015;(January):154–160.

[165] H. Shen, R.H. Gelberman, M.J. Silva, S.E. Sakiyama-Elbert, S. Thomopoulos. BMP12 induces tenogenic differentiation of adipose-derived stromal cells. *PloS ONE* 2013;8(10):e77613.

[166] M. Hayashi, C. Zhao, K.N. An, P.C. Amadio. The effects of growth and differentiation factor 5 on bone marrow stromal cell transplants in an *in vitro* tendon healing model. *J Hand Surg Eur Vol* 2011;36(4):271–279.

[167] C.N. Manning, A.G. Schwartz, W. Liu, J. Xie, N. Havlioglu, S.E. Sakiyama-elbert, M.J. Silva, Y. Xia, R.H. Gelberman, S. Thomopoulos. Controlled delivery of mesenchymal stem cells and growth factors using a nanofiber scaffold for tendon repair. *Acta Biomater* 2013;9:6905–6914.

[168] R. Yanez, M.L. Lamana, J. García-Castro, I. Colmenero, M. Ramirez, J.A. Bueren. Adipose tissue-derived mesenchymal stem cells have in vivo immunosuppressive properties applicable for the control of the graft-versus-host disease. *Stem cells* 2006;24(11):2582–2591.

[169] L. Cui, S. Yin, W. Liu, N. Li, W. Zhang, Y. Cao. Expanded adipose-derived stem cells suppress mixed lymphocyte reaction by secretion of prostaglandin e2. *Tissue Eng* 2007;13(6):1185–1195.

[170] A. Rouhani, A. Tabrizi, E. Ghavidel. Effects of non-steroidal anti-inflammatory drugs on flexor tendon rehabilitation after repair. *Arch Bone Jt Surg* 2013;1(1):28.

[171] C. Hsu, J. Chang. Clinical implications of growth factors in flexor tendon wound healing. *J Hand Surg Am* 2004;29(4):551–563.

[172] M.I. Kulick, S. Smith, K. Hadler. Oral ibuprofen: evaluation of its effect on peritendinous adhesions and the breaking strength of a tenorrhaphy. *J Hand Surg Am* 1986;11(1):110–120.

[173] V. Tan, A. Nourbakhsh, J. Capo, J.A. Cottrell, M. Meyenhofer, J.P. O'Connor. Effects of nonsteroidal anti-inflammatory drugs on flexor tendon adhesion. *J Hand Surg Am* 2010;35(6):941–947.

[174] H.A. Awad, D.L. Butler, G.P. Boivin, F.N. Smith, P. Malaviya, B. Huibregtse, A.I. Caplan. Autologous mesenchymal stem cell-mediated repair of tendon. *Tissue Eng* 1999;5(3):267–277.

[175] S.Y. Woo, D. Smith, K. Hildebrand, J. Zeminski, L. Johnson. Engineering the healing of the rabbit medial collateral ligament. *Med Biol Eng Comput* 1998;36(3):359–364.

[176] K.A. Hildebrand, S.L. Woo, D.W. Smith, C.R. Allen, M. Deie, B.J. Taylor, C.C. Schmidt. The effects of platelet-derived growth factor-BB on healing of the rabbit medial collateral ligament an *in vivo* study. *Am J Sports Med* 1998;26(4):549–554.

[177] S.N. Robinson, J.E. Talmadge. Sustained release of growth factors. *In vivo (Athens, Greece)* 2001;16(6):535–540.

[178] S.E. Sakiyama-Elbert, R. Das, R.H. Gelberman, F. Harwood, D. Amiel, S. Thomopoulos. Controlled-release kinetics and biologic activity of platelet-derived growth factor-bb for use in flexor tendon repair. *J Hand Surg Am* 2008;33(9):1548–1557.

[179] D.L. Butler, S.a. Goldstein, F. Guilak. Functional tissue engineering: the role of biomechanics. *J Biomech Eng* 2000;122(6):570–5.

[180] D.L. Butler, N. Juncosa-Melvin, G.P. Boivin, M.T. Galloway, J.T. Shearn, C. Gooch, H. Awad. Functional tissue engineering for tendon repair: A multidisciplinary strategy using mesenchymal stem cells, bioscaffolds, and mechanical stimulation. *J Orthop Res* 2008;26(1):1–9.

[181] A.P. Breidenbach, S.D. Gilday, A.L. Lalley, N.a. Dyment, C. Gooch, J.T. Shearn, D.L. Butler. Functional tissue engineering of tendon: Establishing biological success criteria for improving tendon repair. *J Biomech* 2013;:1–8.

[182] H.H. Lu, S.D. Subramony, M.K. Boushell, X. Zhang. Tissue engineering strategies for the regeneration of orthopedic interfaces. *Ann Biomed Eng* 2010;38(6):2142–2154.

[183] K. Uehara, C. Zhao, A. Gingery, A.R. Thoreson, K.N. An, P.C. Amadio. Effect of fibrin formulation on initial strength of tendon repair and migration of bone marrow stromal cells *in vitro*. *J Bone Joint Surg Am* 2015;97(21):1792–1798.

[184] C. Zhao, H.F. Chieh, K. Bakri, J. Ikeda, Y.L. Sun, S.L. Moran, K.N. An, P.C. Amadio. The effects of bone marrow stromal cell transplants on tendon healing in vitro. *Medical engineering & physics* 2009;31(10):1271–1275.

[185] F. Qu, J.M.G. Lin, J.L. Esterhai, M.B. Fisher, R.L. Mauck. Biomaterial-mediated delivery of degradative enzymes to improve meniscus integration and repair. *Acta Biomater* 2013;9(5):6393–402.

[186] R.H. Gelberman, H. Shen, I. Kormpakis, B. Rothrauff, G. Yang, R.S. Tuan, Y. Xia, S. Sakiyama-Elbert, M.J. Silva, S. Thomopoulos. Effect of adipose-derived stromal cells and BMP12 on intrasynovial tendon repair: A biomechanical, biochemical, and proteomics study. *J Orthop Res* 2016;34(4):630–640.

[187] D. Amiel, K. Ishizue, E. Billings, M. Wiig, J.V. Berg, W.H. Akeson, R. Gelberman. Hyaluronan in flexor tendon repair. *J Hand Surg Am* 1989;14(5):837–843.

[188] M. Wiig, S.O. Abrahamsson, G. Lundborg. Tendon repair—cellular activities in rabbit deep flexor tendons and surrounding synovial sheaths and the effects of hyaluronan: an experimental study *in vivo* and *in vitro*. *J Hand Surg Am* 1997;22(5):818–825.

[189] J.A. Miller, R.L. Ferguson, D.L. Powers, J.W. Burns, S.W. Shalaby. Efficacy of hyaluronic acid/nonsteroidal anti-inflammatory drug systems in preventing postsurgical tendon adhesions. *J Biomed Mater Res* 1997;38(1):25–33.

[190] U. Khan, N. Occleston, P. Khaw, D. McGrouther. Single exposures to 5-fluorouracil: a possible mode of targeted therapy to reduce contractile scarring in the injured tendon. *Plast Reconstr Surg* 1997;99(2):465–471.

[191] S. Cerovac, A. Afoke, A. Akali, D. McGrouther. Early breaking strength of repaired flexor tendon treated with 5-fluorouracil. *J Hand Surg Br* 2001;26(3):220–223.

[192] H.H. Stark, J. Boyes, L. Johnson, C. Ashworth. The use of paratenon, polyethylene film, or silastic sheeting to prevent restricting adhesions to tendons in the hand. *J Bone Joint Surg Am* 1977;59(7):908–913.

[193] G. Eskeland, T. Eskeland, T. Hovig, J. Teigland. The ultrastructure of normal digital flexor tendon sheath and of the tissue formed around silicone and polyethylene implants in man. *Bone & Joint Journal* 1977;59(2):206–212.

[194] S.E. Sakiyama-Elbert, J.A. Hubbell. Controlled release of nerve growth factor from a heparin-containing fibrin-based cell ingrowth matrix. *J Control Release* 2000;69(1):149–158.

[195] S.E. Sakiyama-Elbert, J.A. Hubbell. Development of fibrin derivatives for controlled release of heparin-binding growth factors. *J Control Release* 2000;65(3):389–402.

[196] L.D. Solorio, L.M. Phillips, A. McMillan, C.W. Cheng, P.N. Dang, J.E. Samorezov, X. Yu, W.L. Murphy, E. Alsberg. Spatially organized differentiation of mesenchymal stem cells within biphasic microparticle-incorporated high cell density osteochondral tissues. *Adv Healthc Mater* 2015;4(15):2306–13.

[197] L.D. Solorio, E.L. Vieregge, C.D. Dhami, P.N. Dang, E. Alsberg. Engineered cartilage via self-assembled hMSC sheets with incorporated biodegradable gelatin microspheres releasing transforming growth factor- β 1. *J Contol Release* 2012;158(2):224–232.

[198] O. Jeon, D.W. Wolfson, E. Alsberg. In-situ formation of growth-factor-loaded coacervate microparticle-embedded hydrogels for directing encapsulated stem cell fate. *Adv Mater* 2015;27(13):2216–2223.

[199] H. Shen, I. Kormpakis, N. Havlioglu, S.W. Linderman, S.E. Sakiyama-Elbert, I.E. Erickson, T. Zarembinski, M.J. Silva, R.H. Gelberman, S. Thomopoulos. The effect of mesenchymal stromal cell sheets on the inflammatory stage of flexor tendon healing. *Stem Cell Research & Therapy* 2016;7(1):144.

[200] C. Erisken, X. Zhang, K.L. Moffat, W.N. Levine, H.H. Lu. Scaffold fiber diameter regulates human tendon fibroblast growth and differentiation. *Tissue Eng Part A* 2013;19(3-4):519–28.

[201] N.M. Wolfman, G. Hattersley, K. Cox, A.J. Celeste, R. Nelson, N. Yamaji, J.L. Dube, E. DiBlasio-Smith, J. Nove, J.J. Song, et al. Ectopic induction of tendon and ligament in rats by growth and differentiation factors 5, 6, and 7, members of the TGF-beta gene family. *J Clin Invest* 1997;100(2):321.

[202] effect of gdf-5 on ligament healing. ????;.

[203] J. Lou, Y. Tu, M. Burns, M. Silva, P. Manske, et al. BMP-12 gene transfer augmentation of lacerated tendon repair. *J Orthop Res* 2001;19(6):1199–1202.

[204] A. Hoffmann, G. Pelled, G. Turgeman, P. Eberle, Y. Zilberman, H. Shinar, K. Keinan-Adamsky, A. Winkel, S. Shahab, G. Navon, et al. Neotendon formation induced by manipulation of the smad8 signalling pathway in mesenchymal stem cells. *J Clin Invest* 2006;116(4):940–952.

[205] A. Park, M.V. Hogan, G.S. Kesturu, R. James, G. Balian, A.B. Chhabra. Adipose-derived mesenchymal stem cells treated with growth differentiation factor-5 express tendon-specific markers. *Tissue Eng Part A* 2010;16(9):2941–2951.

[206] J.Y. Lee, Z. Zhou, P.J. Taub, M. Ramcharan, Y. Li, T. Akinbiyi, E.R. Maharam, D.J. Leong, D.M. Laudier, T. Ruike, et al. BMP-12 treatment of adult mesenchymal stem cells *in vitro* augments tendon-like tissue formation and defect repair in vivo. *PloS One* 2011;6(3):e17531.

[207] L.V. Gulotta, D. Kovacevic, J.D. Packer, J.R. Ehteshami, S.A. Rodeo. Adenoviral-mediated gene transfer of human bone morphogenetic protein–13 does not improve rotator cuff healing in a rat model. *Am J Sports Med* 2011;39(1):180–187.

[208] S.W. Linderman, R.H. Gelberman, S. Thomopoulos, H. Shen. Cell and Biologic-Based Treatment of Flexor Tendon Injuries. *Operative Techniques in Orthopaedics* 2016;In press:1–10.

[209] C.H. Lee, B. Shah, E.K. Moioli, J.J. Mao. CTGF directs fibroblast differentiation from human mesenchymal stem/stromal cells and defines connective tissue healing in a rodent injury model. *J Clin Invest* 2010;120(9):3340–3349.

[210] J. Liu, X. Tao, L. Chen, W. Han, Y. Zhou, K. Tang. CTGF positively regulates BMP12 induced tenogenic differentiation of tendon stem cells and signaling. *Cell Physiol Biochem* 2015;35(5):1831–1845.

[211] connective tissue growth factor mrna expression pattern in cartilages is associated with their type i collagen expression. ????;.

[212] C.C. Würgler-Hauri, L.M. Dourte, T.C. Baradet, G.R. Williams, L.J. Soslowsky. Temporal expression of 8 growth factors in tendon-to-bone healing in a rat supraspinatus model. *J Shoulder Elbow Surg* 2007;16(5):S198–S203.

[213] C.H. Chen, Y. Cao, Y.F. Wu, A.J. Bais, J.S. Gao, J.B. Tang. Tendon healing *in vivo*: gene expression and production of multiple growth factors in early tendon healing period. *J Hand Surg Am* 2008;33(10):1834–1842.

[214] N. Juncosa-Melvin, G.P. Boivin, C. Gooch, M.T. Galloway, J.R. West, M.G. Dunn, D.L. Butler. The effect of autologous mesenchymal stem cells on the biomechanics and histology of gel-collagen sponge constructs used for rabbit patellar tendon repair. *Tissue Eng* 2006;12(2):369–379.

[215] R.G. Young, D.L. Butler, W. Weber, A.I. Caplan, S.L. Gordon, D.J. Fink. Use of mesenchymal stem cells in a collagen matrix for Achilles tendon repair. *J Orthop Res* 1998;16(4):406–413.

[216] L.V. Gulotta, D. Kovacevic, J.R. Ehteshami, E. Dagher, J.D. Packer, S.A. Rodeo. Application of bone marrow-derived mesenchymal stem cells in a rotator cuff repair model. *Am J Sports Med* 2009;37(11):2126–2133.

[217] Y. Morizaki, C. Zhao, K.N. An, P.C. Amadio. The effects of platelet-rich plasma on bone marrow stromal cell transplants for tendon healing *in vitro*. *J Hand Surg Am* 2010;35(11):1833–1841.

[218] M. He, A.W.T. Gan, A.Y.T. Lim, J.C.H. Goh, J.H.P. Hui, A.K.S. Chong. Bone marrow derived mesenchymal stem cell augmentation of rabbit flexor tendon healing. *Hand Surg* 2015;20(03):421–429.

[219] E. Godwin, N. Young, J. Dudhia, I. Beamish, R. Smith. Implantation of bone marrow-derived mesenchymal stem cells demonstrates improved outcome in horses with overstrain injury of the superficial digital flexor tendon. *Equine Vet J* 2012;44(1):25–32.

[220] R.K. Smith. Mesenchymal stem cell therapy for equine tendinopathy. *Disabil Rehabil* 2008;30(20-22):1752–1758.

[221] S. Pacini, S. Spinabella, L. Trombi, R. Fazzi, S. Galimberti, F. Dini, F. Carlucci, M. Petrini. Suspension of bone marrow-derived undifferentiated mesenchymal stromal cells for repair of superficial digital flexor tendon in race horses. *Tissue Eng* 2007;13(12):2949–2955.

[222] C. Thorpe, P. Clegg, H. Birch. A review of tendon injury: why is the equine superficial digital flexor tendon most at risk? *Equine Vet J* 2010;42(2):174–180.

[223] C.H. Lee, F.Y. Lee, S. Tarafder, K. Kao, Y. Jun, G. Yang, J.J. Mao. Harnessing endogenous stem/progenitor cells for tendon regeneration. *J Clin Invest* 2015;125(7):2690–2701. arXiv:arXiv:1011.1669v3.

[224] P.P.Y. Lui, O.T. Wong, Y.W. Lee. Application of tendon-derived stem cell sheet for the promotion of graft healing in anterior cruciate ligament reconstruction. *Am J Sports Med* 2014;42(3):681–689.

[225] L.J. Soslowsky, J.E. Carpenter, C.M. DeBano, I. Banerji, M.R. Moalli. Development and use of an animal model for investigations on rotator cuff disease. *J Shoulder Elbow Surg* 1996;5(5):383–392.

[226] L. Soslowsky, S. Thomopoulos, S. Tun, C. Flanagan, C. Keefer, J. Mastaw, J. Carpenter. Neer award 1999: Overuse activity injures the supraspinatus tendon in an animal model: a histologic and biomechanical study. *J Shoulder Elbow Surg* 2000;9(2):79–84.

[227] S. Thomopoulos, L.J. Soslowsky, C.L. Flanagan, S. Tun, C.C. Keefer, J. Mastaw, J.E. Carpenter. The effect of fibrin clot on healing rat supraspinatus tendon defects. *J Shoulder Elbow Surg* 2002;11(3):239–47.

[228] C.N. Manning, H.M. Kim, S. Sakiyama-Elbert, L.M. Galatz, N. Havlioglu, S. Thomopoulos. Sustained delivery of transforming growth factor beta three enhances tendon-to-bone healing in a rat model. *J Orthop Res* 2011;29(7):1099–1105.

[229] H.M. Kim, L.M. Galatz, C. Lim, N. Havlioglu, S. Thomopoulos. The effect of tear size and nerve injury on rotator cuff muscle fatty degeneration in a rodent animal model. *J Shoulder Elbow Surg* 2012;21(7):847–858.

[230] R. Das, J. Rich, H.M. Kim, A. McAlinden, S. Thomopoulos. Effects of botulinum toxin-induced paralysis on postnatal development of the supraspinatus muscle. *J Orthop Res* 2011;29(2):281–288.

[231] S.H. Coleman, S. Fealy, J.R. Ehteshami, J.D. MacGillivray, D.W. Altchek, R.F. Warren, A.S. Turner. Chronic rotator cuff injury and repair model in sheep. *J Bone Joint Surg Am* 2003;85(12):2391–2402.

[232] Y. Koike, G. Trudel, H.K. Uhthoff. Formation of a new enthesis after attachment of the supraspinatus tendon: A quantitative histologic study in rabbits. *J Orthop Res* 2005;23(6):1433–1440.

[233] F. Matsumoto, H.K. Uhthoff, G. Trudel, J.F. Loehr. Delayed tendon reattachment does not reverse atrophy and fat accumulation of the supraspinatus—an experimental study in rabbits. *J Orthop Res* 2002;20(2):357–363.

[234] G. Trudel, N. Ramachandran, S.E. Ryan, K. Rakhra, H.K. Uhthoff. Supraspinatus tendon repair into a bony trough in the rabbit: mechanical restoration and correlative imaging. *J Orthop Res* 2010;28(6):710–715.

[235] S.A. Rodeo. Biologic augmentation of rotator cuff tendon repair. *J Shoulder Elbow Surg* 2007;16(5):S191–S197.

[236] M.L. Killian, L. Cavinatto, L.M. Galatz, S. Thomopoulos. Recent advances in shoulder research. *Arthritis research & therapy* 2012;14(3):1.

[237] S.C. Gamradt, S.A. Rodeo, R.F. Warren. Platelet rich plasma in rotator cuff repair. *Techniques in Orthopaedics* 2007;22(1):26–33.

[238] R. Castricini, U.G. Longo, M. De Benedetto, N. Panfoli, P. Pirani, R. Zini, N. Maffulli, V. Denaro. Platelet-rich plasma augmentation for arthroscopic rotator cuff repair a randomized controlled trial. *Am J Sports Med* 2011;39(2):258–265.

[239] S.A. Rodeo, D. Delos, R.J. Williams, R.S. Adler, A. Pearle, R.F. Warren. The effect of platelet-rich fibrin matrix on rotator cuff tendon healing a prospective, randomized clinical study. *Am J Sports Med* 2012;40(6):1234–1241.

[240] F.A. Barber, S.A. Hrnack, S.J. Snyder, O. Hapa. Rotator cuff repair healing influenced by platelet-rich plasma construct augmentation. *Arthroscopy* 2011;27(8):1029–1035.

[241] E. Zelzer, E. Blitz, M.L. Killian, S. Thomopoulos. Tendon-to-bone attachment: From development to maturity. *Birth Defects Res C Embryo Today* 2014;102(1):101–12.

[242] R. Schweitzer, E. Zelzer, T. Volk. Connecting muscles to tendons: tendons and musculoskeletal development in flies and vertebrates. *Development* 2010;137(19):3347–3347.

[243] R. Schweitzer, J.H. Chyung, L.C. Murtaugh, a.E. Brent, V. Rosen, E.N. Olson, A. Lassar, C.J. Tabin. Analysis of the tendon cell fate using Scleraxis, a specific marker for tendons and ligaments. *Development* 2001;128(19):3855–66.

[244] D. Kovacevic, A.J. Fox, A. Bedi, L. Ying, X.H. Deng, R.F. Warren, S.A. Rodeo. Calcium-phosphate matrix with or without tgf-β3 improves tendon-bone healing after rotator cuff repair. *Am J Sports Med* 2011;39(4):811–819.

[245] S.A. Rodeo, K. Suzuki, X.h. Deng, J. Wozney, R.F. Warren. Use of recombinant human bone morphogenetic protein-2 to enhance tendon healing in a bone tunnel. *Am J Sports Med* 1999;27(4):476–488.

[246] L.V. Gulotta, D. Kovacevic, J.D. Packer, X.H. Deng, S.A. Rodeo. Bone marrow–derived mesenchymal stem cells transduced with scleraxis improve rotator cuff healing in a rat model. *Am J Sports Med* 2011;39(6):1282–1289.

[247] X. Li, J. Xie, J. Lipner, X. Yuan, S. Thomopoulos, Y. Xia. Nanofiber scaffolds with gradations in mineral content for mimicking the tendon-to-bone insertion site. *Nano Lett* 2009;9(7):2763–8.

[248] K.A. Derwin, S.F. Badylak, S.P. Steinmann, J.P. Iannotti. Extracellular matrix scaffold devices for rotator cuff repair. *J Shoulder Elbow Surg* 2010;19(3):467–476.

[249] C.J. Dy, A. Daluiski, H.T. Do, A. Hernandez-Soria, R. Marx, S. Lyman. The epidemiology of reoperation after flexor tendon repair. *J Hand Surg Am* 2012;37(5):919–924.

[250] H.M. Kim, G. Nelson, S. Thomopoulos, M.J. Silva, R. Das, R.H. Gelberman. Technical and biological modifications for enhanced flexor tendon repair. *J Hand Surg Am* 2010;35(6):1031–7.

[251] J.W. Sperling, R.H. Cofield, C. Schleck. Rotator cuff repair in patients fifty years of age and younger. *J Bone Joint Surg Am* 2004;86(10):2212–2215.

[252] E.S. Paxton, S.A. Teefey, N. Dahiya, J.D. Keener, K. Yamaguchi, L.M. Galatz. Clinical and radiographic outcomes of failed repairs of large or massive rotator cuff tears. *J Bone Joint Surg Am* 2013;95(7):627–632.

[253] P. Calvert, G. Chakrabarty, H. C. Integrity of rotator cuff repairs assessed by MRI and correlated with clinical function [abstract]. In: Sixth International Congress of Surgery of the Shoulder. Helsinki, Stockholm, and Painatuskeskus, Finland; 1995, p. FH156.

[254] J.T. Shearn, K.R. Kinneberg, N.a. Dyment, M.T. Galloway, K. Kenter, C. Wylie, D.L. Butler. Tendon tissue engineering: progress, challenges, and translation to the clinic. *J Musculoskelet Neuronal Interact* 2011;11(2):163–73.

[255] C.A. Cummins, G.A.C. Murrell. Mode of failure for rotator cuff repair with suture anchors identified at revision surgery. *J Shoulder Elbow Surg* 2003;12(2):128–133.

[256] S.W. Linderman, I. Kormpakis, R.H. Gelberman, V. Birman, U.G. Wegst, G.M. Genin, S. Thomopoulos. Shear lag sutures: Improved suture repair through the use of adhesives. *Acta Biomaterialia* 2015;23:229–39.

[257] J.H. Breasted. The Edwin Smith Surgical papyrus (facsimile and hieroglyphic transliteration with translation and commentary, in two volumes). Chicago, Illinois: The University of Chicago Press; 1930.

[258] J.P. Allen. The Art of Medicine in Ancient Egypt. New York, NY: The Metropolitan Museum of Art; 2005.

[259] Unknown, Possibly Imhotep (Egyptian Physician). 3000 - 1600 B.C. Edwin Smith Papyrus. URL: http://archive.nlm.nih.gov/proj/ttp/flash/smith/smith.html. URL Accessed: 12/08/2014.

[260] C. Xu, J. Zhao, D. Li. Meta-analysis comparing single-row and double-row repair techniques in the arthroscopic treatment of rotator cuff tears. *J Shoulder Elbow Surg* 2013;23(2):1–7.

[261] M.L. Killian, L. Cavinatto, S.A. Shah, E.J. Sato, S.R. Ward, N. Havlioglu, L.M. Galatz, S. Thomopoulos. The effects of chronic unloading and gap formation on tendon-to-bone healing in a rat model of massive rotator cuff tears. *J Orthop Res* 2014;32(3):439–47.

[262] D.L. Korvick, J.F. Cummings, E.S. Grood, J.P. Holden, S.M. Feder, D.L. Butler. The use of an implantable force transducer to measure patellar tendon forces in goats. *J Biomech* 1996;29(4):557–561.

[263] N. Juncosa, J.R. West, M.T. Galloway, G.P. Boivin, D.L. Butler. In vivo forces used to develop design parameters for tissue engineered implants for rabbit patellar tendon repair. *J Biomech* 2003;36:483–488.

[264] V. Volkersen. Die Nietkraftverteilung in zugbeanspruchten Nievtverbindungen mit konstanten Laschenquerschnitten. *Luftfahrforschung* 1938;15:41–47.

[265] H. Cox. The Elasticity and Strength of Paper and Other Fibrous Materials. *Br J Appl Phys* 1952;3(3):72.

[266] J.A. Nairn. On the use of shear-lag methods for analysis of stress transfer in unidirectional composites. *Mech Mater* 1997;26(2):63–80.

[267] J.A. Nairn, D.A. Mendels. On the use of planar shear-lag methods for stress-transfer analysis of multilayered composites. *Mech Mater* 2001;33:335–362.

[268] C.N. Maganaris, J.P. Paul. In vivo human tendon mechanical properties. *J Physiol* 1999;521 Pt 1(1999):307–13.

[269] S.S. Raghavan, C.Y.L. Woon, A. Kraus, K. Megerle, M.S.S. Choi, B.C. Pridgen, H. Pham, J. Chang. Human Flexor Tendon Tissue Engineering: Decellularisation of Human Flexor Tendons Reduces Immunogenicity in vivo. *Tissue Eng Part A* 2012;18:796–805.

[270] J. Kondratko-Mittnacht, S. Duenwald-Kuehl, R. Lakes, R. Vanderby. Shear Load Transfer in High and Low Stress Tendons. *J Mech Behav Biomed Mater* 2015;45:109–120.

[271] D. Casey, O. Lewis. Absorbable and nonabsorbable sutures. In: Handbook of biomaterials evaluation: scientific, technical and clinical testing of implant materials; chap. 7. New York, NY: Macmillan Publishers Limited; 1986, p. 86–94.

[272] C.C. Chu, J.A. Von Fraunhofer, H.P. Greisler. Wound closure biomaterials and devices. CRC Press; 1996.

[273] S. Jackson Inc. Supramid product information sheet. 2015. URL: http://www.supramid.com/content/SUPRAMIDEXTRAIIProductInformation.pdf.

[274] Henkel Corporation. 2014. Technical Data Sheet: Loctite 4902. URL: https://tds.us.henkel.com/NA/UT/HNAUTTDS.nsf/web/41BCEE769DD0931C85257CF5004876E3/$File/4902-EN.pdf. URL Accessed: 03/25/2015.

[275] Henkel Corporation. 2014. Technical Data Sheet: Loctite 4903. URL: https://tds.us.henkel.com/NA/UT/HNAUTTDS.nsf/web/0192ED8CF7AABF1685257CF50048CB6A/$File/4903-EN.pdf. URL Accessed: 03/25/2015.

[276] Henkel Corporation. 2005. Technical Data Sheet: Loctite Quicktite Instant Adhesive Gel. URL: https://tds.us.henkel.com/NA/UT/HNAUTTDS.nsf/web/A7685691D5C6B064882571870000DC0D/$File/QuicktiteGel-EN.pdf. URL Accessed: 03/25/2015.

[277] H. Lee, S.M. Dellatore, W.M. Miller, P.B. Messersmith. Mussel-inspired surface chemistry for multifunctional coatings. *Science* 2007;318(5849):426–30.

[278] H. Lee, B.P. Lee, P.B. Messersmith. A reversible wet/dry adhesive inspired by mussels and geckos. *Nature* 2007;448(7151):338–41.

[279] Henkel Corporation. 2014. Loctite Highly Flexible Instant Adhesives. URL: http://www.henkelna.com/us/structure_images/11839_LT6864_CHART507316_338984_web_563W.jpg. URL Accessed: 10/06/2014.

[280] 3M Industrial Adhesives and Tapes Division. 3M Scotch-Weld Neoprene High Performance Rubber & Gasket Adhesives - 1300 and 1300L Technical Data. 2012. URL: http://multimedia.3m.com/mws/mediawebserver?mwsId=66666UgxGCuNyXTtnxfVNXz6EVtQEcuZgVs6EVs6E666666--&fn=1300and1300LDataPage_R2.pdf.

[281] R.O. Babitt. Vanderbilt Rubber Handbook. 13 ed.; R T Vanderbilt; 1990.

[282] C.A. Harper. Handbook of Plastics, Elastomers, and Composites. 3 ed.; McGraw Hill; 1996.

[283] A.N. Azadani, P.B. Matthews, L. Ge, Y. Shen, C.S. Jhun, T.S. Guy, E.E. Tseng. Mechanical properties of surgical glues used in aortic root replacement. *Ann Thorac Surg* 2009;87(4):1154–60.

[284] A.D. Potenza. Detailed evaluation of healing processes in canine flexor digital tendons. *Mil med* 1962;127:34–47.

[285] A.D. Potenza. Tendon healing within the flexor digital sheath in the dog. *J Bone Joint Surg Am* 1962;44-A(1):49–64.

[286] R.H. Gelberman, J. Menon, M. Gonsalves, W.H. Akeson. The effects of mobilization on the vascularization of healing flexor tendons in dogs. *Clin Orthop Relat Res* 1980;153:283–289.

[287] S. Thomopoulos, H.M. Kim, M.J. Silva, E. Ntouvali, C.N. Manning, R. Potter, H. Seeherman, R.H. Gelberman. Effect of bone morphogenetic protein 2 on tendon-to-bone healing in a canine flexor tendon model. *J Orthop Res* 2012;30(11):1702–9.

[288] M.J. Silva, S. Thomopoulos, N. Kusano, M.A. Zaegel, F.L. Harwood, H. Matsuzaki, N. Havlioglu, T.T. Dovan, D. Amiel, R.H. Gelberman. Early healing of flexor tendon insertion site injuries: Tunnel repair is mechanically and histologically inferior to surface repair in a canine model. *J Orthop Res* 2006;24(5):990–1000.

[289] R.L. Lieber, D. Amiel, K.R. Kaufman, J. Whitney, R.H. Gelberman. Relationship Between Joint Motion and Flexor Tendon Force in the Canine Forelimb. *J Hand Surg Am* 1996;21(6):957–962.

[290] D.A. Dillard. Fundamentals of stress transfer in bonded systems. Adhesion science and engineering / series editor, A. V. Pocius; 1 ed.; Amsterdam, The Netherlands: Elsevier; 2002.

[291] M.F. Ashby. Overview No. 80: On the engineering properties of materials. *Acta Metallurgica* 1989;37(5):1273–1293.

[292] M.F. Ashby, L.J. Gibson, U.G.W. Wegst, R. Olive. The mechanical properties of natural materials. I. Material property charts. *Proc R Soc A* 1995;450(1938):123–140.

[293] U.G.K. Wegst, M.F. Ashby. The mechanical efficiency of natural materials. *Philos Mag* 2004;84(21):2167–2186.

[294] D.J. Pring, a.a. Amis, R.R. Coombs. The mechanical properties of human flexor tendons in relation to artificial tendons. *J Hand Surg Eur* 1985;10:331–336.

[295] P.J. Bouten, M. Zonjee, J. Bender, S.T. Yauw, H. van Goor, J.C. van Hest, R. Hoogenboom. The chemistry of tissue adhesive materials. *Prog Polym Sci* 2014;39:1375–1405.

[296] I.A. Trail, E.S. Powell, J. Noble, S. Crank. The role of an adhesive (Histoacryl) in tendon repair. *J Hand Surg-Brit Eur* 1992;17(5):544–9.

[297] A.C. Nassif. An Adhesive for Repair of Tissues: Experiments with Canine Tendon, Bone, Lung, Blood Vessels and Skin, Using a Methyl 2-Cyanoacrylate Adhesive. *J Surg Res* 1965;5(3):108–115.

[298] T. Inoue, T. Taguchi, S. Imade, N. Kumahashi, Y. Uchio. Effectiveness and biocompatibility of a novel biological adhesive application for repair of meniscal tear on the avascular zone. *Sci Tech Adv Mater* 2012;13(6):064219.

[299] H. Ming-Yuan, J.W. Hutchinson. Crack deflection at an interface between dissimilar elastic materials. *Int J Solids Struct* 1989;25(9):1053–1067.

[300] G.M. Genin, J.W. Hutchinson. Composite laminates in plane stress: constitutive modeling and stress redistribution due to matrix cracking. *J Am Ceram Soc* 1997;80(5):1245–1255.

[301] J.C. McNulty, F.W. Zok, G.M. Genin, A.G. Evans. Notch-sensitivity of fiber-reinforced ceramic-matrix composites: Effects of inelastic straining and volume-dependent strength. *J Am Ceram Soc* 1999;82(5):1217–1228.

[302] A. Kelly, W.R. Tyson. Tensile properties of fibre-reinforced metals: copper/tungsten and copper/molybdenum. *J Mech Phys Solids* 1965;13(6):329–350.

[303] R.F. Gibson. Principles of composite material mechanics. 3 ed.; CRC Press; 2011.

[304] S. Lekhnitskiĭ. Theory of elasticity of an anisotropic elastic body. San Francisco, CA: Holden-Day; 1963.

[305] V. Birman. Mechanics and energy absorption of a functionally graded cylinder subjected to axial loading. *Int J Eng Sci* 2014;78:18–26.

[306] S.W. Linderman, M. Golman, T.R. Gardner, V. Birman, W.N. Levine, G.M. Genin, S. Thomopoulos. Enhanced tendon-to-bone repair through adhesive films. *Acta biomaterialia* 2018;70:165–176.

[307] S. Thomopoulos, V. Birman, G.M. Genin. Structural interfaces and attachments in biology. Springer Science & Business Media; 2013.

[308] M.C. Park, N.S. ElAttrache, J.E. Tibone, C.S. Ahmad, B.J. Jun, T.Q. Lee. Part I: Footprint contact characteristics for a transosseous-equivalent rotator cuff repair technique compared with a double-row repair technique. *J Shoulder Elbow Surg* 2007;16(4):461–468.

[309] A. Zosel. Adhesion and tack of polymers: Influence of mechanical properties and surface tensions. *Colloid Polym Sci* 1985;263(7):541–553.

[310] T. Mochizuki, H. Sugaya, M. Uomizu, K. Maeda, K. Matsuki, I. Sekiya, T. Muneta, K. Akita. Humeral insertion of the supraspinatus and infraspinatus: New anatomical findings regarding the footprint of the rotator cuff. *J Bone Joint Surg Am* 2008;90(5):962–969.

[311] J.Y. Rho, R.B. Ashman, C.H. Turner. Young's modulus of trabecular and cortical bone material: ultrasonic and microtensile measurements. *J Biomech* 1993;26(2):111–119.

[312] C.D. Peltz, S.M. Perry, C.L. Getz, L.J. Soslowsky. Mechanical properties of the long-head of the biceps tendon are altered in the presence of rotator cuff tears in a rat model. *J Orthop Res* 2009;27(3):416–420.

[313] G.M. Genin, S. Thomopoulos. The tendon-to-bone attachment: Unification through disarray. *Nat Mater* 2017;16(6):607–608.

[314] F. Fang, A.S. Sawhney, S.P. Lake. Different regions of bovine deep digital flexor tendon exhibit distinct elastic, but not viscous, mechanical properties under both compression and shear loading. *J Biomech* 2014;47(12):2869–2877.

[315] B.K. Ahn, S. Das, R. Linstadt, Y. Kaufman, N.R. Martinez-Rodriguez, R. Mirshafian, E. Kesselman, Y. Talmon, B.H. Lipshutz, J.N. Israelachvili, J.H. Waite. High-performance mussel-inspired adhesives of reduced complexity. *Nat Commun* 2015;6:7.

[316] G.C. Vorys, H. Bai, C. Chandhanayingyong, C.H. Lee, J.T. Compton, J.M. Caldwell, T.R. Gardner, J.J. Mao, F.Y. Lee. Optimal internal fixation of anatomically shaped synthetic bone grafts for massive segmental defects of long bones. *Clinical Biomechanics* 2015;30(10):1114–1118.

[317] A.M. DeHaan, T.W. Axelrad, E. Kaye, L. Silvestri, B. Puskas, T.E. Foster. Does Double-Row Rotator Cuff Repair Improve Functional Outcome of Patients Compared With Single-Row Technique?: A Systematic Review. *Am J Sports Med* 2012;40(5):1176–1185.

[318] S. Patel, A.P. Gualtieri, H.H. Lu, W.N. Levine. Advances in biologic augmentation for rotator cuff repair. *Ann NY Acad Sci* 2016;1383(1):97–114.

[319] M.C. Park, J.E. Tibone, N.S. ElAttrache, C.S. Ahmad, B.J. Jun, T.Q. Lee. Part II: Biomechanical assessment for a footprint-restoring transosseous-equivalent rotator cuff repair technique compared with a double-row repair technique. *J Shoulder Elbow Surg* 2007;16(4):469–476.

[320] J. Hein, J.M. Reilly, J. Chae, T. Maerz, K. Anderson. Retear rates after arthroscopic single-row, double-row, and suture bridge rotator cuff repair at a minimum of 1 year of imaging follow-up: a systematic review. *Arthroscopy* 2015;31(11):2274–2281.

[321] E. Avgoulas, M. Sutcliffe. A Review of Natural Joint Systems and Numerical Investigation of Bio-Inspired GFRP-to-Steel Joints. *Materials* 2016;9(7):566.

[322] E.I. Avgoulas, M.P.F. Sutcliffe. Biomimetic-inspired CFRP to perforated steel joints. *Composite Structures* 2016;152:929–938.

[323] J.J. Boyle, M. Kume, M.A. Wyczalkowski, L.A. Taber, R.B. Pless, Y. Xia, G.M. Genin, S. Thomopoulos. Simple and accurate methods for quantifying deformation, disruption, and development in biological tissues. *J R Soc Interface* 2014;11(100):20140685.

[324] L.J. Hart-Smith. Bonded-bolted composite joints. *J Aircraft* 1985;22(11):993–1000.

[325] G. Kelly. Load transfer in hybrid (bonded/bolted) composite single-lap joints. *Compos Struct* 2005;69(1):35–43.

[326] G. Li, J.H. Chen, M. Yanishevsky, N.C. Bellinger. Static strength of a composite butt joint configuration with different attachments. *Compos Struct* 2012;94(5):1736–1744.

[327] N.M. Chowdhury, W.K. Chiu, J. Wang, P. Chang. Experimental and finite element studies of bolted, bonded and hybrid step lap joints of thick carbon fibre/epoxy panels used in aircraft structures. *Composites Part B* 2016;100:68–77.

[328] N.L. Millar, T.A. Bradley, N.A. Walsh, R.C. Appleyard, M.J. Tyler, G.A.C. Murrell. Frog glue enhances rotator cuff repair in a laboratory cadaveric model. *J Shoulder Elbow Surg* 2009;18(4):639–645.

[329] L.D. Graham, V. Glattauer, M.G. Huson, J.M. Maxwell, R.B. Knott, J.W. White, P.R. Vaughan, Y. Peng, M.J. Tyler, J.A. Werkmeister, J.A. Ramshaw. Characterization of a protein-based adhesive elastomer secreted by the Australian frog *Notaden bennetti*. *Biomacromolecules* 2005;6(6):3300–3312.

[330] L.D. Graham, V. Glattauer, P.R. Vaughan, J.A. Werkmeister, M.J. Tyler, J.A. Ramshaw, et al. An adhesive secreted by australian frogs of the genus notaden. In: Biological adhesives. Springer; 2006, p. 207–223.

[331] C. Heiss, R. Schnettler. Bioresorbable bone adhesives. historical perspective and current status. *Unfallchirurg* 2005;108(5):348–355.

[332] S. Patel, J.M. Caldwell, S.B. Doty, W.N. Levine, S. Rodeo, L.J. Soslowsky, S. Thomopoulos, H.H. Lu. Integrating soft and hard tissues via interface tissue engineering. *J Orthop Res* 2018;36(4):1069–1077.

[333] A.J. Spooner, H.E. Mewhort, L.M. DiFrancesco, P.W. Fedak. Adhesive-enhanced sternal closure: Feasibility and safety of late sternal reentry. *Case Rep Surg* 2017;2017.

[334] E. Hochuli-Vieira, E. Pinto, A.C. Basso, V.A. Pereira-Filho, S. Saska, M.S. Monnazzi. Adhesives based on butyl-cyanoacrylate for fixation of autologous bone graft: Pilot study in rabbits. *Dent Traumatol* 2017;33(4):261–268.

[335] İ. Özyazgan. Septal deviation treatment using bone or cartilage grafts fixed with cyanoacrylate tissue adhesive. *Aesthetic Plast Surg* 2017;41(3):618–627.

[336] E. De Santis, E.R. Silva, E.N. Carneiro Martins, R. Favero, D. Botticelli, S.P. Xavier. Healing at the interface between autologous block bone grafts and recipient sites using n-butyl-2-cyanoacrylate as fixation. Histomorphometric study in rabbits. *J Oral Implantol* 2017;43(6):447–455.

[337] A. Sultan, A. Mohamed. Efficacy and safety of using n-butyl cyanoacrylate in cranial fixation following trauma and other pathologies. *Turk Neurosurg* 2017;28(3).

[338] A. Türer, M.E. Önger. Effects of different tissue adhesives in treating calvarial bone defects. *J Craniofac Surg* 2017;28(7):e682–e685.

[339] C. Heiss, R. Kraus, F. Peters, W. Henn, M. Schnabelrauch, A. Berg, T. Pautzsch, J. Weisser, R. Schnettler. Development of a bioresorbable self-hardening bone adhesive based on a composite consisting of polylactide methacrylates and β-tricalcium phosphate. *J Biomed Mater Res B Appl Biomater* 2009;90(1):55–66.

[340] C. Heiss, N. Schettler, S. Wenisch, S. Cords, F. Schilke, K.S. Lips, V. Alt, R. Schnettler. Bond strength of an alkylene bis (dilactoyl)-methacrylate bone adhesive: a biomechanical evaluation in sheep. *J Biomater Sci Polym Ed* 2010;21(10):1345–1358.

[341] C. Heiss, N. Hahn, S. Wenisch, V. Alt, P. Pokinskyj, U. Horas, O. Kilian, R. Schnettler. The tissue response to an alkylene bis (dilactoyl)-methacrylate bone adhesive. *Biomaterials* 2005;26(12):1389–1396.

[342] R. Kraus, F. Peters, A. Geck, K. Lips, M. Obert, C. Röder, M. Schnabelrauch, R. Schnettler, C. Heiss. Adhesive strength of a β-tricalcium phosphate-enriched bone adhesive. *Z Orthop Unfall* 2011;149(3):271–278.

[343] A. Noori, S.J. Ashrafi, R. Vaez-Ghaemi, A. Hatamian-Zaremi, T.J. Webster. A review of fibrin and fibrin composites for bone tissue engineering. *Int J Nanomedicine* 2017;12:4937.

[344] A. Khodakaram-Tafti, D. Mehrabani, H. Shaterzadeh-Yazdi. An overview on autologous fibrin glue in bone tissue engineering of maxillofacial surgery. *Dent Res J* 2017;14(2):79.

[345] Q. Zhao, D.W. Lee, B.K. Ahn, S. Seo, Y. Kaufman, J.N. Israelachvili, J.H. Waite. Underwater contact adhesion and microarchitecture in polyelectrolyte complexes actuated by solvent exchange. *Nat Mater* 2016;15(4):407–412.

[346] J. Li, A. Celiz, J. Yang, Q. Yang, I. Wamala, W. Whyte, B. Seo, N. Vasilyev, J. Vlassak, Z. Suo, D. Mooney. Tough adhesives for diverse wet surfaces. *Science* 2017;357(6349):378–381.

[347] Z. Wang, Z. Jia, Y. Jiang, P. Li, L. Han, X. Lu, F. Ren, K. Wang, H. Yuan. Mussel-inspired nano-building block assemblies for mimicking extracellular matrix microenvironments with multiple functions. *Biofabrication* 2017;9(3):035005.

[348] D. Lu, H. Wang, T. Li, Y. Li, F. Dou, S. Sun, H. Guo, S. Liao, Z. Yang, Q. Wei, Z. Lei. Mussel-inspired thermo-responsive polypeptide-pluronic copolymers for versatile surgical adhesives and hemostasis. *ACS Appl Mater Interfaces* 2017;9(20):16756–66.

[349] X. Zhao, Y. Han, J. Li, B. Cai, H. Gao, W. Feng, S. Li, J. Liu, D. Li. BMP-2 immobilized PLGA/hydroxyapatite fibrous scaffold via polydopamine stimulates osteoblast growth. *Mater Sci Eng C Mater Biol Appl* 2017;78:658–666.

[350] S. Zhang, H. Li, M. Yuan, M. Yuan, H. Chen. Poly (lactic acid) blends with poly (trimethylene carbonate) as biodegradable medical adhesive material. *Int J Mol Sci* 2017;18(10):2041.

[351] I. Vidovic Zdrilic, I. de Azevedo Queiroz, B. Matthews, J. Gomes-Filho, M. Mina, I. Kalajzic. Mineral trioxide aggregate improves healing response of periodontal tissue to injury in mice. *J Periodontal Res* 2017;52(6):1058–1067.

[352] K.C. Huang, F. Yano, Y. Murahashi, S. Takano, Y. Kitaura, S.H. Chang, K. Soma, S.W. Ueng, S. Tanaka, K. Ishihara, Y. Okamura, T. Moro, S. T. Sandwich-type PLLA-nanosheets loaded with BMP-2 induce bone regeneration in critical-sized mouse calvarial defects. *Acta Biomater* 2017;59:12–20.

[353] J. Li, S.W. Linderman, C. Zhu, H. Liu, S. Thomopoulos, Y. Xia. Surgical Sutures with Porous Sheaths for the Sustained Release of Growth Factors. *Adv Mater* 2016;:4620–4624.

[354] S.W. Linderman, H. Shen, S. Yoneda, R. Jayaram, M.L. Tanes, S.E. Sakiyama-Elbert, Y. Xia, S. Thomopoulos, R.H. Gelberman. Effect of connective tissue growth factor delivered via porous sutures on the proliferative stage of intrasynovial tendon repair. *Journal of Orthopaedic Research*® 2018;36(7):2052–2063.

[355] J. Dhom, D.A. Bloes, A. Peschel, U.K. Hofmann. Bacterial adhesion to suture material in a contaminated wound model: Comparison of monofilament, braided, and barbed sutures. *J Orthop Res* 2017;35(4):925–33.

[356] K.N. Leknes, K.A. Selvig, O.E. Bøe, U.M. Wikesjö. Tissue reactions to sutures in the presence and absence of anti-infective therapy. *J Clin Periodontol* 2005;32(2):130–138.

[357] J.E. Otten, M. Wiedmann-Al-Ahmad, H. Jahnke, K. Pelz. Bacterial colonization on different suture materials—a potential risk for intraoral dentoalveolar surgery. *J Biomed Mater Res B Appl Biomater* 2005;74(1):627–635.

[358] K.M. Wilkins, G.W. Hanlon, G.P. Martin, C. Marriott. The migration of bacteria through gels in the presence of iucd monofilament tails. *Contraception* 1989;39(2):205–216.

[359] S.A. Hacking, J.D. Bobyn, K.K. Toh, M. Tanzer, J.J. Krygier. Fibrous tissue ingrowth and attachment to porous tantalum. *J Biomed Mater Res* 2000;52(4):631–638.

[360] B.R. Levine, S. Sporer, R.A. Poggie, C.J. Della Valle, J.J. Jacobs. Experimental and clinical performance of porous tantalum in orthopedic surgery. *Biomaterials* 2006;27(27):4671–4681.

[361] J.M. Souza, Z.P. Dumanian, A.N. Gurjala, G.A. Dumanian. *In Vivo* Evaluation of a Novel Suture Design for Abdominal Wall Closure. *Plast Reconstr Surg* 2015;135(2):322e–330e.

[362] Y. Li, K.N. Kumar, J.M. Dabkowski, M. Corrigan, R.W. Scott, K. Nusslein, G.N. Tew. New bactericidal surgical suture coating. *Langmuir* 2012;28(33):12134–12139.

[363] J. Schneider, A. Hapfelmeier, J. Fremd, P. Schenk, A. Obermeier, R. Burgkart, S. Forkl, S. Feihl, N. Wantia, B. Neu, et al. Biliary endoprosthesis: a prospective analysis of bacterial colonization and risk factors for sludge formation. *PloS one* 2014;9(10):e110112.

[364] S.H. Cummings, D.a. Grande, C.K. Hee, H.K. Kestler, C.M. Roden, N.V. Shah, P. Razzano, D.M. Dines, N.O. Chahine, J.S. Dines. Effect of recombinant human platelet-derived growth factor-BB-coated sutures on Achilles tendon healing in a rat model: A histological and biomechanical study. *J Tissue Eng* 2012;3(1):2041731412453577.

[365] A. Obermeier, J. Schneider, S. Wehner, F.D. Matl, M. Schieker, R. von Eisenhart-Rothe, A. Stemberger, R. Burgkart. Novel high efficient coatings for anti-microbial surgical sutures using chlorhexidine in fatty acid slow-release carrier systems. *PloS one* 2014;9(7):e101426.

[366] T. Fuchs, C. Surke, R. Stange, S. Quandte, B. Wildemann, M. Raschke, G. Schmidmaier. Local delivery of growth factors using coated suture material. *The Scientific World Journal* 2012;2012.

[367] C. Uggen, J. Dines, M. McGarry, D. Grande, T. Lee, O. Limpisvasti. The effect of recombinant human platelet-derived growth factor BB–coated sutures on rotator cuff healing in a sheep model. *Arthroscopy* 2010;26(11):1456–1462.

[368] S. Tarafder, E. Chen, Y. Jun, K. Kao, K.H. Sim, J. Back, F.Y. Lee, C.H. Lee. Tendon stem/progenitor cells regulate inflammation in tendon healing via jnk and stat3 signaling. *FASEB J* 2017;31(9):3991–3998.

[369] M. Hattori, M. Saito, K. Okajima, K. Kamide. Molecular characterization of nylon 6, 6 and its dissolved state in mixture of calcium chloride and methanol. *Polymer J* 1995;27(6):631–644.

[370] S. Samitsu, R. Zhang, X. Peng, M.R. Krishnan, Y. Fujii, I. Ichinose. Flash freezing route to mesoporous polymer nanofibre networks. *Nat Commun* 2013;4.

[371] S.H. Im, U. Jeong, Y. Xia. Polymer hollow particles with controllable holes in their surfaces. *Nat Mater* 2005;4(9):671–675.

[372] J.T. McCann, M. Marquez, Y. Xia. Highly porous fibers by electrospinning into a cryogenic liquid. *J Am Chem Soc* 2006;128(5):1436–1437.

[373] R.H. Gelberman, S.W. Linderman, R. Jayaram, A.D. Dikina, S. Sakiyama-Elbert, E. Alsberg, S. Thomopoulos, H. Shen. Combined administration of ASCs and BMP-12 promotes an M2 macrophage phenotype and enhances tendon healing. *Clin Orthop Relat Res* 2017;475(9):2318–2331.

[374] E. Walker, A.S. Nowacki. Understanding equivalence and noninferiority testing. *J Gen Int Med* 2011;26(2):192–196.

[375] F. Schuind, M. Garcia-Elias, W.P. Cooney III, K.N. An. Flexor tendon forces: *in vivo* measurements. *J Hand Surg* 1992;17(2):291–298.

[376] P. Burssens, R. Forsyth, A. Steyaert, E. Van Ovost, M. Praet, R. Verdonk. Influence of burst tens stimulation on collagen formation after achilles tendon suture in man. a histological evaluation with movat's pentachrome stain. *Acta Orthop Belg* 2005;71(3):342–6.

[377] H.Z. Movat. Demonstration of all connective tissue elements in a single section; pentachrome stains. *AMA Arch Pathol* 1955;60(3):289–295.

[378] S. Bachman, A. Ramaswamy, B. Ramshaw. Tissue ingrowth, adhesion, and mesh contraction. In: Hernia Repair Sequelae. Springer; 2010, p. 345–352.

[379] J.J. Bauer, M.T. Harris, I. Kreel, I.M. Gelernt. Twelve-year experience with expanded polytetrafluoroethylene in the repair of abdominal wall defects. *The Mount Sinai Journal of Medicine, New York* 1999;66(1):20–25.

[380] P.S. Issack. Use of porous tantalum for acetabular reconstruction in revision hip arthroplasty. *J Bone Joint Surg Am* 2013;95(21):1981–1987.

[381] J. Bobyn, R. Pilliar, H. Cameron, G. Weatherly. Osteogenic phenomena across endosteal bone-implant spaces with porous surfaced intramedullary implants. *Acta Orthop Scand* 1981;52(2):145–153.

[382] J. Bobyn, G. Stackpool, S. Hacking, M. Tanzer, J. Krygier. Characteristics of bone ingrowth and interface mechanics of a new porous tantalum biomaterial. *Bone & Joint Journal* 1999;81(5):907–914.

[383] R.H. Gelberman, V. Khabie, C.J. Cahill. The revascularization of healing flexor tendons in the digital sheath. a vascular injection study in dogs. *J Bone Joint Surg Am* 1991;73(6):868–881.

[384] Y. Hamada, S. Katoh, N. Hibino, H. Kosaka, D. Hamada, N. Yasui. Effects of monofilament nylon coated with basic fibroblast growth factor on endogenous intrasynovial flexor tendon healing. *J Hand Surg* 2006;31(4):530–540.

[385] C.S. Chamberlain, J.S. Lee, E.M. Leiferman, N.X. Maassen, G.S. Baer, R. Vanderby, W.L. Murphy. Effects of bmp-12-releasing sutures on achilles tendon healing. *Tissue Eng Part A* 2014;21(5-6):916–927.

[386] M. Rickert, M. Jung, M. Adiyaman, W. Richter, H.G. Simank. A growth and differentiation factor-5 (gdf-5)-coated suture stimulates tendon healing in an achilles tendon model in rats. *Growth Factors* 2001;19(2):115–126.

[387] M. Younesi, B.O. Donmez, A. Islam, O. Akkus. Heparinized collagen sutures for sustained delivery of pdgf-bb: Delivery profile and effects on tendon-derived cells in-vitro. *Acta Biomater* 2016;41:100–109.

[388] S. Thomopoulos, H.M. Kim, R. Das, M.J. Silva, S.E. Sakiyama-Elbert, D. Amiel, R.H. Gelberman. The Effects of Exogenous Basic Fibroblast Growth Factor on Intrasynovial Flexor Tendon Healing in a Canine Model. *J Bone Joint Surg Am* 2010;92A(13):2285–2293.

[389] J.H. Ajcamo. Surgical suture. 1964. US Patent 3,123,077.

[390] A.R. McKenzie. An experimental multiple barbed suture for the long flexor tendons of the palm and fingers. Preliminary report. *J Bone Joint Surg Br* 1967;49(3):440–7.

[391] H.J. Buncke. Surgical methods using one-way suture. 1999. US Patent 5,931,855.

[392] P. Genova, R.C. Williams III, W. Jewett. Method for cutting a suture to create tissue retainers of a desired shape and size. 2011. US Patent 8,015,678.

[393] N. Maiorino, M.S. Buchter, M.D. Cohen, M. Primavera, T.D. Kosa. Method of forming barbs on a suture. 2012. US Patent 8,161,618.

[394] J.A. Greenberg, J.I. Einarsson. The use of bidirectional barbed suture in laparoscopic myomectomy and total laparoscopic hysterectomy. *J Minim Invasive Gynecol* 2008;15(5):621–623.

[395] J.A. Greenberg. The use of barbed sutures in obstetrics and gynecology. *Rev Obstet Gynecol* 2010;3(3):82–91.

[396] J.A. Greenberg, R.H. Goldman. Barbed Suture: A Review of the Obstetrics and Gynecology. *Rev Obstet Gynecol* 2013;6(3):107–115.

[397] Y. Lin, S. Lai, J. Huang, L. Du. The Efficacy and Safety of Knotless Barbed Sutures in the Surgical Field: A Systematic Review and Meta-analysis of Randomized Controlled Trials. *Scientific Reports* 2016;6:23425.

[398] G.E. Maddox, J. Ludwig, E.R. Craig, D. Woods, A. Joiner, N. Chaudhari, C. Killingsworth, G.P. Siegal, A. Eberhardt, B. Ponce. Flexor tendon repair with a knotless, bidirectional barbed suture: An *in vivo* biomechanical analysis. *J Hand Surg Am* 2015;40(5):963–968.

[399] W.T. McClellan, M.J. Schessler, D.S. Ruch, L.S. Levin, R.D. Goldner. A Knotless Flexor Tendon Repair Technique Using a Bidirectional Barbed Suture. *Plast Reconstr Surg* 2011;128(4):322e–327e.

[400] W.D. Spotnitz, S. Burks. Hemostats, sealants, and adhesives: components of the surgical toolbox. *Transfusion* 2008;48(July):1502–1516.

[401] L.D. Graham, S.J. Danon, G. Johnson, C. Braybrook, N.K. Hart, R.J. Varley, M.D.M. Evans, G.A. McFarland, M.J. Tyler, J.A. Werkmeister, J.A.M. Ramshaw. Biocompatibility and modification of the protein-based adhesive secreted by the Australian frog *Notaden bennetti*. *J Biomed Mater Res A* 2010;93(2):429–441.

[402] W.D. Spotnitz, S. Burks. State-of-the-art review: Hemostats, sealants, and adhesives II: Update as well as how and when to use the components of the surgical toolbox. *Clin Appl Thromb Hemost* 2010;16(5):497–514.

[403] H. Zhang, T. Zhao, P. Duffy, Y. Dong, A.N. Annaidh, E. O'Cearbhaill, W. Wang. Hydrolytically Degradable Hyperbranched PEG-Polyester Adhesive with Low Swelling and Robust Mechanical Properties. *Adv Healthc Mater* 2015;4(15):2260–2268.

[404] O. Jeon, J.E. Samorezov, E. Alsberg. Single and dual crosslinked oxidized methacrylated alginate/PEG hydrogels for bioadhesive applications. *Acta Biomater* 2014;10(1):47–55.

[405] X. Dai, X. Chen, L. Yang, S. Foster, A.J. Coury, T.H. Jozefiak. Free radical polymerization of poly(ethylene glycol) diacrylate macromers: Impact of macromer hydrophobicity and initiator chemistry on polymerization efficiency. *Acta Biomater* 2011;7(5):1965–1972.

[406] B.P. Partlow, C.W. Hanna, J. Rnjak-Kovacina, J.E. Moreau, M.B. Applegate, K.a. Burke, B. Marelli, A.N. Mitropoulos, F.G. Omenetto, D.L. Kaplan. Highly tunable elastomeric silk biomaterials. *Adv Funct Mater* 2014;24(29):4615–4624.

[407] D.N. Rockwood, R.C. Preda, T. Yucel, X. Wang, M.L. Lovett, D.L. Kaplan. Materials fabrication from Bombyx mori silk fibroin. *Nat Protoc* 2011;6(September):1612–1631.

[408] W.L. Stoppel, D. Hu, I.J. Domian, D.L. Kaplan, L.D. Black. Anisotropic silk biomaterials containing cardiac extracellular matrix for cardiac tissue engineering. *Biomedical Materials* 2015;10:034105.

[409] Y. Liu, A.G. Schwartz, V. Birman, S. Thomopoulos, G.M. Genin. Stress amplification during development of the tendon-to-bone attachment. *Biomech Model Mechanobiol* 2014;13(5):973–83.

[410] A.E. Loiselle, K. Yukata, M.B. Geary, S. Kondabolu, S. Shi, J.H. Jonason, H.A. Awad, R.J. O'Keefe. Development of antisense oligonucleotide (ASO) technology against TGF-β signaling to prevent scarring during flexor tendon repair. *J Orthop Res* 2015;33(6):859–66.

[411] C.N. Manning, C. Martel, S.E. Sakiyama-Elbert, M.J. Silva, S. Shah, R.H. Gelberman, S. Thomopoulos. Adipose-derived mesenchymal stromal cells modulate tendon fibroblast responses to macrophage-induced inflammation in vitro. *Stem cell research & therapy* 2015;6(1):74.

[412] L.D. Solorio, C.D. Dhami, P.N. Dang, E.L. Vieregge, E. Alsberg. Spatiotemporal regulation of chondrogenic differentiation with controlled delivery of transforming growth factor-β1 from gelatin microspheres in mesenchymal stem cell aggregates. *Stem Cells Transl Med* 2012;1(8):632–639.

[413] P.N. Dang, L.D. Solorio, E. Alsberg. Driving cartilage formation in high-density human adipose-derived stem cell aggregate and sheet constructs without exogenous growth factor delivery. *Tissue Eng Part A* 2014;20(23-24):3163–75.

[414] M. Yamamoto, Y. Ikada, Y. Tabata. Controlled release of growth factors based on biodegradation of gelatin hydrogel. *J Biomater Sci Polym Ed* 2001;12(1):77–88.

[415] A. Viinikainen, H. Göransson, K. Huovinen, M. Kellomäki, P. Rokkanen. A comparative analysis of the biomechanical behaviour of five flexor tendon core sutures. *J Hand Surg Br* 2004;29(6):536–543.

[416] L.C. Bainbridge, C. Robertson, D. Gillies, D. Elliot. A comparison of post-operative mobilization of flexor tendon repairs with "passive flexion-active extension" and "controlled active motion" techniques. *J Hand Surg Br* 1994;19(4):517–521.

[417] T.M. Lawrence, T.R.C. Davis. A biomechanical analysis of suture materials and their influence on a four-strand flexor tendon repair. *J Hand Surg Am* 2005;30(4):836–841.

[418] J.B. Tang, Y. Zhang, Y. Cao, R.G. Xie. Core suture purchase affects strength of tendon repairs. *J Hand Surg Am* 2005;30(6):1262–1266.

[419] F. Vizesi, C. Jones, N. Lotz, M. Gianoutsos, W.R. Walsh. Stress relaxation and creep: viscoelastic properties of common suture materials used for flexor tendon repair. *J Hand Surg Am* 2008;33(2):241–6.

[420] D.L. Pruitt, M. Aoki, P.R. Manske. Effect of suture knot location on tensile strength after flexor tendon repair. *J Hand Surg Am* 1996;21(6):969–973.

[421] T. Momose, P.C. Amadio, C. Zhao, M.E. Zobitz, K.N. An. The effect of knot location, suture material, and suture size on the gliding resistance of flexor tendons. *J Biomed Mater Res* 2000;53(6):806–811.

[422] Y.R. Wong, C.S. Lee, A.M. Loke, X. Liu, I. Suzana M. J., S.C. Tay. Comparison of Flexor Tendon Repair Between 6-Strand Lim-Tsai With 4-Strand Cruciate and Becker Technique. *J Hand Surg Am* 2015;40(9):1806–1811.

[423] T. Miller, J. Feinblatt, J. Craw, A. Litsky, D. Flanigan. Evaluation of high-strength orthopedic sutures: a head-to-head comparison. *Orthopedics* 2010;33(9):674.

[424] J.D. Kelly, S. Vaishnav, B.M. Saunders, M.A. Schrumpf. Optimization of the racking hitch knot: How many half hitches and which suture material provide the greatest security? *Clin Orthop Relat Res* 2014;472(6):1930–1935.

[425] K.A. Barrie, S.L. Tomak, J. Cholewicki, S.W. Wolfe. The role of multiple strands and locking sutures on gap formation of flexor tendon repairs during cyclical loading. *J Hand Surg Am* 2000;25(4):714–720.

Stephen W. Linderman

Stephen.Linderman@wustl.edu | https://www.linkedin.com/in/stephen-linderman-1a5231b/

EDUCATION AND RESEARCH EXPERIENCE

Washington University School of Medicine **Enrolled: August 2011**
Candidate for M.D. and Ph.D. in Biomedical Engineering **Defended PhD: January 2017**
Medical Scientist Training Program (MSTP), Expected Graduation: May 2019
Ph.D. GPA: 4.00

Ph.D. Thesis Advisor: Dr. Stavros Thomopoulos 2012-2017
Department of Orthopedic Surgery, Washington University School of Medicine
- "Improved orthopaedic repairs through mechanically optimized, adhesive biomaterials"
- Engineered the bone–tendon and tendon–suture interfaces to enhance repair mechanics.
- Developed cell and growth factor delivery platforms and tested in large animal surgeries.
- F30-AR069491 Ruth L. Kirschstein National Research Service Award (NRSA) Individual Predoctoral MD/PhD Fellow, NIAMS, NIH
- T32-AR060719 Metabolic Skeletal Disorders Training Grant – Predoctoral Fellow National Institute of Arthritis and Musculoskeletal and Skin Diseases, NIH

University of Cambridge, Churchill College **Graduated: October 2011**
Master of Philosophy with Distinction in Translational Medicine and Therapeutics

Master's Thesis Advisor: Dr. Thomas Krieg 2010-2011
Clinical Pharmacology Unit, Department of Medicine, University of Cambridge
- Thesis: "Mechanisms of cardioprotection by adenosine A_{2B} receptor activation"
- Conducted animal studies on a pharmaceutical compound for treating myocardial infarctions and investigated the compound's mechanism of action through mitochondria.

Cornell University **Graduated: May 2010**
Bachelor of Science *Summa cum Laude* with Honors in Biological Engineering
Minor: Biomedical Engineering
GPA: 4.12 – Dean's List all semesters

Honors Thesis Advisor: Dr. Matthew DeLisa 2007-2010
Department of Chemical and Biomolecular Engineering, Cornell University
- Thesis: "Developing tools to monitor and engineer protein solubility and interactions in *Escherichia coli*."
- Developed a protein interaction reporter for antibody engineering, studying pathways, etc.

NSF Research Experience for Undergraduates Advisor: Dr. Eben Alsberg Summer 2009
Department of Biomedical Engineering, Case Western Reserve University
- Created and tested a novel system to generate smooth physical and chemical gradients in hydrogel scaffolds to test the effects of various properties on cell migration and function.

TEACHING EXPERIENCE

Teaching Assistant for Interfaces and Attachments, Dr. Guy Genin Fall 2015
Graduate Mechanical Engineering Course, Washington University in St. Louis

Teaching Assistant for Cell and Organ Systems, Dr. Robert Mercer 2014-2015
1st Year Medical Student Physiology Course, Washington University School of Medicine
- Selected by students as WUSM T.A. of the Year, of 21 M.D.-Ph.D. candidate T.A.'s
- Average student evaluation: 4.88 / 5.00, compared to average of 3.32 for other instructors

Course Developer and T.A. for Clinical Needs Identification, Dr. Frank Yin 2014-2015
Sophomore Biomedical Engineering Course, Washington University in St. Louis

Coordinator for Health and Human Rights, Dr. Kim Carmichael, WUSM Spring 2013

PROFESSIONAL

Third Rock Ventures, Intern **April-October 2017**
- Led early-stage scientific and business exploration of cell engineering therapies

LEADERSHIP EXPERIENCE

Sling Health (formerly known as IDEA Labs), Nonprofit Corporation
Founder, Director, and President 2013-2019

- National President 2015-2019
  - Expanded Sling Health platform into a national network with 9 chapters
  - Established collaborations with American Medical Association, Veterans Affairs Center of Innovation, and Forge Health (acquired by Sling Health 2016)
  - Developed a sustainable and scalable infrastructure that is rapidly expanding
  - Created an investor conference with top biotechnology company participation
- St. Louis President, Vice President, Managing Director 2013-2015
  - Developed incubator platform to launch biomedical technology startups
  - Led 20 member executive team in raising funds, managing and supporting teams, establishing and honing operations, marketing, and coordinating Demo Day event
  - Grew to > $125,000 local budget, > 150 active student participants, and > 50 mentors
- Successes to date within the first five years of operation:
  - Created 100+ teams and 70+ prototypes, 25+ provisional patents
  - Supported 15+ finalists in national competitions
  - Teams have collectively raised approximately $6 million in seed funding
- Developed infrastructure to support teams of student entrepreneurs with legal agreements, intellectual property retention, and third party interactions (e.g., *pro bono* legal support)
- Attracted major national keynote speakers, e.g., Mark Levin and Dr. Robert Langer

Innovative Programs to Enhance Research Training (R25) – Advisory Board 2017-2018
Educational program to improve innovation and entrepreneurship in biomedical researchers
Washington University School of Medicine

Young Scientist Program: Continuing Mentoring – Cofounder, Coordinator 2011-2014
Washington University School of Medicine and Soldan High School, St. Louis

HONORS, AWARDS, AND GRANTS

Michael V. Seiden Fellow – Outstanding Accomplishment as MD-PhD – WUSM 2018
Gold Humanism Honor Society 2018
Olin Fellowship – Outstanding Biomedical Doctoral Research – Washington Univ. 2018
2nd Place – SB^{3}C PhD Student Paper Competition 2017
Best Paper – ASME International Mechanical Engineering Conference & Exhibition 2016
Entrepreneurship Citation – Washington University 2016
Predoctoral Fellow – F30 NRSA Individual MD/PhD Fellowship, NIAMS, NIH 2016
Doctoral Research Award – Biomedical Engineering, WUSTL 2016
Co-Investigator – WUSTL Musculoskeletal Research Center Translational Grant for "Adhesive sutures for enhanced flexor tendon repair." 2015
Hertz Fellowship Finalist 2014, 2015
WUSM Distinguished Service Teaching Award – Teaching Assistant of the Year 2015
WUSTL BioEntrepreneurship Core Bench to Business Challenge – 1st Place 2015
Washington University Translational Research Competition Finalist & Grant Awardee 2015
Washington University MSTP Retreat – Best Presentation and Travel Award 2015
Predoctoral Fellow – T32 Metabolic Skeletal Disorders Training Grant, NIAMS, NIH 2014
3rd Place Winner in microMedic National Contest – KinoCOM, IDEA Labs 2013
Churchill Scholar 2010-2011
Scholars' Feast Invitee – Churchill College, University of Cambridge 2010
Merrill Presidential Scholar – Cornell University 2010
Academic Excellence Award – College of Agriculture and Life Sciences, Cornell 2010
Tau Beta Pi Engineering Honor Society 2010
Marshall Scholarship Finalist 2009
Barry M. Goldwater Scholar 2009
Alpha Epsilon, Biological Engineering Honors Society 2009
Hunter R. Rawlings III Cornell Presidential Research Scholars Program 2006-2010

ACTIVITIES

Medical School Musical, *Urinetown* and *Lucky Stiff*, Washington University 2011-2012
Churchill College Boat Club, Men's First VIII Boat 2010-2011
The Class Notes, Cornell University co-ed a cappella 2006-2010

PATENTS PENDING

Adhesive-coated sutures	US2016 0135809A1
Adhesive films for tendon-to-bone repair	US2017 0360554A1
Surgical suture materials with porous sheaths for drug delivery	WO2017 147431A1

INVENTIVE PORTFOLIO

Sticky sutures: Biomechanically optimized, adhesive coated sutures for soft tissue repair

Tissue-to-bone tape: Biomechanical adhesive films for soft tissue to bone repair

Porous sutures: Mechanically equivalent, porous sutures that dramatically increase adhesive or growth factor loading capacity for sustained delivery within tissue

Gradient generator: Pump-based device to make tunable biochemical or mechanical gradients in hydrogels for tissue engineering and other applications

KinoCOM: Modular device to convert stroke patient movements into computer inputs for typing or other functions [advisory role]

Volt Optics: Eyeglasses with rapidly tunable prescription focal length [advisory role]

Protein interaction selector: Assay to rapidly detect and select protein interactions in *E. coli* using reconstituted antibiotic resistance, used to engineer antibodies

Protein folding selector: Assay to rapidly detect and compare competent protein folding in periplasm and cytoplasm of *E. coli*

PUBLICATIONS

[In Press] Avgoulas EI, Sutcliffe MPF, **Linderman SW**, Birman V, Thomopoulos S, Genin GM. "Adhesive-based tendon-to-bone repair: failure modeling and materials selection." *Journal of the Royal Society, Interface* (2019). PMID: pending.

Yoneda S, Kusano N, Okubo H, **Linderman SW**, Silva MJ, Thomopoulos S, Kanaya F, Gelberman RH. "The effect of modified locking methods and suture materials on Zone II flexor tendon repair: An *ex vivo* study." *PLOS ONE* **13**(10):e0205121. (2018). PMID: 30289887.

Shen H, Jayaram R, Yoneda S, **Linderman SW**, Sakiyama-Elbert SE, Xia Y, Gelberman RH, Thomopoulos S. "The effect of adipose-derived stem cell sheets and CTGF on early flexor tendon healing in a canine model." *Scientific Reports*, **8**:11078 (2018). DOI: 10.1038/s41598-018-29474-8. PMID: 30038250.

Linderman SW, Golman M, Gardner TR, Yoon D, Birman V, Ahn K, Genin GM, Thomopoulos S. "Enhanced tendon-to-bone repair through adhesive films." *Acta Biomaterialia*, **70**:165-176 (2018). PMID: 29427745.

Linderman SW, Shen H, Yoneda S, Tanes ML, Sakiyama-Elbert SE, Xia Y, Thomopoulos S, Gelberman RH. "Effect of connective tissue growth factor delivered via porous sutures on the proliferative stage of intrasynovial tendon repair." *J Orthopaedic Research*, (2017). DOI: 10.1002/jor.23842. PMID: 29266404.

Gelberman RH, **Linderman SW**, Jayaram R, Dikina AD, Sakiyama-Elbert SE, Alsberg E, Thomopoulos S, Shen H. "Combined administration of ASCs and BMP12 promotes an M2 macrophage phenotype and enhances tendon healing." *Clinical Orthopaedics and Related Research*, **475**(9):2318-2331 (2017). DOI: 10.1007/s11999-017-5369-7. PMID: 28462460.

Shen H, Kormpakis I, Havlioglu N, **Linderman SW**, Sakiyama-Elbert SE, Erickson IE, Zarembinsk T, Silva MJ, Gelberman RH, Thomopoulos S. "The effect of mesenchymal stromal cell sheets on the inflammatory stage of flexor tendon healing." *Stem Cell Research & Therapy*, **7**(1):144 (2016). DOI: 10.1186/s13287-016-0406-0. PMID: 27677963.

Linderman SW, Gelberman RH, Thomopoulos S, Shen H. "Cell and Biologic-Based Treatment of Flexor Tendon Injuries." *Operative Techniques in Orthopaedics*, **26**(3):206-215 (2016). DOI: 10.1053/j.oto.2016.06.011. PMID: 28042226.

Kormpakis I*, **Linderman SW***, Thomopoulos S, Gelberman RH. "Enhanced Zone II Flexor Tendon Repair through a New Half Hitch Loop Suture Configuration." *PLOS ONE*, **11**(4):e0153822. (2016). PMID: 27101409. [*co-first authors]

PUBLICATIONS (CONTINUED)

Li J, **Linderman SW**, Zhu C, Liu H, Thomopoulos S, Xia Y. "Surgical Sutures with Porous Sheaths for the Sustained Release of Growth Factors." *Advanced Materials*, **28**(23):4620-4624 (2016). DOI: 10.1002/adma.201506242. PMID: 27059654.

Smith L*, Deymier AC*, Boyle JJ, Li Z, **Linderman SW**, Pasteris JD, Xia Y, Genin GM, Thomopoulos S. "Tunability of collagen matrix mechanical properties via multiple modes of mineralization." *Interface Focus*, **6** (2015). DOI: 10.1098/rsfs.2015.0070 [*co-first authors]

Linderman SW, Kormpakis I, Gelberman RH, Birman V, Wegst UGK, Genin GM, and Thomopoulos S, "Shear Lag Sutures: Improved Suture Repair Through the Use of Adhesives." *Acta Biomaterialia*, **23**:229-239 (2015). PMID: 26022966.

Som A, Charanya T, **Linderman SW**, and Siegel JS, "Bridging the gap between invention and commercialization in medical devices", *Nature Biotechnology*, **32**(10):1063-5 (2014). PMID: 25299924.

Jeon O, Alt DS, **Linderman SW**, and Alsberg E, "Biochemical and physical signal gradients in hydrogels to control stem cell behavior", *Adv Mater*, **25**(44):6366-72 (2013). PMID: 23983019.

Mansell TJ, **Linderman SW**, Fisher AC, and DeLisa MP, "A rapid protein folding assay for the bacterial periplasm", *Protein Science*, **19**(5):1079-90 (2010). PMID: 20440843.

Lim HK, Mansell TJ, **Linderman SW**, Fisher AC, Dyson MR, and DeLisa MP, "Mining mammalian genomes for folding competent proteins using Tat-dependent genetic selection in *Escherichia coli*", *Protein Science*, **18**(12):2537-49 (2009). PMID: 19830686.

INVITED TALKS

"Translating orthopedic research into treatments" Orthopaedic Research Society Midwest Musculoskeletal Workshop, Jul 20, 2017, St. Louis, MO.

"Translating Clinical Research: Insights from Sling Health" Washington University TL1 Program, Clinical Research Training Center, Interdisciplinary Research Training in Translation Seminars. Oct 25, 2016, St. Louis, MO.

"Sling Health: Building the innovation ecosystem with the American Medical Association" Health 2.0 Conference "AMA Lunch-and-Learn" Panelist. Sep 27, 2016, Santa Clara, CA.

"Improving orthopaedic repairs through mechanically optimized, adhesive biomaterials" Washington University Biomedical Engineering Day Conference, Doctoral Research Award Presentation. Apr 26, 2016, St. Louis, MO.

"Solving medical problems, training innovators, improving healthcare" Washington U. School of Engineering National Advisory Council Meeting. Apr 8, 2016, St. Louis, MO.

"Improving orthopaedic repairs through mechanically optimized, adhesive biomaterials" Hospital for Special Surgery, Tissue Eng., Regen. & Repair. Mar 17, 2016, New York, NY.

"Adhesive Films for Rotator Cuff Repair" Columbia University, Orthopaedic Surgery, Shoulder and Sports Group. Mar 15, 2016, New York, NY.

"Translation via Commercialization - Stories from the field" Washington University Clinical Research Training Center, Career Development Seminar. Jan 12, 2016, St. Louis, MO.

"Improved orthopaedic repairs through mechanically optimized, adhesive biomaterials" Washington U. Medical Scientist Training Program Seminar. Dec 10, 2015, St. Louis, MO.

"Solving medical problems, training innovators, improving healthcare" Washington U. School of Medicine National Advisory Council Meeting. Dec 1, 2015, St. Louis, MO.

"Making entrepreneurship attainable for students" Washington U Board of Trustees Meeting. Apr 30, 2015, St. Louis, MO.

"IDEA Labs: Students improving healthcare through innovation" Cerner Corporation. Sep 12, 2014, Kansas City, MO.

CONFERENCE PRESENTATIONS

"Adhesive films for enhanced tendon-to-bone repair" **Linderman SW**, Golman M, Gardner TR, Yoon D, Birman V, Levine WN, Genin GM, and Thomopoulos S, Summer Biomechanics, Bioengineering, and Biotransport Conference, 2017, Tucson, AZ. *2nd place, PhD Student Paper Competition*

"Sustained delivery of growth factor on porous sutures to modulate the proliferative stage of canine flexor tendon repair" **Linderman SW**, Shen H, Yoneda S, Tanes ML, Jayaram R, Xia Y, Sakiyama-Elbert SE, Thomopoulos S, and Gelberman RH, American Physician Scientists Association, 2017, Chicago, IL.

"Strengthening tendon-to-bone repair with mechanically-optimized adhesives" **Linderman SW**, Golman M, Yoon D, Birman V, Genin GM, and Thomopoulos S, Orthopaedic Research Society Annual Meeting, 2017, San Diego, CA.

"Shear lag sutures: Improved suture repair mechanics through the use of adhesives" **Linderman SW**, Kormpakis I, Gelberman RH, Birman V, Wegst UGK, Thomopoulos S, and Genin GM, ASME International Mechanical Engineering Conference & Exhibition, 2016, Phoenix, AZ. *Best Paper 1st place in Track 4: Biomedical and Biotechnology Eng.*

"Improved tendon suture repairs through the use of adhesive biomaterials" **Linderman SW**, Li J, Kormpakis I, Gelberman RH, Birman V, Kaplan DL, Genin GM, and Thomopoulos S, Musculoskeletal Research Center Winter Symposium, 2016, St. Louis, MO.

"Improved orthopaedic repairs through mechanically optimized, adhesive biomaterials" **Linderman SW**, Thomopoulos S, WUSTL Medical Scientist Training Program Retreat, 2015, St. Louis, MO. *Best Presentation Award.*

"Sticky Sutures: Improved Suture Repair Mechanics Through the Use of Adhesives" **Linderman SW**, Kormpakis I, Gelberman RH, Birman V, Genin GM, and Thomopoulos S, Orthopaedic Research Society Annual Meeting, 2015, Las Vegas, NV.

"Shear Lag Sutures: Improved Suture Repair Mechanics Through the Use of Adhesives" **Linderman SW**, Kormpakis I, Gelberman RH, Birman V, Wegst UGK, Genin GM, and Thomopoulos S, Musculoskeletal Research Center Winter Symposium, 2015, St. Louis, MO.

"IDEA Labs: University students bridging the gap between invention and commercialization in medical devices" **Linderman SW**, Talent Pipeline Management Roundtable, US Chamber of Commerce Foundation, 2014, Las Vegas, NV.

"Improving regulatory systems for pharmaceutical development and biotechnology" **Linderman SW**, Global Scholars' Symposium, 2011, Oxford, UK.

"Mechanisms of A_{2B} adenosine receptors in protecting rat cardiomyocytes following ischemia" **Linderman SW** and Krieg T, University of Cambridge and Glaxo-SmithKline's Translational Medicine & Therapeutics Research Day, 2011, Cambridge, UK.

"Engineering Antibody Interactions in the Periplasm of *Escherichia coli*" **Linderman SW**, Mansell TJ, and DeLisa MP, Cornell University Institute of Biological Engineering's 8th Annual Bio-Expo, 2010, Ithaca, NY.

"Monitoring and Engineering Protein-Protein Interactions in the Bacterial Periplasm" **Linderman SW**, Mansell TJ, and DeLisa MP, 35th Annual NE Bioengineering Conference, 2009, Boston, MA.

"Examining and Engineering Protein-Protein Interactions in the Bacterial Periplasm" **Linderman SW**, Mansell TJ, DeLisa MP, Cornell Undergraduate Research Board's 24th Annual Spring Research Forum, 2009, Ithaca, NY.

"Reporting protein-protein interactions in the bacterial periplasm" **Linderman SW**, Mansell TJ, and DeLisa MP, Institute of Biological Eng. Regional Conference, 2008, Ithaca, NY.

PEER-REVIEWER

Journal of Orthopedic Research
Journal of Biomechanical Engineering, Journal of Biomechanics
American Chemical Society: Biomaterials Science & Engineering